New insights into portal tract morphogenesis: from 3D imaging to the roles of axon guidance genes in hepatic artery development

Catalina De Schrevel

2018-2023

Acknowledgements

Au terme de ces quatre années et demie de travail, j'aimerais prendre le temps de remercier les personnes qui m'ont permis d'entreprendre et de progresser dans mon projet scientifique ainsi que de finaliser cette folle odyssée doctorale. Elles m'ont été importantes, tant scientifiquement que moralement, elles ont cru en moi, m'ont soutenue, m'ont aidée et m'ont fait grandir.

Mes premiers remerciements vont à mon promoteur, Frédéric. Vous avez cru en ma capacité à mener à bien le projet en commençant par le défendre face au jury du FRIA. Vous m'avez accompagnée durant ce premier challenge pour me laisser ensuite voler de mes propres ailes. Durant tout mon cheminement, j'ai toujours pu compter sur vos conseils et votre expertise. Un très grand merci pour la correction minutieuse de mon manuscrit de thèse mais surtout merci de m'avoir ouvert les portes de votre labo pour vivre une belle aventure qui aujourd'hui touche à sa fin.

Je remercie également chaleureusement les membres de mon comité pour leur suivi bienveillant tout au long de mon parcours. J'ai apprécié les échanges que nous avons eus durant nos réunions annuelles. Merci pour votre intérêt, votre temps et votre regard extérieur. Merci aux membres externes de mon jury pour leurs apports critiques, la relecture attentive de ma thèse et vos questions challengeantes. Lors de ma défense privée, j'ai beaucoup apprécié de pouvoir discuter avec vous des résultats et difficultés de ma thèse.

ACKNOWLEDGEMENTS

Avant de remercier ceux qui ont fait partie de mon quotidien, je souhaiterais remonter dans le temps. Car rien n'aurait été possible sans plusieurs belles rencontres . Tout a commencé le vendredi 27 septembre 2012, incertaine, désorientée et un peu perdue je ne savais pas quelle direction prendre afin de m'épanouir dans des études supérieures. Alors que mon tram avait du retard, j'ai naïvement passé le coup de fil qui allait changer le cours de ma vie. J'ai appelé le responsable académique des études de sciences biologiques à l'UCL, le professeur André Lejeune. Après une discussion animée et passionnée, j'étais convaincue et le lendemain je m'inscrivais au programme 1 ère bachelier biologie pour l'année 2012-2013. Les premières années furent difficiles et c'est en grande partie grâce à l'accompagnement et aux conseils de Monsieur Lejeune que j'ai surmonté l'énorme défi des premières années à l'université pour ensuite m'épanouir dans mes études. C'est donc bien mieux outillée que j'ai entamé un Master en Biochimie et biologie moléculaire et cellulaire de l'UCL. Durant ces deux années j'ai fait de nouvelles rencontres qui ont marqué un tournant dans mon parcours scientifique. Le professeur René Rezsohazy, en charge du master et du cours d'embryologie (un signe ?), m'a apporté un accompagnement sans faille pour la recherche du lieu de mémoire et de stage ainsi que leur suivi. C'est lors de mon mémoire, que j'effectuais dans le laboratoire du professeur Isabelle Donnay sous la supervision de Matthew Dallemagne, que nous devenons voisin de bureau. Une chose est sûre, c'est que je n'aurais pas pu mieux tomber. Un encadrement de qualité, une ambiance de laboratoire du tonnerre ainsi qu'une réelle envie de partager et d'enseigner. C'est dans ce cadre fabuleux que j'ai pu apprendre ce qu'était le travail en laboratoire et la recherche scientifique. Alors que ce n'était pas une évidence pour moi c'est à grâce à ce soutien bienveillant que j'ai pu envisager d'entreprendre une thèse de doctorat. C'est alors que je quitte Louvain-la-Neuve pour entamer mon nouveau travail de doctorante à l'Institut de Duve. Il fallait garder un lien avec

cette période cruciale pour moi et que rêver de mieux que d'avoir Monsieur Rezsohazy comme membre de mon jury. Je me demande toujours si il n'a pas accepté cette proposition afin de me remercier d'avoir animé les brocantes qu'il organisait dans mon bureau durant mon mémoire.

Revenons à nos moutons et plutôt qu'au troupeau, à la tribu LPAD et GEPI. Je tenais à remercier tous les membres de l'équipe pour l'atmosphère d'entraide, la disponibilité, mais aussi les pauses de midi, les activités de labo, les drinks, les marchés de Noël et j'en passe. Un grand merci à l'équipe de mes débuts, celle au sein de laquelle j'ai été accueillie, ai trouvé ma place, fait mes armes. Mine de rien, il y en a eu du passage pendant ces quatre années et demi et la relève est venue renforcer cette équipe, merci donc à cette deuxième fournée de m'avoir permis de m'épanouir. Dans tout de mouvement il y a bien eu une constante, Sabine, que je tenais à remercier tout particulièrement pour sa sympathie, ses conseils, son sourire communicatif, son soutien inconditionnel mais surtout pour tous les moments de qualité passés ensemble. Voilà pour celles et ceux qui ont fait partie de mon quotidien au labo . Celles et ceux qui ont fêté les manips qui marchent et encore plus celles qui foirent. Celles et ceux qui comprennent parce qu'ils ou elles vivent la même chose. C'est pour cette dernière raison que je remercie également Marie, Julie, Morgane, Pauline et Mathieu, mes copains d'université avec lesquels j'ai tant partagé. Dans le même milieu mais chacun à sa manière, un amitié qui tient dans la durée. Vous êtes toujours de bon conseils et je chéris chacunes de nos retrouvailles.

Je tenais aussi à remercier quelques personnes en dehors du labo. Toujours dans un cadre scientifique, merci à Morgane Belle, la spécialiste de la microscopie 3D. Quelle chance de t'avoir rencontré, quel partage. Merci pour nos échanges d'égale

à égale alors que j'avais tout à apprendre et que tu étais une pro. Merci de m'avoir transmis ton amour pour l'imagerie, ta gentillesse, ta patience, ta disponibilité et surtout tes nombreux conseils judicieux. Avec l'aide de Stéphane vous avez rendu tous mes séjours à Paris chaleureux, drôles et enrichissants. Afin d'en mettre plein la vue avec mes images 3D, je remercie également l'équipe de la plateforme d'imagerie de l'ULB ainsi que les organisateurs et les participants du « EMBO pratical course on 3D Developmental Imaging » qui a eu lieu au Portugal. C'est grâce à toutes ces rencontres formidables que j'ai pu m'épanouir dans mon projet scientifique en me passionnant pour l'imagerie.

Merci également aux personnes qui ont toujours été à l'écoute de mes joies, mes déceptions sans toujours tout comprendre, qui se sont intéressés à mon travail et m'ont changé les idées quand c'était nécessaire. Je pense à mes amis de toujours le Club83, les Bibiches, les Cobras et j'en passe. Mais plus particulièrement, merci à ma famille, mes frères mais surtout mes parents. Maman et Papa, merci pour tous ces blocus passés aux petits soins chez vous durant mes études et après ! Merci pour votre encouragement, votre aide et votre soutien sans faille. Vous avez toujours cru en moi et m'avez accompagnée et épaulée durant ces longues années. Un petit mot aussi pour ma Mamy, qui habite tout près du laboratoire , quel bonheur de venir passer de merveilleuses pauses chez toi tout en repartant avec un bon potage histoire de reprendre des forces.

Pour finir, je tiens à mettre à l'honneur mon partenaire de tous les jours, Sweat P. Tu es indispensable à mon équilibre. Scientifique mais pas doctorant, fêtard et casanier, gourmet , drôle et attentif autant d'éléments qui font que toi est moi nous formons un beau duo. J'aime le soutien que tu m'as apporté et la compréhension

dont tu as fait preuve tout au long de ma thèse. Merci du fond du cœur d'avoir été là et d'avoir si bien pris soin de moi.

Il est l'heure de clore un long et beau chapitre de ma vie. Grâce à vous tous celle que je suis aujourd'hui n'est pas tout à fait celle que j'étais auparavant. Je me suis enrichie de clés, d'outils, de connaissance, de rencontres et de découvertes pour aborder la prochaine étape sereinement.

TABLE OF CONTENTS

ACKNOWLEDGEMENTS **3**

JURY MEMBERS **11**

ABBREVIATIONS **13**

SUMMARY **17**

INTRODUCTION **19**

I. THE ADULT LIVER HISTOLOGY AND FUNCTIONS 21

II. OVERVIEW OF THE FETAL MOUSE LIVER DEVELOPMENT 25

III. THE BILIARY TREE IN MAMMALS 27

i. Organization and function of the biliary system *27*

ii. Morphogenesis of the intrahepatic bile duct *30*

iii. Molecular mechanisms governing IHBD development *34*

IV. THE LIVER MESENCHYME 39

i. Origin and mesenchyme subpopulations *40*

ii. Epithelial-mesenchyme interaction driving liver development *45*

V. THE LIVER VASCULATURE 46

i. Organization and function of the hepatic vasculature *46*

ii. Overview of the fetal liver venous system *48*

iii. Origin and morphogenesis of the hepatic artery *49*

VI. RECIPROCAL INTERACTIONS BETWEEN ENDOTHELIAL, MESENCHYMAL, AND EPITHELIAL CELLS DURING DEVELOPMENT AND MORPHOGENESIS OF TISSUES AND ORGANS 53

i. Classical axon guidance receptors and their ligands in mammals *54*

ii. Roles for axon guidance pathways in embryonic tissue architecture *59*

iii. Axon guidance cues in the liver *70*

VII. IMAGING TISSUE AND ORGAN MORPHOGENESIS 74

i. Main clearing techniques *75*

ii. 3D microscopy *78*

iii. Practical considerations *79*

AIMS AND STRATEGIES OF OUR RESEARCH **81**

TABLE OF CONTENTS

RESULTS 83

I. NEW INSIGHT INTO THE 3D DEVELOPMENT OF THE LIVER PORTAL -------AREA 83

i. Introduction 83

ii. Materials and methods 84

iii. Results 88

iv. Discussion 107

v. References 113

II. AXON GUIDANCE GENES CONTROL HEPATIC ARTERY DEVELOPMENT 117

i. Abstract 118

ii. Introduction 119

iii. Results 120

iv. Discussion 144

v. Materials and methods 147

vi. References 159

GENERAL DISCUSSION 177

I. THE STUDY OF ORGAN DEVELOPMENT IN 3D 179

i. Imaging the liver development: the tip of the iceberg 179

ii. Perspectives 181

II. THE ROLE OF AXON GUIDANCE MOLECULES DURING PORTAL TRACT DEVELOPMENT: DREAM OR REALITY? 183

i. Theory that holds great promise 183

ii. The study of axon guidance genes in liver development: more or no more? ... 184

III. HOW FAR ARE WE FROM APPLICATIONS? 195

CONCLUDING REMARKS 197

BIBLIOGRAPHY 199

Jury members

President

Chistophe Pierreux

de Duve Institute, UCLouvain

Internal members

René Rezsohazy

Louvain Institute of Biomolecular Science and Technology, UCLouvain

Wen-Hui Lien

de Duve Institute, UCLouvain

External members

Pedro Baptista

Aragon Health Institute, Saragoza, Spain

Isabelle Migeotte

Institut de Recherche Interdisciplinaire en Biologie Humaine et Moléculaire, Université libre de Bruxelles

Promoter

Frédéric Lemaigre

de Duve Institute, UCLouvain

Abbreviations

2D	Two-dimensional
3D	Three-dimensional
3DISCO	3D imaging of solvent-cleared organs
αSMA	α Smooth muscle actin
βCAT	Beta-catenin
BMP	Bone morphogenic protein
BSA	Bovine serum albumin
CD	Cluster of differentiation
DUCT	Double resin casting computed tomography
CCL4	Carbon tetrachloride
CEACAM	Carcinoembryonic antigen-related cell adhesion molecule
CLDN	Claudin
CNN	Calponin
COL15A1	Collagen Type XV Alpha 1 Chain
CUBIC	Clear, unobstructed brain/body imaging cocktails and computational analysis
CK	Cytokeratin
DBE	Dibenzyl ether
DCC	Deleted in colorectal cancer
DCM	Dichloromethane
DES	Desmin
DNMT1	DNA (cytosine-5)-methyltransferase 1
E-CAD	Epithelial cadherin
ECM	Extracellular matrix
EHBD	Extrahepatic bile duct
ELN	Elastin
EMT	Epithelial-mesenchymal transition
EphB	Ephrin receptor b
eYFP	Enhanced yellow fluorescent protein
FB	Fibroblasts

FBLN	Fibulin
FFPE	Formalin-fixed paraffin embedded
FGF	Fibroblast growth factor
GFP	Green fluorescent protein
HSC	Hepatic stellate cells
HNF	Hepatocyte nuclear factor
IHBD	Intrahepatic bile duct
IHC	Immunohistochemistry
JAG1	Jagged1
LYVE-1	Lymphatic vessel endothelial hyaluronan receptor 1
MicroCT	Microcomputed tomography
MUC	Mucin
NEO	Neogenin
NTN	Netrin
OCT	Optimal cutting temperature compound
OPN	Osteopontin
PBS	Phosphate-buffered saline
PBSGT	PBS containing 0,2%gelatine, 0,5% Triton X-100
PDGF	Platelet-derived growth factor
PFA	Paraformaldehyde
PV	Portal vein
qPCR	Quantitative polymerase chain reaction
RAC1	Ras-related C3 botulinum toxin substrate 1
RBPJκ	Recombination signal binding protein for immunoglobulin kappa J
RhoA	Ras homolog gene family, member A
RI	Refractive index
ROBO	Roundabout
RGM	Repulsive guidance molecules
RT	Room temperature
scRNA seq	Single cell RNA sequencing
SEMA	Semaphorin
SM22α	Smooth muscle protein 22 α
snRNA seq	Single nucleus RNA sequencing

SMTN	Smoothelin
SOX	SRY-related HMG box transcription factor
STM	Septum transversum mesenchyme
TAGLN	Transgelin
TβRII	Tgfβ receptor II
TGFβ	Transforming growth factor β
THF	Tetrahydrofuran
THY1	Thymocyte differentiation antigen 1
TPM	Transcripts per million
TUBB3	Tubulin class III
YAP1	Yes-associated protein 1
VEGF-A	Vascular endothelial growth factor A
VEGFR	VEGF receptor
VIM	Vimentin
VSMC	Vascular smooth muscle cells
WWTR1	WW domain-containing transcription regulator protein 1 (= TAZ)

Summary

The liver performs vital functions, such as production and excretion of bile, regulation of energy metabolism, nutrient processing, metabolite detoxification or secretion of plasma proteins. This requires that the various cell types of the liver are organized into three-dimensional (3D) structures commonly referred to as hepatic lobules. The latter are the functional units of the liver and consist of hepatocyte cords and sinusoids that radiate from the portal area to the central vein. The portal area contains a branch of the portal vein, a hepatic artery, a bile duct and mesenchymal cells. Previous work has shown that embryonic development of the bile ducts, hepatic artery and periportal mesenchyme is functionally interdependent. However, how these three structures coordinately develop in 3D in the portal tract has not been described in detail. Also, how the molecular crosstalk between mesenchyme, duct and artery is orchestrated to shape the portal tract in 3D remains poorly characterized.

To address these questions, we first optimized tissue clearing methods to visualize 3D development of the portal tract in mouse embryonic liver using light-sheet fluorescence microscopy. This optimization was needed to analyze the entire liver and entire hepatic lobes at cellular resolution. It enabled us to describe how the periportal mesenchyme forms hepatic arteries, in parallel with the morphogenesis of the bile ducts.

Second, to search for signaling pathways driving portal tract morphogenesis, we purified cholangiocytes and adjacent periportal mesenchymal cells at distinct

stages of liver development and analyzed their transcriptome by bulk RNA sequencing. These data suggested that axon guidance genes are candidate regulators of portal tract development. Following our identification of the cell-specific and spatial expression profiles of selected genes, we focused on Slit/Robo and Netrin/Netrin receptor pairs on the basis of their preferential expression near forming ducts and arteries. We inactivated selected genes in the developing mouse liver and discovered that Slit/Robo and Rgma/Neogenin1 signaling were dispensable for biliary morphogenesis, but that Slit2/Robo2 signaling is required within the mesenchyme for normal hepatic artery formation.

To conclude, we provide a workflow to comprehensively investigate the architectural organization and coordinated development of the portal tract components. We highlight the close spatial and temporal relationship between mesenchyme and biliary cells during development and uncover that Slit2/Robo2 signaling is a new player in development of the liver vasculature.

Introduction

Although the liver has the unique capacity to regenerate, in advanced cases of acute and chronic liver disease, regeneration is impaired. In this setting, as well as in in genetic or congenital diseases with severe liver deficiency, liver transplantation is often the only curative therapy. Due to the shortage of donor organs, tissue engineering appears as a most promising alternative. However, implementing this strategy requires a detailed understanding of the biological processes that drive liver organogenesis in space and time.

In this section, I provide the background for studying liver organogenesis, specifically in the context of mammalian development, and outline how my thesis can contribute to gain new knowledge. I start by giving a brief overview of adult liver architecture and mouse fetal liver development. As tubular structures play essential roles in transport and exchange of nutrients and metabolites, I focus on the development of the liver portal tract (bile duct, periportal mesenchyme, portal vein, hepatic artery) which constitutes a coherent functional unit. I summarize the current understanding of intrahepatic bile duct and artery development while highlighting the gaps of knowledge. Subsequently, given that cell-cell and cell-matrix communication is fundamental for proper tissue development, I narrowed my focus on describing the role of axon guidance molecule in the interaction between endothelial, mesenchymal, and epithelial cells during organogenesis. Finally, I summarize how the description of organ morphogenesis can be improved by implementing advanced in 3D imaging technology.

I. The adult liver histology and functions

The liver is the largest internal organ in the body, located in the upper right quadrant in human and occupying the entire space under the diaphragm in mice. The rodent liver differs from human liver by its smooth, uninterrupted surface and lobe patterns (Fig. 1). The physiological function is similar in the two species, and consists in nutrient processing, protein production, controlling energy homeostasis and detoxification. Overall, similarities in structure and function between the two species far outweigh the differences, and rodents remain the most widely studied laboratory models of mammalian liver development (Rogers & Dintzis, 2018; Trefts, Gannon, & Wasserman, 2017).

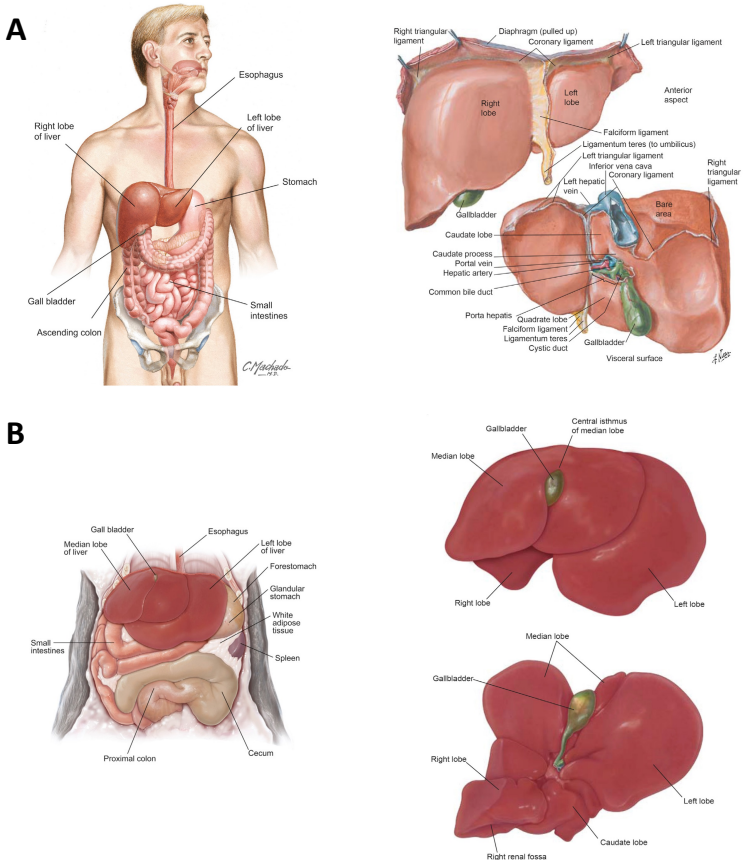


Figure 1: Schematic representation of the human and mouse liver anatomy. (A) The human liver occupies the upper right quadrant of the abdominal cavity, prominently septated near the left lobe by the falciform ligament. It has four lobes: right, left, caudate and quadrate. **(B)** The mouse liver spans the entire subdiaphragmatic space in the abdomen and does not have prominent surface ligaments. It also has four lobes: left, right, median, and caudate. Figure adapted from (Rogers & Dintzis, 2018).

The functions of the liver rely on a particular 3-dimensional (3D) tissue architecture in which the different cell types are organized as hepatic lobules. This lobular architecture is highly conserved in mammals and consists of chords of polarized hepatocytes lined by sinusoids organized in an approximately hexagonal shape around the central vein. At the extremities of the hexagons are the portal spaces containing branches of the bile ducts, the hepatic artery, the portal vein, lymphatics, and nerve fibers, all embedded in connective tissue known as the portal mesenchyme (Fig. 2A) (Krishna, 2013; Mescher, 2010).

Oxygen-rich blood from the hepatic artery mixes with nutrient-rich blood from the portal circulation in the sinusoids and flows towards the central vein while exchanging metabolites with the hepatocytes. Bile, an exocrine secretion from the hepatocytes which is required for lipid digestion in the gut, travels in the opposite direction towards the bile ducts in the portal spaces. This organization induces functional zonation of the lobules whereby hepatocytes and sinusoidal cells are exposed to gradients of oxygen, nutrients and morphogens along a porto-central axis. Three distinct zones (periportal, midzonal, centrilobular) can be described in the lobule, each possessing hepatic cells with different gene expression and functionality as well as different damage susceptibility (Fig. 2B) (Paris & Henderson, 2022; Ramachandran, Matchett, Dobie, Wilson-Kanamori, & Henderson, 2020).

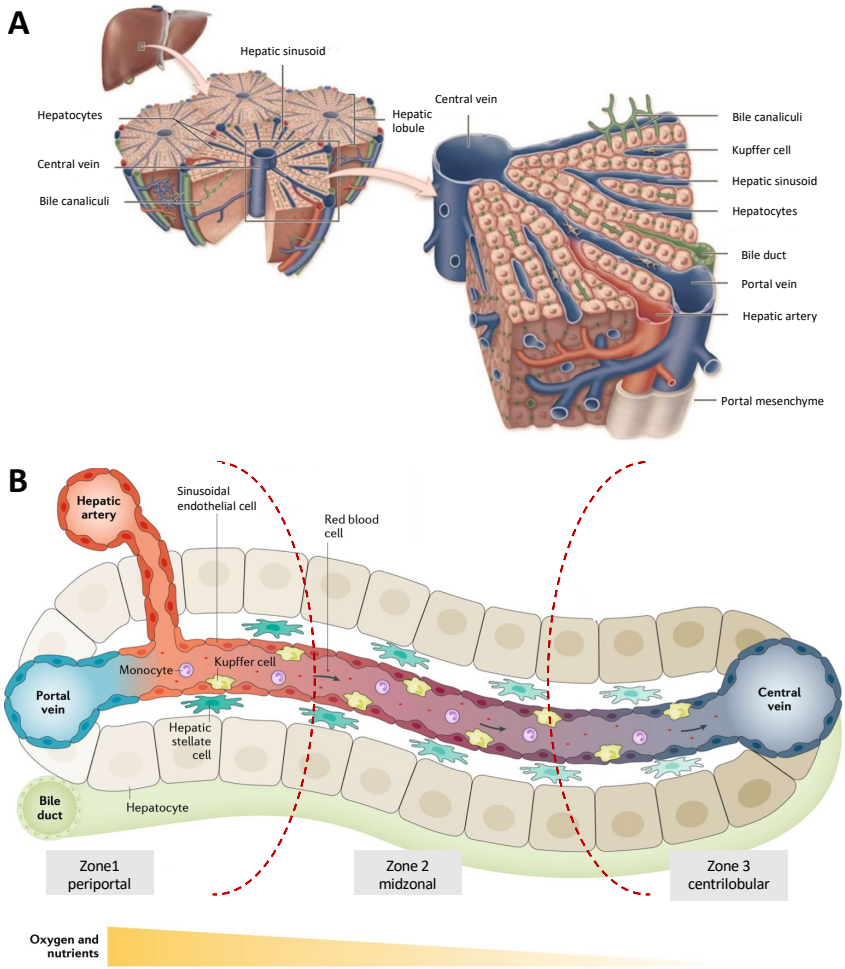


Figure 2: Schematic representation of the liver organization. (A) The liver is composed of lobules. Hepatocyte cords radiate from the peripheral portal areas towards a centrilobular vein. Each portal area contains a portal vein, a bile duct and a hepatic artery, collectively referred to as portal triad and surrounded by portal mesenchyme. **(B)** Non-parenchymal cells associated with the sinusoid include fenestrated liver sinusoidal endothelial cells, Kupffer cells and hepatic stellate cells which reside in the space of Disse. Oxygen and nutrients are depleted along the sinusoids, thereby creating a gradient. Figure adapted from (Mescher, 2010; Ramachandran et al., 2020).

In addition to the hepatocytes which constitute 80% of total liver volume, several other cell types contribute to the liver functions. Cholangiocytes are parenchymal cells that line the bile ducts and modify the composition of bile. Non-parenchymal

cells provide essential supportive and homeostatic functions, and include immune cells (dendritic cells, Kupffer cells, natural killer and T cells), sinusoidal endothelial cells, hepatic stellate cells (HSCs), vascular smooth muscle cells (VSMCs) and fibroblasts (FBs) (Dobie et al., 2019; Ishibashi, Nakamura, Komori, Migita, & Shimoda, 2009). The cholangiocytes and the three mesenchymal cell types are described with more detail in chapter III and IV.

II. Overview of the fetal mouse liver development

The liver and the gastrointestinal tract derive from the definitive endoderm. During formation of the primitive gut tube, the endoderm is patterned along the anterior-posterior axis into foregut, midgut, and hindgut. Signals from the overlying cardiac mesoderm and septum transversum mesenchyme (STM) specify hepatic identity and promote migration of hepatoblasts, which are the liver parenchymal progenitors emerging from the endoderm (Lotto et al., 2020). Hepatoblasts intermingle with endothelium and mesenchyme and express liver-specific proteins (Ober & Lemaigre, 2018; Sosa-Pineda, Wigle, & Oliver, 2000; Zaret, 2016). Over time, hepatoblasts give rise to both hepatocytes and cholangiocytes which form bile canaliculi and bile ducts, respectively. Their differentiation proceeds during gestation, and their functional and structural maturation terminates in the postnatal period (Gordillo, Evans, & Gouon-Evans, 2015; Tanimizu, 2022; Tanimizu, Miyajima, & Mostov, 2007; Zorn & Wells, 2007).

Development of the liver vasculature and initiation of hematopoiesis occur in parallel. The fetal liver is indeed a hematopoietic organ during the foetal period (Soares-da-Silva, Peixoto, Cumano, & Pinto-do-Ó, 2020): stem and progenitor cells migrate to the liver which offers a microenvironment that promotes hematopoiesis (Popescu et al., 2019). Starting at the end of gestation, hematopoietic cells leave the liver and migrate to their permanent bone marrow niche. The liver then rearranges its tissular architecture to optimize its metabolic functions (Beath, 2003).

Liver organogenesis is tightly controlled by a network of signaling molecules and transcription factors (Fig. 3). Prominent signaling pathways are activated by fibroblast growth factors (FGF), bone morphogenic proteins (BMP), transforming growth factor β (TGFβ), and WTN/β-catenin. Moreover, the Hippo pathway, a serine/threonine kinase cascade, is a known key regulator of liver size (Driskill & Pan, 2021). Notch signaling is required for differentiation of the biliary lineage.

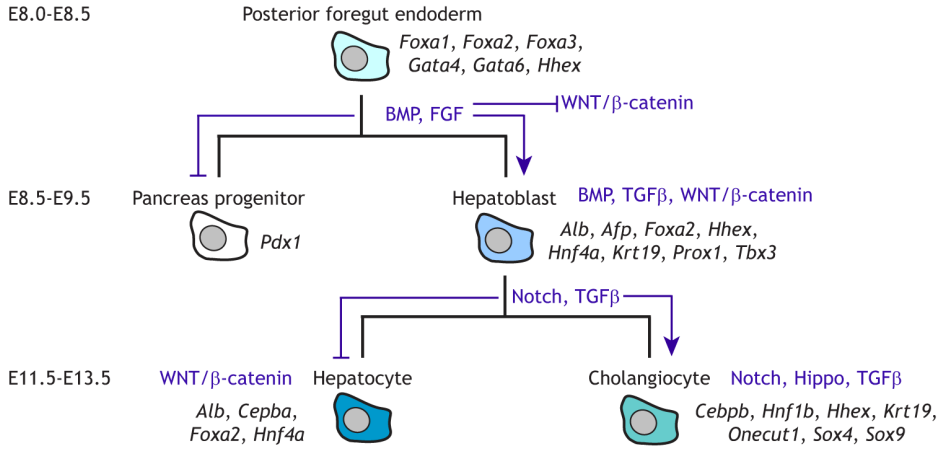


Figure 3: Key signaling pathways and transcription factors driving liver development. Specification and differentiation of endoderm, hepatoblasts, hepatocytes and cholangiocytes are controlled by several signaling pathways and by a network of liver-enriched transcription factors. Figure from (Campbell et al., 2021).

Although early liver development is relatively well described, the 3D organization and remodelling of the liver components during late embryonic development are poorly understood. As tubular structures are indispensable for proper liver function, I focus on the development of the liver portal tract (bile duct, portal vein, hepatic artery and surrounding mesenchyme). The next chapters zoom in these different components as well as in their coordinated development.

III. The biliary tree in mammals

i. Organization and function of the biliary system

The biliary tree is a large 3D network of ducts whose main purpose is to collect and transport bile produced by hepatocytes inside the liver and to drain it to the gut. Bile is a digestive fluid responsible for fat emulsification. It is composed of water, bile acids/salts, cholesterol, bilirubin, lipids, organic ions, and xenobiotic compounds. Bile acids play a key role in the physiological function of bile, and they represent the primary route of cholesterol catabolism (Boyer, 2013). While bile transport in the canalicular compartment is diffusion-dominated, the biliary epithelium absorbs and secretes ions and metabolites to modify the composition, fluidity and flow of bile (de Jong, van Leeuwen, Lisman, Gouw, & Porte, 2018; Vartak et al., 2021) . The lumen of the biliary tree is lined by a single layer of cholangiocytes. The biliary system not only provides a transportation channel for bile, but also acts as a barrier to protect liver parenchyma and other surrounding structures against harmful endogenous and exogenous biliary substances (Beuers et al., 2010).

The biliary tree is composed of the extra- and intra-hepatic biliary systems with ducts enlarging from the periphery of the liver towards the small intestine. The extrahepatic biliary ducts (EHBDs) include the common hepatic duct, the common bile duct and the cystic duct, the latter being connected with the gallbladder. In the liver, the intrahepatic bile ducts (IHBDs) are constituted by the ramification of the left and right hepatic ducts into smaller intrahepatic bile ducts from the hilum to the periphery (Fig. 4). Bile canaliculi, the smallest branches of the bile duct system, are delineated by the apical poles of adjacent hepatocytes and are connected to

intrahepatic bile ducts via the canals of Hering, which are lined by cholangiocytes and hepatocytes (de Jong et al., 2018; Morini, Carpino, Carotti, & Gaudio, 2020).

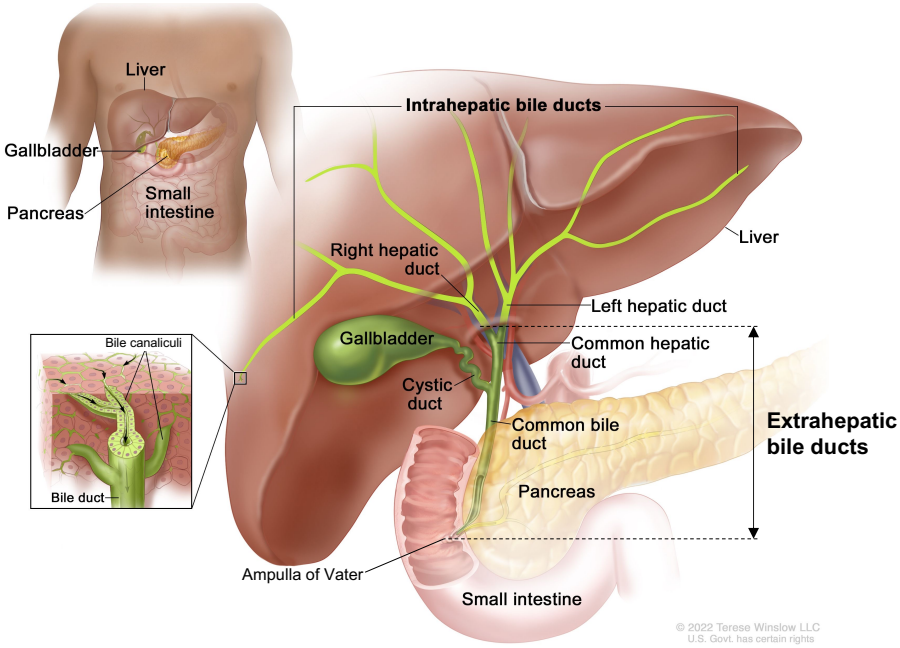


Figure 4: Schematic representation of the extra- and intra-hepatic biliary trees. The extrahepatic biliary system is composed of the common hepatic duct and the common bile duct. Bile is stored in the gallbladder and flows in the cystic duct to reach the small intestine via the common bile duct. The intrahepatic biliary system is composed of the right and the left hepatic ducts that ramify to form the intrahepatic bile ducts. Figure adapted from (https://www.teresewinslow.com/#/digestion/).

The biliary epithelium is known for many years to be heterogeneous at the functional and morphological level (Kanno, LeSage, Glaser, Alvaro, & Alpini, 2000). The cholangiocytes' secretory function modulated by hormones, peptides, and neurotransmitters, many of which act on a subpopulation of ductal epithelium (Maroni et al., 2015), and the cells' differential response after ductal injury are good examples (Kamimoto et al., 2016; Miyajima, Tanaka, & Itoh, 2014). At the morphological level, the biliary epithelial cells differ in size, with “small”

cholangiocytes residing in proximal ductules near the canals of Hering and “large” cholangiocytes in larger ducts (Brevini, Tysoe, & Sampaziotis, 2020; Maroni et al., 2015; Strazzabosco & Fabris, 2008).

Recent single cell RNA sequencing (scRNA seq) analyses provided extensive details on this heterogeneity (T. S. Andrews et al., 2022; Guilliams et al., 2022; Pepe-Mooney et al., 2019). In human liver, cholangiocyte heterogeneity has been studied by a combination of scRNA seq and single nucleus RNA sequencing (snRNA seq), which revealed six transcriptionally distinct subpopulations ranging from progenitor-like to hepatocyte-like and mature cholangiocytes (T. S. Andrews et al., 2022). Knowledge about this heterogeneity is important because cholangiopathies affect distinct categories of cholangiocytes.

Underneath the single layer of cholangiocytes delineating the central lumen, the large IHBD and EHBD are encircled by a fibrous tissue which provides most of its thickness and tensile strength. This periductal tissue contains connective tissue, nerves, blood vessels, lymphatics, and the intramural peribiliary glands. The IHBDs are maintained in the fibrous connective tissue of the portal tract, whereas EHBD have a similar fixing in the hepatoduodenal ligament. The amount of periductal tissue is proportionate to the diameter of the bile ducts and the number of smooth muscle cells increases along the common bile duct near the Ampulla of Vater (de Jong et al., 2018).

ii. Morphogenesis of the intrahepatic bile duct

The first descriptions of IHBD tubulogenesis were based on two-dimensional (2D) analysis and can be summarized as follows (Fig. 5A). Bile duct morphogenesis is initiated at around E13.5–15.5 in mice and develops in association with the portal vein, starting from the hilum and extending towards the periphery of the liver. It is initially characterized by the development of the ductal plate, which on 2D sections of embryonic tissue resembles a nearly continuous single layer of cholangiocytes around the branches of the portal vein. This process depends on periportal mesenchyme, which is rich in laminin, collagen and fibronectin and promotes differentiation of hepatoblasts to a biliary phenotype. The latter is characterized by increased expression of SRY-related HMG box transcription factor 9 (SOX9), which is the earliest marker of cholangiocyte differentiation. Around E15.5-16.5, asymmetrical structures develop from the ductal plate, and small lumina become detectable. These asymmetrical structures, also called primitive ductal structures, are lined by cholangiocytes (negative for Hepatocyte Nuclear factor (HNF)4α and positive for SOX9) on the portal side and by hepatoblasts (positive for HNF4α and negative for SOX9) on the parenchymal side, while becoming surrounded by mesenchyme. Progressively, hepatoblasts lining the primitive ductal structures differentiate into cholangiocytes, giving rise to mature bile ducts entirely lined by cholangiocytes and surrounded by mesenchyme (Antoniou et al., 2009; Poncy et al., 2015; Zong et al., 2009). Thus, the lumen expands in parallel with recruitment of an increasing number of polarized cells. Importantly, the shaping of the ductular structures also requires apical constriction of the cells lining the lumen, and secretion of fluid into the lumen (Benhamouche-Trouillet et al., 2018; Van Liedekerke et al., 2022). Maturation and finalization of duct morphogenesis involves remodeling of the tubes, with a decrease in the number of ducts and the differentiation of a subset of ductal plate cells into periportal hepatocytes

(Carpentier et al., 2011). Around E18.5-E19.5 the expression of cytokeratin-7 (CK7), another marker of biliary cells, is initiated in large bile ducts and reaches the periphery of the biliary tree after birth (Lemaigre, 2020; Morini et al., 2020).

3D analysis using thick section confocal imaging and computer-assisted analysis has improved the understanding of duct morphogenesis (Takashima, Terada, Kawabata, & Suzuki, 2015; Vestentoft et al., 2011). Initially, a 3D model of IHBD morphogenesis was proposed as an attempt to integrate the conclusions of classical 2D histology, thick section imaging and computer-assisted 3D reconstruction (Ober & Lemaigre, 2018) (Fig. 5B). It described that duct growth is discontinuous: along the axis of the future duct, the ductal plate forms small luminal spheres which progressively connect with each other, thereby elongating the duct. In parallel, a perivenous biliary plexus forms which eventually remodels into a dense network of small tubules connected to one or two main ducts (Takashima et al., 2015).

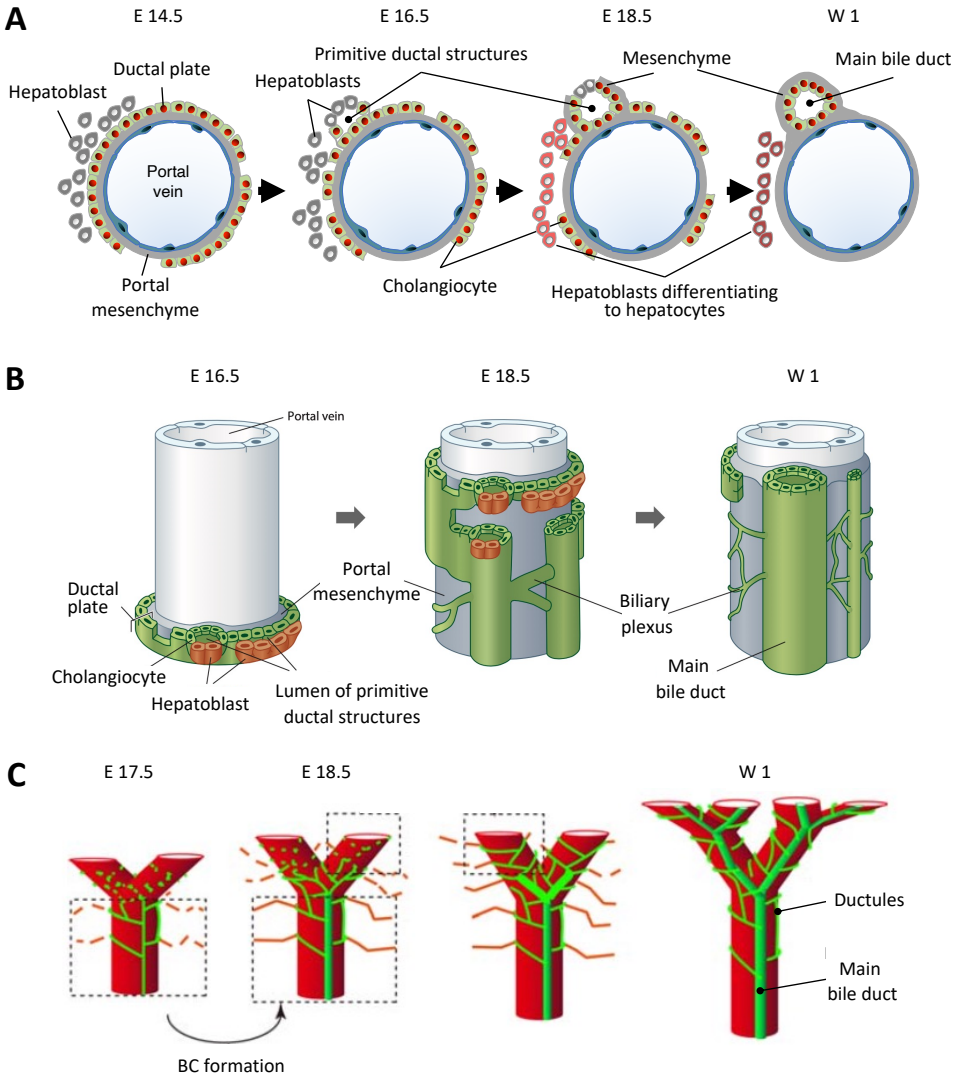


Figure 5: Morphogenesis of IHBD. (A) Cholangiocytes first form a cell layer, ductal plate, near the portal vein (PV) around E14.5. Cholangiocytes generate the luminal space with hepatoblasts ("forming duct" structure). **(B)** Model of bile duct morphogenesis. Cholangiocytes form a cell layer, ductal plate, near the portal vein (PV) around E16.5 and then progressively reorganize it to form tubules **(C)** The 3D model of IHBD morphogenesis. Cholangiocytes are discontinuously differentiated from hepatoblasts, which are eventually interconnected to form the homogeneous luminal network. The homogeneous luminal network is rearranged to a hierarchical network. This transition correlates with formation of the bile canalicular network. Figure adapted from (Ober & Lemaigre, 2018; Tanimizu, Ichinohe, & Mitaka, 2018).

Almost at the same time, the tubular network of IHBDs was analyzed by alternative 3D imaging techniques, including retrograde injection of resin into IHBDs from the common bile duct (Walter, Vanderpool, Cast, & Huppert, 2014), retrograde carbon ink injection (Kaneko, Kamimoto, Miyajima, & Itoh, 2015) and the combination of 3D confocal imaging and retrograde carbon ink injection (Tanimizu et al., 2016). Based on these analyses, IHBD morphogenesis has been divided into three steps (Fig. 5C): at the start, cholangiocytes are discontinuously differentiated from hepatoblasts around the portal veins; subsequently they form a continuous homogeneous luminal network consisting of only small ductules; later, the homogenous luminal network is dramatically re-arranged into a hierarchical mature network, with one or two main ducts running parallel to the portal vein, interconnected with a mesh-like ductular network branching from the large ducts and surrounding the portal vein. This reorganization takes place between E17.5 and 18.5 at the same time as bile canalicular formation. A clear understanding of the mechanism that drives this transition is still lacking. Moreover, whether the luminal enlargement observed in the hierarchical network occurs through localized proliferation of cholangiocytes, movement and incorporation of nearby cholangiocytes, or stretching and enlargement of cholangiocytes cell size remains to be experimentally determined. The IHBD architecture remains immature at the liver periphery of mice until 1 week of age. Indeed, tubular morphogenesis further proceeds at the periphery of the lobes during the early postnatal period, by incorporation of newly differentiated cholangiocytes into the tubular network (Kaneko et al., 2015; Takashima et al., 2015; Tanimizu et al., 2016)

Although our understanding of duct morphogenesis has improved with help of novel imaging technology, each technical approach has its specific limitations. There is still a need to fill the gap between the 2D histology-based description that focuses on cellular organization of the biliary cells and the 3D analysis of luminal structure using ink injection which visualizes the biliary tree at the lobe or organ level. Wholemount imaging using light-sheet microscopy should provide more complete insight into 3D duct morphogenesis both at the cellular and at the lobe or organ level. This technique will also allow a better understanding of the 3D spatio-temporal development of the portal area since several structures will be visualized in parallel. In particular, the bile ducts, the adjacent portal mesenchyme, the portal vein and the hepatic artery which are known to have a coordinated development will be investigated. We focus on the developmental stages from E17.5 to P6 because the basic tubular structures of the biliary system are established in late fetal period (Chapter III ii) and because portal tract morphogenesis further proceeds in neonates (Chapter V iii; cfr Results I).

iii. Molecular mechanisms governing IHBD development

Several signaling mechanisms play a role in biliary morphogenesis. Since differentiation of hepatoblasts to cholangiocytes and formation of 3D ductal structures are tightly associated processes, it remains difficult to distinguish mechanisms promoting differentiation from those regulating morphogenesis. Below are examples of signaling mechanisms important for tubular morphogenesis.

TGFβ

TGFβ signaling is critical at the stage of cholangiocyte differentiation and is dynamically controlled during biliary morphogenesis. Once hepatoblasts differentiate into immature cholangiocytes, they need to shut off the expression of TGFβ receptor II (TβRII) since a prolonged expression is associated with delayed maturation of cholangiocytes and abnormal duct morphogenesis. The mechanisms of this repression are not clearly understood, but there is evidence that it occurs via a TGFβ-induced negative feedback loop (Antoniou et al., 2009; Kaylan, Ermilova, Yada, & Underhill, 2016; Poncy et al., 2015).

Wnt

Unsurprisingly, the canonical Wnt pathway is active during biliary tubulogenesis. This finding results from studies in which β-catenin was either inactivated or stabilized in cholangiocytes. These studies showed that β-catenin was dispensable for the first step of morphogenesis, but that its activity must be contained within strict limits to avoid hyperplasia of the bile ducts and cholangiocytes dedifferentiation (Cordi et al., 2016).There is also evidence from *in vitro* experiments using a hepatoblast line that Wnt5a-induced noncanonical signaling reduces bile duct size (Kiyohashi et al., 2013). These results suggest that harmonious biliary morphogenesis requires appropriately balanced canonical and noncanonical Wnt signaling.

Jagged-Notch

The involvement of Notch signaling in biliary development was initially proposed following the finding that Alagille syndrome (Alagille et al., 1987), a genetic disease associated with intrahepatic bile duct paucity, resulted from mutations in *JAG1* or *NOTCH2*. Subsequently, the role of Notch signaling in the lineage commitment of

cholangiocytes from hepatoblasts was investigated and several mutant mouse models with depletion of components of the Notch signaling (*Notch2*, *Rbpjk*, *Jag1*) were generated. The mice displayed reduced numbers of cholangiocytes and mature ducts, confirming a role in differentiation and tubulogenesis (reviewed in (Tanimizu, 2022; Tanimizu et al., 2018). However, how Notch signaling properly regulates tubular morphogenesis remains unclear. Tanimizu et al. proposed that the appropriate activation of Notch is required to supply enough cholangiocytes to generate the tubular structure of IHBDs (Tanimizu et al., 2016).

Recent evidence shows that multiple proteins, such as FRINGE proteins, were able to modulate the length and strength of the Notch signal to fine-tune the Notch pathway for the development of a well patterned and functional biliary tree (Martinez Lyons & Boulter, 2021). Finally, Notch signaling has also been proposed to influence the proper distribution of apical proteins and thus directly or indirectly influencing cholangiocytes apical-basal polarity (Andersson et al., 2018; Fiorotto et al., 2013; Lozier, McCright, & Gridley, 2008).

Extracellular matrix

The extracellular matrix (ECM) is a 3D network of proteins and non-protein components that provides the structural and biochemical scaffolds for surrounding cells in tissues. It is composed of two major classes of biomolecules, fibrous proteins and glycosaminoglycans (Matsuda & Seki, 2020). ECM plays a vital role in the maturation of ductal structures and tubulogenesis. An even distribution of α1-laminin, produced by the periportal mesenchyme, is detected at the basal side of all cholangiocytes at the onset of ductal plate development and disappears as biliary development proceeds. On the contrary, α5-LAMININ is produced by the developing cholangiocytes and is first detected at the basal pole of the

cholangiocytes, facing the periportal mesenchyme. Later, α5-laminin is observed all around the ducts, indicating that the rise in its expression coincides with duct maturation. Further, gene inactivation studies in mice showed that α5-LAMININ is dispensable for differentiation, but that it is required for the formation of mature ductal lumens of the proper size (Tanimizu, Kikkawa, Mitaka, & Miyajima, 2012). Together, these data combined with *in vitro* experiments addressing the functional role of α1-LAMININ, indicate that α1-LAMININ is necessary for cholangiocyte differentiation and that, subsequently, α5-LAMININ controls tubulogenesis. In line with the spatiotemporal expression of LAMININS, it is noteworthy that the LAMININ receptors, namely β1- and β4-INTEGRINS, also present distinct temporal expression patterns.

Hippo

The role of the ECM in biliary morphogenesis is likely linked with that of the Hippo/Yap pathway. Indeed, activation of Yes-associated protein 1 (YAP1) and TAZ/WW Domain-Containing Transcription Regulator Protein 1 (WWTR1) is thought to induce the secretion of ECM proteins such as Laminin and Collagen IV, and these proteins are proposed to locally affect the stiffness of the matrix (D. H. Lee et al., 2016). In turn, those localized stiffness determinants could contribute to the control of morphogenesis. Impairment of laminin-integrin signaling has been shown to block murine bile duct morphogenesis (Tanimizu et al., 2012). However, whether YAP1 directly regulates the synthesis of laminins and integrins and/or whether this process depends on communication with the adjacent portal mesenchyme, remains unclear. Still, inactivation of YAP1 in developing liver inhibits the development of biliary cells (N. Zhang et al., 2010). Moreover, the formation of primary cilia was also impaired in developing cholangiocytes after YAP1 loss, suggesting a defect in cell polarization that could impact tubulogenesis (Molina,

Nejak-Bowen, & Monga, 2022). Finally, YAP1 is required during adult biliary cell homeostasis, as deletion of *Yap1* leads to loss of bile duct morphology, integrity, and widespread liver damage (Driskill & Pan, 2021; L. Molina et al., 2022).

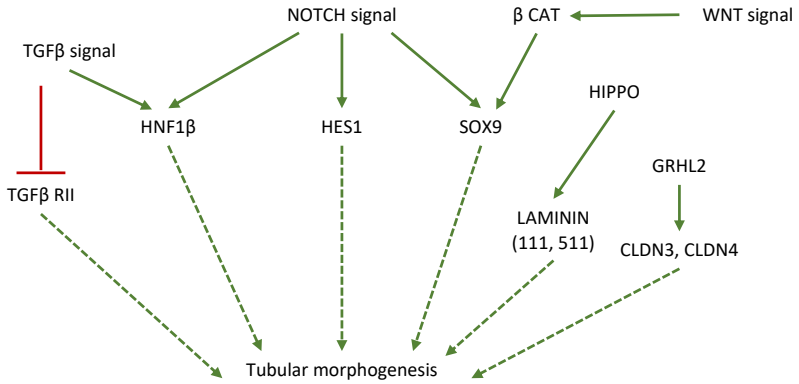


Figure 6: Molecular Mechanisms Governing IHBD Development. Figure adapted from (Lemaigre, 2020; Si-Tayeb, Lemaigre, & Duncan, 2010; Tanimizu, 2022).

How the above-mentioned pathways promote differentiation of hepatoblasts to cholangiocytes is rather well understood and has been summarized in detail elsewhere (Lemaigre, 2020; Tanimizu et al., 2018). However, the dynamic signaling that controls morphogenesis as described here still does not provide much explanation about the mechanisms promoting the spatio-temporal organization of the tubular network. 3D ducts morphogenic events such as branching, remodeling or spatial organization in the lobule remain poorly understood. Also, information on initial lumen formation and connection is limited. This highlights the need to further investigate the proper 3D development of the IHBD in this thesis and the signaling mechanism involved. IHBD morphogenesis will not be investigated alone as many signaling molecules described above are expressed in the adjacent mesenchyme, thereby highlighting an important crosstalk between the two cell types. This topic is addressed in the following chapters IV and VI.

IV. The liver mesenchyme

Liver mesenchyme is a heterogenous cell population that includes several cell subtypes. Mesothelial and sub-mesothelial cells populate the capsular lining the liver, while HSCs, FBs and VSMCs are present within the liver parenchyma. Recent data from scRNA seq and snRNA seq analyses, in adult mice and human livers have revealed an unprecedented level of heterogeneity between seemingly homogeneous mesenchymal cells subtypes (T. S. Andrews et al., 2022; Brancale & Vilarinho, 2021; Dobie et al., 2019; Lei et al., 2022a). Andrews et al. showed improved capture of mesenchymal cell using snRNA-seq and identified seven mesenchymal cluster in the parenchyma, including three HSC clusters, two FB clusters and two VSMC clusters (T. S. Andrews et al., 2022). Spatial transcriptomics confirmed that HSC gene expression was dispersed throughout the liver lobule, whereas FBs and VSMCs were predominantly located periportally. Housset's laboratory focused on periportal mesenchyme in adult mice and identified 5 FB, 5 VSMC, 1 HSC, 4 endothelial and 1 mesothelial cell clusters (Lei et al., 2022a).

Although liver mesenchymal roles have been explored more in depth in adults and especially in the context of disease (Mederacke et al., 2013; Ramachandran et al., 2020), comparatively little is known about their physiology and function during embryonic development. This situation reflects great challenges in cell isolation, with embryonic mesenchymal cells representing a very small and heterogenous proportion of cells characterized by a rapidly changing gene expression pattern during development (Friedman, 2008; Ramadori, Saile, Ramadori, & Saile, 2002; Wells, 2014). Nonetheless, mesenchymal cells are indispensable for proper liver organogenesis (Lotto et al., 2020; Tanimizu et al., 2012; Wells, 2014) and require better characterization.

i. Origin and mesenchyme subpopulations

During mouse embryogenesis, the septum transversum mesenchyme is the tissue from which many mesenchymal populations originate. At the onset of hepatoblast migration, a portion of the ventral-most septum transversumnal cells delaminate and populate the surface of the heart, forming the epicardium, while those that remain located adjacent to the liver contribute to the liver mesothelium. Morphological studies and lineage tracing of mesothelial cells showed that they migrate inward from the liver surface and give rise to HSCs, FBs, and VSMCs (Asahina, Zhou, Pu, & Tsukamoto, 2011; Lotto et al., 2020; Lua & Asahina, 2016).

Hepatic stellate cells

HSCs exist in the liver in a quiescent or activated state. In the quiescent homeostatic state, HSCs store vitamin A droplets, while in the activated state, *i.e.* following liver injury, they become the main producer of collagen whose accumulation leads to fibrosis. In the homeostatic liver, HSCs represent approximately one third of nonparenchymal cells and are localized in the space of Disse, namely between the sinusoidal endothelial cells and hepatocytes. scRNA seq analysis in adult mice demonstrated spatial and functional zonation of HSCs. Two distinct subpopulations were described, namely portal vein-associated HSC and central vein-associated HSCs. The fact that both subpopulations are the predominant collagen-producing HSC in different liver injuries, demonstrates that the activated zonal HSC population reflects the location of injury (Dobie et al., 2019; Matsuda & Seki, 2020; Paris & Henderson, 2022; Rosenthal et al., 2021). Studying the mesenchyme at unprecedented resolution has allowed deeper interrogation of traditional HSC markers. Beyond the known markers (Lecithin retinol acyltransferase, Glial fibrillary acid protein, Desmin), novel highly specific HSC markers were discovered, such as

Reelin in mice and Regulator of G protein signaling 5 in human (Dobie et al., 2019). Activated HSC-derived myofibroblasts are contractile and characterized by the up-regulation of alpha-smooth muscle actin (αSMA); they produce both collagen and tissue inhibitor of metalloproteinase 1 leading to fibrosis.

Determining the embryonic origin of HSCs has been challenging since these cells express a range of different germ layer markers. However, when hepatoblasts invade the STM, STM cells adjacent to the gut tube become trapped within the hepatic cords, and form HSCs. In addition to direct differentiation from STM, HSCs are also generated from mesothelial cells trough a mesothelial-to-mesenchymal transition. Wt1-creERT2 lineage tracing suggests roughly 15% of HSCs are generated through a sub-mesothelial intermediate (Asahina et al., 2011). Throughout development, hepatic stellate cells are located near endothelial, hematopoietic, and hepatic epithelial cells, which suggests that HSCs may modulate the growth, differentiation, or morphogenesis of these cells (Yin, Evason, Asahina, & Stainier, 2013), and *vice-versa*.

Portal fibroblasts

In adults, the portal FBs, resident FBs of the portal tract, are found surrounding the bile ducts, the portal vein, but not around the pericentral blood vessels neither within the space of Disse. Portal FBs are heterogenous and represent one of the several FB populations in the liver. These cells express Fibulin2, Elastin, Thy1 and Ectonucleotidase 2 *in situ.* Nonetheless, there is significant variability between developmental stages and none of the markers listed have been validated as both sensitive and specific across all developmental stages (Lemoinne, Cadoret, El Mourabit, Thabut, & Housset, 2013; Wells, 2014). Portal FBs are defined

morphologically as cells with an elongated, flat, and spindle shape in culture. Functionally they have the capacity to give rise to a myofibroblast population distinct from HSC myofibroblasts with a significant role in biliary fibrosis (Lei et al., 2022a; Lemoinne, Thabut, & Housset, 2016; Lua & Asahina, 2016; Wells, 2014). In addition to a role in fibrosis, other niche-specific function of portal FBs has been studied. These include the production of elastin for elastic fibers that provides mechanical stability to the bile ducts and the portal vasculature (Wells, 2014), as well as interactions between portal FBs and cholangiocyte that regulate the latter's proliferation (Cordero-Espinoza et al., 2021; Jhandier, Kruglov, Lavoie, Sévigny, & Dranoff, 2005). Interestingly, another specific function of fibroblast is migration cell guidance as they express axon guidance genes in a site-specific way (H. Y. Chang et al., 2002; Wells, 2014). But no data implicating portal FBs in cell migration have yet been reported.

Therefore, the portal FBs remain poorly understood nonparenchymal cells that require further investigation, especially in the context of morphological guidance.

Hepatic vascular smooth muscle cells

Surprisingly, very little is known about the VSMCs located in the liver. This cell type is an important component of blood vessel wall (Fig. 7A). In the liver VSCMs are in the media of the hepatic artery and to a lesser extent of the portal vein walls. They form the muscular *tunica media* whose contractile function regulates vascular tone and diameter, blood pressure and blood flow distribution to tissues. VSMCs differ from skeletal and cardiac myocytes as they retain a high degree of cellular plasticity allowing VSMCs to alter their phenotype in response to environmental cues and extracellular signals.

In a mature healthy vessel, VSMCs exhibit a differentiated quiescent contractile state and rarely proliferate. This differentiated phenotype is characterized by the expression of a repertoire of smooth muscle-specific contractile and contractile-associated proteins including Smooth-muscle-myosin heavy chain 11, αSMA, Smooth muscle protein 22 α (SM22α, also called Transgelin), calponin1, h-caldesmon and smoothelin, the latter being used as marker of mature VSMCs (Chakraborty et al., 2021; Trávníčková et al., 2018). Depending on environmental stimuli or cell culture conditions, VSMC can dedifferentiate to a "synthetic" and proliferative phenotype. This switch can be monitored by the downregulation of the contractile marker genes and loss of contractility (Fig 7B). Many signals influence VSMC phenotype, including contractility, mechanical forces, integrins, ECM, cytokines, and growth factors, through multiple distinct signaling pathways. We refer to reviews for more details (Chakraborty et al., 2021; Shi & Chen, 2016).

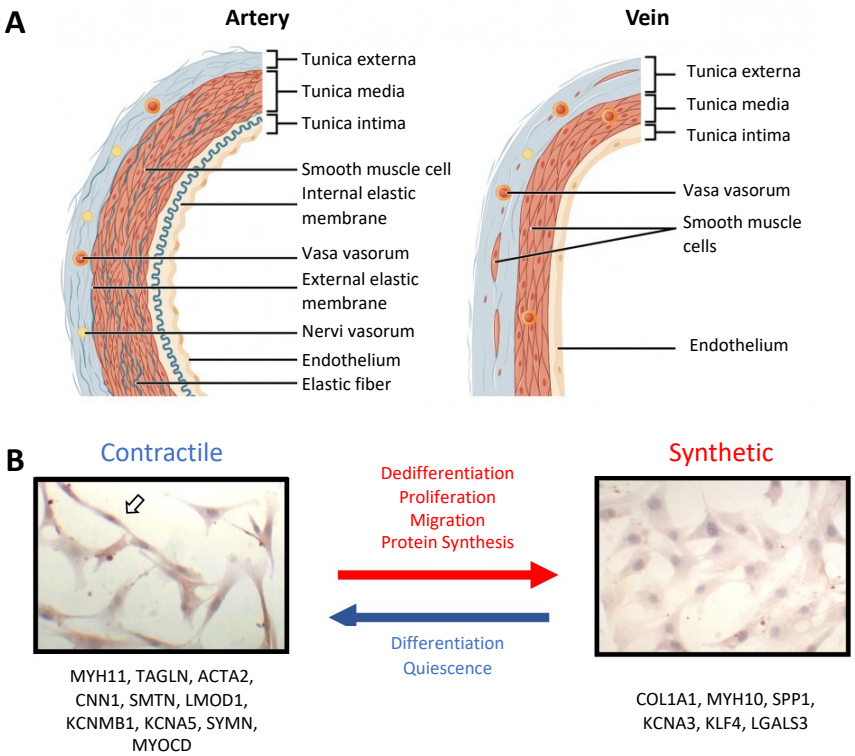


Figure 7: Localization and characteristics of hepatic vascular smooth muscle cells (A) Comparative histology of artery and vein. **(B)** Characteristics of the differentiated contractile and dedifferentiated "synthetic" vascular smooth muscle cell phenotypes. Figure adapted from (Chakraborty et al., 2021; Shi & Chen, 2016).

Further studies on the mechanisms underlying a transition from mesothelial to hepatic VSMCs, with aspects of spatiotemporal evolution of specific gene expression and specific localization, may lead to better understanding of cell fate regulation and morphogenesis in both embryonic and adult livers.

ii. Epithelial-mesenchyme interaction driving liver development

As described in the previous chapters, during early liver development, hepatic specification is induced by BMPs from the septum transversum mesenchyme and later hepatoblast proliferation is regulated by interaction with surrounding endothelial cells and hepatic mesenchyme (Ober & Lemaigre, 2018). Crosstalk between hepatic progenitors and the portal mesenchyme also controls biliary differentiation and morphogenesis. Differentiation of hepatoblasts towards the biliary lineage requires exposure to ligands of the Notch and TGFβ signaling pathways. These ligands are expressed in the mesenchyme and their cognate receptor are found in the adjacent cholangiocytes (Lemaigre, 2020). Later, in adult liver, a population of mesenchymal cells, likely fibroblasts, maintains cholangiocytes in a quiescent state in a Notch-dependent manner (Cordero-Espinoza et al., 2021). Reciprocally, bile duct morphogenesis impacts development of the portal mesenchyme. Indeed, inactivation of genes coding for transcription factors specifically expressed in cholangiocytes, such as SOX4 and SOX9, leads to disruption of the bile ducts and hypotrophy of the portal mesenchyme (Poncy et al., 2015).

Although, a crosstalk between the developing bile ducts and the portal mesenchyme controls biliary differentiation and morphogenesis further investigation is needed to properly understand the dynamic evolution and spatial organization of the mesenchymal subpopulations during liver embryogenesis. In the present thesis, we focus on the spatio-temporal heterogeneity of mesenchymal cells, its 3D organization and the stromal niche-to-epithelial cell interaction during portal tract organization.

V. The liver vasculature

The vascular system of vertebrates consists of an organized, branched network of arteries, veins and capillaries that penetrates all the tissues of the body including the liver. Vasculogenesis provides the primitive vascular network via *de novo* blood vessels formation and angiogenesis allows growth of new blood vessels by sprouting from preexisting ones. From a developmental point of view, the circulatory system is the first functioning physiological system to emerge during vertebrate embryogenesis in combination with the hematological system (Ribatti, 2006). Apart from supplying blood, there is increasing evidence that blood vessels provide instructive signals to surrounding non-vascular target cells during embryonic development (Crivellato, 2011). Here, we briefly describe the liver vasculature and then discuss, in chapter VI, the importance of the crosstalk between endothelial, mesenchymal, and epithelial cells during organogenesis.

i. Organization and function of the hepatic vasculature

The liver vasculature comprises vascular, sinusoidal and lymphatic endothelial cells. The liver receives both nutrient-rich blood from the portal vein and oxygenated blood from the hepatic artery. The portal vein supplies about 70–80% of the blood to the liver, while the remaining is provided by the hepatic artery. Hepatic veins, which merge with the inferior vena cava, drain blood out of the liver. The portal vein carries blood from the gastrointestinal tract, spleen and pancreas and enters the liver at the hilum. It then subdivides into right and left branches, which arborize throughout the liver and discharge blood into the sinusoids. The hepatic artery originates from the celiac trunk via the descending aorta, first as a common hepatic artery, which divides into the gastroduodenal artery and the proper hepatic artery.

The latter reaches the liver where it runs and divides parallel to the portal vein. Extrahepatically, the hepatic artery gives rise to the cystic artery and to branches that vascularize the extrahepatic biliary ducts (Fig. 8) (Morini et al., 2020).

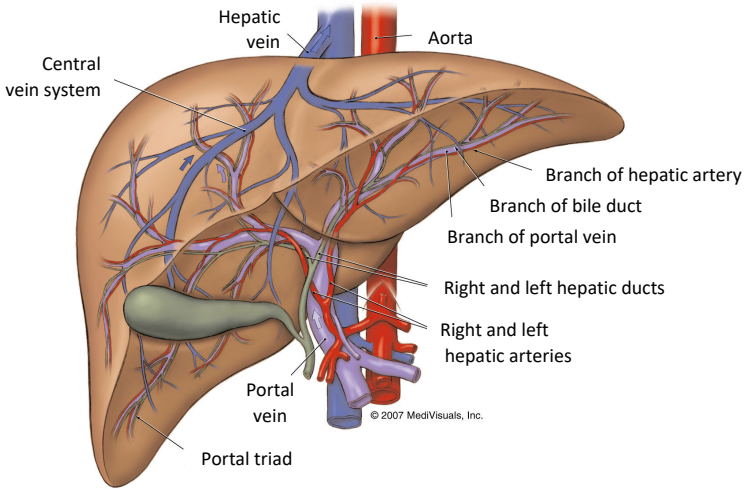


Figure 8: Schematic representation of the portal vein and hepatic artery. Figure from (https://www.sgihealth.com/liver-functioning/).

Sinusoids collect the blood from the portal vein and hepatic artery. Liver function critically depends on the proper organization and morphology of the sinusoids. Their large fenestrae and lack of basement membrane create the most permeable endothelial barrier in the body, allowing optimized exchanges between blood and liver cells. Besides their barrier properties, sinusoids exert many immune functions which have been recently reviewed by Amersfoort et al. 2022 (Amersfoort, Eelen, & Carmeliet, 2022). Like hepatocytes, sinusoidal endothelial cells are zonated (Paris & Henderson, 2022). Lymphatic vessels are present in the liver only in the connective tissue of the portal spaces and provide drainage for interstitial fluid of the parenchyma (Ohtani & Ohtani, 2008).

ii. Overview of the fetal liver venous system

Cells from the endocardium migrate with hepatoblasts in the STM, forming early capillaries. As the liver bud expands, the hepatic venous system derives from the umbilical and vitelline veins, with the vitelline veins ramifying in the STM and giving rise to at least part of the sinusoids. The umbilical veins give rise to intra- and extra-hepatic branches, of which the latter progressively regress while the left intrahepatic branch forms the ductus venosus, a vessel which allows blood from the placenta to bypass the liver during the fetal period. With continued development, the left vitelline vein degenerates and the right vitelline vein gives rise to the hepatic portal vein (Fig. 9) (DeSesso, 2017; Lotto et al., 2020; Morini et al., 2020; H. Zhang et al., 2016).

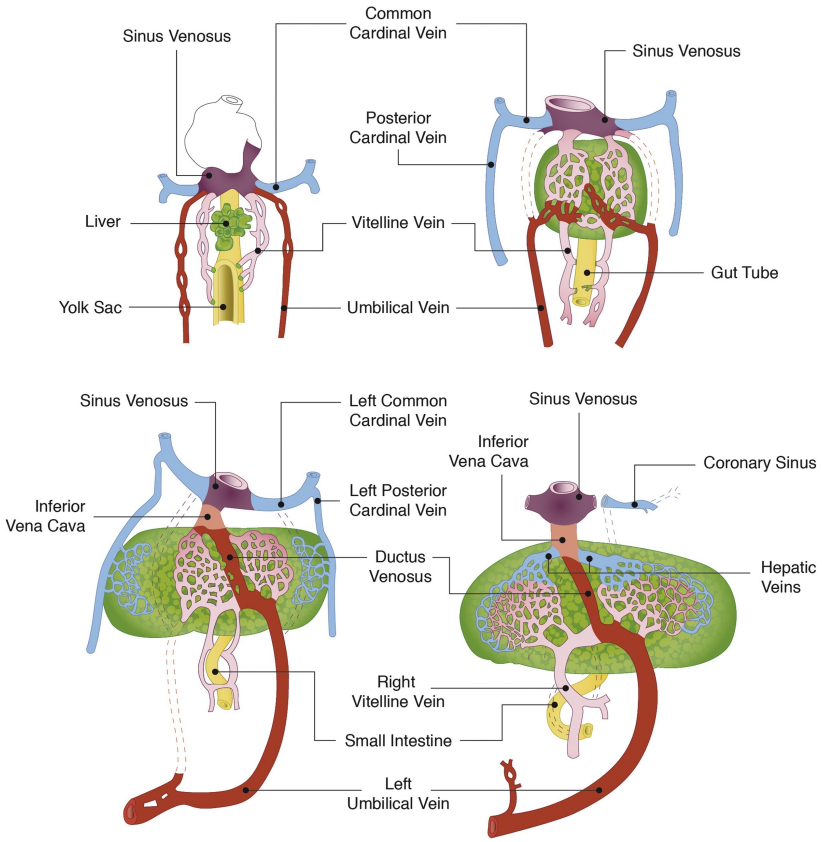


Figure 9: Schematic representation of vascular development in the liver. Adapted from (DeSesso, 2017)**.**

The hepatic sinusoids are the first vessels to appear around E10–E10.5 and the portal vein is identified between E10.5–E12.5(Collardeau-Frachon & Scoazec, 2008; Swartley, Foley, Livingston, Cullen, & Elmore, 2016). The mesenchyme and hepatoblasts were identified as stimulators of sinusoid morphogenesis and maturation (Takebe et al., 2013). Sinusoidal development occurs in three phases. Initially, endothelial cells are non-fenestrated and lined by a basement membrane. Stabilin 2 and lymphatic vessel endothelial hyaluronan receptor 1 (LYVE-1) start to be expressed in the sinusoidal endothelial cells at E9.5 and E10.5. Fenestrae develops in a second phase, namely around E14-E15, and the composition of the basement membrane changes. These changes are controlled by the hepatoblasts, at least in part via VEGF signaling. Thirdly, at birth, the size of the fenestrae evolves and becomes graded along the porto-central axis, in parallel with zonation of endothelial functions (Paris & Henderson, 2022). Portal vessels express the arterial markers EPHRIN-B2 and Neuropilin-1, but not the venous marker EphB4 during embryonic development. This expression profile is inverted at the end of gestation, with the transition into a venular phenotype (Khan et al., 2016). In adult livers, endothelial cells of portal and hepatic veins strongly express CD31, while it is absent or weakly detected in sinusoidal endothelial cells (Sugiyama et al., 2010; Takebe et al., 2013).

iii. Origin and morphogenesis of the hepatic artery

During development, the portal vein is the first to establish its branching architecture, followed by IHBD and lastly the hepatic artery. Whereas the morphogenesis of the first two have been deeply investigated and is still a major

topic of research for IHBD development, very few studies have tackled the subject of hepatic artery development. Nonetheless, the anatomical association between bile ducts and the surrounding arteries indicates that biliary and hepatic arterial development are highly interwoven as highlighted by the concept that the integrity and functionality of the bile ducts dictates arterial development (Clotman et al., 2003; Fabris et al., 2008). As an example, mutant mice with a primary defect in the cholangiocytes (*e.g.* HNF6 or HNF1β knockout mice) fail to develop normal ducts and also fail to develop normal arteries (Clotman et al., 2002). Still, how the hepatic artery develops and how it interacts with the bile ducts remain poorly characterized.

As an explanation for this coordinate development, few studies suggest that signals from the bile ducts direct the intrahepatic development of the hepatic artery through secretion of angiogenic factors (Clotman et al., 2003; Fabris et al., 2008; Gouysse et al., 2002). Vascular endothelial growth factor-A (VEGF-A) is secreted by ductal plate cells and widely expressed in developing liver. It recruits Vascular Endothelial Growth Factor Receptor (VEGFR)-2-positive endothelial progenitor cells to the portal mesenchyme near the ductal plate, where they aggregate as VEGFR-1-positive endothelial cells. The latter assemble into primitive vascular cluster with myofibroblast-derived mural cells expressing TIE-2, a receptor for Angiopoietin-1 secreted by hepatoblasts. Arterial remodelling and lumen formation is then likely promoted by autocrine secretion of Angiopoietin-2 by mural cells (Fig. 10).

As bile duct and hepatic artery maturation process, the forming tubular structure are incorporated within the mesenchyme of the developing portal space. In parallel, a vascular peribiliary plexus develops, but its origin remains debated as it may result from branching of the hepatic artery or from local vasculogenesis

(Gouysse et al., 2002; Terada & Nakanuma, 1993). The interaction between developing bile ducts and hepatic arteries may differ slightly in humans and mice, since arterial morphogenesis in humans occurs along the ductal plate, whereas in mice, arteries only form postnatally and alongside mature bile ducts (Korzh et al., 2008).

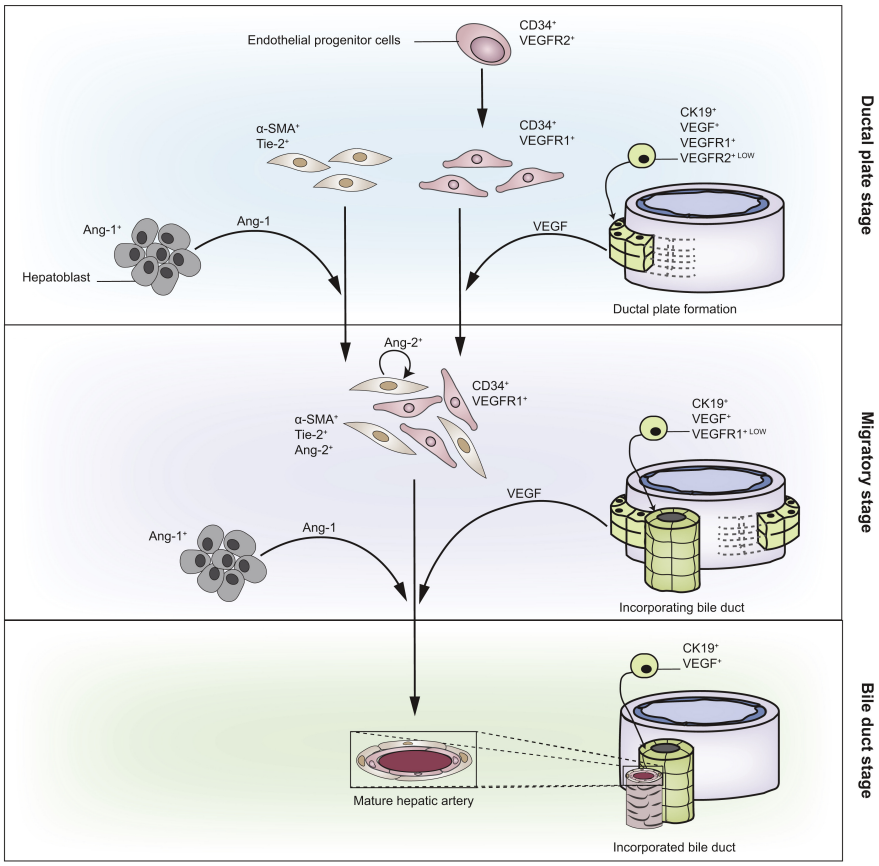


Figure 10: Schematic representation of a model for hepatic artery development. Details are explained in the text above. Figure from (Mariotti, Fiorotto, Cadamuro, Fabris, & Strazzabosco, 2021).

The proposed model of hepatic artery formation at first sight fits with a vasculogenic process, *i.e.* from endothelial cell precursors present in the portal spaces, as suggested by immunohistochemical studies (Fabris et al., 2008; Gouysse et al., 2002). Nevertheless, it does neither identify the origin of the cells involved, nor their 3D organization and assembly. Moreover, it does not allow to exclude a process of angiogenesis by which the intrahepatic hepatic artery would derive from small branches sprouting from the extrahepatic part of the hepatic artery that progressively extend into the portal spaces.

As the mechanisms driving hepatic arteriogenesis is to our knowledge essentially limited to gene expression data it justifies our study on hepatic artery development in the present thesis. With a particular focus on the origin of the arterial muscle cells and the 3D organization of the forming hepatic artery.

In parallel, since ductal plate cells are already known to synthesize large amounts of VEGF, a potent pro-angiogenic factor (Gouysse et al., 2002), it is interesting to determine whether ductal plate cells or adjacent periportal mesenchyme secrete axon guidance molecules, such as netrins and semaphorins, which have been shown to play at role in growth and migration of arterial vessels (Lu et al., 2004). The next chapter will go into more detail on this topic.

VI. Reciprocal interactions between endothelial, mesenchymal, and epithelial cells during development and morphogenesis of tissues and organs

A fundamental feature of the architecture and functional design of vertebrate animals is a stroma, composed of ECM and mesenchymal cells, which provides a structural scaffold for the organ constituents. Reciprocal interactions between mesenchymal and epithelial cells are known to play a critical role in orchestrating the development and morphogenesis of tissues and organs. A mutual influence between organ cells and penetrating vasculature is also primordial for proper organogenesis (Cleaver & Melton, 2003; Coultas, Chawengsaksophak, & Rossant, 2005).

As described in the previous chapters, the liver portal tract is a great example of such interactions as the portal mesenchyme instructs bile duct morphogenesis and normal development of the latter is required for hepatic artery formation. For example, Notch and TGFβ signals from the periportal mesenchyme promote cholangiocyte differentiation and inhibit hepatocyte differentiation (Chen et al., 2018) whereas hepatic epithelial cells are thought to recruit endothelial progenitor and mural cells for hepatic artery vasculogenesis via angiogenic factors (Fabris et al., 2008). However, the complete molecular signals that underlie epithelial-mesenchyme interaction during portal tract morphogenesis remain however incompletely understood. There is a need for a better understanding of those interactions in specifying its proper 3D architecture during development. In addition, the roles played by specific stromal subpopulations has never been described.

In this context we decided to take a closer look at axon guidance genes during liver development, knowing that studies on their function outside the nervous system and in tissue morphogenesis have mushroomed in recent years. Interestingly, these cues are present in the extracellular environment and are either expressed at the cell surface or secreted into the ECM (Yuasa-Kawada, Kinoshita-Kawada, Tsuboi, & Wu, 2022). By shaping the tissues in 3D during portal tract development, axon guidance genes may display wide-ranging morphogenic properties that go well beyond their known neurite guidance function.

i. Classical axon guidance receptors and their ligands in mammals

First described in the neuronal system as guidance cues for axons, they allowed axons projection of newly differentiated neurons to reach their synaptic targets and form functional circuits. Historically, guidance signaling axes have been categorized as “attractive” or “repulsive” based on the responses of the growth cone to ligand-receptor binding (Stoeckli, 2018). Nowadays it is commonly accepted that axon guidance genes play much more versatile roles during tissue morphogenesis (Hinck, 2004).

During development, both neurons and other cells must acquire specific fates through changes in their locations, morphology, and gene expression. The four families Netrin (NTN), Slit, Semaphorin (SEMA), and Ephrin have structural differences, but all guidance factors direct the motility of cells and facilitate the regulation of cell-cell communication and cell movement (Hinck, 2004). There is also accumulating evidence that they contribute to tissue development by regulating the transcription and translation of genes encoding key morphogenic factors.

Here, we provide an overview of the ligand–receptor pairs that were studied in this thesis. An in-depth discussion of ligand–receptor structures and signaling mechanisms, can be found in a recent review from Zang et al. (Zang, Chaudhari, & Bashaw, 2021). Examples of their roles during tissue architecture are described in the following section.

SEMAPHORIN-PLEXIN

SEMAs are a large and diverse family of signaling ligands, including secreted, cell surface-attached and membrane-bound members, that have been categorized into eight classes (Fig. 11). All SEMAs share a common extracellular domain which facilitates homodimerization and interaction with SEMA receptors. SEMAs mainly mediate their functions through two types of receptors, plexins and neuropilins. In addition to acting as signaling ligands, transmembrane SEMAs can also act as receptors, a phenomenon known as reverse signaling (Alto & Terman, 2017; Jongbloets & Pasterkamp, 2014). The SEMAs were first described as repulsive cues of axon pathfindings during neuronal development (Luo, Raible, & Raper, 1993). Later, they have been studied in development (Hinck, 2004), in the immune system (Feinstein & Ramkhelawon, 2017; Kanth, Gairhe, & Torabi-Parizi, 2021) and in cancer (Neufeld et al., 2016). During development they have been shown to regulate neuronal circuit assembly, bone formation and angiogenesis mainly via regulation of cytoskeletal dynamic, and influence of cell shape, differentiation, motility, and survival (Alto & Terman, 2017; Jongbloets & Pasterkamp, 2014).

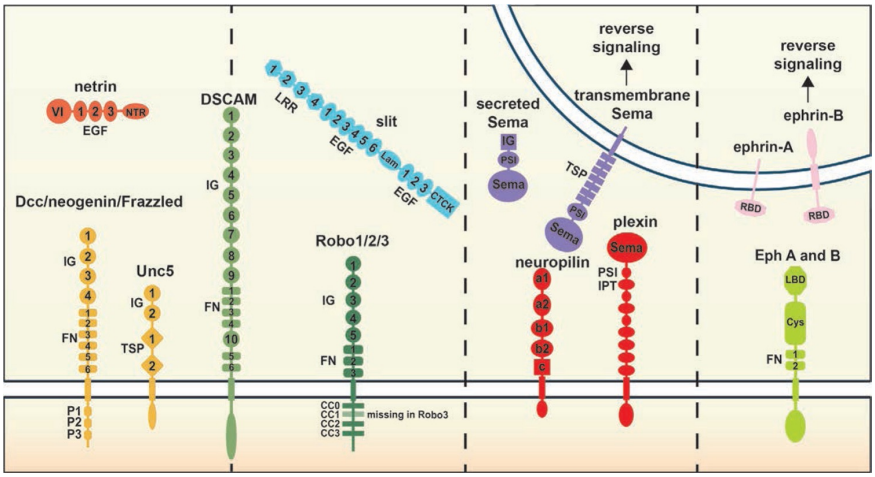


Figure 11: Domain structures of axon guidance receptors and their ligands. Netrin and its receptors DCC, NEO1, and Unc5; SLITs and its receptors ROBO1, 2, and 3; transmembrane and secreted SEMAs and their plexin and neuropilin receptors; and Ephrin and its Eph receptors. Down syndrome cell adhesion molecule can interact with both netrin and slit. Transmembrane Semas and ephrins can also induce reverse signaling. CTCK, C-terminal cysteine knot; Cys, cysteine-rich domains; EGF, epidermal growth factor-like domains; FN, fibronectin type III domains; IG, immunoglobulin-like domains; IPT, immunoglobulin-plexin-transcription domains; Lam, laminin-type domains; LRR, leucine-rich-repeat domains; NTR, the netrin module; PSI, plexin-semaphorin-integrin domain; RBD, receptor binding domains; LBD, ligand binding domains; TSP, thrombospondin type 1 domains. Figure from (Zang et al., 2021).

EPHRIN-EPH

EPH receptors are a large class of receptor tyrosine kinases encompassing two subclasses: EPH-A and EPH-B, based on sequence homology and binding preferences (Kania & Klein, 2016; Taylor, Campbell, & Nobes, 2017). EPHRIN ligands are classified into glycosylphosphatidylinositol-anchored EPHRIN-As and transmembrane EPHRIN-Bs (Fig. 11). Because both EPHRIN and EPH are located at the cell membrane, signaling primarily occurs between adjacent cells. Although EPH-EPHRIN signaling may also be mediated between non-adjacent cells through cellular protrusions or through release of EPH and EPHRIN by exosomes (Cayuso et

al., 2016; J. Gong, Körner, Gaitanos, & Klein, 2016). Like SEMA-plexin signaling, EPH-EPHRIN signaling is bidirectional. In general, ligation promotes clustering of the Eph and allows for transphosphorylation and kinase activation (Finney & Orr, 2018; Kania & Klein, 2016; Taylor et al., 2017).Thanks to its ability to sense the surrounding cellular microenvironment and to respond accordingly, EPH-EPHRIN signaling is critical in a wide variety of developmental contexts. They play important role in normal physiological processes, including embryonic tissue boundary formation (Cayuso et al., 2016), angiogenesis and guidance, while in adult tissue they help in wound healing and cell population maintenance (R. H. Adams & Eichmann, 2010; Kania & Klein, 2016; Taylor et al., 2017; Wilkinson, 2014).

NETRINs and their receptors

NTNs are laminin-like molecules and the netrin family consists of secreted NTN-1 to -5, and glycosylphosphatidylinositol-anchored NTN-G1 and -G2 (Lai Wing Sun, Correia, & Kennedy, 2011; Meijers, Smock, Zhang, & Wang, 2020). All NTN receptors are transmembrane proteins which belong to the immunoglobulin superfamily of cell- adhesion molecules (Lai Wing Sun et al., 2011). Secreted NTNs signal via several receptors, namely deleted in colorectal cancer (DCC), the DCC paralog NEOGENIN1 (NEO1), the UNC- 5 homologs UNC5A-D. NTN-G1 and -G2 lack affinity for classical NTN receptors and bind to LRRC4C and LRRC4 receptors, respectively (Lai Wing Sun et al., 2011). NTNs elicit different cellular responses depending on the receptors involved (Chaturvedi & Murray, 2022), with the different receptors acting either alone or forming a wide range of different complexes (Robinson et al., 2021; K. Xu et al., 2014). In addition to their NTN-induced activities, NTN receptors act as “dependence receptors”, meaning that they can have a pro-apoptotic response when not bound to their Netrin ligand (Ardito et al., 2012; Lai Wing Sun et al., 2011; Laws & Bashaw, 2022; Murray, 2017;

Negulescu & Mehlen, 2018). In addition to the DCC and UNC family receptors, netrins have also been associated with other receptors, including Down syndrome cell adhesion molecule and integrins. Conversely, other ligands for netrin receptors have been identified such as the repulsive guidance molecules (RGMs) for NEO1. Since its discovery in the early 1990s, it is now becoming clear that the NTN gene family exhibit a wealth of biological functions, with significance beyond neural development, and contributes to the organization of multiple tissues.

SLIT-ROUNDABOUT

The SLIT-ROBO axon guidance family consists of three SLIT ligands and four ROUNDABOUT (ROBO) receptors. SLITs are secreted glycoproteins that contain multiple leucine-rich repeats and epidermal growth factor repeats. The ROBO receptors are single-pass transmembrane proteins (Fig. 11). In addition to alternative splice isoforms, post-translational modifications further expand the repertoire of ROBO proteins (Blockus & Chédotal, 2016). Major effectors of SLIT-ROBO signaling are regulators of the actin cytoskeleton, mainly via activity of small GTPases of the Rho family leading to actin polymerization and cell migration. In addition to motility, SLIT-ROBO signaling also impacts cell adhesion by modulating N-cadherin and E-cadherin affinity (Blockus & Chédotal, 2016). Much knowledge on SLIT-ROBO was gained during the study of commissural axon projection in developing spinal cord. SLIT-ROBO is not only involved in axon guidance, but also in the proliferation and migration of central nervous system progenitor cells, and the control of dendrite development (Yuasa-Kawada et al., 2022). In addition, SLIT-ROBO is an important regulator of angiogenesis, organ development, tumorigenesis and other diseases (W. D. Andrews, Barber, & Parnavelas, 2007; Blockus & Chédotal, 2016).

ii. Roles for axon guidance pathways in embryonic tissue architecture

Neuronal network development, blood vessel morphogenesis, branching morphogenesis of epithelia are seemingly disparate developmental processes which, nevertheless, share a wide expression of axon guidance molecules throughout all developmental stages. These findings may explain why peripheral nerves and blood vessels follow parallel paths along developing epithelial tubes if they share response to common axon guidance cues. Below are illustrative examples of the role of axon guidance molecules during vascular patterning, tissue morphogenesis and branching morphogenesis.

Vascular development

In contrast to neurons where the body of single cells extend, in the vascular system, proliferation is tightly linked to branching morphogenesis of cooperating groups of cells. During angiogenesis, endothelial tip cells, which share many of the morphological characteristics of neuronal growth cones, direct vascular patterning by sensing VEGF-A and axon guidance cues (R. H. Adams & Eichmann, 2010; Larrivée, Freitas, Suchting, Brunet, & Eichmann, 2009).

Semaphorins

SEMA signaling is involved in vasculogenesis, angiogenesis, heart formation and lymphatic development (R. H. Adams & Eichmann, 2010; Alto & Terman, 2017; Crivellato, 2011; Elpek, 2015). Interestingly, SEMAs antagonize the effects of VEGFs on endothelial cells (Alto & Terman, 2017; Crivellato, 2011; H. Nakayama, Kusumoto, Nakahara, Fujiwara, & Higashiyama, 2018). For example, SEMA-3E, a PLEXIN-D1 ligand, acts as a key repellent in endothelial cells, whereas VEGF-A is a major attractant (R. H. Adams & Eichmann, 2010). Interestingly, RHOJ, a GTPase, integrates these directional cues in endothelial cells. RHOJ coordinates interactions

between SEMA3a, VEGFA and their receptors, namely PLEXIN-D1, NEUROPILIN-1 and VEGFR2, and controls their endocytic trafficking and degradation (Fukushima et al., 2020; Yuasa-Kawada et al., 2022). In addition, VEGFRs may also serve as signal transducing receptors for SEMAs. Fluid shear stress is an additional regulator of vascular development and homeostasis. In endothelial cells, PLEXIN-D1 senses force by forming a mechano-sensing complex with NEUROPILIN-1 and VEGFR2. In response to shear force, this complex activates integrin signaling and focal adhesion formation (Mehta et al., 2020). On the other hand, SEMA-3 suppresses integrin activation and focal adhesion formation, via neuropilins/plexins, leading to inhibition of vascular remodeling during embryonic development (Serini et al., 2003). Thus, PLEXIN-D1 acts either as a SEMA-3E receptor or as mechanosensor.

EPHRIN AND EPH

EPHRIN-EPH signaling is required during angiogenesis and is a determinant of arterial/venous characteristics. In the developing circulatory system, the specific expressions of EPHRIN-B2 in the arteries and EPHRIN-B4 receptor in the venous endothelium, provide one of the earliest known molecular distinctions between arteries and veins (Herbert et al., 2009; Lindskog et al., 2014; H. U. Wang, Chen, & Anderson, 1998). EPHRIN-B2 - EPH-B4 interactions mediate repulsive signaling, but a clear cellular mechanism of this activity has yet to be determined (Kania & Klein, 2016). During development Ephrin-B2 is also necessary for the normal function of mural cells of the mesenchymal lineage, such as pericytes and VSMCs. Conditional inactivation of the mouse *Ephrin-B2* gene in mural cells changes their morphology and behavior, ultimately altering vessel architecture and causing hemorrhaging (Foo et al., 2006; A. Nakayama et al., 2013). Mechanistically, the function of EPHRIN-B2 in mural cells is coupled to the membrane distribution, endocytosis and

signaling output of platelet-derived growth factor receptor-β, which suppresses the differentiation and promotes the proliferation of VSMCs (Kania & Klein, 2016).

NETRINs

The role of NTNs in vascular growth remains controversial, as it was reported either as an inhibitor (Larrivée et al., 2007; Lejmi et al., 2008; X. Lu et al., 2004) or a promoter (Park et al., 2004; B. D. Wilson et al., 2006; N. H. Wilson & Key, 2006). Deletion of *Unc5b* in mice causes excessive extension of filopodia by endothelial tip cells and increases branching during developmental angiogenesis, suggesting that UNC5B functions as a repulsive NTN receptor in this process (X. Lu et al., 2004). In apparent contrast, injection of NTN1 causes robust neovascularization in the mouse and NTN1 appears to be as potent as VEGF in inducing postnatal angiogenesis (Park et al., 2004). Another study reported that the overexpression of NTN1 induces an increased recruitment of VSMCs at sites of neovascularization (B. D. Wilson et al., 2006). As reported in the earlier study, screening of endothelial cells failed to identify significant expression of any NTN receptors. By contrast, NEO1 was detected on VSMCs, and the authors proposed that this receptor may mediate the observed angiogenic effects of NTN-1 by promoting the recruitment of smooth muscle cells (B. D. Wilson et al., 2006). These observations imply that the signaling mechanisms that underlie the decision between attraction to and repulsion from NTN are conserved in neurons and other cell types and that NTNs can exert both effects during angiogenesis, depending perhaps on developmental stage, tissue involved and that they may target different vascular cell types through distinct receptors pathways.

SLIT-ROBO

Other guidance receptors and their ligands are implicated in vascular system patterning. SLIT-ROBO signaling was found to display pro- and anti-angiogenic functions and behaves as a regulator of blood vessel permeability (Blockus & Chédotal, 2016; Wu, Liao, Wang, & Chang, 2017). For example, ROBO4 is highly expressed in endothelial cells. In response to SLIT, ROBO4 signaling stabilizes the vasculature by suppressing VEGFA-induced angiogenesis and vascular leakage (Jones et al., 2009). However, it was also reported that SLIT2 does not bind to ROBO4 but promotes angiogenesis via ROBO1/2 by promoting endothelial cell motility and polarity (Dubrac et al., 2016; Koch et al., 2011; Rama et al., 2015). Unexpectedly, ROBO4 binds to UNC5B and inhibits VEGFR2 signaling leading to blood vessels stabilization and angiogenesis inhibition (Koch et al., 2011). But it is unclear how NTNs and ROBO4 exert different effects on endothelial cells through UNC5B. SLIT3 also promotes endothelial cell migration by inducing ROBO4-dependent RAC1 and RHO-A activation (B. Zhang et al., 2009) or through activation of RHO-A/RHO kinase pathway (Dou et al., 2018). Interestingly, the impact of SLIT and ROBO on angiogenesis seems to depend on cell-type specificity and on the Slit-Robo pairs.

Mammary gland

Mammary gland development occurs in three stages: during embryogenesis, tubes are established and reticulate into their primary structure; during puberty, they elongate and form secondary branches; during pregnancy, they form tertiary branches, and the luminal epithelium divides to give rise to the secretory alveoli (Hinck, 2004; Silberstein, 2001). During puberty, terminal end buds are highly mitotic and facilitate ductal morphogenesis, and several axon guidance signals are

important for this process. Growth is primarily driven by cap cells, which form a single layer at the extremity of the terminal bud (Fig. 12). Cap cells proliferate to give rise to myoepithelial cells, which contribute to the elongation and morphogenesis of the duct (Williams & Daniel, 1983).

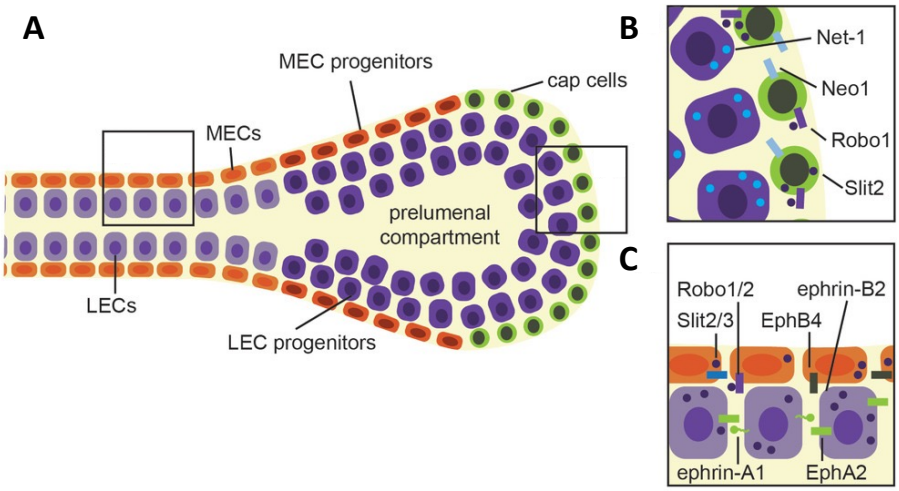


Figure 12: Axon guidance factors control mammary gland remodeling. (A) The mammary gland terminal end bud guides gland growth and elaboration within the fat pad. Proliferative cap cells at the bud extremity (green). In the prelumenal compartment, cap cells primarily give rise to progenitor cells (dark orange) fated to become basal myoepithelial cells (MECs;light orange). Luminal epithelial cells (LECs; light purple) are primarily derived from body cells in the inner mass of the terminal end bud (dark purple). **(B)** Members of the NTN-NEO (blue) and SLIT-ROBO pathways (purple) are expressed in the prelumenal compartment and in cap cells at the terminal end bud. EPHRIN-B2 expression, not pictured, also extends to the prelumenal compartment. **(C)** Members of the SLIT-ROBO pathway (blue) and Ephrin-Eph pathway (green) are expressed in LECs and MECs. Figure from (Laws & Bashaw, 2022).

NETRINs

In the terminal end buds of pubertal mice, NTN1 and NEO1 are expressed in complementary patterns: NTN1 is expressed by luminal cells, while NEO1 expression is limited primarily to cap cells (Srinivasan, Strickland, Valdes, Shin, & Hinck, 2003). Deletion of NTN1 or NEO1 causes a similar disorganization of the

terminal end bud with a dissociation of the two cell layers. The basement membrane appears to be partially disrupted, and there is an increased influx of cap cell into the preluminal compartment. This suggests that NTN-1 functions as a short-range cue to maintain intercellular adhesion among cap cells and close apposition of the cap cell layer to both the prelumenal compartment and the basement membrane (Srinivasan et al., 2003; Strickland, Shin, Plump, Tessier-Lavigne, & Hinck, 2006).

SLIT-ROBO

SLIT-ROBO signaling also regulates terminal end bud morphology in mouse mammary glands. SLIT2 and SLIT3 are expressed in myoepithelial cells and inner luminal epithelial cells along the mammary duct, but SLIT2 alone is expressed in cap cells at terminal end buds during ductal outgrowth (Strickland et al., 2006). Mammary glands from *Slit2* null, but not from *Slit3* null, mice have disorganized terminal end buds. Ductal adhesion defects in glands from *Slit2* mutant mice are recapitulated in *Robo1* null mice, indicating that SLIT2 signals through ROBO1 to control terminal end bud morphology. While the terminal end bud phenotype in *Slit-Robo* mutants closely resembles that in NTN-1 and NEO1 mutant mice, duct adhesion defects in glands from *Slit2* mutant mice are made worse by removal of NTN-1, suggesting that the two pathways act in parallel (Strickland et al., 2006). In contrast to NTN-1 mutant mammary glands, where cell adhesion appears to be largely responsible for the mutant phenotype (Srinivasan et al., 2003), ROBO1 suppresses cap cell proliferation (Macias et al., 2011). Knowing that mammary gland branching requires cell proliferation, the role of SLIT-ROBO in suppressing proliferation would also suppress branching (Ochoa-Espinosa & Affolter, 2012). Terminal end bud proliferation provides the cells necessary for lateral branching in the pubertal mammary gland (P. Lu, Ewald, Martin, & Werb, 2008). Consequently,

while mammary epithelia from *Robo1* or *Slit2;3* null mice transplanted into donor mice grow to the same length as those transplanted from wild-type mice, they are significantly more branched (Macias et al., 2011). Furthermore, exogenous SLIT2 introduced into the fat pad limits ductal branching. One possible mechanism for Slit-Robo branching inhibition is that it interacts with the Wnt signaling pathway. Experimental data are consistent with a model in which SLIT2-ROBO1 signaling prevents β CATENIN target gene expression and, ultimately, proliferation (Teulière et al., 2005).

EPHRIN- EPH

EPHRIN-EPH signaling cues are also expressed in the mammary gland and may also regulate mammary gland proliferation and branching morphogenesis (Vaught, Chen, & Brantley-Sieders, 2009). EPHRIN-B2 is expressed by luminal cells, and its receptor EPH-B4, is expressed in a complementary pattern by myoepithelial cells. Mammary-specific conditional knockout of *Ephrin-B2* perturbates gland architecture highlighting a role in the maintenance of mammary gland epithelia (Weiler et al., 2009). As for the EPH-A2-deficient animals, they demonstrate that EPH-A2 receptor function is required for mammary epithelial growth and branching morphogenesis. Loss of EPH-A2 decreased penetration of mammary epithelium into fat pad, reduced epithelial proliferation, and inhibited epithelial branching. While an EPH-A2 ligand, EPHRIN-A1, is also expressed in luminal epithelial cells, it remains to be seen if it is similarly required for mammary gland morphogenesis (Vaught et al., 2009).

Pancreas architecture

Approximately 95% of the pancreas is a tubular and acinar exocrine organ that secretes digestive enzymes. The remaining 5%, the endocrine pancreas, comprises

spheroid islets (islets of Langerhans), responsible for regulating glucose homeostasis. Islets in both humans and mice consist primarily of insulin-secreting β cells and also contain additional endocrine cells, including α cells and δ cells, which secrete respectively glucagon and somatostatin. The spatial architecture of endocrine cell types within the islet is important for their function, as physical contact and secreted signals between certain cell types optimizes hormone secretion (Brereton, Vergari, Zhang, & Clark, 2015). During development, islet cells differentiate and migrate to their final location within the pancreas (Pan & Wright, 2011). A large body of research has highlighted the importance of guidance receptors in both morphological development and secretory function of islets of Langerhans (Fig. 13) (Laws & Bashaw, 2022; Waters & Blum, 2022).

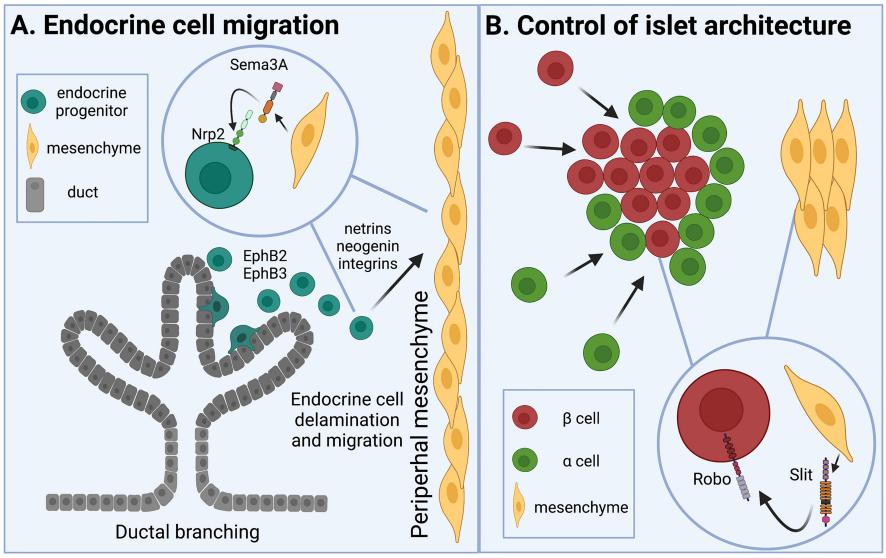


Figure 13: Axon guidance molecules are involved in islet morphogenesis and cell-cell contact. (A) Islet development begins as proendocrine cells delaminate from branching ducts and migrate across the pancreatic mesenchyme. EPH receptors are involved in epithelial cell branching. SEMAs expressed by peripheral mesenchyme draw NEUROPILIN receptor-expressing proendocrine cells away from the ducts. NETRINs, NEO1, and INTEGRINs are also known to regulate epithelial cell migration. **(B)** As endocrine cells aggregate into islets, SLIT from pancreatic mesenchyme interacts with ROBO on β cells to direct cell type sorting and establish appropriate islet architecture. Figure from (Waters & Blum, 2022).

SEMAPHORINS-NEUROPILINS

NEUROPILIN-2 is expressed in islet endocrine progenitor cells and *Nrp2* constitutive knockout mice exhibit improper migration of endocrine progenitor cells away from the ductal structures. Later the endocrine cells aggregate around the ductal structures indicating that NEUROPILIN-2 is required for proper islet cell migration (Pauerstein et al., 2017; Waters & Blum, 2022).

SEMA-3A is expressed in the peripheral pancreatic mesenchyme during development and *in vitro*, β cells migrate towards SEMA-3A-soaked beads (Pauerstein et al., 2017). This raises the possibility that mesenchyme-derived SEMA-3A signals through NEUROPILIN-2 to regulate endocrine cell migration within the pancreas.

EPHRIN-EPH

Most of the known impact of EPHRIN-EPH signaling in the islet has been characterized in the context of hormone secretion in mature islets. However, there is evidence that this signaling pathway may play a role in islet development with implication in epithelial branching and proendocrine cell identity. This was demonstrated by EPH-B2/EPH-B3 knockout mice who displayed branching defects and by studies showing that EPH-B3 was transiently expressed during development and marked delaminating epithelial endocrine-committed cells (Villasenor 2010 & 2012). In addition, a recent study has revealed a potential role of EPHRIN-EPH signaling in establishing islet architecture via changes in Notch signaling. RNA sequencing of islets from a gain-of-function Notch mutant mouse revealed an increase in EPHRIN signaling. Treatment with soluble ligand EPHRIN-A5-Fc increased repulsion among β cells and blocked pseudo-islet formation (Bartolome

2022). Together, these data show that EPHRINS and EPHs may be involved in both endocrine cell differentiation and endocrine cell migration.

SLIT-ROBO

Axon guidance molecules SLIT and ROBO are involved in early pancreatic differentiation. Mice with mesenchyme-specific inactivation of the transcription factor PBX1 showed significant reduction in pancreatic proendocrine cells during development. In this model, *Slit* expression was also reduced and exogenous SLIT applied to pancreatic explants was sufficient to rescue the number of insulin-positive cells (Cozzitorto et al., 2020). Similarly, ROBO is required for pancreatic progenitors to maintain endocrine identity (Escot, Willnow, Naumann, Di Francescantonio, & Spagnoli, 2018). Both studies highlight roles of mesenchymal SLIT and epithelial ROBO in islet development. As early endocrine cells migrate within the pancreas, they also begin to cluster together to form the islets with the typical architecture of a β cell core and α cell mantle. A process that also required mesenchymal SLIT and epithelial ROBO signaling for proper spatial architecture in the islet. Deleting *Robo* in the β cells, but not in the α cells, of developing mice results in cell type intermixing and loss of classic murine core-mantle architecture (M. T. Adams, Gilbert, Hinojosa Paiz, Bowman, & Blum, 2018) implicating *Robo* expression in the β cell for appropriate endocrine cell- type sorting. Data suggest that SLIT-2 and -3 from the pancreatic mesenchyme may interact with ROBO in the β cell to regulate endocrine cell migration and establish islet architecture (Gilbert, Adams, Sharon, Jayaraaman, & Blum, 2020).

NETRINs

As for the NTNs, the understanding of the activity of this axon guidance family in islet morphogenesis is limited. NTN-1 is expressed in fetal rat endocrine and exocrine pancreas during the time of islet morphogenesis (De Breuck, Lardon, Rooman, & Bouwens, 2003), suggesting that it may be involved in crosstalk among these tissues. NTN-4 is more widely expressed in ductal epithelial cells, as well as endothelial cells, and localizes at the basement membrane (Yebra et al., 2011). While DCC receptor is not expressed in the pancreas, another receptor, NEO1, is expressed in fetal pancreas (De Breuck et al., 2003). The expression of NTNs and their receptors during development, as well as the epithelial-mesenchymal expression of these binding pairs, suggests that NTNs and their receptors play a role in islet morphogenesis. So far, NTN signaling was only shown to impact the migration and adhesion of fetal epithelial cells via interaction with INTEGRINs α6β4 and α3β1 (Yebra et al., 2003).

To sum up, many axon guidance genes are important for proper establishment of the embryonic tissue architecture. Although the same receptor ligand couples do not always have similar functions, these cues always impact cell motility, cell shape, proliferation and adhesion. A clear molecular mechanism of axon guidance signaling is often lacking from these knockout studies. Nevertheless, axon guidance molecules are thought to mainly act via regulation of the cytoskeletal dynamics through RhoGTPases as well as actin and microtubules effectors. Still, it often remains challenging to visualize the functional link between surface receptors and the cytoskeleton (Stoeckli, 2018; Zang et al., 2021).

iii. Axon guidance cues in the liver

Surprisingly few data are available in the context of liver development, although axon guidance pathways have been demonstrated to control the development of organs that share close developmental and structural similarities with the liver. As described above, axon guidance molecules are crucial for pancreas morphogenesis as well as lung and mammary gland branching development. Axon guidance cues were also shown to be essential for the morphogenesis of vascular systems (Laws & Bashaw, 2022). Below we summarize the available data about axon guidance in the liver.

SEMAPHORINs

In the fetal liver, NEUROPILIN-1 is expressed by CD45+ hematopoietic cells. It binds and enhances VEGF165 function, through VEGFR-2 on endothelial cells, thereby promoting development of endothelial cells and blood vessel formation (Yamada et al., 2003). In the adult liver, NEUROPILIN-1 is expressed in HSCs and liver sinusoidal endothelial cells. NEUROPILIN-1 expression in hepatocytes is associated with malignant transformation and may play a role in tumor behavior (Elpek, 2015). Studies of chronic liver diseases indicated that, besides its influence on angiogenesis, SEMAs contribute to the progression of liver fibrosis. Activated HSCs increase their production of SEMA-7A upon TGFβ stimulation, and this is associated with a rise in fibrogenic and inflammation markers (De Minicis et al., 2013). Moreover, in a mouse model of liver injury, SEMA-3E was produced by degenerating hepatocytes and induced contraction of sinusoidal endothelial cells leading to the activation of HSCs (Yagai, Miyajima, & Tanaka, 2014). Finally, NEUROPILIN-1, which was originally described as a class III SEMA-binding protein, was found to bind PDGF-β and TGF-β1 and stimulate their downstream pathways. This contributes to HSC activation and liver fibrosis (Cao et al., 2010). In the context

of liver cirrhosis, NEUROPILIN-1 also promotes angiogenesis by upregulating the expression and activation of VEGFR2 through the PI3KT/AKT signaling pathways (Y. Wang et al., 2019).

EPHRIN-EPH

Positioning organs in the body often requires the movement of multiple tissues, yet the molecular and cellular mechanisms coordinating such movements are largely unknown. Cayuso et al. showed that bidirectional signaling between EPHRIN-B1 and EPH-B3 coordinates the movements of the hepatic endoderm and adjacent lateral plate mesoderm, resulting in bud formation and asymmetrical positioning of the zebrafish liver (Cayuso et al., 2016). EPRIN-EPH signaling also displays a pro-fibrotic effect via EPH-B2 (Mimche et al., 2018). Upregulation of EPH-B2 is a prominent feature of two mouse models of hepatic fibrosis and is also observed in humans with liver cirrhosis. For example, EPH-B2 is upregulated and activated in mouse HSCs following chronic carbon tetrachloride (CCl_4) exposure. EPH-B2 deficiency attenuates liver fibrosis and inflammation, and this is correlated with an overall reduction in pro-fibrotic markers, inflammatory chemokines and cytokines.

NETRINs

In addition to regulating epithelial morphogenesis, NTNs can, in some circumstances, promote the dissociation of epithelia. Such conclusions were drawn from *in vitro* and *in vivo* studies (Murray, 2017). *In vitro*, hepatocellular carcinoma cells respond to hypoxia and in such conditions NTN-1 expression is increased and an epithelial-mesenchymal transition (EMT) takes place. The upregulation of NTN-1 is causative since the EMT is blocked by knockdown of NTN-1 and the overexpression of NTN-1 alone can induce the EMT (Yan et al., 2014). *In vivo*, Netrin-1 can increase the invasiveness of human colon tumor xenografts into nude mice (Murray, 2017).

An immunomodulatory property of NTN-1 has also been reported. Schlegel *et al.* demonstrated that NTN-1 impacts the resolution of inflammation and promotes hepatic repair and regeneration during liver ischemia/reperfusion injury (Schlegel et al., 2016). Later, Barnault and coworkers elegantly showed that NTN-1 is a secreted inflammation-inducible factor in the liver and contributes to hepatic inflammation by promoting cytokine production and accumulation of Ly6Chi proinflammatory macrophages. Furthermore, the humanized anti-NTN-1 antibody NP137 was able to effectively inhibit the hepatic inflammation in mice, suggesting that NTN-1 inhibition is a promising target in liver inflammation (Barnault et al., 2022). Finally, the role of NTN-1 during inflammation prompted researchers to evaluate the impact of administering NTN-1 to a mouse model of acetaminophen-induced hepatotoxicity. They demonstrated that exogenous NTN-1 enhances tissue regeneration (Duan, Woolbright, Jaeschke, & Ramachandran, 2020).

SLIT-ROBO

Here again, knowledge on the function of SLIT-ROBO signaling is limited in the context of liver development and the focus has been on the analysis of hepatic disease mechanisms. Three studies uncovered a function of SLIT2 in liver fibrosis. First, increased serum SLIT2 levels and hepatic expression of SLIT2 and ROBO1 were observed in patients with liver fibrosis. In addition, overexpression of SLIT2 exacerbated liver inflammation and injury in response to CCl4 exposure, whereas partially deletion of *Robo1/2* made mice less vulnerable to CCl4-induced liver injury and fibrosis. In combination with *in vitro* studies on an HSC cell line (LX-2) expressing *Robo1*, it was concluded that SLIT2 and ROBO1 promote activation of HSCs through activation of the SMAD2/3 and PI3K/Akt pathways, leading to liver fibrosis (J. Chang et al., 2015). Similarly, SLIT2-ROBO2 signaling promotes the production of pro-fibrogenic mediators, including COLLAGEN 1, TGFβ1 and CTGF,

via the PI3K/Akt pathway. In this study, SLIT2 bound to ROBO2 in the mouse hepatic cell line JS1 and the HSCs of mouse liver (Zeng et al., 2018). The third study also described SLIT2-ROBO1 binding as an activator of HSCs, contributing to the survival and proliferation of HSCs via activation of ERK1/2 and p38 signaling. Their *Robo1-/-* mouse model showed that these mutant mice less readily develops HSC activation and liver fibrosis after bile duct ligation (C. Li et al., 2019).

In hepatocellular carcinoma, ROBO1 and ROBO2 are upregulated, whereas SLIT3 is downregulated (Avci, Konu, & Yagci, 2008). The repression of SLIT3 in HCC induces tumor proliferation via the GSK3β/β-catenin pathway (Ng et al., 2018). Moreover, ROBO1 promotes tumor invasion partly by the upregulation of mouse metalloprotease 2 and promotes tumor angiogenesis in HCC through activation of CDC42 (Ao et al., 2015; Yuan et al., 2016). Quantifications of SLIT-ROBO transcripts in HCC cell lines and liver tumor tissues revealed that ROBO1, ROBO4 AND SLIT2 could predict tumor stage and differentiation status (Avci et al., 2008).

Taken together, these results reveal a role for axon guidance genes in liver diseases, but the lack of information on these pathways during liver development underscores the need for research on axon guidance molecules in embryonic liver. Axon guidance genes may impact bile duct and hepatic artery development, either through repulsive and attractive guidance signals of cellular components required for the formation of these tubular structures, or through cell-cell and cell-ECM contact that will influence cell adhesion, shape, differentiation and maturation during morphogenesis. Axon guidance genes have also been shown to regulate VEGF signaling which is thought to mediate epithelial-mesenchyme interaction during hepatic artery morphogenesis (cfr Fig. 10).

VII. Imaging tissue and organ morphogenesis

Physical sectioning of samples is the gold standard histological technique for obtaining high resolution microscopic images. Typically, samples are fixed, and cut on a microtome into sections with a thickness of approximatively 6 µm. These sections are then processed by immunolabelling, and finally mounted under a coverslip for microscopic inspection. This procedure has proven flexible and efficient in research and routine diagnosis. In the context of voluminous specimens, when the features of interest span several millimeters or even centimeters, such as vascular network or organ architecture, there is a need for 3D imaging. These samples are often investigated by serial physical sectioning and 3D volume reconstruction. However, these serial section techniques are generally destructive to the tissue and the 3D reconstruction is time consuming. The recent rise of optical tissue-clearing techniques makes physical sectioning of samples obsolete in many cases. The previously unattained clarity and transparency of large samples now allows optical sectioning of thick samples. Entire organs are thus imaged as a whole, using several equipment including confocal microscopes and light-sheet fluorescence microscopes (LSFM). The overall process of 3D imaging can be divided into several major steps: fixation, decolorization (optional), labeling, delipidation, refractive index (RI) matching and image acquisition and analysis.

Many reviews have discussed tissue-clearing methods, with either an in-depth focus on the chemical principles (Richardson et al., 2021; Richardson & Lichtman, 2015; Tainaka, Kuno, Kubota, Murakami, & Ueda, 2016) or on guiding to select clearing methods or imaging strategies (Ariel, 2017; Molbay, Kolabas, Todorov, Ohn, & Ertürk, 2021; Vieites-Prado & Renier, 2021; Weiss, Voigt, Shepherd, &

Huisken, 2021). Below, we address briefly the different clearing protocols and 3D imaging modalities relevant for this thesis.

i. Main clearing techniques

Tissue opacity is one of the major obstacles in whole-organ imaging. Tissues contain various substances with different optical properties (Tuchin, 1997). Therefore, when the light goes through tissues, light distribution and intensity become broadened and decayed due to light scattering and light absorption, respectively, which causes blurred and weakened images, especially in deeper regions of the tissue. Thus, the purpose of tissue clearing is mainly to minimize light disturbance for better optical imaging. Efficient tissue clearing contributes to improve imaging depth and contrast (Susaki & Ueda, 2016). Tissue clearing can be achieved by homogenization of optical property inside the tissue sample so that light is transmitted straight in the forward direction. The RI is a simple indicator of optic properties and can be used to compare different systems. Discontinuity of RIs causes light scattering. Various tissue substances (e.g., proteins and lipids) have different RIs, and they are overall higher (around 1.4 to 1.6) than surrounding water (1.33). Therefore, tissue optical clearing works as it enables RI matching inside the sample (Weiss et al., 2021).

Organic solvent-based clearing protocols

All organic solvent clearing protocols aim at creating a RI homogeneity by three steps: 1) dehydration; 2) delipidation; 3) RI matching to the average refractive index of the remaining constituents of the sample (around 1,55). While dehydration is usually achieved by an alcohol gradient, delipidation and RI matching are both achieved by infiltrating the specimens with organic solvents.

The original protocol was first described over 100 years ago, with a tissue clearing protocol using a mixture of benzyl alcohol and methyl salicylate. This protocol was then modified to BABB (Murray's clear), a fast and well-suited clearing protocol using a mixture of benzyl alcohol and benzyl benzoate that was used as early as the 1980s. Significant drawbacks of the method are the induced tissue shrinkage, fast and irreversible quenching of genetically encoded fluorescent proteins and high toxicity (Dent, Polson, & Klymkowsky, 1989). Other organic solvents were further screened in later studies giving rise to the DISCO family of clearing protocols. The use of tetrahydrofuran (THF) for dehydration, dichloromethane (DCM) for lipid extraction and dibenzyl ether (DBE) as a clearing agent, allowed for better results especially for clearing efficiency and genetically expressed fluorescent proteins (Ertürk et al., 2012). Among the main advantages are quality and speed of the clearing but the limitations remain the use of toxic and/or corrosive chemicals as well as tissue shrinkage (Molbay et al., 2021).

Aqueous-based clearing protocols

Aqueous clearing methods have emerged due to their ability to better preserve fluorescence labels that often do not tolerate dehydration. Hydrophilic clearing passively removes lipids content with detergents or amino alcohols and uses hydrophilic RI matching solutions (final RI in the 1,38-1,48 range). The main advantages being biocompatibility and biosafety although the tissue-clearing performance are sometimes inferior to that of organic solvent-based clearing methods and can take several weeks of clearing for large samples.

The different version of CUBIC and Scale methods are grouped in this family. The original version of the Scale method (which was extremely slow) has been superseded by ScaleS, which is faster, avoids tissue expansion and preserves lipids

such that lipid staining is possible (Hama et al., 2015). The first version used urea for tissue clearing which cause hydration leading to tissue expansion. The second use a mix of urea and sorbitol to improves the procedure (Hama et al., 2015). Sorbitol causes dehydration, leading to tissue shrinkage, by balancing both effects, they achieved tissue clearing while preserving the original sample volume.

CUBIC protocols were created by modifying and optimizing the urea-based SCALE clearing solutions. The procedure involved immersion in or perfusion by a first reagent containing Triton X-100 and urea for delipidation and (ethylenedinitrilo)tetra-2-propanol (Quadrol) for decolorization, followed by immersion with a second reagent containing triethanolamine, urea and sucrose for refractive index matching to n = 1.49. A variety of solution variants optimized for different sample types are available and have been described in detail, including organ specific protocols (Molbay et al., 2021). The main disadvantage is that clearing can take several weeks for large samples.

Hydrogel based clearing protocols

Hydrogel-based methods increase protein crosslinking to stabilize the structure of the tissue to enable the use of stronger detergents and accelerated transport through the sample. They utilize an acrylamide monomer to form a tissue-hydrogel hybrid, which allows immobilizing most of the amino group containing molecules by cross-linking, thus keeping large tissues intact and decreasing structural damage. The founder of this methods is the CLARITY protocol, after fixing the tissue and embedding in a hydrogel scaffold, the sample is subjected to delipidation using sodium dodecyl sulfate (SDS) detergent. This clearing process involves electrophoresis-driven lipid removal in a solution with an RI between 1,38-1,45. The nature of the reagents also facilitates tissue expansion which potentially reveals

hidden structures. Among the downsides of this approach are the longer incubation times required for clearing and the need for special equipment.

ii. 3D microscopy

Improved and new imaging technologies are capable of extracting stacks of 2D images from intact 3D samples by identifying and blocking or removing out-of-focus light from the fluorescence images.

Confocal microscopy

Confocal microscopes are the best choice for studies requiring precise signal colocalization and high resolution on smaller samples. Confocal microscopy uses a pinhole in the image plane to block out-of-focus light from entering the photon detector. These microscopes combine well with protocols that clear less efficiently but offer the best fluorescence preservation.

Light-sheet microscopy

The full potential of optical clearing techniques, however, is realized in light-sheet microscopy. Light-sheet microscopes generate a thin plane of light through the sample, while an orthogonal imaging objective collects the image from the illuminated plane. With this approach, optical sectioning is achieved by exciting fluorescence only in the plane of focus, while out-of-focus parts of the sample are left in the dark. This allows gentle imaging at high speed of thousands of sections in the z axis and multiple tiles in the x and y axes (if needed) within minutes.

Light-sheet microscopes with large open sample chambers (e.g. the Miltenyi Ultramicroscope II or Blaze) can scan bigger samples fast but require high transparencies. Therefore, they best combine with organic solvent-based methods, such as DISCO. Light-sheet systems using smaller closed chambers, such as

spectrophotometer cuvettes (e.g. the Zeiss Z7) prevent the evaporation of the imaging solution, and thus allow for more a flexible use of diverse tissue-clearing protocols. They are, however, more restricted regarding sample sizes. These two systems are the best all-purpose choice. Nonetheless, even when maximizing the attainable resolution, light-sheet imaging still produces relatively low-resolution images compared with sections from epifluorescence or confocal microscopes.

iii. Practical considerations

Whole-mount sample preparation and tissue clearing introduce many unique challenges not seen in traditional slide-based 2D microscopy. During sample preparation, one can no longer assume uniform fixation and antibody penetration as in a thin sliced. During imaging, one can no longer simply rotate an objective turret to try a new lens as we now face challenges associated with RI matching, working distance limitations and chemical compatibility in addition to resolution and magnification. However, there are also similarities to traditional sample preparation such as the importance of fixation, minimizing autofluorescence, and labeling. Moreover, there are similarities to traditional imaging including photobleaching and the trade-offs between signal-to-noise ratio, resolution, imaging time and cost (Weiss et al., 2021). One of the major challenges when designing the architecture of a 3D imaging infrastructure for numerous large, cleared samples, is the amount of data generated. This requires sufficient computing power for rendering and analysis, as well as storage capacity. Concerning the latter, however, which is a frequent concern, one should keep in mind that storage of hundreds of thousands of histological glass slides filling cupboards in the corridors has always been a challenge. The difference is that today, when using appropriate image analysis and rendering software such as

Arivis, Fiji or Imaris hundreds or even thousands of images can be viewed and analyzed simultaneously in their 3D spatial (and for live samples, temporal) context.

Nevertheless, more than a century after the birth of tissue optical clearing, there still is no one-size-fits-all approach for all types of samples. Significant progress has been made for many types of specimens, but every researcher still faces a difficult choice when embarking with new kinds of samples into this rapidly enlarging ocean of clearing technologies. The good news is that all the available techniques essentially follow the same principles with just minor differences. In general, solvent-based techniques are great because they are inexpensive and reproducible. However, they can shrink tissue significantly, are less likely to be compatible with fluorescent proteins and may wipe out low-expression proteins during the clearing process. Aqueous techniques offer better support for fluorescent-protein-expressing tissue, while methods that encase the tissue in a hydrogel can improve protein retention. These techniques are thus great for low-expressing targets (Paysan, 2021).

Aims and strategies of our research

The functional microarchitecture of the liver consists in lobules that contain cords of hepatocytes aligned along sinusoids. Blood is supplied to the sinusoids by the portal vein and hepatic artery, and the bile produced by the hepatocytes is collected in biliary ducts. During liver morphogenesis, bile ducts, portal vein and hepatic artery develop coordinately to form the portal tract.

Earlier work using molecular approaches, transgene technology and mainly 2D imaging has demonstrated that the portal mesenchyme is instructive for differentiation of the biliary cells lining the bile ducts, and normal bile duct formation is required for morphogenesis of the hepatic artery. However, how the portal mesenchyme organizes in three-dimensions, how it contributes to shape the 3D architecture of the bile duct and hepatic artery, remains unknown. Also, how the signaling crosstalk between mesenchyme, duct and artery is orchestrated to allow coordinated development is not well understood.

Therefore, in the present thesis we aimed to better describe the development of the portal tract and identify mechanisms that control its morphogenesis by:

1. Providing a 3D description of the coordinated development of portal mesenchyme, bile ducts and hepatic artery at several developmental stages in the mouse liver, and at the level of the entire liver and entire lobes.
2. Unraveling, the cell-cell interactions driving development of the liver portal tract by profiling gene expression in the developing ducts and adjacent portal mesenchyme, and investigating the function of axon guidance genes in duct and hepatic artery formation using transgenic mice.

Results

I. New insight into the 3D development of the liver portal area

i. Introduction

The proper establishment of the complex architecture of the liver plays an essential role in ensuring the functional integrity of the adult organ (Mescher, 2010). The microarchitecture of the liver is organized into lobules. The portal space at the apex of each lobule contains a branch of the portal vein, the bile duct and the hepatic artery, all surrounded by portal mesenchyme (Krishna, 2013). The biliary tubular network plays a crucial role because the bile produced by the hepatocytes must be transported to the intestine. During liver morphogenesis, the bile ducts, portal vein, and hepatic artery develop in an orchestrated manner to form the portal tract (Clotman et al., 2003; Ober & Lemaigre, 2018). The coordinated actions of cell growth, differentiation, maturation, and spatial organization of cells in the portal tract are tightly regulated and synchronized on a spatiotemporal scale.

Most efforts to decipher the mechanisms of portal tract development have focused on identifying regulators of cell fate specification and differentiation, with most attention directed towards the biliary tree (Brevini et al., 2020; Sampaziotis et al., 2015; Zong & Stanger, 2012). However, how the 3D tissue architecture of the liver develops in the embryo remains incompletely understood. Although several models have been proposed to describe the stages of bile duct development (as

elaborated in the thesis introduction-chapter III), they all suffer from several limitations. First, they result primarily from analysis of 2D tissue sections and short segments of IHBD, meaning that the development of IHBD at the lobe or organ level remains unclear. Second, although retrograde ink injection and micro-tomography have been able to visualize the luminal network of bile ducts in the entire liver, ink and resin injections cannot be easily implemented in the embryonic liver at early stages of biliary development. In addition, these techniques do not show nascent ductal structures that lack connectivity. Third, these models do not address the spatial organization of cell types other than cholangiocytes during liver organogenesis.

In this work, we focused on adapting recent advances in tissue clearing and 3D optical imaging systems to enable analysis of embryonic liver development. We were able to: (1) optimize the 3DISCO clearing protocol for mouse embryonic and postnatal livers from E17.5 to P6; (2) resort to light-sheet fluorescence microscopy to provide an accurate 3D description of bile duct development at cellular resolution; (3) visualize in 3D the organization of portal mesenchyme during liver development, in parallel with bile duct formation.

ii. Materials and methods

2D Immunofluorescence, immunohistochemistry, and confocal imaging

Immunofluorescence and immunohistochemistry were performed on 6 µm sections of formalin-fixed paraffin-embedded (FFPE) or sucrose-embedded frozen tissues. FFPE tissue sections were deparaffinized 3x 3 min in xylene, 3 min in 99%, 95%, 70% and 30% ethanol and deionized water. Antigen retrieval was performed by micro-wave heating for 10 min in 10 mM citrate pH 6. Sections were

permeabilized for 5 min in 0.3% Triton X-100 in PBS before blocking for 45 min in 3% milk,10% BSA, 0.3% Triton X-100 in PBS. For preparation of frozen sections, livers were collected, briefly washed in PBS, and fixed overnight in 4% paraformaldehyde. Tissues were incubated in sucrose 15% in PBS for 6-12 h and overnight in sucrose 30% in PBS, before embedding in OCT and freezing in liquid nitrogen-cooled isopentane. Frozen sections were thawed at RT for 20 min and rehydrated in PBS for 10 min. Antigen retrieval was performed by 5 min incubation in 10 mM citrate pH 6 preheated at 95°C, and sections were rinsed in deionized water and PBS, before blocking as above.

Primary antibodies were diluted in blocking solution at 4°C overnight and secondary antibodies were diluted in 10% BSA, 0.3% Triton X-100 in PBS at 37°C for 1 h. For IHC, antibody binding was visualised using 3,3'-diaminobenzidine tetrachloride (#ab64238, Abcam, Cambridge, UK), and 30% haematoxylin (#109249, Merck Millipore) was used to counterstain the tissue. Pictures were taken with Cell Observer Spinning Disk (Carl Zeiss) and Zen blue software, or with CaseViewer on scanned tissues. Primary and secondary antibodies are described in Tables S1.

Whole mount labeling and three-dimensional microscopy

Tissue Collection and Processing

For embryos the developmental age was assessed based on the day of the vaginal plug and for newborns from the day of birth. Dissected livers from CD1 embryos and newborns mice were fixed by immersion in 4% PFA at 4°C overnight. The different liver lobes were further dissected after fixation and post-fixed in 4% PFA at 4°C overnight. The tissue was bleached to remove pigmentation and reduce signal-to-noise ratio (Renier et al., 2014). The samples were dehydrated for 2h at

RT in ascending concentrations of methanol in PBS (50%, 80%, 100%). The samples were then treated overnight at 4°C with a 6% hydrogen peroxide solution in 100% methanol. Samples were re-hydrated for 2h at RT in descending concentrations of methanol (100% twice, 80%, 50%) and washed two times in PBS during 1h. Samples were kept at 4°C until further processing.

Whole-Mount Immunostaining

For immunostaining, samples were permeabilized and blocked by agitation in PBS containing 0.2% gelatin (Merck), and 0.5% Triton X-100 (Roth) (PBSGT) at RT (Belle et al., 2014). They were transferred to a solution containing 0.1% saponin (10 µg/mL) and heparin (10 µg/mL) in PBSGT together with the primary antibodies (listed in the Table 1) and placed at 37°C with agitation for 10 days. This was followed by six washes of 1 h in PBSGT at RT. Next, secondary antibodies (listed in the Table 1) were diluted in a solution containing 0.1% saponin (10 µg/mL) and heparin (10 µg/mL) in PBSGT and passed through a 0.22 µm filter. Samples were incubated overnight at 37°C in the secondary antibody solution. After six washes of 1h in PBSGT at RT, samples were stored in the dark at 4°C until tissue clearing.

Tissue Clearing: 3DISCO

For all tissue clearing, a optimized 3DISCO clearing protocol was developed. All incubation steps were performed in dark conditions at RT in a fume hood, on an agitator, using a 15 mL centrifuge tube (TPP, Dutscher). Samples were first dehydrated in ascending concentrations (50%, 80%, and 2x 100%) of tetrahydrofuran (THF; #186562, Sigma) diluted in H_2O for 2h each. Samples next underwent delipidation for 30 min in dichloromethane (DCM; Sigma-Aldrich) followed by overnight clearing in dibenzyl ether (DBE; Sigma-Aldrich). Samples were then stored in individual light-absorbing glass vials (Rotilabo, Roth) at RT. In

these conditions, samples could be stored and imaged for up to 9 months without any significant loss of fluorescence.

3D Imaging and Image Processing

Three-dimensional image acquisitions were performed by using an ultramicroscope I (LaVision BioTec-Miltenyi Biotec) with the ImspectorPro software (LaVision BioTec-Miltenyi Biotec). The light sheet was generated by a laser (wavelength 560 or 640 nm, Coherent Sapphire Laser, LaVision BioTec-Miltenyi Biotec) and focused using two cylindrical lenses with 150ms time exposure. Two adjustable protective lenses were applied for small and large working distances. A binocular stereomicroscope (MXV10, Olympus) with a 2x objective (MVPLAPO, Olympus) was used at different magnifications (0.63x, 0.8x, 1x, 1.25x, 1.6x, 2x, 2.5x, 3.2x, 4x, 5x, and 6.3x). The corresponding zoom factors and numerical apertures are available on manufacturer website (https://www.miltenyibiotec.com/BE-en/products/objective-lenses-for-ultramicroscopes.html#150-000-493). Samples were placed in an imaging reservoir made of 100% quartz (LaVision BioTec-Miltenyi Biotec) filled with DBE and illuminated from the side by the laser light. A Zyla SCMOS CCD camera (2,048 × 2,048 pixel size, Andor Oxford Instrument) was used to acquire images. The step size between each image was fixed at 1 and 2 µm. All tiff images are generated in 16-bit.

For image processing, images, 3D volume, and movies were generated using Imaris software (version 9.9.0, Bitplane-Oxford Instrument). Stack images were first converted to imaris file (.ims) using ImarisFileConverter and 3D reconstruction was performed using the volume rendering function. 3D pictures and movies were generated using the “snapshot” and “animation” tools.

iii. Results

Protocol optimization for 3D bile ducts visualization

One key obstacle in exploring bile duct morphogenesis is the limited view provided by the traditional 2D imaging techniques. However, light-sheet fluorescence microscopy and tissue clearing techniques helped us to overcome the optical limitations of large sample visualization to evaluate the 3D models of IHBD development at the liver lobe level.

With help of Morgane Belle (Imaging platform, Vision Institute, Paris) we selected and adapted the 3DISCO organic solvent-based clearing technique to our embryonic and postnatal mouse liver samples. With the SCALEA2 and CUBIC clearing protocols, we did not obtain sufficient transparency of the samples, or clearing required 45 days (only 2 days with 3DISCO). Several parameters were adapted to embryonic liver, such as quality of chemicals, duration of tissue permeabilization, temperature. The selection of secondary antibody was critical to obtain a good signal-to-noise ratio. Using the green fluorescence spectrum yielded much autofluorescence of the liver. Even if, such autofluorescence can prove useful to image the liver vasculature by reverse autofluorescence (Adori et al., 2021).

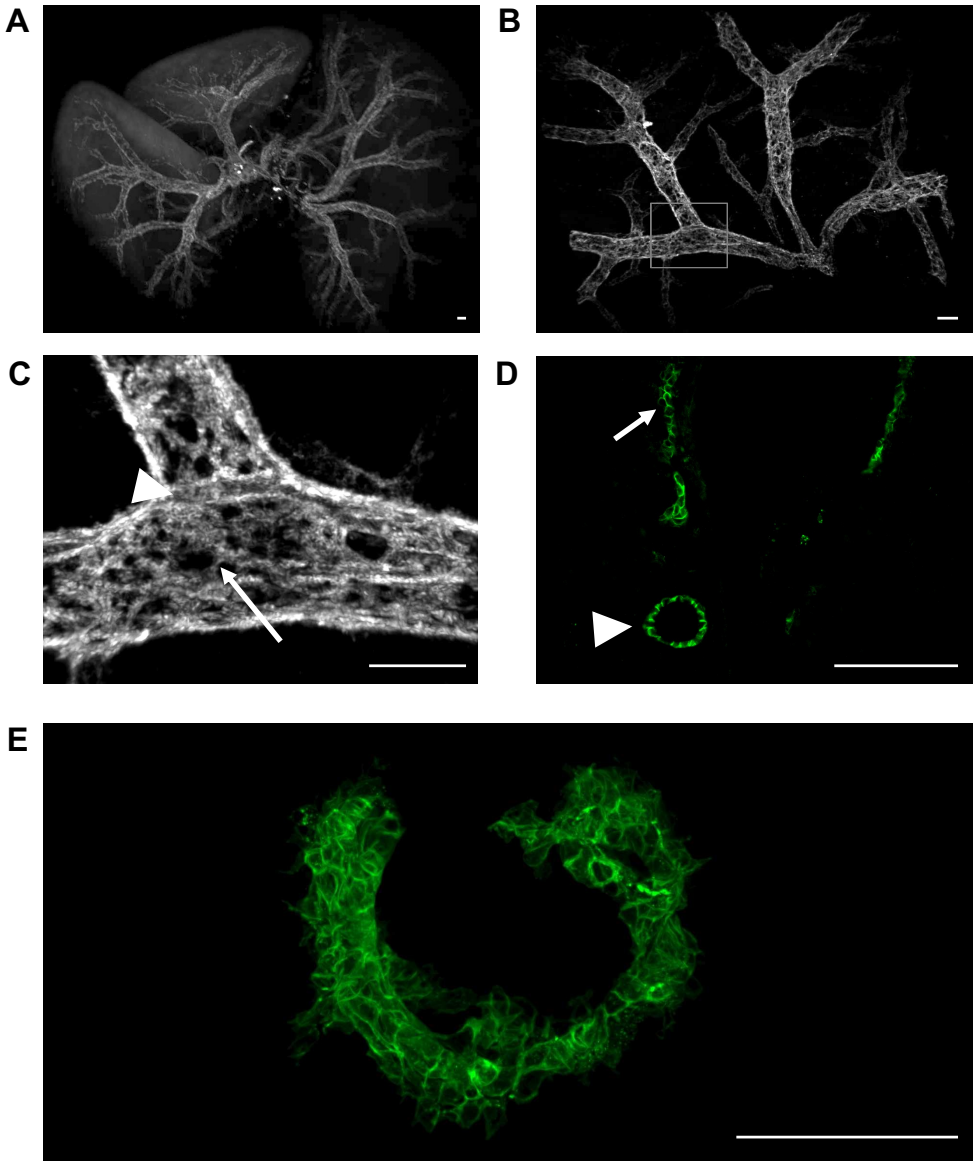


Figure 1: 2D and 3D morphology of the intrahepatic bile ducts. (A) 3D whole liver image acquisition using light sheet fluorescence microscopy illustrates cholangiocytes (CLDN7 staining; white) around the portal vein at E18.5. (**B, C)** Zoomed image acquisitions at the lobe level, of E18.5 liver. Whole mount immunostaining of CLDN7 (white) shows a mesh-like luminal network of small ductules (arrow) and larger ducts (arrowhead) running along the portal vein. **(D, E)** Thin and thick sections imaged using confocal microscopy showed the same hierarchical organization of the developing bile ducts as observed in 3D. Picture E is extracted from a video available in annex. Size bars: 100 µm.

The 3D network of IHBDs was stained with an antibody against the cholangiocyte-specific marker, Claudin7 (CLDN7). At E18.5, we provided the first visualization of the entire developing IHBD network (Fig. 1A). The sample size was optimized to achieve the right compromise between good antibody penetration, efficient clearing and reasonable scan time and file size. We did so while keeping our primary objective in mind, namely that of being able to study the detailed structure of IHBD in 3D at high resolution. Thus, for each sample we imaged the entire liver lobe at low resolution to obtain spatial information such as the proximity to the hilum where the development of the IHBDs is initiated (Fig. 1B). We then zoomed in on the hilum and periphery to acquire high resolution images to investigate the detailed organization of the biliary cells. We compared our zoomed-in 3D images (Fig. 1C) with a classical 2D images (Fig. 1D). Near the hilum, we observed a dense biliary network with a main bile duct running along the portal vein (arrowhead) connected to a thinner biliary plexus (arrow) organized around the portal vein. Importantly, at this stage of development, the biliary network forms a dense network with many connections. This indicates that the ductal plate interpreted from 2D sections as a sleeve or fragmented sleeve around the portal vein actually corresponds to a 3D mesh-like structure (Fig. 1E & video 1F; thesis intro Fig. 5B).

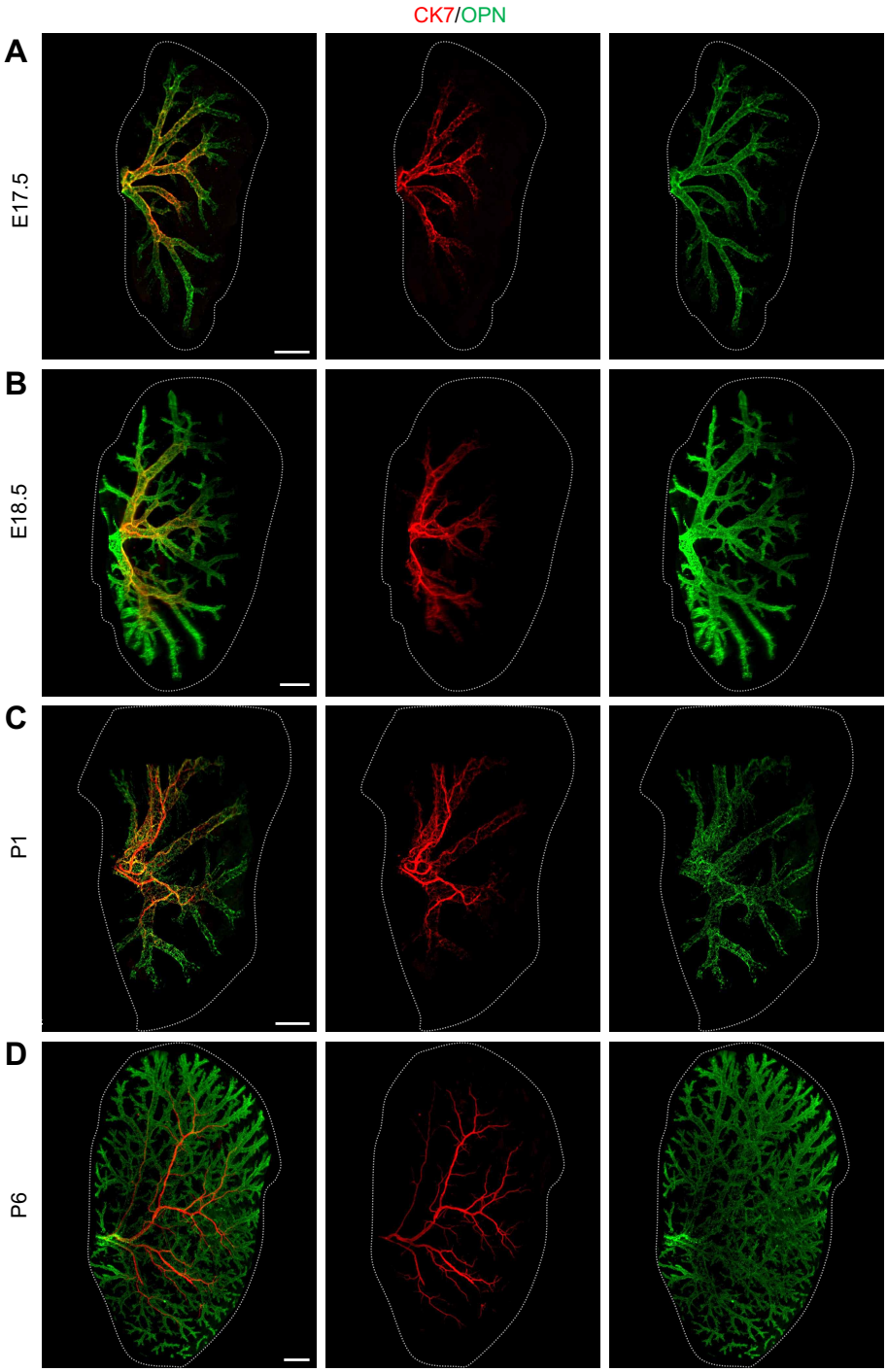

CK7/OPN
A
E17.5
B
E18.5
C
P1
D
P6

Figure 2: 3D morphology of maturing intrahepatic bile ducts. (A-D) 3D whole liver lobe imaging using light sheet fluorescence microscopy illustrates cholangiocytes (OPN staining; the apical pole of cholangiocytes is labelled in green, CK7 staining; the membrane of mature cholangiocytes is labeled in red) around the portal vein at E17.5, E18.5, P1 and P6. White lines delineate lobe boundary. Videos in annex. Size bars: 500 µm

3D visualization of the bile duct maturation process at the lobe level

We applied our improved protocol to different stages of IHBD morphogenesis, visualizing a whole liver lobe at E17.5, E18.5, P1 and P6. We sought to observe the sequence of events characterizing the embryonic development of intrahepatic bile ducts by examining the expression of cholangiocyte-specific markers. Bile ducts were visualized using osteopontin (OPN) staining to mark the luminal structure of bile ducts, with the anti-OPN antibody marking the apical pole of cholangiocytes. This early marker of differentiation was complemented by the terminal differentiation marker cytokeratin7 (CK7) that labels the membrane of mature biliary cells. Both markers had been used by others for 3D imaging of short segments of developing bile ducts (Kaneko et al., 2015; Tanimizu et al., 2016).

Our double-staining procedure confirmed that the development of IHBDs is characterized by progressive development from the hilum to the periphery of the lobes. Our data also confirmed that IHBDs first form a homogeneous network which evolves to a hierarchical organization starting around E18.5 (Tanimizu et al., 2016). In addition, we found a hitherto undescribed heterogeneity in the gene expression profile of cholangiocytes forming the main ($CK7^{+}$ OPN^{+}) or secondary branches ($CK7^{-/low}$ OPN^{+}) (Fig. 2).

To examine in detail the structural changes of IHBDs during liver organogenesis, we zoomed in near the hilum and periphery (Fig. 3, 4). We observed that at E17.5, OPN staining label the cholangiocyte population localized mainly around the large portal

veins (Fig. 2A). The expression pattern of the two biliary markers illustrates three steps at the lobe level. First, cholangiocytes differentiate from the hilum to the periphery as OPN^+ cells near the portal vein. OPN^+ cholangiocytes are initially more scattered at the periphery where they connect to form a continuous biliary network (Fig. 3A). Second, cholangiocytes mature and start expressing CK7. Again, this maturation happens from the hilum to the periphery (Fig. 2). Third, starting at E18.5 the biliary network becomes hierarchical, with formation of large ducts running along the portal vein and smaller surrounding ductules (Fig. 2B, 3B).

Interestingly, we found that the hierarchical network undergoes remodeling. The large ducts indeed evolve from a multidirectional wavy shape to a straight shape running parallel to the portal vein. In parallel, the large ducts and the meshwork of ductules show differential CK7 expression (Fig. 2), revealing that final morphogenic rearrangement goes pairwise with final differentiation of ducts and biliary plexus. During this process, large $OPN^+/CK7^{high}$ ducts remains well connected to the $OPN^+/CK7^{low}$ biliary plexus (Fig. 4B).

Together, our observations confirm and extend earlier data (Kaneko et al., 2015; Tanimizu et al., 2016): we illustrate bile duct morphogenesis at the lobe level and show the differentiation status of cells lining the hierarchical network which so far had essentially been investigated by means of ink injections to visualize the biliary lumina. Moreover, we visualized a hitherto unnoticed reorganization of the main duct architecture which progressively aligns straight along the portal vein.

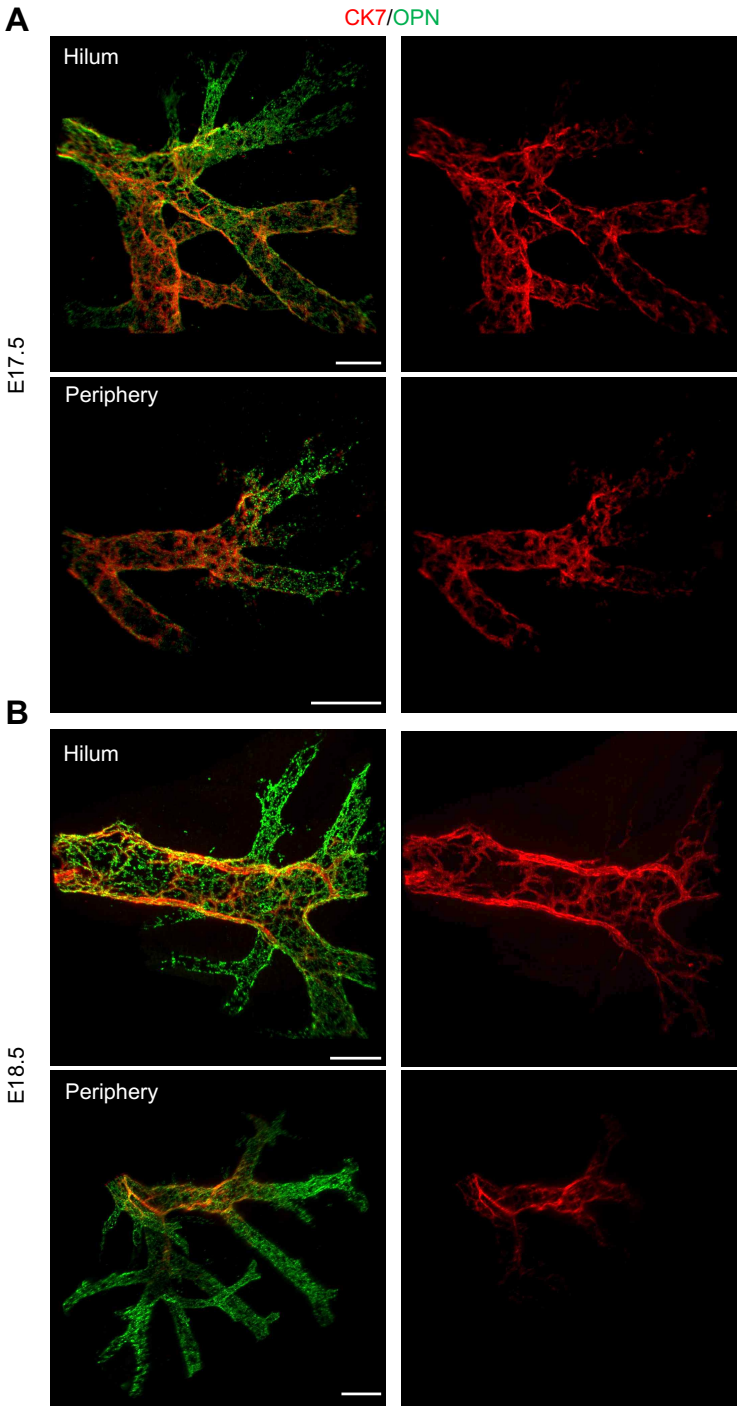


Figure 3: Zoom 3D imaging of the intrahepatic bile ducts during late embryonic. (A-B) Zoomed light-sheet fluorescence microscopy images illustrate cholangiocytes (OPN staining; the apical pole of cholangiocytes is labelled in green, CK7 staining; the membrane of mature cholangiocytes is labeled in red) organization around the portal vein at E17.5 and E18.5. Videos in annex. Size bars: 200 µm.

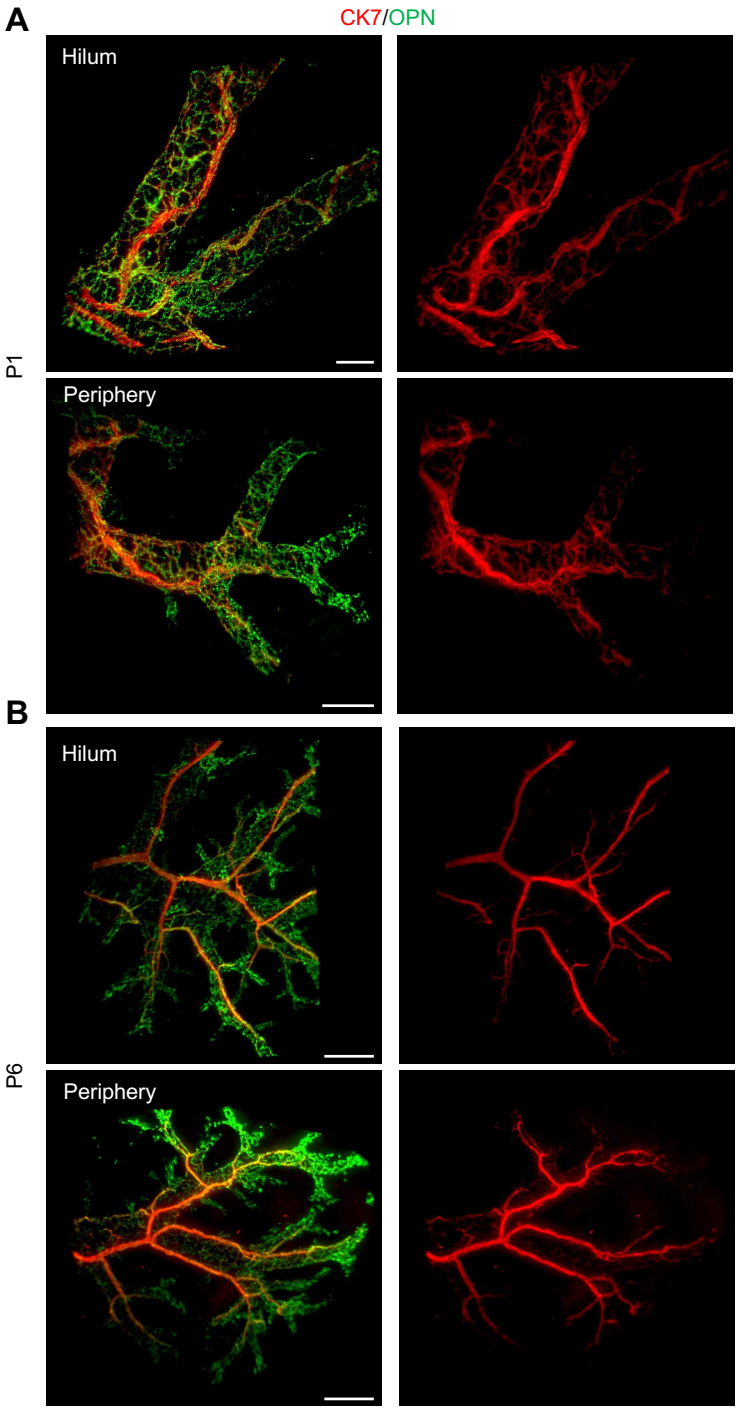


Figure 4: Zoom 3D imaging of the intrahepatic bile ducts during early postnatal stages. (A-B) Zoomed light-sheet fluorescence microscopy images illustrate cholangiocytes (OPN staining; the apical pole of cholangiocytes is labelled in green, CK7 staining; the membrane of mature cholangiocytes is labeled in red) organization around the portal vein at P1 and P6. Videos in annex.
Size bars: 200 µm.

Progressive differentiation and network formation of cholangiocytes from the hilum to the periphery visualized at the cellular level

To better visualize the organization of cholangiocytes and compare their spatiotemporal distribution between the hilum and the periphery, we resorted to the image processing tool called "clipping plane". This consists in cutting the portal vein longitudinally in the center to observe only the biliary cells present on one side of the vein. In other terms, we truncated the image along a given plane in 3D space by cutting away objects to one side of the plane.

Figure 5, is composed of such images, illustrating the evolution of cholangiocyte organization as a function of embryonic stage and location in the lobe. At E17.5, near the hilum, OPN^+ cholangiocytes form a mesh-like network, but this network is interrupted at various places. As the liver develops, the OPN^+ cholangiocytes form a more continuous network which, as illustrated above, reorganizes into a hierarchical structure. The clipping plane approach confirms at higher resolution that the main duct remains connected to the ductules. It also shows that the biliary plexus is remodeled as the number of OPN^+ ductules exists at a lower density at P6.

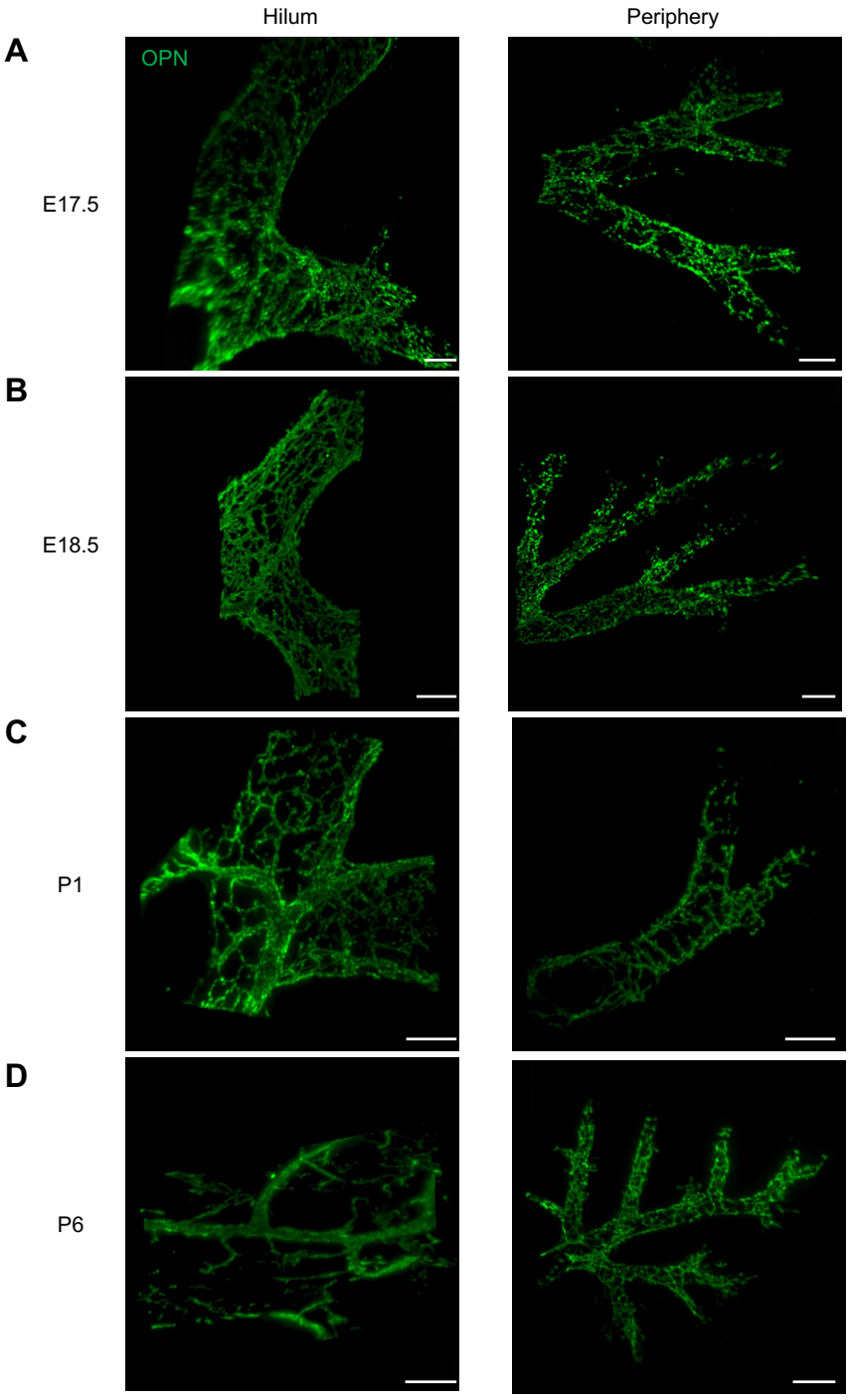

Hilum
Periphery
A
OPN
E17.5
B
E18.5
C
P1
D
P6

Figure 5: Organization of the OPN$^+$ cholangiocytes around the portal vein at E17.5, E18.5, P1 and P6. (A-D) Whole mount immunostaining of the biliary cells (OPN staining; green) is shown around the portal vein. Intrahepatic bile duct development is initiated at the liver hilum and gradually extends towards the periphery. Cholangiocytes from a dense network structure near the hilum whereas at the periphery, individual newly differentiated cholangiocytes are far away and apparently disconnected from one another. Videos in annex. Size bars: 100 µm.

At the periphery of the lobes at E17.5, OPN$^+$ cholangiocytes are much more dispersed around the portal vein than near the hilum. During development, these peripheral cholangiocytes connect with each other to form a homogeneous network that eventually reaches the periphery of the lobe. At P6, only the immature homogeneous network and not the more mature hierarchical network has reached the liver margin (Fig. 5). Thus, it will take more time before the entire biliary network has been remodeled as the immature and homogeneous luminal network gradually reorganizes into a mature hierarchical network during liver enlargement.

The OPN-CK7 antibody combination allows us to compare biliary cell maturation and duct remodeling, yet it does neither facilitate detection of individual cells nor does it permit to evaluate if the distance between cholangiocytes is evolutive. The SOX9 antibody marks the nuclei and is therefore an excellent tool to study the distribution of cholangiocytes during embryonic and postnatal development. Our analysis reveals that cholangiocytes are much more scattered near the edge of the lobe (Fig. 6).

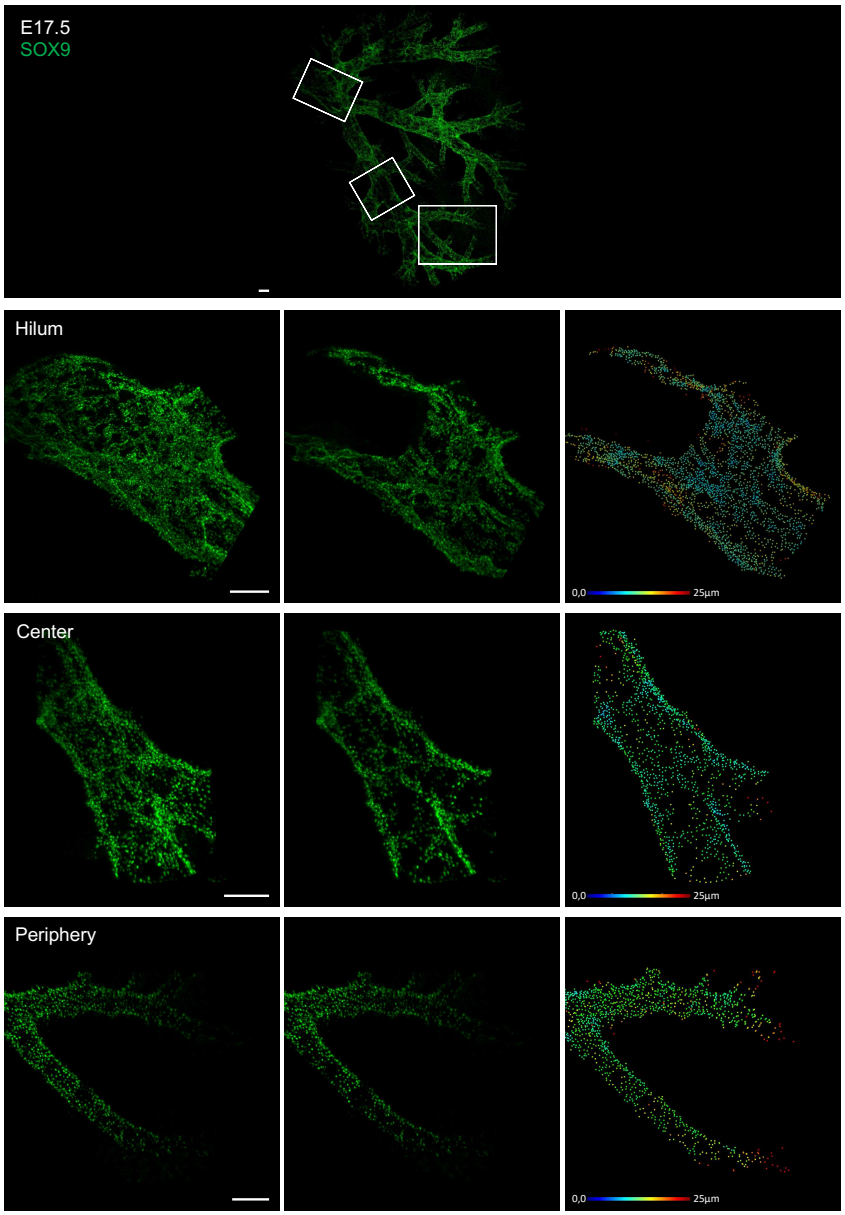


Figure 6: Organization of the SOX9+ cholangiocytes around the portal vein at E17.5. Whole mount immunostaining of the biliary cells (SOX9 staining; green) is shown around the portal vein. Cholangiocyte differentiation is initiated at the liver hilum and gradually extends towards the periphery. Boxed regions near the hilum and periphery (upper panel) are magnified in the lower panels, with middle panels illustrating clipped versions of the left panels. Colors codes illustrate average distances between 9 nearest neighboring nuclei. Videos in annex. Size bars: 100 µm.

To link differentiation with intercellular distance, we performed a double SOX9-CK7 staining to label immature ($SOX9^+$ $CK7^-$) and mature cholangiocytes ($SOX9^+$ $CK7^+$). Using the Imaris Spot function, we labeled each individual cholangiocyte and analyzed the average distance between each $SOX9^+$ nucleus and its 9 closest neighbors (Fig. 7B). Newly differentiated cholangiocytes at the lobe periphery were located further from each other than cells near the hilum. Next, we created a surface encompassing the CK7 staining as a representation of the area of the mature biliary structures (Fig. 7C). We compared cholangiocytes inside and outside this surface. We observed that most $SOX9^+$ cells within this surface tend to be closer to each other as compared to less mature area.

Collectively, our observations confirm that cholangiocyte differentiation proceeds continuously from the hilum toward the lobe's periphery. In addition, we found that the intercellular distance between cholangiocytes narrows down during differentiation, suggesting that close neighborhood is a prerequisite or a consequence of maturation. How the differentiating cells cholangiocytes connect and get closer to each other, and how cells become part of a large duct instead of the ductules forming the biliary plexus is not known.

3D visualization of the portal mesenchyme in the developing liver

Previous work has demonstrated that the portal mesenchyme is instructive for the differentiation of cholangiocytes lining the bile ducts, and that normal bile duct formation is required for the morphogenesis of the hepatic artery (Ober & Lemaigre, 2018). However, it is still unknown how the portal mesenchyme organizes in three dimensions.

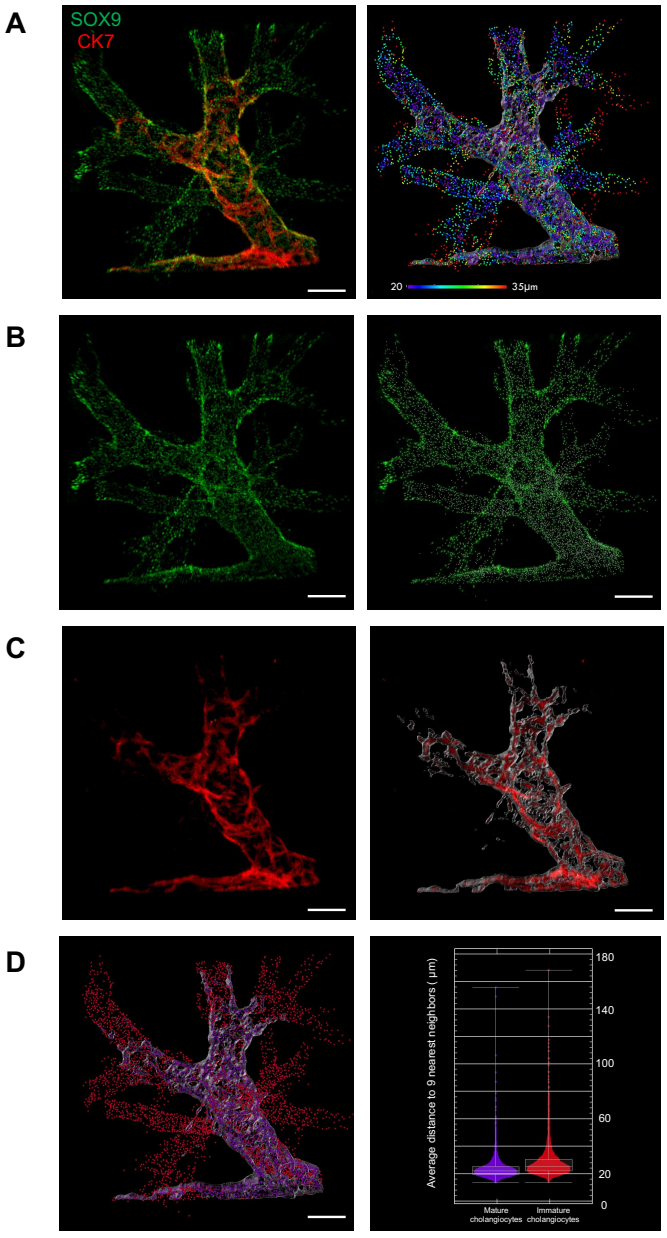


Figure 7: (A) Organization of immature (SOX9$^+$ CK7$^-$) and mature cholangiocytes (SOX9$^+$ CK7$^+$) around the portal vein at E19.5. (B) Calculation of the average distance between each SOX9$^+$ nucleus and its 9 closest neighbors. **(C)** Surface creation encompassing the CK7 staining as a representation of the area containing mature cholangiocytes. **(D)** Distance comparison between immature (SOX9$^+$ CK7$^-$; Red) and mature cholangiocytes (SOX9$^+$ CK7$^+$; purple). Video in annex. Size bars: 200 µm.

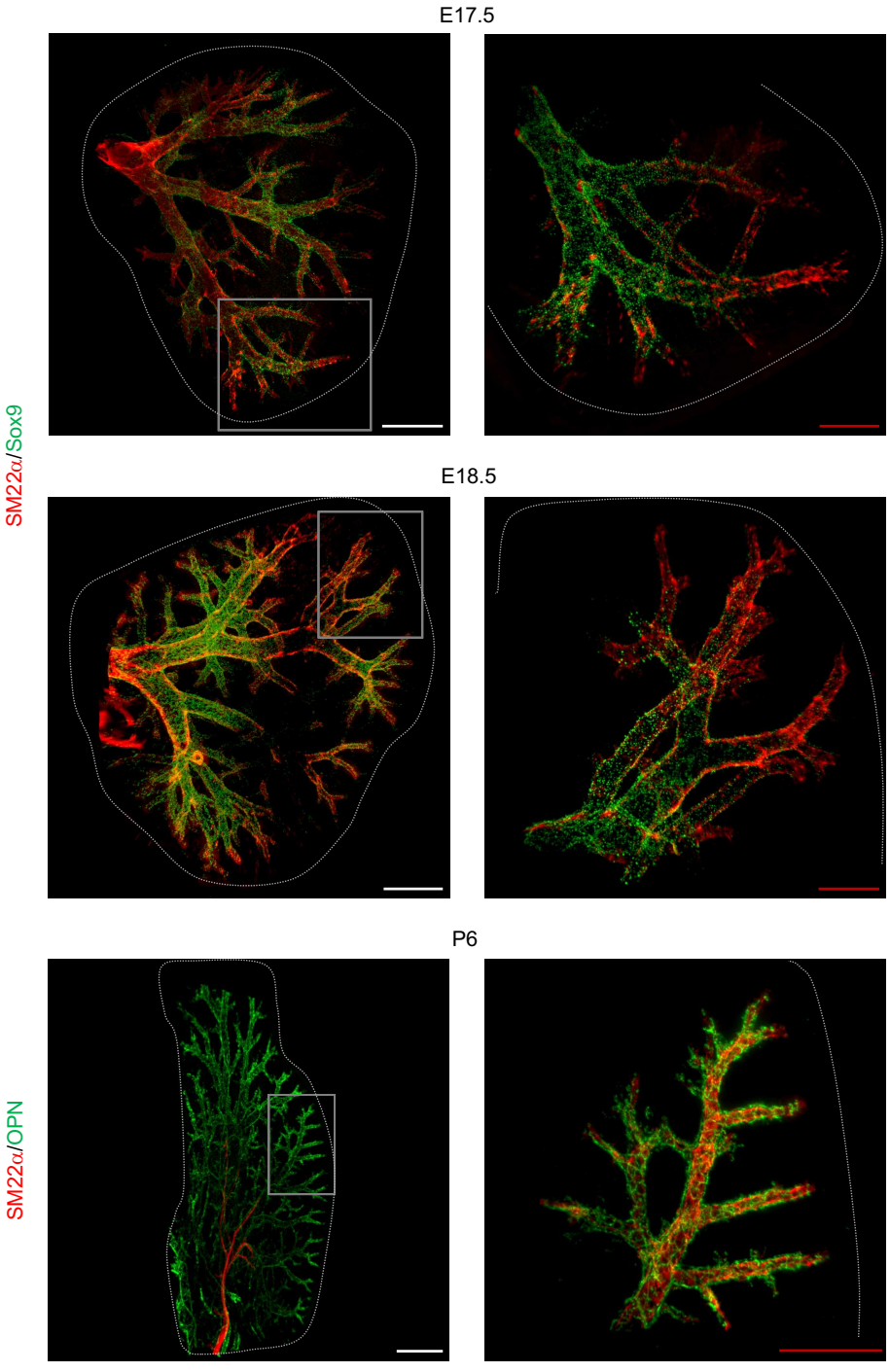

E17.5
E18.5
P6
SM22α/Sox9
SM22α/OPN

Figure 8: Organization of the cholangiocytes and portal mesenchyme around the portal vein. Whole mount immunostaining of the biliary cells (Sox9 or OPN staining; green) and portal mesenchyme (SM22α staining; red) is shown around the portal vein. Intrahepatic bile duct development is initiated at the liver hilum and gradually extends towards the periphery. At embryonic stages, mesenchyme development precedes cholangiocyte differentiation. White lines delineate the lobe boundary. White size bars: 500 µm, red size bars: 200 µm.

The development of the ducts was visualized in parallel with the vasculature (not shown) and portal mesenchyme to study their spatial relationship during development. We collected images from E17.5 to P6, the mesenchyme and bile ducts being immunostained with antibodies against Smooth muscle protein 22α (SM22α; synonum: transgelin) and OPN or SOX9. As anticipated and as evidenced at the lobe periphery, development of the mesenchyme precedes cholangiocyte differentiation (Fig. 8). This is consistent with the fact that signals within the portal mesenchyme instruct differentiation of hepatoblasts to cholangiocytes (Ober & Lemaigre, 2018). Furthermore, neither SM22α^+ portal mesenchyme nor biliary cells are homogeneously distributed around portal veins; a pattern appears to emerge with preferential areas of expression. The spatial organization of the SM22α^+ portal mesenchyme evolves during liver development. Indeed, SM22α^+ cells comprise the precursors of the vascular smooth muscle cells. They were distributed irregularly in the periportal space during development and became progressively restricted to the *tunica media* of the hepatic artery and portal vein (Fig. 9A). This heterogeneous distribution was also confirmed by high-resolution confocal microscopy (Fig. 9B).

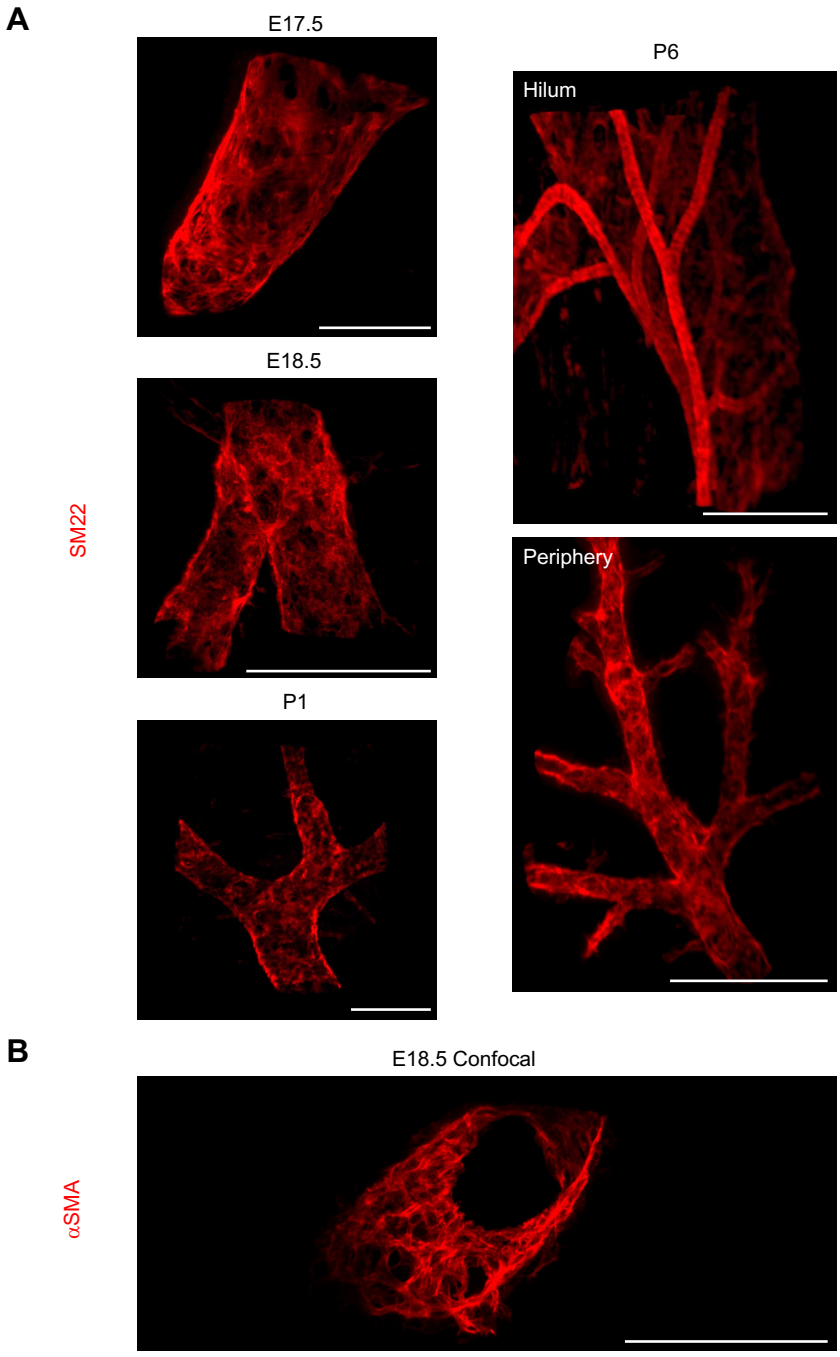


Figure 9: 3D histology of the portal mesenchyme from E17.5 to P6. (A) Whole mount immunostaining of the portal mesenchyme (SM22α staining; red) is shown around the portal vein. Portal mesenchyme is heterogeneously distributed at embryonic and early

postnatal stages. Six days after birth when mesenchymal subpopulations are more mature SM22α staining becomes restricted to vascular smooth muscle cell forming the hepatic artery and portal vein wall. This maturation is initiated at the liver hilum and gradually extends towards the periphery. (**B)** Thick section immunostaining and confocal imaging of the portal mesenchyme (αSMA staining; red) is shown around the portal vein and confirms the heterogenous distribution of the cells. Videos in annex. Size bars: 200 μm.

The heterogeneous distribution of SM22α$^+$ mesenchymal cells results from at least two distinct phenomena. First, SM22α$^+$ cells represent only a fraction of the portal mesenchyme. In adults, the latter is composed of vascular smooth muscle cells, portal fibroblasts and stellate cells. Yet, when and how these periportal cells differentiate from mesenchyme precursors remains poorly known (cfr Introduction chapter IV). Our observations provide evidence that some mesenchymal maturation occurs in the early postnatal period. As early as P1, we found that mesenchymal cells located in the vicinity of the bile ducts begin to express portal fibroblast markers such as CD90 (cfr article Fig. 2) while at the same time the number of αSMA$^+$ cells diminishes in the portal area (Fig. 10A). After birth, at P6, the mesenchyme is even more specialized as the hepatic artery is formed. At that time, αSMA becomes a specific marker of muscle cells forming the wall of the hepatic artery and portal vein. Second, the liver is a hematopoietic organ and a subset of hematopoietic cells, namely CD45$^+$ leukocytes are found in large numbers around the portal veins (Fig. 10B). Because they are distinct from the mesenchyme labeled by eYFP in *Sm22α-Cre;Rosa26ReYFP*, we speculated that they might fill the gaps observed in 3D between mesenchymal cells.

In conclusion, our observations illustrate how development of the mesenchyme precedes morphogenesis and differentiation of the bile ducts, and how mesenchymal cells that express vascular smooth muscle cell markers are distributed along the portal vein and hepatic artery during development.

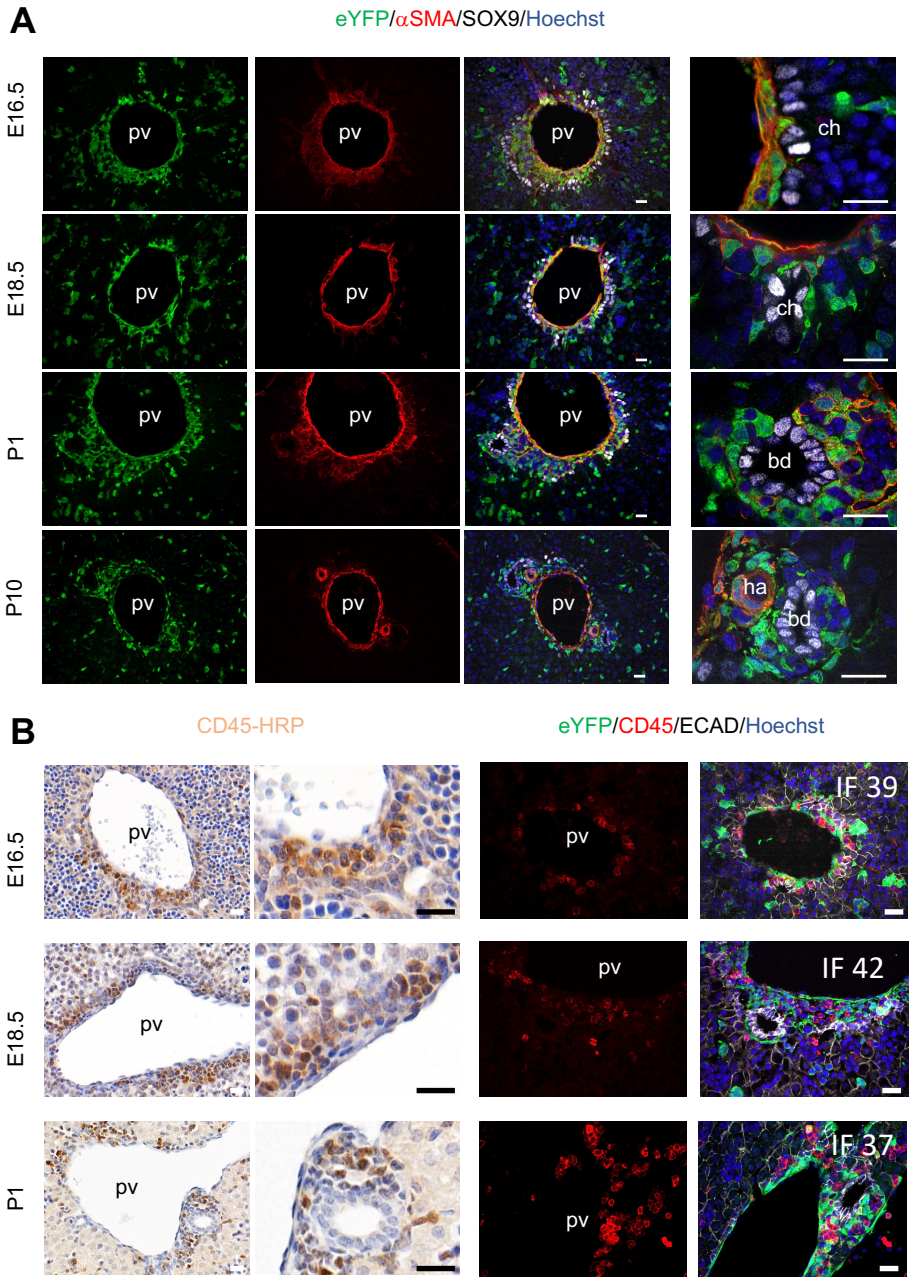


Figure 10: 2D histology of cells located in the portal mesenchyme (A) Staining of αSMA, CD45 and eYFP, in *Sm22α-Cre;Rosa26ReYFP* livers, at E16.5, E18.5, P1 and P6 reveals localization of progenitors of vascular smooth muscle cells. **(B)** CD45+ cells are located next to eYFP+ mesenchymal cells in *Sm22α-Cre;Rosa26ReYFP* livers. Ch, cholangiocytes; ha, hepatic artery; bd, bile duct; pv, portal vein. Size bars: 20 µm.

iv. Discussion

Protocol optimization

Since the development of IHBDs differs between the liver periphery and the hilum, it is important to visualize the largest possible extent of liver tissue, optimally the entire liver, to understand biliary and portal tract morphogenesis. Reconstructions from a stack of 2D sections would require continuous sections of the entire liver, which is time-consuming, labor-intensive and results in significant loss of z-axis information (Takashima et al., 2015). Tissular deformation upon sectioning is also a source of difficulty when aligning the sections. Retrograde ink injection is effective in studying the evolution of the luminal organization of the biliary tree, but it provides a 2D image, which precludes 3D analysis of the architecture (Kaneko et al., 2015; Tanimizu et al., 2016). Other limitations are the inability to study the spatial relationship with surrounding cells as well as low cellular resolution. In addition, the size of the visualized ducts that are possible to image is dependent on the carbon particle size of the ink used. More importantly, this technique can give inaccurate and subjective results due to the difficulty in accurately controlling the total amount of perfused solution.

MicroCT is the original method used to measure the biliary tree, nevertheless it offers suboptimal resolution, especially for distal bile ducts. Recently, Hankeova et al. have brilliantly developed a novel approach for the 3D analysis of the biliary tree called DUCT, double resin casting computed tomography. DUCT has revealed architectural mechanisms contributing to bile duct regeneration (Hankeova et al., 2021b). The technique allows for dual 3D analysis of vascular and biliary networks in adult mice using a custom-written MATLAB pipeline, ImageJ, or qualitative visual assessment. Although this technique provides info about the lumen, internal

diameter, perfusion and connectivity of the injected tree, it suffers from several limitations. DUCT cannot visualize lumens smaller than 5 μm due to the viscosity of the resin used. Data analysis, such as segmentation can be time consuming and require robust computational powers. In addition, retrograde ink and resin injections cannot be easily implemented in the early embryonic liver and do not show nascent ductal structures that lack connectivity.

An alternative is whole mount immunofluorescence staining combined with tissue clearing to assess the complete 3D architecture of the liver during morphogenesis. Although 3D imaging of thick sections of tissue or organ "blocks" is useful for regions of interest (Chen et al., 2020; Kamimoto et al., 2016; Tanimizu et al., 2016), our 3D imaging technique reveals the complete 3D network of IHDBs over an entire liver lobe. To our knowledge, our work is the first to optimize the 3DISCO protocol of tissue clearing for embryonic and postnatal liver samples. Only few protocols have been primarily developed for developmental stages (Vieites-Prado & Renier, 2021). Embryonic liver, in particular, has proven hard to image in 3D due to high pigmentation and tissue autofluorescence. Moreover, the fragility and heterogeneity of the different lobes of the liver require adaptations when using tissue-clearing protocols originally designed for adult samples.

To study the developmental stages of intrahepatic bile ducts and the organization of the hepatic portal mesenchyme, we decided to focus on the larger lobes to facilitate imaging, as the smaller ones can be difficult to manipulate. An inclusion step in agarose before the dehydration in organic solvent is a good optional step to facilitate their handling or the use of an expansion protocol to improve spatial resolution. Our adapted 3DISCO protocol allows direct visualization of IHBDs in a simple and efficient manner. Using light-sheet imaging we captured an image of

the entire biliary tree and its changes at different stages of late embryonic and early postanal development. As compared to other approaches cited above, our method has the advantage to produce high resolution images enabling detailed visualization of biliary cell nuclei. The spatial organization and even the relationship between cholangiocytes and the adjacent portal mesenchyme is clearly detectable at the lobe level.

IHBD development

Classical histological sections of the liver normally represent the bile duct as a simple tubular epithelial structure with a clearly detectable lumen located adjacent to the portal vein. Notably, cholangiocytes, without an apparent tubular structure are often not considered. Another controversial structure is the ductal plate described as a plane sheet structure surrounding the branches of the portal vein. We show here that ductules exist in abundance and correspond to the biliary plexus observed in the adult. During the development of the IHBDs, these ductules are the first to form and are then reorganized during morphogenesis. As for the ductal plate, our 3D imaging techniques support that it resembles a mesh-like network of ductules forming a dense and homogeneous network around the portal vein.

Our findings are in line with previous data, which we extend here by showing IHBD development at the lobe level with a higher cellular resolution. We confirm the sequential stages of intrahepatic bile duct development described by Tanimizu et al. (Tanimizu et al., 2016; Tanimizu & Mitaka, 2017) and provide a new level of precision regarding the heterogeneity of cholangiocytes during this process. We validate that in the periphery of E17.5 livers and later stages, newly committed cholangiocytes are not yet incorporated into the homogenous network structure

as they are located too far from each other. This suggests that hitherto unknown mechanisms drive connection of the biliary cells during formation of the ducts.

Next, we describe the maturation process of cholangiocytes using the combination of anti-OPN and anti-CK7 antibodies. We believe that until E17.5, cholangiocytes indeed continuously differentiate near the portal veins to extend the homogenous ductules network and that in parallel, starting from the hilum, a dynamic maturation process occurs giving rise to mature OPN^+ $CK7^+$ cholangiocytes. Later, this more mature part of the homogenous luminal network reorganizes into a hierarchical structure with OPN^+ $CK7^+$ ducts branched to an OPN^+ $CK7^{low}$ biliary plexus. The underlying mechanisms inducing the continuity of the luminal networks are currently unknown as for the one driving the transition from a homogenous to a hierarchical network. Tanimizu et al. suggest that a sufficient number of committed cholangiocytes must be supplied to generate the continuous tubular network and that physical stress induced by bile flow is an important factor promoting hierarchy within this homogenous network (Tanimizu et al., 2016; Tanimizu & Mitaka, 2017). Further, more precise studies, using our protocol on the mouse models used to reach these conclusions, are needed to better understand these pivotal steps in bile duct tubulogenesis.

An unexpected finding during the final stage of maturation of the biliary tree was the restructuring of a convoluted main duct to a straight duct running parallel to the vein. The driving forces for such reshaping may be multiple. Increased intraluminal pressure as a result of evolving bile content in the postnatal period may play a role. However, such change in pressure has, to the best of our knowledge, not been measured and remains speculative. Movement of mesenchymal cells surrounding the duct may allow a change in shape of the ducts.

The composition of the periportal space indeed changes at birth, at least in part with the departure of the hematopoietic cells to the bone marrow.

Finally, it is virtually impossible to count or even estimate the number of bile cells residing in the biliary tree using conventional histological analysis techniques such as tissue sections. It was therefore essential to develop a 3D imaging method that could provide detailed and reliable images of the number of bile cells allowing a quantitative assessment.

Mesenchyme 3D organization

Available data point to mutual interactions between developing bile ducts and the adjacent portal mesenchyme, a tissular structure that is so far very poorly characterized during embryonic development. The goal of the present study was to provide a 3D description of the development of portal mesenchyme, bile ducts and hepatic artery at several developmental stages in the mouse liver.

So far, we visualized bile ducts in parallel with the portal mesenchyme and investigate their spatial relationship and maturation process. We observed that SM22α-expressing mesenchymal cells, which comprise precursors of the *tunica media* of the portal vein and hepatic artery, were irregularly distributed around the portal vein during development, and progressively became restricted to the developing hepatic artery and portal vein. Moreover, we also show that differentiation of the portal mesenchyme around the portal vein precedes that of the biliary cells. Together, our data provide the first description of the 3D spatial and temporal relationship of developing bile ducts, portal mesenchyme and hepatic artery. The close association between IHBDs and portal mesenchyme suggests that

mesenchyme secrete factors inducing portal tract morphogenesis. In the next chapter, we implement gene expression profiling of developing ducts and adjacent portal mesenchyme and investigate the function of genes important for portal tract morphogenesis using transgenic mice.

Summary and perspective

To conclude, our research (i) provides an approach and workflow to comprehensively study bile ducts and/or portal mesenchyme, even simultaneously, at high resolution and in 3D, in experimental animal models, (ii) identify anti-claudin 7, anti-CK7, anti-OPN and anti-SOX9 antibodies as excellent tools to visualize cholangiocyte organization, maturation and remodelling in 3D from embryonic to postnatal stages, (iii) extend earlier observations on the close relationship between mesenchyme and cholangiocytes. While our observations in the current study are still static and based on snapshots at fixed time points, we expect that future time-lapse analysis of the cellular dynamics, such as those employing intravital live imaging system, should uncover the active remodelling process of the biliary epithelial architecture and its surroundings.

v. References

Adori, C., Daraio, T., Kuiper, R., Barde, S., Horvathova, L., Yoshitake, T., . . . Hökfelt, T. (2021). Disorganization and degeneration of liver sympathetic innervations in nonalcoholic fatty liver disease revealed by 3D imaging. *Sci Adv, 7*(30). doi:10.1126/sciadv.abg5733

Brevini, T., Tysoe, O. C., & Sampaziotis, F. (2020). Tissue engineering of the biliary tract and modelling of cholestatic disorders. *Journal of Hepatology, 73*(4), 918-932. doi:https://doi.org/10.1016/j.jhep.2020.05.049

Chen, Y., Bai, L., Zhou, Y., Zhang, X., Zhang, J., & Shi, Y. (2020). Fine-scale visualizing the hierarchical structure of mouse biliary tree with fluorescence microscopy method. *Biosci Rep, 40*(5). doi:10.1042/bsr20193757

Clotman, F., Libbrecht, L., Gresh, L., Yaniv, M., Roskams, T., Rousseau, G. G., & Lemaigre, F. P. (2003). Hepatic artery malformations associated with a primary defect in intrahepatic bile duct development. *J Hepatol, 39*(5), 686-692. doi:S0168827803004094 [pii]

Hankeova, S., Salplachta, J., Zikmund, T., Kavkova, M., Van Hul, N., Brinek, A., . . . Andersson, E. R. (2021). DUCT reveals architectural mechanisms contributing to bile duct recovery in a mouse model for Alagille syndrome. *Elife, 10*. doi:10.7554/eLife.60916

Kamimoto, K., Kaneko, K., Kok, C. Y., Okada, H., Miyajima, A., & Itoh, T. (2016). Heterogeneity and stochastic growth regulation of biliary epithelial cells dictate dynamic epithelial tissue remodeling. *Elife, 5*. doi:10.7554/eLife.15034

Kaneko, K., Kamimoto, K., Miyajima, A., & Itoh, T. (2015). Adaptive remodeling of the biliary architecture underlies liver homeostasis. *Hepatology, 61*(6), 2056-2066. doi:10.1002/hep.27685

Mescher, A. (2010). *Junqueira's Basic Histology: Text & Atlas (12th ed.), by Anthony L. Mescher*.

Ober, E. A., & Lemaigre, F. P. (2018). Development of the liver: Insights into organ and tissue morphogenesis. *J Hepatol, 68*, 1049-1062. doi:10.1016/j.jhep.2018.01.005

Renier, N., Wu, Z., Simon, D. J., Yang, J., Ariel, P., & Tessier-Lavigne, M. (2014). iDISCO: a simple, rapid method to immunolabel large tissue samples for volume imaging. *Cell, 159*(4), 896-910. doi:10.1016/j.cell.2014.10.010

Sampaziotis, F., Cardoso de Brito, M., Madrigal, P., Bertero, A., Saeb-Parsy, K., Soares, F. A., . . . Vallier, L. (2015). Cholangiocytes derived from human induced pluripotent stem cells for disease modeling and drug validation. *Nat Biotechnol, 33*(8), 845-852. doi:10.1038/nbt.3275

Takashima, Y., Terada, M., Kawabata, M., & Suzuki, A. (2015). Dynamic three-dimensional morphogenesis of intrahepatic bile ducts in mouse liver development. *Hepatology, 61*(3), 1003-1011. doi:10.1002/hep.27436

Tanimizu, N., Kaneko, K., Itoh, T., Ichinohe, N., Ishii, M., Mizuguchi, T., . . . Mitaka, T. (2016). Intrahepatic bile ducts are developed through formation of homogeneous continuous luminal network and its dynamic rearrangement in mice. *Hepatology, 64*(1), 175-188. doi:10.1002/hep.28521

Tanimizu, N., & Mitaka, T. (2017). Epithelial Morphogenesis during Liver Development. *Cold Spring Harb Perspect Biol, 9*(8). doi:10.1101/cshperspect.a027862

Vieites-Prado, A., & Renier, N. (2021). Tissue clearing and 3D imaging in developmental biology. *Development, 148*(18). doi:10.1242/dev.199369

Zong, Y., & Stanger, B. Z. (2012). Molecular mechanisms of liver and bile duct development. *Wiley Interdiscip Rev Dev Biol, 1*(5), 643-655. doi:10.1002/wdev.47

Table S1 Primary antibodies

Primary antibodies	Species	Dilution	Application	Antigen retrieval	Reference
Claudine7	Rabbit	1/200	Wholemount 3D	/	Abcam (AB27487)
CK7	Rabbit	1/5000	Wholemount 3D	/	Abcam (AB181598)
OPN	Goat	1/200	Wholemount 3D	/	R&D system (AF808)
SOX9	Goat	1/100	Wholemount 3D		R&D system (AF3075)
Sm22	Rabbit	1/100	Wholemount 3D	/	Proteintech (10493-1-AP)
αSMA	Goat	1/100	Wholemount 3D	/	Novus biologicals (NB300-978)
E-Cadherin	Mouse IgG2a	1/200	IF, paraffin section	MW, citrate	BD Biosciences (610181)
αSMA	Mouse IgG2a	1/75	IF, paraffin section	MW, citrate or EDTA	Agilent Dako (M085101-2)
GFP	Goat	1/100	IF, paraffin section	PT-module, EDTA	Abcam (AB6673)
CD45	Rat	1/50	IF, frozen or paraffin section	Water bath, citrate	BD Biosciences (550539)
CD45	Rabbit	1/100	IHC	Water bath, citrate	Abcam (Ab10558)
Ter119	Rabbit	1/500	IF, paraffin section	MW, citrate	Biolegend (116233)
GFP	Chicken	1/1000	IF, frozen or paraffin section	Water bath, citrate	Abcam (AB13970)
SOX9	Rabbit	1/200	IF, paraffin section	MW, citrate	R&D system (AF3075)

Table S2 Secondary antibodies

Secondary antibodies	Species	Dilution	Applications	Reference
Anti-Rabbit HRP	Goat	1/1000	IHC	Invitrogen (31460)
Donkey Anti-Rabbit IgG (H+L) Cy TM3 AffiniPure	Rabbit	1/500	Wholemount 3D	Jackson Immunores. (711-165-152)
Donkey Anti-Goat igG Alexa Fluor 594	Donkey	1/500	Wholemount 3D	Invitrogen (A2144)
Anti-Rabbit Alexa Fluor 647	Donkey	1/500	Wholemount 3D	Invitrogen (A31573)
Donkey Anti-Rabbit Alexa Fluor 594	Donkey	1/500	Wholemount 3D	Invitrogen (A21207)
Anti-Goat Alexa Fluor 647	Donkey	1/500	Wholemount 3D	Invitrogen (A21447)
Anti-Rabbit Alexa Fluor 647	Donkey	1/1000	IF, frozen or paraffin section	Invitrogen (A31573)
Anti-Mouse total Alexa Fluor 594	Goat	1/1000	IF, frozen or paraffin section	Invitrogen (A32744)
Anti-Rat Alexa Fluor 594	Goat	1/1000	IF, frozen or paraffin section	Invitrogen (A21209)
Anti-Goat Alexa Fluor 488	Donkey	1/1000	IF, frozen or paraffin section	Invitrogen (A11055)
Anti-Chicken Alexa Fluor 488	Goat	1/1000	IF, frozen or paraffin section	Invitrogen (A11039)
Anti-Mouse total Alexa fluor 647	Donkey	1/1000	IF, frozen or paraffin section	Invitrogen (A31571)

Annex:

Videos in mp4 format are available via TRANSVOL.

II. Axon guidance genes control hepatic artery development

Catalina De Schrevel[1,*], Lila Gannoun[1,*], Morgane Belle[2,§], Nicolas Dauguet[3], Younes Achouri[4], Axelle Loriot[1], Christophe Vanderaa[1], Sabine Cordi[1], Yves Heremans[5], Ilse Rooman[5], Patrick Jacquemin[1], Laurent Gatto[1], Frédéric P. Lemaigre[1,6].

[1] de Duve Institute, Université catholique de Louvain, Brussels, Belgium

[2] Sorbonne Universités, UPMC Université Paris 06, INSERM, CNRS, Institut de la Vision, Paris, France

[3] Flow cytometry CYTF platform, Université catholique de Louvain, Brussels, Belgium

[4] Transgene technology platform TRSG, Université catholique de Louvain, Brussels, Belgium

[5] Laboratory of Medical and Molecular Oncology, Vrije Universiteit Brussel, Brussels, Belgium

[6] Corresponding author: Frédéric P. Lemaigre, Avenue Hippocrate 75/B1-7503, 1200 Brussels, Belgium. Tel: +32 2 764 75 83; Email: frederic.lemaigre@uclouvain.be

* These authors contributed equally to the work.

[§] current address: Neurotrials, Paris Brain Institute, Paris, France

Running title: Hepatic artery development

Keywords: Liver development, Slit-Robo signaling, liver mesenchyme.

Summary statement: The hepatic artery is an essential component of the liver vasculature. Here we show how this artery forms and how its development is controlled by Slit/Robo signalling, a pathway best known to control neural development.

i. Abstract

Hepatic lobules consist of hepatocyte cords and sinusoids that radiate from the portal area which contains the portal vein, a bile duct and the hepatic artery. Earlier data demonstrated that development of the bile duct, portal mesenchyme and hepatic artery is interdependent, yet how this interdependency is orchestrated remains unknown. Here, using 2D and 3D imaging, we first describe how mesenchymal cells organize around the portal vein to form hepatic arteries. Next, we searched for intercellular signaling active during portal area development and found that axon guidance genes display differential expression between embryonic stages of bile duct and portal mesenchyme development. We focused on the *Repulsive guidance molecule BMP co-receptor A* (*Rgma*)/*Neogenin 1* (*Neo1*) and *Roundabout 2* (*Robo2*)/*Slit2* ligand receptor pairs and investigated their function in mice using tissue-specific gene inactivation. While *Rgma* and *Neo1* were dispensable for portal area development, *Robo2*/*Slit2* signaling in the portal mesenchyme was required for normal development of the hepatic artery by stimulating the maturation of the vascular smooth muscle cells that form the *tunica media*. In conclusion, our work identifies a new player in development of the liver vasculature.

ii. Introduction

The liver is composed of lobules consisting of hepatocyte cords and sinusoids that radiate from the portal area to the central vein. Each portal area contains a portal vein surrounded by a dense mesenchyme in which hepatic arteries, bile ducts, nerves and lymphatics are encapsulated (Krishna, 2013). Portal lymphatics collect fluid filtered through the sinusoids and drained via the space of Disse (Tanaka & Iwakiri, 2016). Nerves regulate blood flow in the liver and their development is controlled through bile duct-mediated secretion of nerve growth factor (Tanimizu et al., 2018). Bile ducts drain bile produced by hepatocytes toward the intestine. Finally, the portal vein provides nutrients and oxygen to the liver; the artery contributes less than half (~25%) of the hepatic blood flow but supplies ~50% of the oxygen.

During development, the portal mesenchyme derives from the *septum transversum* (Asahina et al., 2009; Asahina et al., 2011). It instructs differentiation of liver progenitors (hepatoblasts) towards biliary cells (cholangiocytes), and subsequently promotes bile duct morphogenesis (reviewed in (Gordillo et al., 2015; Lemaigre, 2020; Ober & Lemaigre, 2018; Tanimizu & Mitaka, 2017). Reciprocally, unknown signals from the bile ducts promote perinatal expansion of the portal mesenchyme, as evidenced by the hypotrophy of the mesenchyme resulting from cholangiocyte-specific inactivation of the SRY-related HMG box transcription factors (SOX) 4 and SOX9 (Poncy et al., 2015).

Hepatic arteries develop in close proximity to the maturing bile ducts. The arteries' endothelium is likely recruited by developing cholangiocytes through secretion of Vascular Endothelial Growth Factor-A (Fabris et al., 2008; Gouysse et al., 2002). The VSMCs forming the artery's *tunica media* are considered to derive from portal

mesenchymal cells (Libbrecht, Cassiman, Desmet, & Roskams, 2002; Villeneuve et al., 2009). Proper arrangement of the arterial VSMCs requires the integrity of the bile ducts, since Hepatocyte Nuclear Factor (HNF)6 or HNF1β knockout mouse livers have disrupted bile ducts and fail to develop normal arteries (Clotman et al., 2003). Development of the hepatic artery occurs according to a similar pattern in mice and humans, except that artery morphogenesis in mice takes place postnatally, while human hepatic arteries form during the foetal period (Clotman et al., 2003).

Here, our objective is to identify genes and signaling pathways that control morphogenesis of the hepatic artery. Our strategy was to search for ligand-receptor pairs expressed in the developing portal mesenchyme and bile ducts and to test their function using gene inactivation strategies. With this approach we uncovered that several axon guidance genes were expressed in the developing portal area. While *Repulsive guidance molecule BMP co-receptor A* (*Rgma*)/*Neogenin 1* (*Neo1*) were dispensable for development of the hepatic artery, we found that *Roundabout 2* (*Robo2*)/Slit2 signaling promotes development of the VSMCs lining the hepatic artery.

iii. Results

Maturation of the portal mesenchyme and hepatic artery development.

At the onset of portal mesenchyme development in human embryonic liver, the smooth muscle cell marker αSMA is known to be detected in most mesenchymal cells. Later, around 20 weeks of development, it becomes restricted to VSMCs lining the artery and portal vein, while the rest of the mesenchyme is αSMA-negative (Libbrecht et al., 2002; Villeneuve et al., 2009). We found that this process is

conserved in mice but takes place in the perinatal period: αSMA expression was detected throughout the portal mesenchyme at postnatal day (P) 1, and progressively became confined to the *tunica media* of the hepatic artery (Fig. 1A). Staining of Smooth Muscle Protein 22 α (SM22α; also called Transgelin, TAGLN), which is co-expressed with αSMA (Fig. S1), was used to visualize the cells in three dimensions (Fig. 1B, Suppl. video 1). SM22α-expressing cells irregularly surrounded the portal vein at E17.5 and P1. At P6 these cells concentrated to form the hepatic arteries near the hilum, while the periphery of the lobes still displayed SM22α-expressing cells scattered in the mesenchyme around the portal vein. Bile duct morphogenesis undergoes profound changes between E16.5 and E18.5 (Takashima et al., 2015; Tanimizu et al., 2016) and, accordingly, preceded formation of the arteries, as illustrated using SOX9 and Osteopontin (OPN) staining (Fig. 1).

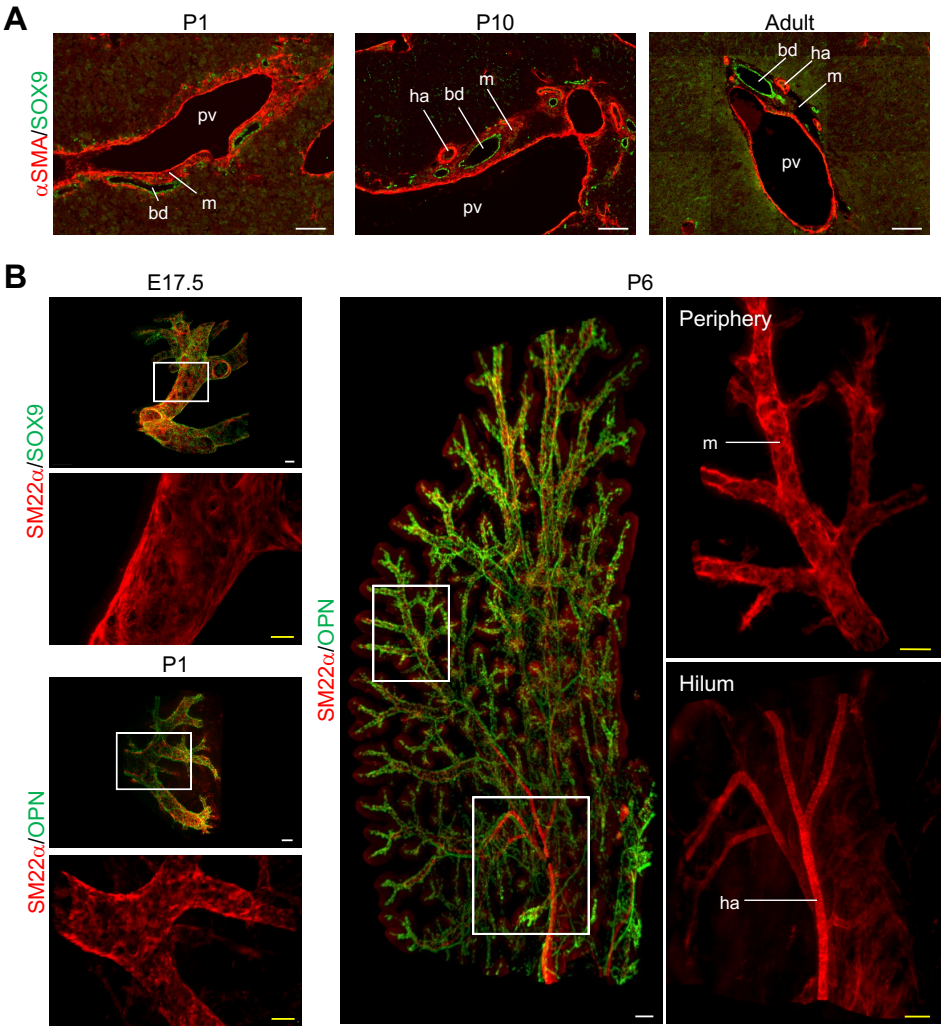


Figure 1: Expression of the smooth muscle cell marker αSMA in the developing portal area. (A) 2D sections show that αSMA-expressing cells are scattered in the portal mesenchyme of postnatal mouse livers and become restricted to the *tunica media* of hepatic arteries when artery development proceeds. **(B)** The same process is illustrated in 3D, using SM22α staining. Development of the artery is first seen near the hilum of the liver, while SM22α-expressing cells are still scattered in the mesenchyme around the portal vein. SOX9 and OPN labeling illustrate bile duct morphogenesis. bd, bile duct; ha, hepatic artery; m, mesenchyme; pv, portal vein. Scale bars: 50 μm (white) and 100 μm (yellow).

Axon guidance signals are expressed in developing bile ducts and portal mesenchyme

To search for novel mesenchyme-bile duct interactions driving hepatic artery development, we separately purified the portal mesenchyme and cholangiocytes from mouse livers at E16.5 and E18.5. We reasoned that these stages correspond to the initiation of intense bile duct remodelling and may therefore also represent a potential transition between developmental stages of the portal mesenchyme. Cholangiocytes were purified from *Sox9-GFP* livers which express GFP specifically in cholangiocytes (Demarez et al., 2018), and mesenchymal cells were isolated from *Sm22α-Cre;Rosa26R*^{eYFP} livers. The latter express eYFP from the *Rosa26* locus when recombined by *Sm22α-Cre* which is reportedly active in the developing portal mesenchyme (Hofmann et al., 2010). We confirmed that *Sm22α-Cre* is active in portal mesenchymal cells: eYFP colocalized in prenatal *Sm22α-Cre;Rosa26R*^{eYFP} livers with αSMA^{+} and αSMA^{-} mesenchymal cells, and postnatally with the VSMCs lining the portal vein and hepatic artery (Fig. 2). Labelling of the mesenchyme using *Sm22α-Cre* was further confirmed by co-staining of eYFP in portal fibroblasts expressing CD90 (Fig. 2). We did not detect eYFP in bile ducts, hepatocytes or endothelial cells. We concluded that *Sm22α-Cre* is appropriate to investigate gene function in developing portal mesenchymal cells.

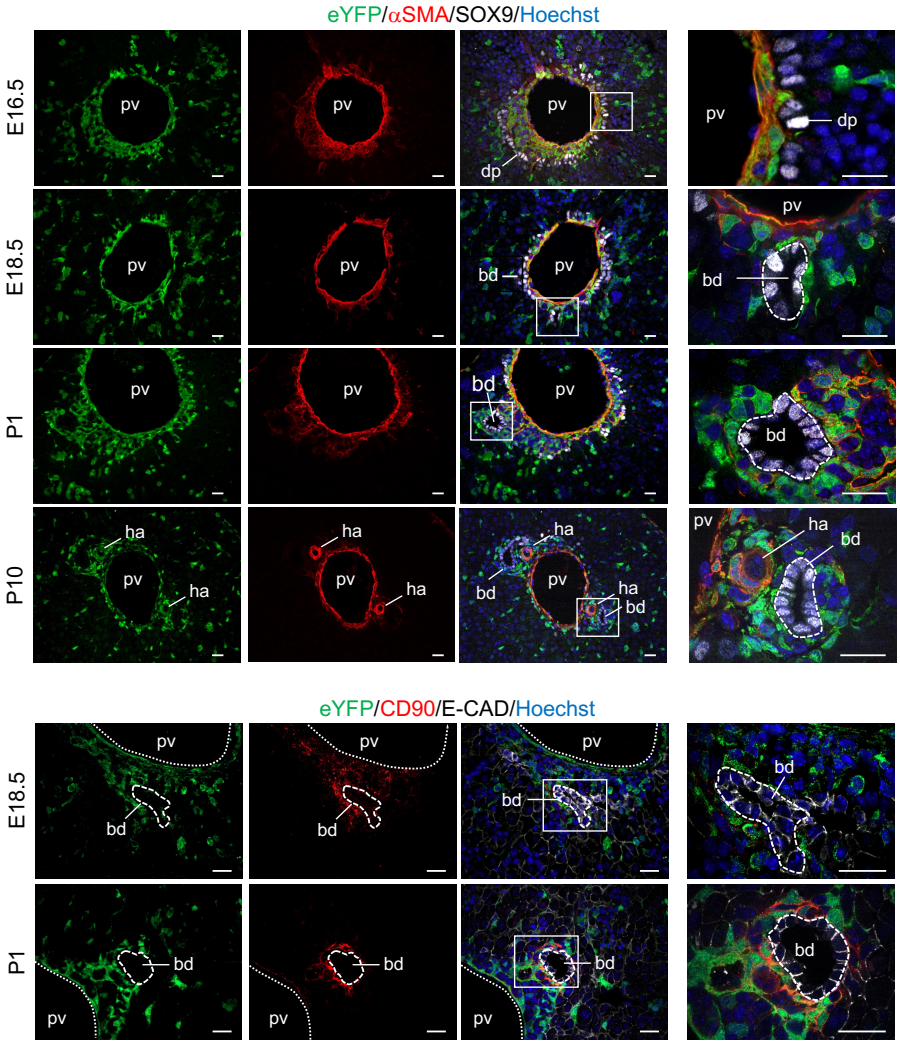


Figure 2: Activity of *Sm22α-Cre* in developing liver. eYFP staining of livers from *Sm22α-Cre;Rosa26R*^{eYFP} mice reflects the activity of *Sm22α-Cre* in the portal tract at the indicated developmental stages. eYFP expression is found in the portal tract mesenchyme, including in αSMA-expressing cells and CD90^{+} fibroblasts, but not in SOX9^{+}/E-CAD^{+} biliary cells. bd, bile duct; dp, ductal plate; ha, hepatic artery; pv, portal vein. Scale bars: 20 μm.

GFP^{+} cholangiocytes and eYFP^{+} mesenchymal cells were purified at E16.5 and E18.5 and subjected to RNA sequencing (Fig. 3A-B). We postulated that genes involved in hepatic artery development should display differential expression between E16.5

and E18.5. Further, we focused on genes coding for ligands produced by cholangiocytes and for their cognate receptors in mesenchymal cells; or *vice-versa*. Fig. 3B provides a pathway enrichment analysis of genes showing a $\log_2$ fold increase ≥ 1 (p_{adj} <0.05) from E16.5 to E18.5.

Our attention was caught by the axon guidance pathway which was enriched during development of both the portal mesenchyme and cholangiocytes. We then decided to focus on the receptor *Roundabout 2* (*Robo2*) and its ligand *Slit2* which earlier single cell RNA sequencing data had identified as the predominantly expressed *Robo* and *Slit* genes during liver development (X. Wang et al., 2020); in addition their expression also showed significant increase from E16.5 to E18.5 in our RNA sequencing analysis (Fig. 3C). We also investigated the *Repulsive guidance molecule BMP co-receptor A* (*Rgma*)/*Neogenin 1* (*Neo1*) pair since, like *Slit/Robo*, it showed significant increase in expression from E16.5 to E18.5 (Fig. 3C).

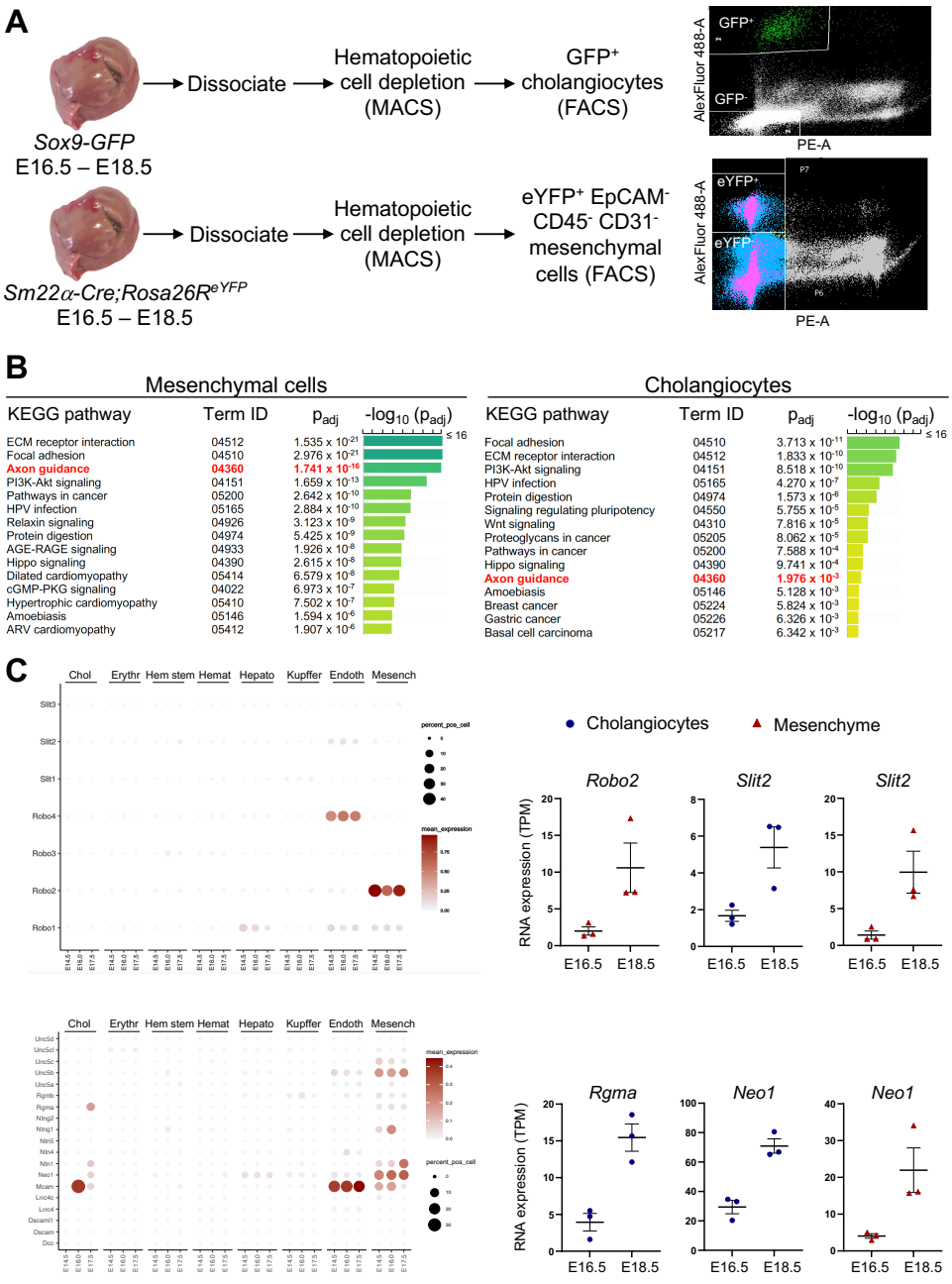


Figure 3: Purification and gene expression in developing cholangiocytes and portal mesenchymal cells. (A) FACS purification procedure to isolate eYFP+ mesenchymal cells and GFP+ cholangiocytes from *Sm22-Cre;Rosa26R*^{eYFP} and *Sox9-GFP* livers, respectively. **(B)** Pathway enrichment analysis of genes upregulated at E18.5 as compared to E16.5 (log_2 fold

change ≥ 1, p_{adj}<0.05) identifies the axon guidance pathway both in mesenchymal cells and cholangiocytes. **(C)** Left panels illustrate Slit/Robo and Netrin signaling genes in single cell RNA sequencing analyses from Wang *et al.* (2020). Right panels show transcripts per million (TPM) detected in bulk RNA sequencing from purified developing cholangiocytes and mesenchymal cells.

Rgma and *Neo1* in developing portal tract

To gain insight into the spatial expression of *Rgma* and *Neo1*, we turned to immunostaining and RNAscope *in situ* hybridization of *Repulsive guidance molecule BMP co-receptor A* (*Rgma*)/*Neogenin 1* (*Neo1*), depending on the availability of functional antibodies. *Rgma* expression was predominantly detected in a subset of developing cholangiocytes at all stages tested; it was also found in very rare mesenchymal cells (Fig. 4A). NEO1 was detected by immunostaining in the developing portal mesenchyme, cholangiocytes and hepatic artery (Fig. 4B). These data prompted us to investigate the morphogenic role of *Rgma* and *Neo1* by conditional inactivation of *Rgma* in developing cholangiocytes using *Sox9-Cre^{ER};Rgma$^{loxP/loxP}$* mice, and by cholangiocyte- and mesenchyme-specific inactivation of *Neo1* using *Sox9-Cre^{ER};Neo1$^{loxP/loxP}$* and *Sm22α-Cre;Neo1$^{loxP/loxP}$* mice.

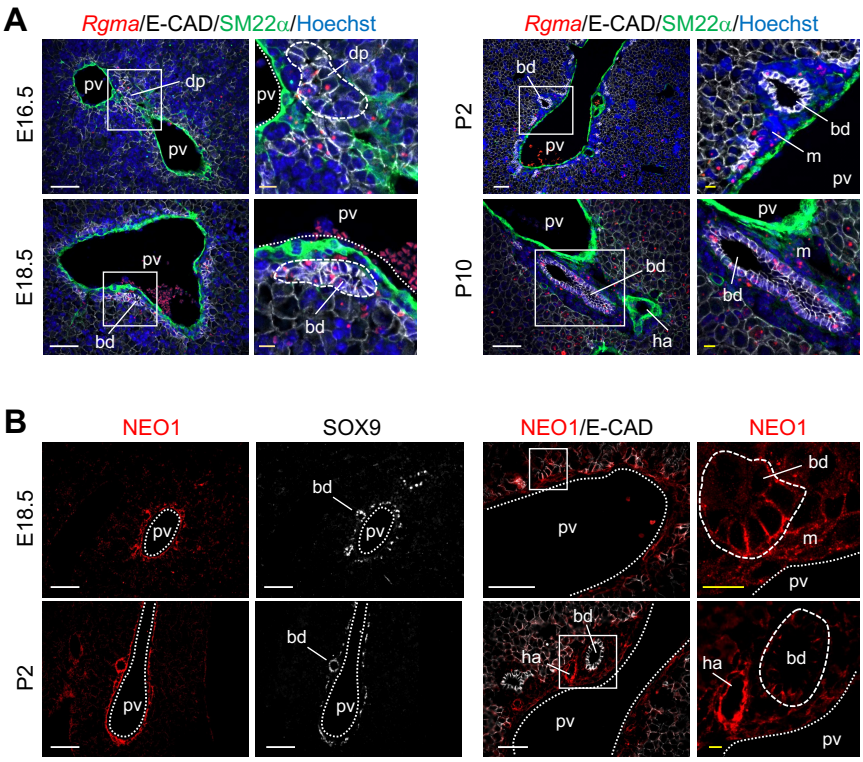


Figure 4: Expression of *Rgma* and NEO1 in the developing portal tract. (A) *In situ* hybridization (RNAscope) detects *Rgma* in a developing cholangiocytes and rare mesenchymal cells. **(B)** NEO1 is found by immunostaining in the developing portal mesenchyme, cholangiocytes and hepatic artery. bd, bile duct; dp, ductal plate; ha, hepatic artery; me, mesenchyme; pv, portal vein. Scale bars: 20 μm.

Females bearing *Sox9-Cre*^{ER};*Rgma*$^{loxP/loxP}$ embryos were injected with tamoxifen at E14.5, and the impact of cholangiocyte-specific inactivation of *Rgma* on portal tract morphogenesis was analyzed at P7 (Fig. 5A). Bile ducts had developed normally and were embedded in portal mesenchyme. They were lined by well-polarized and well-differentiated cholangiocytes, as evidenced by their expression of MUCIN-1 at the apical pole and of the cholangiocyte marker SOX9; the cells did not express the hepatocyte/hepatoblast marker HNF4α. Morphology of the hepatic artery appeared normal as well, as shown by CD31 and αSMA stainings, which label the

endothelium and *tunica media*, respectively. Similarly, at two months of age, no anomaly of the portal tract was noticed (Fig. 5A). The inactivation of *Rgma* in cholangiocytes was confirmed by RNAscope *in situ* hybridization: no *Rgma* RNA could be detected in *Sox9-Cre*^{ER};*Rgma*$^{loxP/loxP}$ livers (Fig. 5B). We concluded that *Rgma* expression in cholangiocytes is dispensable for normal development of the bile ducts and hepatic artery.

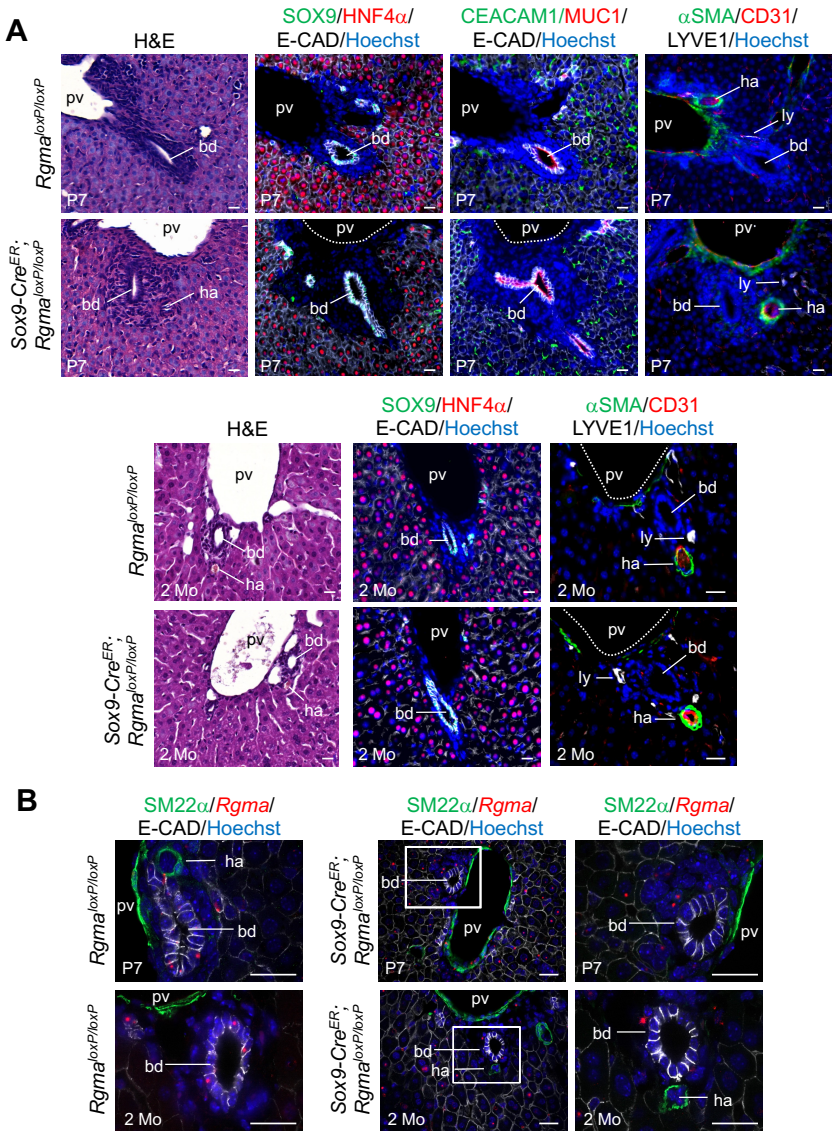


Figure 5: Development of the portal tract in *Sox9-Cre^{ER};Rgma$^{loxP/loxP}$* mice. (A) Cholangiocyte-specific inactivation of *Rgma* during development does not impact morphogenesis of the bile ducts, portal mesenchyme, and hepatic artery, as assessed at P7 (n=3) and 2 months (n=4) following administration of tamoxifen at E14.5. Immunostaining labels cholangiocytes (SOX9, MUC1, E-CAD), hepatocytes (HNF4α, CEACAM1, E-CAD), VSMCs (αSMA, SM22α), endothelium (CD31), and lymphatics (LYVE1). **(B)** *In situ* hybridization confirms the inactivation of *Rgma* in *Sox9-Cre^{ER};Rgma$^{loxP/loxP}$* livers. bd, bile duct; ha, hepatic artery; ly, lymphatics; m, mesenchyme; pv, portal vein. Scale bars: 20 μm.

Cholangiocyte-specific and mesenchyme-specific inactivation of *Neo1* was analyzed at P7 and 2 months in *Sox9-Cre^{ER};Neo1$^{loxP/loxP}$* and *Sm22α-Cre;Neo1$^{loxP/loxP}$* mice which have been injected with tamoxifen at E14.5. The results again showed no morphogenic defect of the portal mesenchyme, bile duct hepatic artery as evidenced by the expression of markers of cholangiocytes (SOX9, E-cadherin), hepatocytes (HNF4α, CEACAM1, E-CADHERIN), hepatic artery (αSMA, VIMENTIN), mesenchyme (VIMENTIN), endothelium (CD31) and apical polarity of cholangiocytes (MUCIN-1) (Fig. 6A and 7A). The inactivation of *Neo1* was confirmed: the basolateral staining in cholangiocytes and mesenchymal staining of NEO1 were abrogated in the knockout livers at E18.5 and E19.5 (Fig. 6B and 7B). Therefore, *Neo1* expression in required neither in cholangiocytes nor in portal mesenchyme for normal morphogenesis of the bile ducts and hepatic artery.

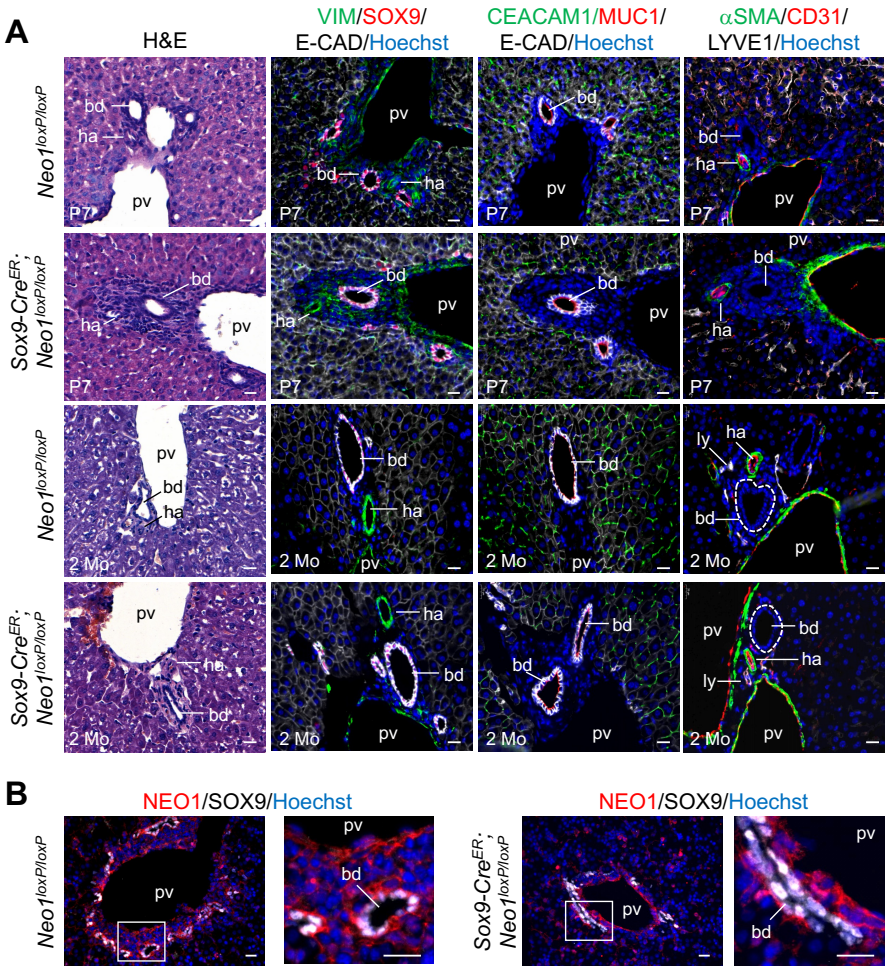


Figure 6: Development of the portal tract in the absence of NEO1 in cholangiocytes. (A) Cholangiocyte-specific inactivation of *Neo1* does not affect morphogenesis of the bile ducts, portal mesenchyme, and hepatic artery, as assessed at P7 (n=3) and 2 months (n=4) in *Sox9-Cre^{ER};Neo1$^{loxP/loxP}$* livers injected with tamoxifen at E14.5. Immunostaining labels Immunostaining labels cholangiocytes (SOX9, MUC1, E-CAD), hepatocytes (CEACAM1, E-CAD), mesenchyme (VIM), VSMCs (αSMA), endothelium (CD31), and lymphatics (LYVE1). **(B)** Immunostaining confirms the absence of NEO1 in *Sox9-Cre^{ER};Neo1$^{loxP/loxP}$* livers at E18.5. bd, bile duct; ha, hepatic artery; ly, lymphatics; pv, portal vein. Scale bars: 20 μm.

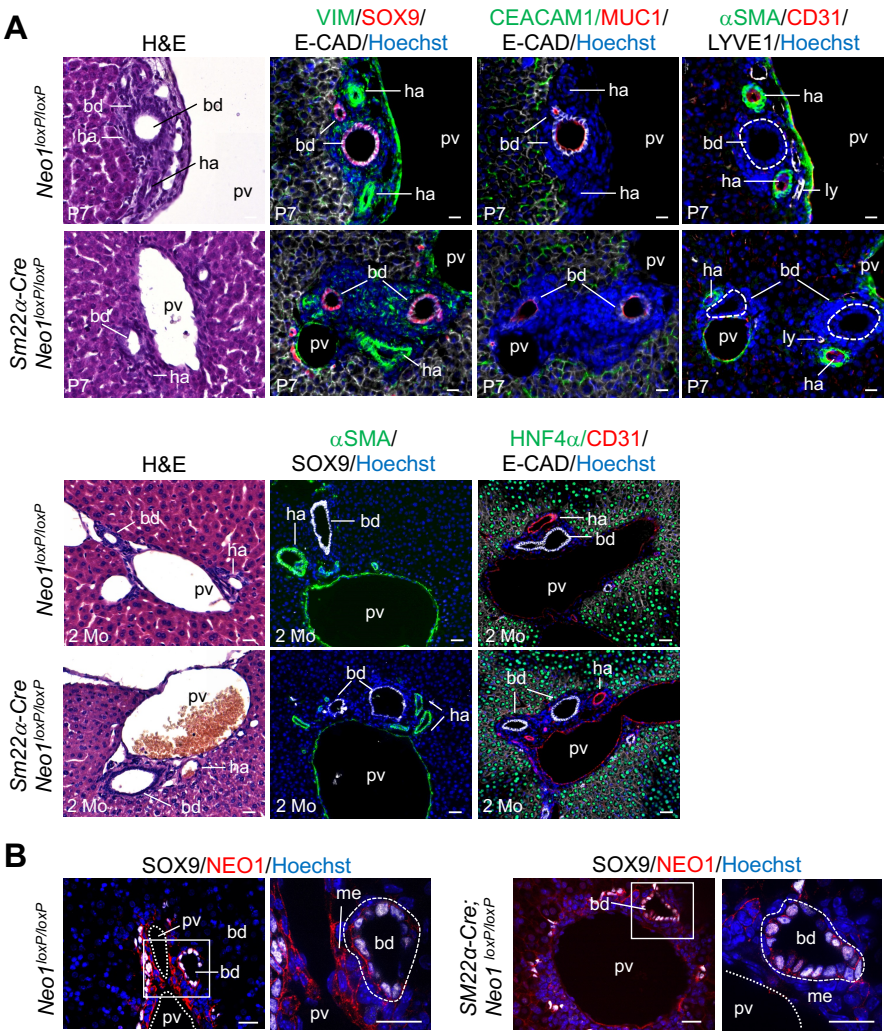


Figure 7: Development of the portal tract in the absence of NEO1 in the portal mesenchyme. (A) Mesenchyme-specific inactivation of *Neo1* does not affect morphogenesis of the bile ducts, portal mesenchyme, and hepatic artery, as assessed at P7 (n=4) and 2 months (n=4) in *Sm22α-Cre;Neo1*$^{loxP/loxP}$ livers. Immunostaining labels Immunostaining labels cholangiocytes (SOX9, MUC1, E-CAD), hepatocytes (CEACAM1, E-CAD), mesenchyme (VIM), VSMCs (αSMA), endothelium (CD31), and lymphatics (LYVE1). (B) Immunostaining confirms the absence of NEO1 in *Sm22α-Cre;Neo1*$^{loxP/loxP}$ livers at E19.5. bd, bile duct; ha, hepatic artery; ly, lymphatics; pv, portal vein. Scale bars: 20 μm.

Expression of *Slit*/*Robo* genes

We then decided to focus on the receptor *Roundabout 2* (*Robo2*) which earlier single cell RNA sequencing data had identified as being strongly expressed in mesenchymal cells during liver development (X. Wang et al., 2020). Its expression showed significant increase from E16.5 to E18.5 in the portal mesenchyme, according to our RNA sequencing analysis (Fig. 3C). Spatially, expression of *Robo2* was detected in the portal mesenchyme: RNAscope *in situ* hybridization mainly identified *Robo2* mRNA in the embryonic portal mesenchyme, predominantly in cells adjacent to developing ducts (E16.5-E18.5); this observation was confirmed at the protein level by immunostaining (Fig. 8A). After birth, at P1 and P10, the number of *Robo2*- expressing cells in the portal mesenchyme progressively decreased. It was detected at low levels in a limited number of periportal CD90-expressing fibroblasts (white arrowheads in Fig. 8A) and in a subset of αSMA-expressing cells at P1. Later, at P10, it was no longer found in αSMA-expressing VSMCs lining the portal vein or hepatic artery (Fig. 8A), in line with single cell RNA-sequencing data which, in adult liver mesenchymal cells, had detected *Robo2* in fibroblasts but not in VSMCs (Fig. S2A). Most *Robo2*$^{+}$ cells were located near the duct and artery. Less relevant to hepatic artery development but confirming earlier data (Lei et al., 2022b), *Robo2* was co-expressed with DESMIN in parenchymal stellate cells (Fig. S2A-B).

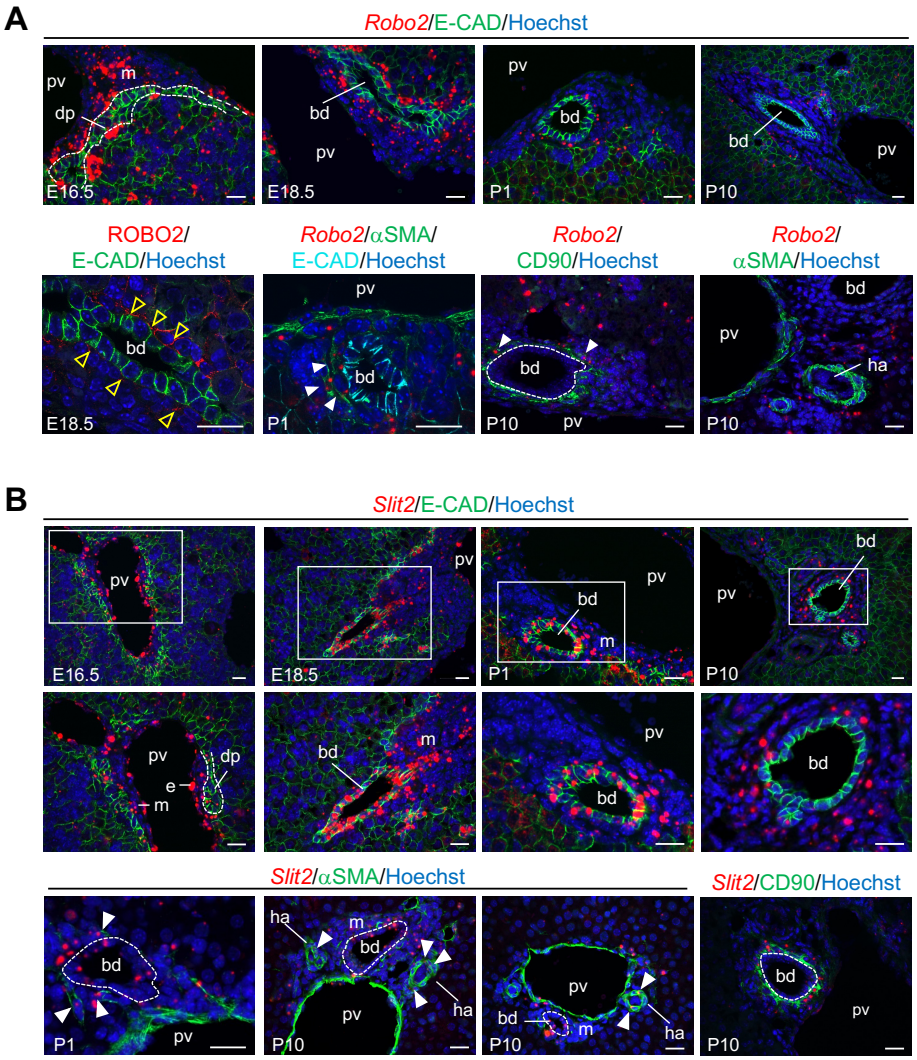


Figure 8: **Expression of *Slit* and *Robo* genes in developing liver. (A)** RNAscope i*n situ* hybridisation and immunostaining reveals *Robo2* RNA and protein (open yellow arrowheads) are expressed in the embryonic and neonatal portal mesenchyme. In the mesenchyme, Robo2 is detected in a subset of CD90+ fibroblasts and at P1 in some αSMA+ cells (white arrowheads). At P10, Robo2 is not detected in the VSMC lining the hepatic artery. **(B)** *Slit2* is transiently expressed in developing cholangiocytes (high E-CAD expression; E16.5 to P1), as well as in the portal mesenchyme at all stages tested. In the mesenchyme, *Slit2* is detected in CD90+ fibroblasts and in a subset of αSMA^{+} cells (white arrowheads) near the bile ducts or lining the artery. bd, bile duct; dp, ductal plate; e, endothelium; ha, hepatic artery; m, mesenchyme; pv, portal vein. Scale bars: 20 µm.

The ROBO ligands are SLIT-1, -2 and -3. Their expression was below detection level in the single cell RNA sequencing analyses of embryonic liver (X. Wang et al., 2020). However, using the more sensitive RNAscope *in situ* hybridization, we detected *Slit3* in portal endothelial cells at a distance from the developing bile ducts and in a small subset of cholangiocytes; *Slit1* was barely detectable in the developing portal area (Fig. S2B). SLIT2 was considered more attractive as a regulator of hepatic artery development. Indeed, *Slit2* expression in liver was strongest in the portal area, where it was detected in cholangiocytes lining developing ducts, in mesenchymal cells and in portal endothelium (Fig. 8B). This expression was transient in biliary cells (E16.5 to postnatal day (P) 1) and portal endothelium (E16.5-E18.5) but was detected at all pre- and postnatal stages tested in the mesenchyme. In the mesenchyme, *Slit2* was detected in $CD90^{+}$ fibroblasts. lt was also detected in αSMA-positive cells near the bile ducts at P1, *i.e.* prior artery formation, as well as in a subset of VSMCs lining the artery at P10 (white arrowheads in Fig. 8B), Parenchymal DESMIN-expressing stellate cells did not show Slit2 expression (Fig. S2B). This fitted with the single cell RNA-sequencing data of Henderson's and Housset's teams who, later in adult liver mesenchymal cells essentially detected *Slit2* in fibroblasts and in a subset of VSMCs (Fig. S2A) (Dobie et al., 2019; Lei et al., 2022b).

We concluded that SLIT2/ROBO2 signaling, either between $ROBO2^{+}$ and $SLIT2^{+}$ mesenchymal cells or between $ROBO2^{+}$ mesenchyme and $SLIT2^{+}$ cholangiocytes, was a candidate regulator of hepatic artery development.

Slit2 expression in developing cholangiocytes is dispensable for hepatic artery and bile duct morphogenesis

To investigate if production of SLIT2 by cholangiocytes might impact hepatic artery formation or bile duct morphogenesis, we conditionally inactivated its expression by mating *Slit2*$^{loxP/loxP}$ mice with *Alfp-Cre* mice. The *Alfp-Cre* transgene induces recombination of loxP-flanked genes in hepatoblasts, meaning that the progeny of these cells, namely cholangiocytes and hepatocytes, have their loxP-flanked alleles inactivated. Hepatic arteries displayed a normal phenotype in P10 *Alfp-Cre;Slit2*$^{loxP/loxP}$ knockout livers, as shown by immunostaining of their *tunica media* using antibodies against SM22α and αSMA, or by detection of ELASTIN (Fig. S3A). Moreover, the *Alfp-Cre*;*Slit2*$^{loxP/loxP}$ mice showed normal biliary ducts (Fig. S3B). The ducts were delineated by well-differentiated and well-polarized cholangiocytes, as evidenced by their transcription factor profile (SOX9^{+}, HNF4α^{-}, C/EBPα^{-}), and by the location of β-CATENIN and E-CADHERIN at the basolateral sides, and MUCIN1 at the apical poles. The muscular layer surrounding the portal vein appeared normal as well and neural class III tubulin (TUBB3)-expressing nerves were also detected in the portal space of the mutant livers (Fig. S3C). We concluded that expression of *Slit2* is dispensable for normal development of the portal vasculature and bile ducts.

Slit2 expression in mesenchymal cells is dispensable for bile duct development but is required for normal morphogenesis of hepatic arteries

We next addressed the role of *Slit2* expression in the portal mesenchyme by mating the above described *Sm22α-Cre* mice with *Slit2*$^{loxP/loxP}$ mice. Here again we found no biliary anomaly: at P10, *Sm22α-Cre;Slit2*$^{loxP/loxP}$ mice developed bile ducts with normal morphology and surrounded by well-polarized and well-differentiated

cholangiocytes (Fig. S4A). There was no evidence of cholestasis as shown by normal levels of plasma bilirubin (Fig. S4B). Moreover, retrograde injection of ink in the common bile duct followed by tissue clearing did not reveal anomalies of the intrahepatic biliary tree (Fig. S5C). TUBB3-expressing nerves were detected in the portal space of the control and mutant livers, as well as $LYVE1^{+}$ lymphatics (Figs. 9A and S4A).

However, when immunostaining to detect αSMA, SM22, and SMOOTHELIN, we observed arterial anomalies in the *Sm22α-Cre;Slit2*$^{loxP/loxP}$ mice at P10. The arterial phenotype was variable, with approximately 50% of animals (6 out of 11) displaying no detectable phenotype, the others (5 out of 11) presenting with a reduction in the thickness of the *tunica media* ranging from nearly no VSMCs surrounding the arterial endothelium to a limited decrease in the arterial wall's thickness. Fig. 9A illustrates three phenotypes observed in *Sm22α-Cre;Slit2*$^{loxP/loxP}$ mice, namely the presence of normal arteries, the lack of detectable VSMCs around the arteries, and an intermediate phenotype with reduced thickness of the artery's muscular layer. This phenotype was confirmed quantitatively (Fig. 9B). We measured the ratio of the surface of the muscle layer to the total artery area; this was significantly reduced in the knockouts. Accordingly, the ratio of the arterial luminal area to the total artery area was increased in the mutant livers.

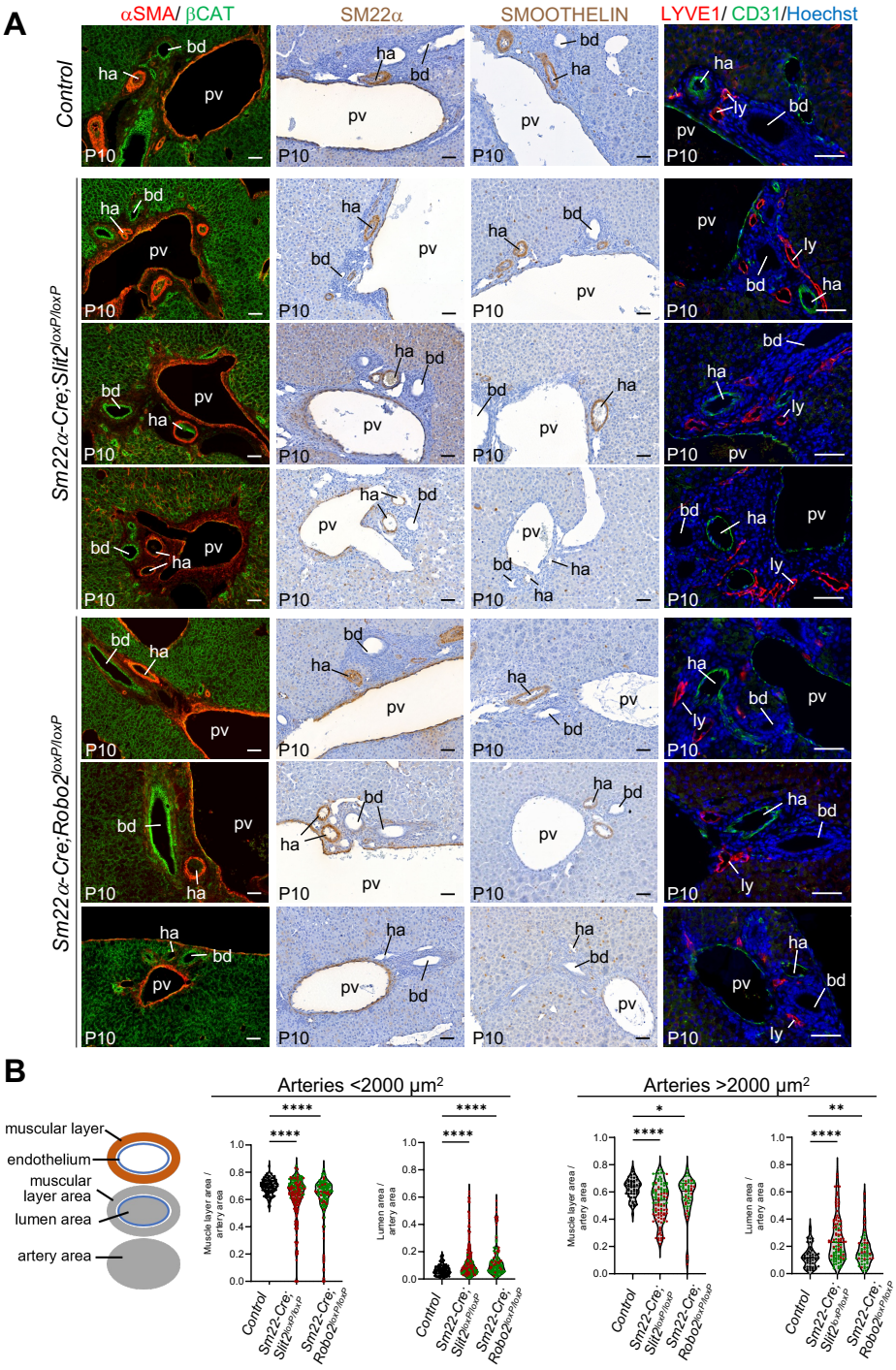

A
αSMA/ βCAT
SM22α
SMOOTHELIN
LYVE1/ CD31/Hoechst
Control
Sm22α-Cre;Slit2loxP/loxP
Sm22α-Cre;Robo2loxP/loxP
bd
ha
pv
ly
P10
B
muscular layer
endothelium
muscular layer area
lumen area
artery area
Arteries <2000 µm²
Arteries >2000 µm²
Muscle layer area / artery area
Lumen area / artery area
Control
Sm22-Cre; Slit2loxP/loxP
Sm22-Cre; Robo2loxP/loxP

Figure 9: *Slit2* or *Robo2* inactivation in portal mesenchymal cells perturbs muscle layer formation around hepatic arteries. (A) Immunostaining of αSMA, SM22α and SMOOTHELIN reveals normal muscle layer (6 out of 11 *Sm22α-Cre;Slit2$^{loxP/loxP}$* and 5 out of 7 *Sm22α-Cre;Robo2$^{loxP/loxP}$*), a decrease in muscle layer thickness (4 out of 11 *Sm22α-Cre;Slit2$^{loxP/loxP}$* and 1 out of 7 *Sm22α-Cre;Robo2$^{loxP/loxP}$*) or a lack of muscle layer (1 out of 11 *Sm22α-Cre;Slit2$^{loxP/loxP}$* and 1 out of 7 *Sm22α-Cre;Robo2$^{loxP/loxP}$*) around the hepatic arteries. Immunostaining of CD31 and LYVE1 shows normal endothelial cells and presence of lymphatic vessels in wild-type and mutant mice. bd, bile duct; ha, hepatic artery; L, lymphatic vessel; pv, portal vein. Scale bars: 50 μm. **(B)** The muscle layer and lumen area of hepatic arteries were measured, showing a significantly reduced thickness of the muscle layer and increased lumen area, both in small (<2000 μm^2) and large (>2000 μm^2) arteries. Two-tailed t-test with Welch's correction* p<0.5; ** p<0.1; ***p<0.01; **** p<0.001). Dots represent individual measurements (Table S3). Black dots, hepatic arteries in wild-type mice; green dots, hepatic arteries in mutant mice showing a normal muscle layer; red dots, hepatic arteries in mutant mice with decreased muscle layer thickness. Black line is median.

To avoid a potential bias related to arterial size, these measurements were performed on hepatic arteries that have a cross-sectional area inferior or superior to 2000 μm^2. The number of animals and hepatic arteries measured in these experiments is shown in Table S1. The phenotypic heterogeneity did not reflect variable efficiency of *Sm22α-Cre*-mediated inactivation of the *Slit2* gene. *Sm22α-Cre* is indeed widely active in the portal mesenchyme of all animals as determined by eYFP induction in *Sm22α-Cre;Rosa26R^{eYFP}* livers (Figs. 2). Moreover, *in situ* RNA hybridization using a BaseScope probe targeting the floxed exon 8 of *Slit2* showed efficient inactivation of the gene, in all portal areas (Fig. S5). Therefore, the heterogeneous phenotype resulted from biological but not from technical variability.

We next hypothesized that the reduced *tunica media*, may impact the overall morphology of the hepatic artery and therefore visualized the artery using ink injection. The results showed that control livers displayed straight artery branches, whereas localized distortions were observed in a subset of artery branches of *Sm22α-Cre;Slit2$^{loxP/loxP}$* livers (red arrows in Fig. 10). Portal vein morphology was

normal as evaluated by ink injections (Fig. S6). Consistent with the phenotypic variability of the mice, only a subset of mice displayed the morphological anomalies.

We concluded that the expression of *Slit2* in the portal mesenchyme is not required for bile duct formation but is necessary for normal development of the VSMCs that constitute the *tunica media* of the hepatic artery.

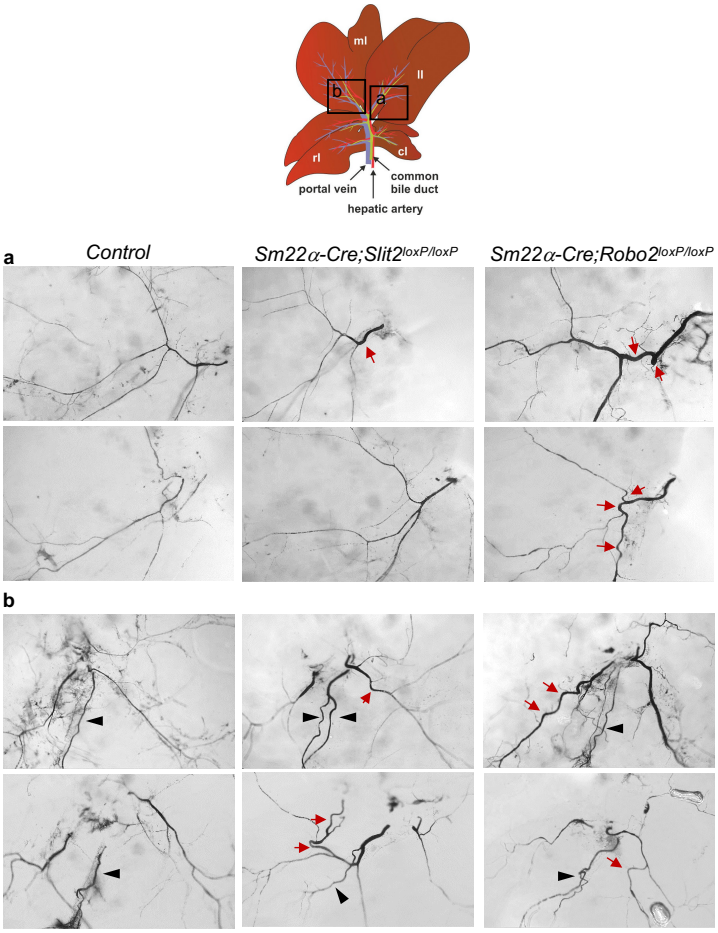


Figure 10: *Slit2* or *Robo2* inactivation in portal mesenchymal cells modifies the shape of hepatic arteries. Ink injection in the gastroduodenal artery followed by clearing of median lobe (a) and left lobe (b) shows a irregularly-shaped morphology (red arrowheads) of the

arteries in 2 month-old *Sm22α-Cre;Slit2*$^{loxP/loxP}$ (2 out of 4) and *Sm22α-Cre;Robo2*$^{loxP/loxP}$ (2 out of 4) mice, compared to wild-type mice (n=5). Black arrowhead, gallbladder artery.

Robo2 expression in mesenchymal cells is dispensable for bile duct development but is required for normal morphogenesis of hepatic arteries

Since SLIT2 is a ligand of ROBO2, we hypothesized that the latter is involved in hepatic artery development and generated *Sm22α-Cre;Robo2*$^{loxP/loxP}$ mice in which *Robo2* is inactivated in the mesenchyme. Similar to *Slit2* inactivation in the mesenchyme, no evidence was found for abnormal differentiation and polarity of cholangiocytes, or for abnormal morphogenesis of bile ducts in *Sm22α-Cre;Robo2*$^{loxP/loxP}$ mice (Fig. S4). Portal nerves (TUBB3^{+}) and lymphatics (LYVE1^{+}) were also detected normally, and liver function assessed by plasma levels of hepatic enzymes, albumin and bilirubin was unaffected (Figs. 9A and S4A-B). The efficiency of *Sm22α-Cre*-mediated inactivation of *Robo2* was demonstrated using ROBO2 protein immunostaining and BaseScope *in situ* hybridization targeting the floxed exon 5 (Fig. S5).

However, again similar to *Sm22α-Cre;Slit2*$^{loxP/loxP}$ mice, a subset of *Sm22α-Cre;Robo2*$^{loxP/loxP}$ mice displayed hepatic artery anomalies. Two mice out of 7 showed reduced or lack of detectable muscular layer, as evidenced by αSMA, SM22α, SMOOTHELIN and ELASTIN stainings (Figs. 9A and 11A). This phenotype was confirmed quantitatively using the same measurements as those performed in *Sm22-Cre; Slit2*$^{loxP/loxP}$ livers (Fig. 9B). Ink injection into the hepatic artery further revealed perturbed morphology, with artery branches showing localized distortions, again like in SLIT2-deficient livers (Fig. 10B). Portal vein morphology was normal (Fig. S6).

Since, the phenotype resulting from *Robo2* inactivation in the portal mesenchyme is similar to that of *Slit2* inactivation, we suggests that ROBO2 is the receptor of SLIT2 during development of the hepatic artery's *tunica media*.

SLIT2/ROBO2 signaling controls differentiation of vascular smooth muscle cells lining the hepatic artery

During vessel formation, VSMCs undergo profound changes which includes their differentiation from an immature synthetic state characterized by proliferation and synthesis of extracellular matrix, to a mature and quiescent contractile state identified by the production of contractile markers specific to smooth muscle (Owens, Kumar, & Wamhoff, 2004). Although such distinction between the two states does not perfectly reflect the entire phenotypic spectrum of VSMCs, it remains useful to characterize potential anomalies occurring during development. To address the possibility that SLIT2/ROBO2 signaling is required for the hepatic artery's VSMCs to mature from a synthetic to contractile state we measured the expression of phenotypic markers. Since this transition is expected to occur perinatally, *i.e.* when the VSMCs aggregate around the hepatic artery endothelium (Fig. 1), we purified the portal mesenchyme at P10 and measured the expression of synthetic and contractile markers. Considering the inter- and intra-organ heterogeneous arterial phenotype (Fig. 9), and the need for sufficient amounts of liver tissue for purification of portal mesenchyme, it is not possible to keep a part of the tissue for histological analysis and to verify if a collected liver belongs to the category of those that display or not a morphological arterial defect. To circumvent this problem, we decided to evaluate the state of the mesenchyme by RT-qPCR analysis of a phenotypic index that corresponds to the ratio of expression of synthetic (*Col15A1*, *Fbln2, Dnmt1*) versus contractile (*Cnn1*, *Eln*, *Smtn*) markers.

Expression of these markers was normalized to that of the pan-mesenchyme marker Vimentin. This was justified by our observation that expression of mature contractile markers SMOOTHELIN and ELASTIN is reduced in *Sm22α-Cre;Slit2*$^{loxP/loxP}$ and *Sm22α-Cre;Robo2*$^{loxP/loxP}$ mice at P10 (Figs. 9A and 11A). The phenotypic index, calculated as indicated in Fig. 11B, shows that the synthetic state is increased in purified portal mesenchymal cells from mice that lack *Slit2* or *Robo2* expression, reflecting that the number of cells reaching VSMC maturity is reduced. Proliferation of aSMA+ cells at P10, analyzed by phospho-histone H3 labeling, was low or undetectable at P10 in control liver as well as in mutant livers (Fig. 11C). Therefore, we concluded that the increased ratio of synthetic versus contractile gene expression reflects that VSMCs fail to mature normally in the mutant livers.

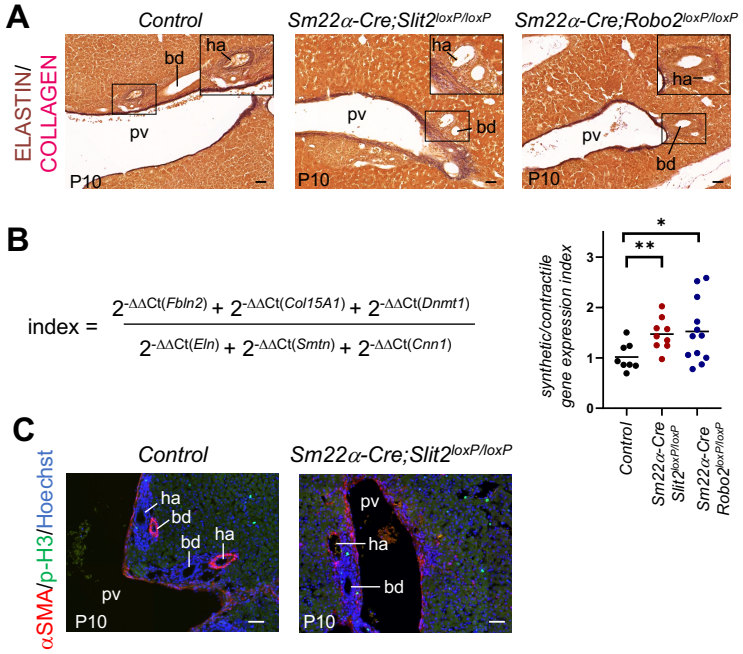


Figure 11: *Slit2* or *Robo2* inactivation in portal mesenchymal cells affects the maturation of VSMCs (A) Reduced ELASTIN staining around hepatic arteries in *Sm22α-Cre;Slit2*$^{loxP/loxP}$ and *Sm22α-Cre;Robo2*$^{loxP/loxP}$ mice. **(B)** Left: the maturation of VSMCs was evaluated using an index calculated by the sum of expression of markers of the synthetic state divided by the sum of expression of markers of the contractile state. Expression levels are relative to

the pan-mesenchymal marker *Vimentin* and were calculated by RT-qPCR using the ΔΔCt formula. Right: maturation index of VSMCs in *Sm22α-Cre;Slit2$^{loxP/loxP}$* and *Sm22α-Cre;Robo2$^{loxP/loxP}$* mice at P10 suggests that the lack of *Slit2* or *Robo2* expression favours maintenance of a synthetic state. *Cnn1*, *Calponin1*; *Col15A1*, *Collagen15A1*; *Dnmt1*, *DNA methyltransferase1*, *Eln*, *Elastin*; *Fbln2*, *Fibuline2*; *Smtn*, *Smoothelin*. **(C)** Proliferation visualised using phospho-histone H3 (p-H3) labeling does not uncover a difference in the proliferation of αSMA$^+$ cells in control and Slit2-deficient portal mesenchyme. bd, bile duct; ha, hepatic artery; pv, portal vein. Scale bars: 50 µm.

iv. Discussion

Available knowledge on the role of axon guidance genes in the liver is mainly restricted to disease conditions. More specifically, the SLIT/ROBO pathway was studied during fibrosis and ductular reactions and was shown to promote fibrosis and neoangiogenesis (J. Chang et al., 2015; Coll et al., 2022; Lei et al., 2022b; Pi et al., 2022; Zeng et al., 2018). In hepatocellular carcinoma, expression levels of *ROBO* and *SLIT* genes are predictive of tumor stage (Avci et al., 2008). In the present manuscript we illustrate how portal mesenchymal cells organize to form the hepatic artery and propose that SLIT2/ROBO2 signaling regulates the formation of the artery's *tunica media* by promoting maturation of the VSMCs.

Expression of *Robo2* and *Slit2* was found at P1, *i.e.* prior to artery formation, in CD90$^+$ portal fibroblasts and αSMA$^+$ cells located near the bile ducts. When the artery wall had developed at P10, *Slit2* but not *Robo2* was detected in the VSMCs forming the *tunica media*. No expression of *Slit2* or *Robo2* was detected in the hepatic artery's endothelium. This profile raises the possibility that during hepatic artery development SLIT2/ROBO2 signalling occurs between fibroblasts and αSMA$^+$ cells that are VSMC precursors. In this scenario fibroblasts would promote VSMC maturation. Alternatively, SLIT2/ROBO2-mediated signalling between αSMA$^+$ VSMC precursors may be required for VSMC maturation. Yet another alternative is

that SLIT2/ROBO2-mediated interactions between fibroblasts would secondarily impact on VSMC development. How intercellular signalling is mediated to control VSMC development remains unknown.

While the heterogeneity of the liver mesenchyme has been well characterized in adults (T. S. Andrews et al., 2022; Dobie et al., 2019; Lei et al., 2022b), investigation of the cell-cell and molecular mechanisms driving VSMC maturation requires better knowledge of the portal mesenchymal cell populations in the pre- and perinatal periods. Lei et al. identified 5 subpopulations of VSMCs characterized by specific markers (Lei et al., 2022a). However, these markers were expressed at too low levels for accurate investigation in mesenchyme purified at P10 (data not shown), likely indicating that VSMC maturation is not yet terminated at that stage. Further, increased knowledge of the spatial functions of the mesenchymal cells in the portal space is needed. Indeed, we note that *Robo2* expression is predominantly localised in the vicinity of bile ducts, and that inactivating *Slit2* or *Robo2* did not impact development of the narrow muscular layer surrounding the portal vein.

Several guidance molecules play a role in artery patterning, but the role of SLIT-ROBO signalling in this context remains obscure (Finney & Orr, 2018). SLIT2 produced by endothelial cells and VSMCs is a known repellent of arterial VSMCs (D. Liu et al., 2006). This function was investigated *in vitro* but the physiological relevance of this observation is unclear. Portal VSMCs fated to form the hepatic artery may exhibit migrational defects in the absence of SLIT2/ROBO2 signaling. Such defect could be associated with a lack of VSMC maturation. Migrational anomalies cannot easily be investigated *in vivo* in developing mouse liver. We currently lack information about VSMC precursors to be able to purify these cells and track their migrational behavior *in vitro* in response to SLIT-ROBO stimuli. Also,

in vitro data on VSMCs have yielded several data that were contradicting *in vivo* findings (Owens et al., 2004), thereby prompting the need to design assays that recapitulate the hepatic arteries' specificities *in vitro*. Endothelial cells can recruit VSMCs during arteriogenesis. The lack of *Slit2* or *Robo2* detection in the hepatic artery's endothelium prompts us to rule out that the arterial defect seen in the mutant mice results from an endothelial cell defect.

Future investigation of hepatic mesenchyme development requires *Cre*-driver mice with higher cell-specificity than *Sm22α-Cre*. Greenhalgh *et al.* listed mouse lines with Cre activity in non-parenchymal cells of the liver (Greenhalgh, Conroy, & Henderson, 2015). *Pdgfrb-Cre* and *Lrat-Cre* are active in adult portal mesenchyme but no information is available on prenatal activity (Henderson et al., 2013; Mederacke et al., 2013). In the present manuscript, we selected the *Sm22α-Cre* line described by Holtwick *et al.* (Holtwick et al., 2002). The alternative *Sm22α-CreKI* is reportedly not functional in the embryo (J. Zhang et al., 2006). *Vimentin-Cre^{ER}* is not active in the portal mesenchyme of homeostatic liver (Troeger et al., 2012). *Gata4-G2-Cre* marks the *septum tranversum* cells, but also a subset of CD45^{+} leucocytes, which may interfere with our objective to investigate portal mesenchymal cells since CD45^{+} cells are present in the periportal space (Delgado et al., 2014).

In conclusion, our work raises novel questions and identifies future needs to tackle the function of the portal mesenchyme in development. It also uncovers that SLIT/ROBO signaling is a novel regulator of the development of the liver vasculature.

v. Materials and methods

Animals

Mice (*Mus musculus*) received humane care and the research protocol was approved by the Animal Welfare Committee of the Université Catholique de Louvain with numbers 2018/UCL/MD/014 and 2022/UCL/MD/16. All mice were housed under a 12h light/dark cycle in individually ventilated cages supplied with RM3 chow (#801700, Tecnilab, Someren, Netherlands), acidified water, and polyvinyl chloride play tunnels. *Alfp-Cre*, *Smα22-Cre*, *Sox9-Cre^{ER}*, *Robo1$^{-/-}$;Robo2$^{loxP/loxP}$*, *Robo2$^{loxP/loxP}$*, *Rgma$^{loxP/loxP}$* and *Slit2$^{loxP/loxP}$* mice have been described (Holtwick et al., 2002) (Kellendonk, Opherk, Anlag, Schutz, & Tronche, 2000; Kopp et al., 2011; Long et al., 2004; W. Lu et al., 2007; Rama et al., 2015) and were kindly provided by F. Tronche, W. Martinet, M. Sander, F. Spagnoli, V. Mirakaj and A. Chédotal. *Rosa26R^{eYFP}* and *Sox9-GFP* mice have been described (S. Gong et al., 2003; Srinivas et al., 2001).

Neo1$^{loxP/loxP}$ mice were generated using the cloning-free CRISPR-Cas9 system (Aida et al., 2015). Guide RNAs were designed using CRISPRdirect (Naito, Hino, Bono, & Ui-Tei, 2015). Two guide RNAs targeting sequences 5' and 3' of exon 4 were designed. Each guide RNA consists of a crRNA (20 nucleotides), corresponding to the target sequence with a tail (16 nucleotides), and a tracRNA (67 nucleotides; 1072534, Integrated DNA Technologies, Leuven, Belgium), containing the hairpin recognized by CAS9 with an extremity complementary to the crRNA tail. Two long single-strand oligonucleotides containing homology arms and loxP sequence were synthesized (Integrate DNA Technologies) as Ultramer DNA and used as repair template for homologous direct repair. crRNAs and single-stranded DNA

oligonucleotides are as follows: crRNA-1 (5'), 5' CGGCTGTTTGTACCCTCGTG 3'; crRNA-2 (3'), 5' ACATCAACCCCTCTACTGAC 3'; Ultramer 1 (5'), 5'AGTCAGTAGGAAGGGACACACAGGTATTGAGTTTGTTTAGTCTCGGCTGTTTGTACCC TCGCTAGCataacttcgtataATGTATGCtatacgaagttatGTGTGGTATTGTATAGATTCATGTT GTGTGTTCCTCATGTGACCAGAAAGCACCATGTAA 3'; Ultramer 2 (3'), 5'CTTGAAAGGCATTTTTATGTTGTGTCTATGGTGTTTAAAGAAAAAGCATGCTTTCCAGT CGAATTCataacttcgtataATGTATGCtatacgaagttatAGTAGAGGGGTTGATGTTGCTGCTG CTGCTGTTAACCTTCATTATAGCTAGCTTGCAAGG 3'.

Annealed crRNA/tracrRNA (2.4 pmol/µl), recombinant CAS9 nuclease V3 (200ng/µl; Integrated DNA Technologies) and both single-strand DNA donors (5 ng/µl each) were mixed in IDTE buffer (11-01-02-02, Integrated DNA technologies) and injected into the pronucleus of B6D2F2 mouse zygotes. Injected zygotes were incubated in KSOM medium at 37°C for at least 2 hours before being transferred into oviducts of CD1 pseudo-pregnant female mice. Identification of the positive founders with insertion of both loxP sites was done by PCR genotyping and confirmed by Sanger sequencing. Cre-mediated recombination induces the deletion of loxP-flanked exon 4, creating a frame shift and premature stop codon, leading to a putative small protein of 255 aa instead of full-length NEOGENIN.

Purification of mesenchymal cells and cholangiocytes

For RNA sequencing analysis of embryonic cells, pools of 15 livers at embryonic day E16.5 or E18.5 were dissected and mechanically dissociated using scalpel blades as described (Van Liedekerke et al., 2022). Briefly, *Sox9-GFP* or *Sm22α-Cre;Rosa26R^{eYFP}* livers were used for purification of cholangiocytes or mesenchymal cells, respectively. Subsequent chemical dissociation was performed in DMEM-F12 (#31870-025, Gibco, Life technologies, Lederberg, Belgium) containing 1 mg/ml

collagenase IV (#43E14253, Worthington, New Jersey, USA), 1 mg/ml dispase (#17105-041, Gibco, Life Technologies) and 0.1 mg/ml of DNAse I (#11284932001, Roche, Mannheim, Germany) for 30 min at 37°C. An equal volume of 10% fetal bovine serum (FBS) in phosphate buffered saline (PBS) was added to stop the digestion, and cells were resuspended in 2 mM EDTA, 0.5% bovine serum albumin (BSA) in PBS and filtered on 40 µm cell strainer (#087711, Fisher Scientific Merelbeke, Belgium). Hematopoietic cells were eliminated by magnetic cell sorting using the Lineage cell depletion kit (#130090858, Miltenyi Biotech Paris, France) which contains antibodies against CD5, CD45R (B220), CD11b, Gr-1 (Ly-6G/C), 7-4, Ter-119. The cells were subjected to flow cytometry (BD FACSAria III, sample and collection tubes maintained at 4°C) and GFP^+ cholangiocytes or $eYFP^+$ $CD45^-$ $CD31^-$ $EpCAM^-$ mesenchymal cells were purified. Antibodies used in flow cytometry are listed in Table S2.Total RNA was isolated using RNAqueous® Micro kit (#AM1931, Invitrogen) according to manufacturer's protocol. RNA quality was evaluated using the Agilent RNA 6000 Pico Kit (#50671513, Agilent Technologies) and Bioanalyzer™ (Agilent Technologies) for measuring concentration and calculation of RNA integrity number (RIN).

For RT-qPCR analysis of portal mesenchymal cells at P10, control and transgenic livers at P10 were dissected and mechanically dissociated using scalpel blades as described above. Trypsin-EDTA 0.05% (#25300054, Gibco, Life Technologies) was used 3 min at 37°C to help dissociation. Cells were resuspended in 2 mM EDTA, 5% FBS in PBS, filtered on 40 µm cell strainer and centrifuged at 50 g with a minimum deceleration. Supernatant was collected and centrifuged for 5 min at 290 g to keep the pellet. Total RNA was isolated using RNeasy Mini Kit (#74104, Qiagen) according to manufacturer's protocol, and was processed for reverse transcription using the First Strand cDNA Synthesis Kit (#K1612, Thermo Fisher Scientific). cDNA was used

to perform qPCR using KAPA SYBR® FAST Universal 2X qPCR Master Mix (#KK4602, Sopachem life sciences) and primers designed to amplify target genes (Table S4), on the CFX96 Real Time System (Bio-Rad) thermal cycler. Gene expression levels were determined by the $2^{-\Delta\Delta CT}$ method following normalisation to *Vimentin* reference gene. Technical triplicates were run for all samples and, as a control, a reaction without cDNA was performed.

Sequencing and bioinformatics workflow

Read quality control was performed using FastQC software v0.11.7 (Babraham Institute, Cambridge, UK). Low quality reads were trimmed and adapters were removed using Trimmomatic software v0.35 (RWTH Aachen University, Germany). Reads were aligned using HISAT2 software v2.1.0 (Johns Hopkins University School of Medicine, Center for Computational Biology, Baltimore, MD, USA) on GRCm38 mouse genome. Gene counts were generated using HTSeq-count (v0.5.4p3) software and gencode.vM15.annotation.gtf annotation file and raw counts were further converted in transcripts per million (TPM). Pathway analysis was performed using g:Profiler (Raudvere et al., 2019).

The RNA-seq data have been deposited in the Gene Expression Omnibus database and assigned the identifier GSE163062 and GSE224219.

Dual RNAScope/Immunofluorescence and BaseScope

RNAScope RNA *in situ* hybridization was performed on 6 µm sections of formalin-fixed paraffin-embedded tissues, according to the manufacturer's protocol for manual RNAscope®2.5 HD Assay—RED (#322350, Advanced Cell Diagnostics Inc.). The tissue sections were incubated at 60°C for 1h, deparaffinized 2x 5 min in xylene

and dehydrated 2x 2 min in 99% ethanol. Endogenous peroxidase was blocked with hydrogen peroxide for 10 min at room temperature (RT) followed by two short washings with deionized water. Slides were heated for 10 sec at 100°C in deionized water, and antigen retrieval was performed for 15 min at 100°C using RNAscope®Target retrieval. Tissue sections were washed in deionized water and 99% ethanol. Slides were dried for 5 min at RT and tissues were delineated using an ImmEdge Hydrophobic Barrier Pen (#310018, Advanced Cell Diagnostics Inc.). Slides were incubated for 15 min with RNAscope®Protease plus (diluted at 1/5 in deionized water) at 40°C, washed with deionized water and incubated with the probe for 2h at 40°C. The tissue sections were washed with RNAscope®Wash buffer and six amplifications were performed (using six reagents AMP1-AMP6). The signal detection followed using RNAscope®Fast A and B reagents for 10 min at RT. The slides were kept in PBS overnight and immunostaining was performed: sections were blocked for 45 min at RT in 3% milk, 10% BSA, 0.3% Tween 20 in PBS. Primary and secondary antibodies were diluted in 10% BSA, 0.3% Tween 20 in PBS and incubated respectively for 1h30 at 37°C and 1h30 at RT. Pictures were taken with Cell Observer Spinning Disk (Carl Zeiss) and Zen blue software. Primary and secondary antibodies are described in Tables S1-2.

BaseScope RNA *in situ* hybridization was performed on 6 µm sections of formalin-fixed paraffin-embedded tissues, according to the manufacturer's protocol for BaseScope RED v2 kit, as described (Martens et al., 2021). The custom probes were designed to bind specifically to exon 8 of the *Slit2* gene or to exon 5 of the *Robo2* gene.

Immunofluorescence and immunohistochemistry

Immunofluorescence and immunohistochemistry (IHC) were performed on 6 µm sections of formalin-fixed paraffin-embedded (FFPE) or sucrose-embedded frozen tissues. FFPE tissue sections were deparaffinized 3x 3 min in xylene, 3 min in 99%, 95%, 70% and 30% ethanol and deionized water. Antigen retrieval was performed by micro-wave heating for 10 min or using the Lab Vision PT Module (Thermo Fisher Scientific, Waltham, MA), in 10 mM citrate pH 6 or Tris-EDTA pH 9, depending on the antibody. Sections were permeabilized for 5 min in 0.3% Triton X-100 in PBS before blocking for 45 min in 3% milk,10% BSA, 0.3% Triton X-100 in PBS. For preparation of frozen sections, livers were collected, briefly washed in PBS, and fixed overnight in 4% paraformaldehyde. Tissues were incubated in sucrose 15% in PBS for 6-12 h and overnight in sucrose 30% in PBS, before embedding in OCT and freezing in liquid nitrogen-cooled isopentane. Frozen sections were thawed at RT for 20 min and rehydrated in PBS for 10 min. Antigen retrieval was performed by 5 min incubation in 10 mM citrate pH 6 preheated at 95°C, and sections were rinsed in deionized water and PBS, before blocking as above.

Primary antibodies were diluted in blocking solution at 4°C overnight and secondary antibodies were diluted in 10% BSA, 0.3% Triton X-100 in PBS at 37°C for 1 h. For IHC, antibody binding was visualized using 3,3'-diaminobenzidine tetrachloride (#ab64238, Abcam, Cambridge, UK), and 30% haematoxylin (#109249, Merck Millipore) was used to counterstain the tissue. Pictures were taken with Cell Observer Spinning Disk (Carl Zeiss) and Zen blue software, or with CaseViewer on scanned tissues. Primary and secondary antibodies are described in Tables S2 and S3.

Haematoxylin-Eosin (H&E) and Elastin-Collagen staining

The stainings were performed on 6 µm sections of formalin-fixed paraffin-embedded tissues. For H&E staining, tissue sections were deparaffinized 3x 3 min in xylene, 3 min in 99%, 95%, 70% and 30% ethanol and deionized water. Tissue sections were stained 7 sec in 100% haematoxylin solution (#109249, Merck Millipore), washed 2 min in tap water, stained 14 sec in eosin solution (#3137.2, Carl Roth) and washed with tap water until stain fades. Dehydration was performed in 30%, 70%, 95%, 99% and 100% ethanol and slides were washed in xylene until mounting slides with DPX (#1005790500, VWR).

For Elastin-Collagen staining, the Elastica Van Gieson Staining Kit (#8275.1, Carl Roth) was used, and the manufacturer's protocol was adapted to our tissues. Tissue sections were deparaffinized 3x 3 min in xylene, rehydrated 3 min in 99% and 80% ethanol, and stained 30 min in the esorcinol fuchsine solution. Slides were washed with tap water until stain fades, washed with deionized water, differentiated few seconds with ethanol 80% and washed with deionized water to interrupt the differentiation. Finally, tissue sections were stained 3 min with the Van Gieson solution and shortly washed with 70%, 95% and 100% ethanol, and xylene before mounting slides with DPX.

Blood collection and plasma analysis

Six- to eight-week-old mice were anesthetized and blood was collected using intracardiac puncture. Plasma samples were analyzed for total bilirubin, albumin, alkaline phosphatase, aspartate aminotransferase, alanine aminotransferase and lactate dehydrogenase (Fuji Dri-Chem NX500 analyzer).

Ink injection and tissue clearing

Six- to eight-week-old mice were anesthetized and transcardially perfused with PBS for 3 min (perfusion rate 5 ml/1 min). Protocols for bile duct and portal vein injections are described (Hankeova et al., 2021a) and were adapted for ink injection. Briefly, black ink (Higgins Drawing Ink) was injected in the common bile duct using a PE10 tubing (#427401, BD Bioscience) attached to a 30 g needle/2ml syringe. White ink (Higgins Drawing Ink) was injected in the portal vein, using a catheter (Peripheral IV cannulae, #BDAM381312, VWR) attached to a 5 ml syringe. To visualize the hepatic arteries, we injected ink in the gastroduodenal artery according to a protocol adapted from that described for rats (Sheu, Zhang, Omary, & Larson, 2013; Shinozaki, Ebert, Kournioti, Tai, & Woo, 2004; Tada et al., 2006). The gastroduodenal artery was cleaned from surrounded tissue, and surgical suture (SURGICRYL 910, #15150217, SMI AG) was loosely wrapped around the artery. An incision was made in the gastroduodenal artery using a spring scissor (2mm, #15000-03, Fine Science Tools). A PE10 tubing was attached to a 30 g needle/5ml syringe, and the end of the tubing was stretched and cut at an angle to create a beveled end. The common hepatic artery was clamped, the tubing was inserted in the gastroduodenal artery, and the suture was tightened on the tubing, before injecting ink. Following ink injection, liver lobes were incubated on a rocking platform in 50% methanol for 4 h at RT, in 100% methanol overnight at RT and in benzyl alcohol (BA), benzyl benzoate (BB) solution (1BA: 2 BB) for a few hours at RT. Pictures were taken with a Stereo Microscope Stemi SV6 (Zeiss) and a Moticam X3 camera.

Tissue labeling and three-dimensional microscopy

Embryos and newborns were fixed overnight in 4% paraformaldehyde (PFA) at 4°C. The liver lobes were dissected after fixation and post-fixed in 4% PFA at 4°C overnight. Tissue bleaching was as described (Renier et al., 2014). The samples were dehydrated for 2h at RT in ascending concentrations of methanol in PBS (50%, 80%, 100%), and then incubated overnight at 4°C with a 6% hydrogen peroxide solution in 100% methanol. Samples were re-hydrated for 2h at RT in descending concentrations of methanol (100% twice, 80%, 50%) and washed 2x for 1h in PBS. Samples were kept at 4°C for further processing.

For immunostaining, the samples were permeabilized and blocked in PBS containing 0.2% gelatin (Merck), and 0.5% Triton X-100 (Roth) (PBSGT) at RT (Belle et al., 2014). They were transferred to a solution containing primary antibodies (Table S2), 0.1% saponin (10 µg/ml) and heparin (10 µg/ml) in PBSGT for 10 days at 37°C with agitation. Samples were then washed 6x 30 min in PBSGT at RT. Secondary antibodies (Table S3) were diluted in a solution containing 0.1% saponin (10 µg/mL) and heparin (10 µg/mL) in PBSGT and filtered through a 0.22 µm filter. Samples were incubated overnight at 37°C in the secondary antibody solution. After six washes of 30 min in PBSGT at RT, samples were stored in the dark at 4°C until tissue clearing.

For tissue clearing, a modified 3DISCO clearing protocol was used. All incubation steps were performed in the dark at RT in a fume hood, on an agitator, using a 15 ml centrifuge tube. Samples were first dehydrated in ascending concentrations (50%, 80%, and 100%) of tetrahydrofuran (THF) diluted in H_2O. An initial overnight

incubation in 50% THF was followed by 2h in 80% THF and 2h in 100% THF. Samples next underwent delipidation for 30 min in dichloromethane (DCM, Sigma-Aldrich) followed by overnight clearing in dibenzyl ether (DBE; Sigma-Aldrich). Samples were then stored in individual light-absorbing glass vials (Roth) at RT. In these conditions, samples could be stored and imaged for up to 9 months without significant loss of fluorescence.

Three-dimensional image acquisitions were performed by using an ultramicroscope I (LaVision BioTec-Miltenyi Biotec) with the ImspectorPro software (LaVision BioTec-Miltenyi Biotec) The light sheet was generated by a laser (wavelength 560 or 640nm, Coherent Sapphire Laser, LaVision BioTec-Miltenyi Biotec) and focused using two cylindrical lenses. Two adjustable protective lenses were applied for small and large working distances. A binocular stereomicroscope (MXV10, Olympus) with a 2x objective (MVPLAPO, Olympus) was used at different magnifications (0.63x, 0.8x, 1x, 1.25x, 1.6×, 2x, 2.5x, 3.2x, 4x, 5x, and 6.3x). The corresponding zoom factors and numerical apertures are available on manufacturer website (https://www.miltenyibiotec.com/BE-en/products/objective-lenses-for-ultramicroscopes.html#150-000-493). Samples were placed in an imaging reservoir made of 100% quartz (LaVision BioTec-Miltenyi Biotec) filled with DBE and illuminated from the side by the laser light. A Zyla SCMOS CCD camera (2,048 × 2,048 pixel size, Andor Oxford Instrument) was used to acquire images. The step size between each image was fixed at 1 and 2 µm. All tiff images are generated in 16-bit.

For image processing, images, 3D volume, and movies were generated using Imaris software (version 9.9.0, Bitplane-Oxford Instrument). Stack images were first converted to imaris file (.ims) using ImarisFileConverter and 3D reconstruction was

performed using the volume rendering function. 3D pictures and movies were generated using the “snapshot” and “animation” tools.

Statistical analysis

Single comparisons between two experimental groups measuring plasma levels were done using a paired Student’s t test. For morphometric analyses of hepatic arteries, significance was assessed by a Student’s t-test with Welch’s correction. For calculation of adjusted p-value in gene expression analyses, a Benjamini-Hochberg correction was applied. P-value <0.05 was considered significant. Statistical analyses were performed using Graphpad Prism 9.

ACKNOWLEDGEMENTS

We thank François Tronche, Wim Martinet, Maike Sander, Francesca Spagnoli, Valbona Mirakaj and Alain Chédotal for providing mouse strains; Cheng-Ran Xu for sharing raw data on single cell analyses of developing liver; Chantal Housset and the members of the Lemaigre laboratory for discussions; the Imaging facility of the Institut de la Vision (Paris, France; Dr. Stéphane Fouquet), of the Université Libre de Bruxelles (LIMIF, Brussels, Belgium; Prof. Jean-Marie Vanderwinden) for help.

COMPETING INTEREST

The authors declare no competing or financial interests

AUTHOR CONTRIBUTIONS

Conceptualization: LiG, CDS, PJ, FPL; Methodology: LiG, CDS, MB, ND, YA, YH, IR; Formal analysis: LiG, CDS, MB, AL, CV, LaG; Investigation: LiG, CDS, SC, YH; Writing-original draft: LiG, CDS, FPL; Writing-review: LiG, CDS, ND, AL, CV, IR, PJ, LaG, FPL; Supervision: LaG, PJ, FPL; Project administration: FPL; Funding acquisition: FPL.

FUNDING

The work of F.P.L. was supported by grants from the Fonds de la Recherche Scientifique FRS-FNRS (Belgium; grants J.0115.21 and T.0158.20); from D.G. Higher Education and Scientific Research of the French Community of Belgium (grant ARC 15/20-065); from the Agence Nationale de la Recherche (France, program iLITE, ANR-16-RHUS-0005-16). L.G. and C.D.S. held fellowships from the Fonds pour la formation à la Recherche dans l'Industrie et l'Agriculture and from the UCLouvain (Belgium: grants 1.E071.18 and 1.E.053.19). P.J. is Research Director at FRS-FNRS, Belgium.

vi. References

Aida, T., Chiyo, K., Usami, T., Ishikubo, H., Imahashi, R., Wada, Y., Tanaka, K. F., Sakuma, T., Yamamoto, T., Tanaka, K. (2015). Cloning-free CRISPR/Cas system facilitates functional cassette knock-in in mice. *Genome Biol*. **16**, 87.

Andrews, T. S., Atif, J., Liu, J. C., Perciani, C. T., Ma, X. Z., Thoeni, C., Slyper, M., Eraslan, G., Segerstolpe, A., Manuel, J., et al. (2022). Single-Cell, Single-Nucleus, and Spatial RNA Sequencing of the Human Liver Identifies Cholangiocyte and Mesenchymal Heterogeneity. *Hepatol Commun*. **6**, 821-840.

Asahina, K., Tsai, S. Y., Li, P., Ishii, M., Maxson, R. E., Jr., Sucov, H. M., Tsukamoto, H. (2009). Mesenchymal origin of hepatic stellate cells, submesothelial cells, and perivascular mesenchymal cells during mouse liver development. *Hepatology*. **49**, 998-1011.

Asahina, K., Zhou, B., Pu, W. T., Tsukamoto, H. (2011). Septum transversum-derived mesothelium gives rise to hepatic stellate cells and perivascular mesenchymal cells in developing mouse liver. *Hepatology*. **53**, 983-95.

Avci, M. E., Konu, O., Yagci, T. (2008). Quantification of SLIT-ROBO transcripts in hepatocellular carcinoma reveals two groups of genes with coordinate expression. *BMC Cancer*. **8**, 392.

Belle, M., Godefroy, D., Dominici, C., Heitz-Marchaland, C., Zelina, P., Hellal, F., Bradke, F., Chedotal, A. (2014). A simple method for 3D analysis of immunolabeled axonal tracts in a transparent nervous system. *Cell Rep*. **9**, 1191-201.

Chang, J., Lan, T., Li, C., Ji, X., Zheng, L., Gou, H., Ou, Y., Wu, T., Qi, C., Zhang, Q., et al. (2015). Activation of Slit2-Robo1 signaling promotes liver fibrosis. *J Hepatol*. **63**, 1413-20.

Clotman, F., Libbrecht, L., Gresh, L., Yaniv, M., Roskams, T., Rousseau, G. G., Lemaigre, F. P. (2003). Hepatic artery malformations associated with a

primary defect in intrahepatic bile duct development. *J Hepatol*. **39**, 686-92.

Coll, M., Arino, S., Martinez-Sanchez, C., Garcia-Pras, E., Gallego, J., Moles, A., Aguilar-Bravo, B., Blaya, D., Vallverdu, J., Rubio-Tomas, T., et al. (2022). Ductular reaction promotes intrahepatic angiogenesis through Slit2-Roundabout 1 signaling. *Hepatology*. **75**, 353-368.

Delgado, I., Carrasco, M., Cano, E., Carmona, R., Garcia-Carbonero, R., Marin-Gomez, L. M., Soria, B., Martin, F., Cano, D. A., Munoz-Chapuli, R., et al. (2014). GATA4 loss in the septum transversum mesenchyme promotes liver fibrosis in mice. *Hepatology*. **59**, 2358-70.

Demarez, C., Gerard, C., Cordi, S., Poncy, A., Achouri, Y., Dauguet, N., Rosa, D. A., Gunning, P. T., Manfroid, I., Lemaigre, F. P. (2018). MicroRNA-337-3p controls hepatobiliary gene expression and transcriptional dynamics during hepatic cell differentiation. *Hepatology*. **67**, 313-327.

Dobie, R., Wilson-Kanamori, J. R., Henderson, B. E. P., Smith, J. R., Matchett, K. P., Portman, J. R., Wallenborg, K., Picelli, S., Zagorska, A., Pendem, S. V., et al. (2019). Single-Cell Transcriptomics Uncovers Zonation of Function in the Mesenchyme during Liver Fibrosis. *Cell Rep*. **29**, 1832-1847 e8.

Fabris, L., Cadamuro, M., Libbrecht, L., Raynaud, P., Spirli, C., Fiorotto, R., Okolicsanyi, L., Lemaigre, F., Strazzabosco, M., Roskams, T. (2008). Epithelial expression of angiogenic growth factors modulate arterial vasculogenesis in human liver development. *Hepatology*. **47**, 719-28.

Gong, S., Zheng, C., Doughty, M. L., Losos, K., Didkovsky, N., Schambra, U. B., Nowak, N. J., Joyner, A., Leblanc, G., Hatten, M. E., et al. (2003). A gene expression atlas of the central nervous system based on bacterial artificial chromosomes. *Nature*. **425**, 917-25.

Gordillo, M., Evans, T., Gouon-Evans, V. (2015). Orchestrating liver development. *Development*. **142**, 2094-108.

Gouysse, G., Couvelard, A., Frachon, S., Bouvier, R., Nejjari, M., Dauge, M. C., Feldmann, G., Henin, D., Scoazec, J. Y. (2002). Relationship between

vascular development and vascular differentiation during liver organogenesis in humans. *J Hepatol*. **37**, 730-40.

Greenhalgh, S. N., Conroy, K. P., Henderson, N. C. (2015). Cre-ativity in the liver: transgenic approaches to targeting hepatic nonparenchymal cells. *Hepatology*. **61**, 2091-9.

Hankeova, S., Salplachta, J., Zikmund, T., Kavkova, M., Van Hul, N., Brinek, A., Smekalova, V., Laznovsky, J., Dawit, F., Jaros, J., et al. (2021). DUCT reveals architectural mechanisms contributing to bile duct recovery in a mouse model for Alagille syndrome. *Elife*. **10**, e60916.

Henderson, N. C., Arnold, T. D., Katamura, Y., Giacomini, M. M., Rodriguez, J. D., McCarty, J. H., Pellicoro, A., Raschperger, E., Betsholtz, C., Ruminski, P. G., et al. (2013). Targeting of alphav integrin identifies a core molecular pathway that regulates fibrosis in several organs. *Nat Med*. **19**, 1617-24.

Hofmann, J. J., Zovein, A. C., Koh, H., Radtke, F., Weinmaster, G., Iruela-Arispe, M. L. (2010). Jagged1 in the portal vein mesenchyme regulates intrahepatic bile duct development: insights into Alagille syndrome. *Development*. **137**, 4061-72.

Holtwick, R., Gotthardt, M., Skryabin, B., Steinmetz, M., Potthast, R., Zetsche, B., Hammer, R. E., Herz, J., Kuhn, M. (2002). Smooth muscle-selective deletion of guanylyl cyclase-A prevents the acute but not chronic effects of ANP on blood pressure. *Proc Natl Acad Sci U S A*. **99**, 7142-7.

Kellendonk, C., Opherk, C., Anlag, K., Schutz, G., Tronche, F. (2000). Hepatocyte-specific expression of Cre recombinase. *Genesis*. **26**, 151-3.

Kopp, J. L., Dubois, C. L., Schaffer, A. E., Hao, E., Shih, H. P., Seymour, P. A., Ma, J., Sander, M. (2011). Sox9+ ductal cells are multipotent progenitors throughout development but do not produce new endocrine cells in the normal or injured adult pancreas. *Development*. **138**, 653-65.

Krishna, M. (2013). Microscopic anatomy of the liver. *Clin Liver Dis (Hoboken)*. **2**, S4-S7.

Lei, L., Bruneau, A., El Mourabit, H., Guegan, J., Folseraas, T., Lemoinne, S., Karlsen, T. H., Hoareau, B., Morichon, R., Gonzalez-Sanchez, E., et al. (2022). Portal fibroblasts with mesenchymal stem cell features form a reservoir of proliferative myofibroblasts in liver fibrosis. *Hepatology*. **76**, 1360-1375.

Lemaigre, F. (2020). Development of the intrahepatic and extrahepatic biliary tract: a framework for understanding congenital diseases. *Annu Rev Pathol Mech Dis* **15**, 1-22.

Libbrecht, L., Cassiman, D., Desmet, V., Roskams, T. (2002). The correlation between portal myofibroblasts and development of intrahepatic bile ducts and arterial branches in human liver. *Liver*. **22**, 252-8.

Liu, D., Hou, J., Hu, X., Wang, X., Xiao, Y., Mou, Y., De Leon, H. (2006). Neuronal chemorepellent Slit2 inhibits vascular smooth muscle cell migration by suppressing small GTPase Rac1 activation. *Circ Res*. **98**, 480-9.

Long, H., Sabatier, C., Ma, L., Plump, A., Yuan, W., Ornitz, D. M., Tamada, A., Murakami, F., Goodman, C. S., Tessier-Lavigne, M. (2004). Conserved roles for Slit and Robo proteins in midline commissural axon guidance. *Neuron*. **42**, 213-23.

Lu, W., van Eerde, A. M., Fan, X., Quintero-Rivera, F., Kulkarni, S., Ferguson, H., Kim, H. G., Fan, Y., Xi, Q., Li, Q. G., et al. (2007). Disruption of ROBO2 is associated with urinary tract anomalies and confers risk of vesicoureteral reflux. *Am J Hum Genet*. **80**, 616-32.

Martens, S., Coolens, K., Van Bulck, M., Arsenijevic, T., Casamitjana, J., Fernandez Ruiz, A., El Kaoutari, A., Martinez de Villareal, J., Madhloum, H., Esni, F., et al. (2021). Discovery and 3D imaging of a novel DeltaNp63-expressing basal cell type in human pancreatic ducts with implications in disease. *Gut*. **71**, 2030-42.

Mederacke, I., Hsu, C. C., Troeger, J. S., Huebener, P., Mu, X., Dapito, D. H., Pradere, J. P., Schwabe, R. F. (2013). Fate tracing reveals hepatic stellate cells as dominant contributors to liver fibrosis independent of its aetiology. *Nat Commun*. **4**, 2823.

Naito, Y., Hino, K., Bono, H., Ui-Tei, K. (2015). CRISPRdirect: software for designing CRISPR/Cas guide RNA with reduced off-target sites. *Bioinformatics*. **31**, 1120-3.

Ober, E. A., Lemaigre, F. P. (2018). Development of the liver: Insights into organ and tissue morphogenesis. *J Hepatol*. **68**, 1049-1062.

Owens, G. K., Kumar, M. S., Wamhoff, B. R. (2004). Molecular regulation of vascular smooth muscle cell differentiation in development and disease. *Physiol Rev*. **84**, 767-801.

Pi, L., Sun, C., Jn-Simon, N., Basha, S., Thomas, H., Figueroa, V., Zarrinpar, A., Cao, Q., Petersen, B. (2022). CCN2/CTGF promotes liver fibrosis through crosstalk with the Slit2/Robo signaling. *J Cell Commun Signal*.

Poncy, A., Antoniou, A., Cordi, S., Pierreux, C. E., Jacquemin, P., Lemaigre, F. P. (2015). Transcription factors SOX4 and SOX9 cooperatively control development of bile ducts. *Dev Biol*. **402**, 136-148.

Rama, N., Dubrac, A., Mathivet, T., Ni Charthaigh, R. A., Genet, G., Cristofaro, B., Pibouin-Fragner, L., Ma, L., Eichmann, A., Chedotal, A. (2015). Slit2 signaling through Robo1 and Robo2 is required for retinal neovascularization. *Nat Med*. **21**, 483-91.

Raudvere, U., Kolberg, L., Kuzmin, I., Arak, T., Adler, P., Peterson, H., Vilo, J. (2019). g:Profiler: a web server for functional enrichment analysis and conversions of gene lists (2019 update). *Nucleic Acids Res*. **47**, W191-W198.

Renier, N., Wu, Z., Simon, D. J., Yang, J., Ariel, P., Tessier-Lavigne, M. (2014). iDISCO: a simple, rapid method to immunolabel large tissue samples for volume imaging. *Cell*. **159**, 896-910.

Sheu, A. Y., Zhang, Z., Omary, R. A., Larson, A. C. (2013). Invasive catheterization of the hepatic artery for preclinical investigation of liver-directed therapies in rodent models of liver cancer. *Am J Transl Res*. **5**, 269-78.

Shinozaki, K., Ebert, O., Kournioti, C., Tai, Y. S., Woo, S. L. (2004). Oncolysis of multifocal hepatocellular carcinoma in the rat liver by hepatic artery infusion of vesicular stomatitis virus. *Mol Ther*. **9**, 368-76.

Srinivas, S., Watanabe, T., Lin, C. S., William, C. M., Tanabe, Y., Jessell, T. M., Costantini, F. (2001). Cre reporter strains produced by targeted insertion of EYFP and ECFP into the ROSA26 locus. *BMC Dev Biol*. **1**, 4.

Tada, M., Hatano, E., Taura, K., Nitta, T., Koizumi, N., Ikai, I., Shimahara, Y. (2006). High volume hydrodynamic injection of plasmid DNA via the hepatic artery results in a high level of gene expression in rat hepatocellular carcinoma induced by diethylnitrosamine. *J Gene Med*. **8**, 1018-26.

Takashima, Y., Terada, M., Kawabata, M., Suzuki, A. (2015). Dynamic three-dimensional morphogenesis of intrahepatic bile ducts in mouse liver development. *Hepatology*. **61**, 1003-11.

Tanaka, M., Iwakiri, Y. (2016). The Hepatic Lymphatic Vascular System: Structure, Function, Markers, and Lymphangiogenesis. *Cell Mol Gastroenterol Hepatol*. **2**, 733-749.

Tanimizu, N., Ichinohe, N., Mitaka, T. (2018). Intrahepatic bile ducts guide establishment of the intrahepatic nerve network in developing and regenerating mouse liver. *Development*. **145**, pii: dev159095.

Tanimizu, N., Kaneko, K., Itoh, T., Ichinohe, N., Ishii, M., Mizuguchi, T., Hirata, K., Miyajima, A., Mitaka, T. (2016). Intrahepatic bile ducts are developed through formation of homogeneous continuous luminal network and its dynamic rearrangement in mice. *Hepatology*. **64**, 175-88.

Tanimizu, N., Mitaka, T. (2017). Epithelial Morphogenesis during Liver Development. *Cold Spring Harb Perspect Biol*. **9**.

Troeger, J. S., Mederacke, I., Gwak, G. Y., Dapito, D. H., Mu, X., Hsu, C. C., Pradere, J. P., Friedman, R. A., Schwabe, R. F. (2012). Deactivation of hepatic stellate cells during liver fibrosis resolution in mice. *Gastroenterology*. **143**, 1073-83 e22.

Van Liedekerke, P., Gannoun, L., Loriot, A., Johann, T., Lemaigre, F. P., Drasdo, D. (2022). Quantitative modeling identifies critical cell mechanics driving bile duct lumen formation. *PLoS Comput Biol*. **18**, e1009653.

Villeneuve, J., Pelluard-Nehme, F., Combe, C., Carles, D., Chaponnier, C., Ripoche, J., Balabaud, C., Bioulac-Sage, P., Lepreux, S. (2009). Immunohistochemical study of the phenotypic change of the mesenchymal cells during portal tract maturation in normal and fibrous (ductal plate malformation) fetal liver. *Comp Hepatol*. **8**, 5.

Wang, X., Yang, L., Wang, Y. C., Xu, Z. R., Feng, Y., Zhang, J., Wang, Y., Xu, C. R. (2020). Comparative analysis of cell lineage differentiation during hepatogenesis in humans and mice at the single-cell transcriptome level. *Cell Res*. **30**, 1109-1126.

Zeng, Z., Wu, Y., Cao, Y., Yuan, Z., Zhang, Y., Zhang, D. Y., Hasegawa, D., Friedman, S. L., Guo, J. (2018). Slit2-Robo2 signaling modulates the fibrogenic activity and migration of hepatic stellate cells. *Life Sci*. **203**, 39-47.

Zhang, J., Zhong, W., Cui, T., Yang, M., Hu, X., Xu, K., Xie, C., Xue, C., Gibbons, G. H., Liu, C., et al. (2006). Generation of an adult smooth muscle cell-targeted Cre recombinase mouse model. *Arterioscler Thromb Vasc Biol*. **26**, e23-4.

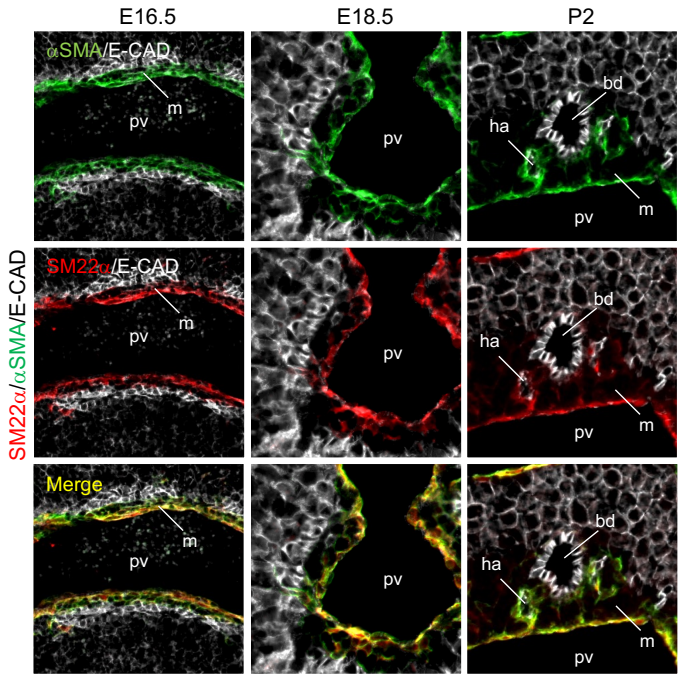


Fig. S1. αSMA and SM22α are co-expressed in the developing portal mesenchyme and hepatic artery. E-cadherin (E-CAD) labels the cholangiocytes lining the bile ducts and the hepatocytes. bd, bile duct; ha, hepatic artery; m, mesenchyme; pv, portal vein.

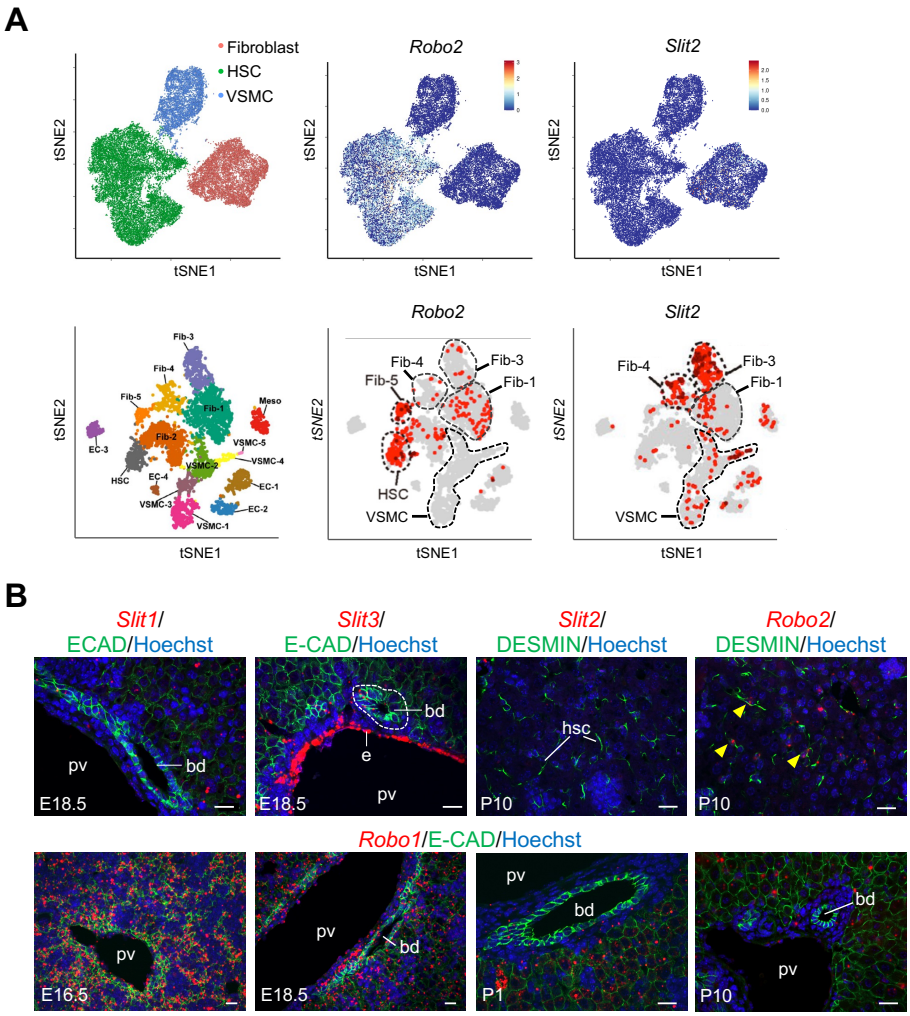


Fig. S2. Expression of *Robo* and *Slit* genes in portal mesenchyme. (A) Single cell RNA sequencing of adult mouse liver detected *Robo2* mainly in stellate cells but also in fibroblasts. *Slit2* was found in fibroblasts and VSMCs. Upper and lower panels are data extracted from Dobie *et al.* (2019) and Lei *et al.* (2022), respectively. (B) Using RNAscope *in situ* hybridisation of embryonic mouse liver, *Slit1* was barely detected; *Slit3* was found in portal vein endothelium and at very low level in a subset of cholangiocytes. Robo2, but not *Slit2*, was detected in DESMIN-expressing stellate cells. RNAscope *in situ* hybridisation detects *Robo1* RNA in prenatal hepatoblasts, cholangiocytes, mesenchyme and endothelial cells. After birth, *Robo1* expression progressively decreases in the portal area. bd, bile duct; e, endothelium; hsc, hepatic stellate cells; pv, portal vein. Scale bars: 20 µm.

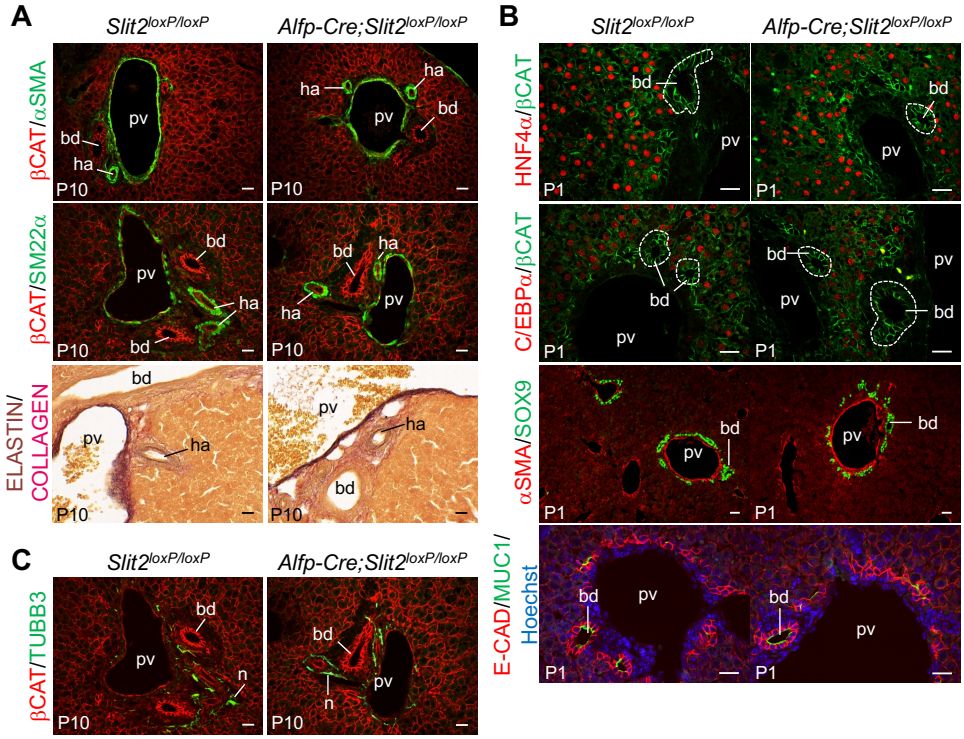


Fig. S3. Hepatic artery and biliary morphogenesis does not require *Slit2* expression in cholangiocytes. (A) The absence of SLIT2 in cholangiocytes is associated with normal development of hepatic arteries, as shown by αSMA, SM22α, ELASTIN and COLLAGEN staining in *Alfp-Cre;Slit2*$^{loxP/loxP}$ mice (n=7). (B) Bile ducts are normal and delineated by well-differentiated and well-polarised cholangiocytes in the absence of SLIT2 in hepatic epithelial cells of *Alfp-Cre;Slit2*$^{loxP/loxP}$ mice (n=7). (C) TUBB3 staining shows periportal nerves (n=7). Immunostaining labels hepatocytes (HNF4α, C/EBPα, βCAT, E-CAD), cholangiocytes (SOX9, βCAT, E-CAD, MUC1), and VSMCs (αSMA, SM22α). bd, bile duct; ha, hepatic artery; n, nerve; pv, portal vein. Scale bars: 20 μm.

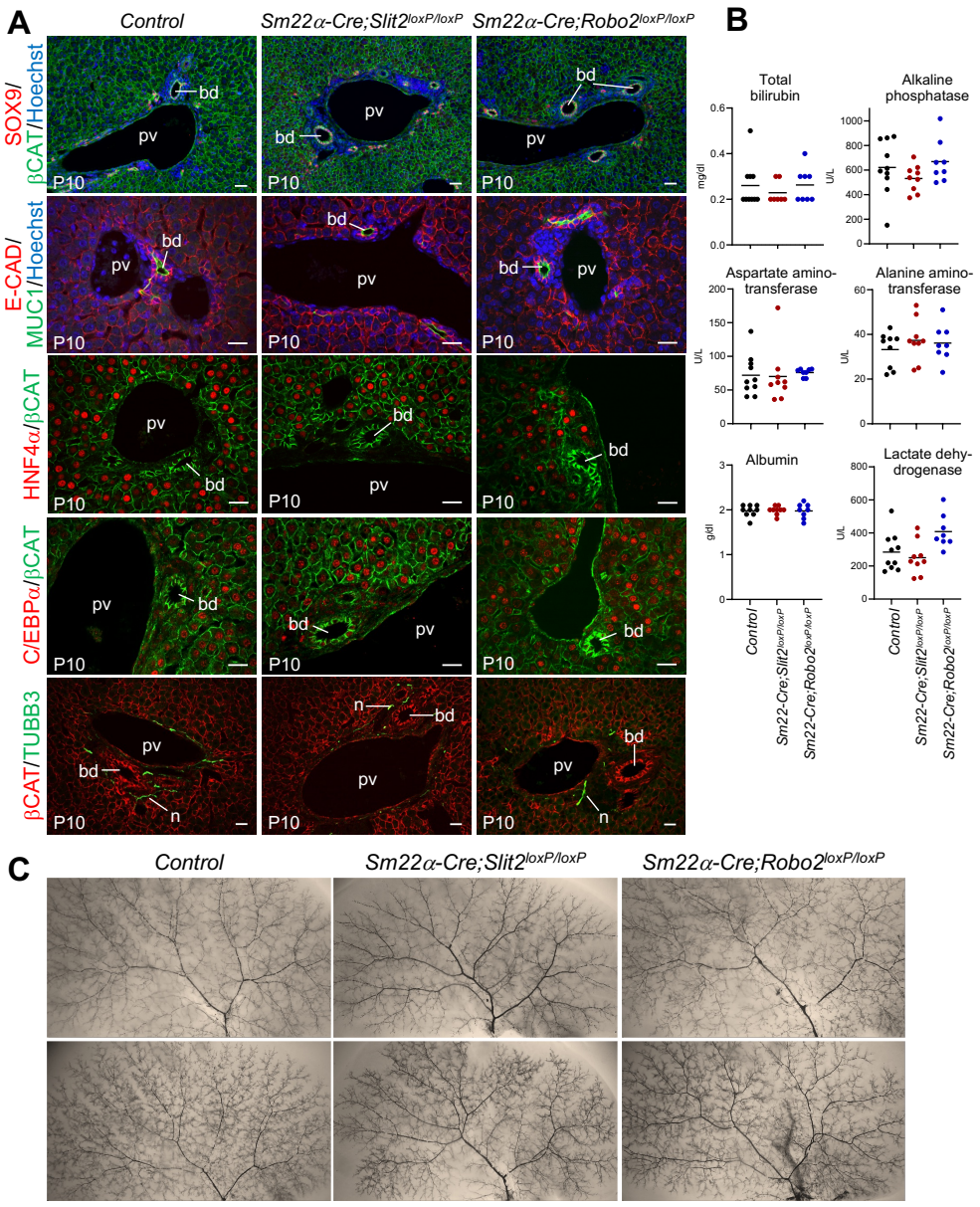


Fig. S4. Biliary morphogenesis does not require *Slit2* or *Robo2* expression in portal mesenchymal cells. (A) Bile ducts are well-formed and delineated by well-differentiated and well-polarised cholangiocytes in the absence of SLIT2 or ROBO2 in the mesenchyme of *Sm22α-Cre;Slit2*$^{loxP/loxP}$ (n=11) and *Sm22α-Cre;Robo2*$^{loxP/loxP}$ (n=7) mice. (B) At 2 months, serum levels of total bilirubin, albumin, alkaline phosphatase, aspartate aminotransferase, alanine aminotransferase and lactate dehydrogenase do not show a significant difference between *Sm22α-Cre;Slit2*$^{loxP/loxP}$ (n=9), *Sm22α-Cre;Robo2*$^{loxP/loxP}$ (n=8) and wild-type (n=10) mice. Dots represent individual measurements. (C) Retrograde injection of ink in the common bile duct followed by tissue clearing reveals normal biliary tree in 2 months-old wild-type (n=6), *Sm22α-Cre;Slit2*$^{loxP/loxP}$ (n=7) and *Sm22α-Cre;Robo2*$^{loxP/loxP}$ (n=4) mice. Immunostaining labels hepatocytes (HNF4α, C/EBPα, βCAT, E-CAD), cholangiocytes (SOX9, βCAT, E-CAD, MUC1), and nerves (TUBB3). bd, bile duct; n, nerve; pv, portal vein. Scale bars: 20 µm.

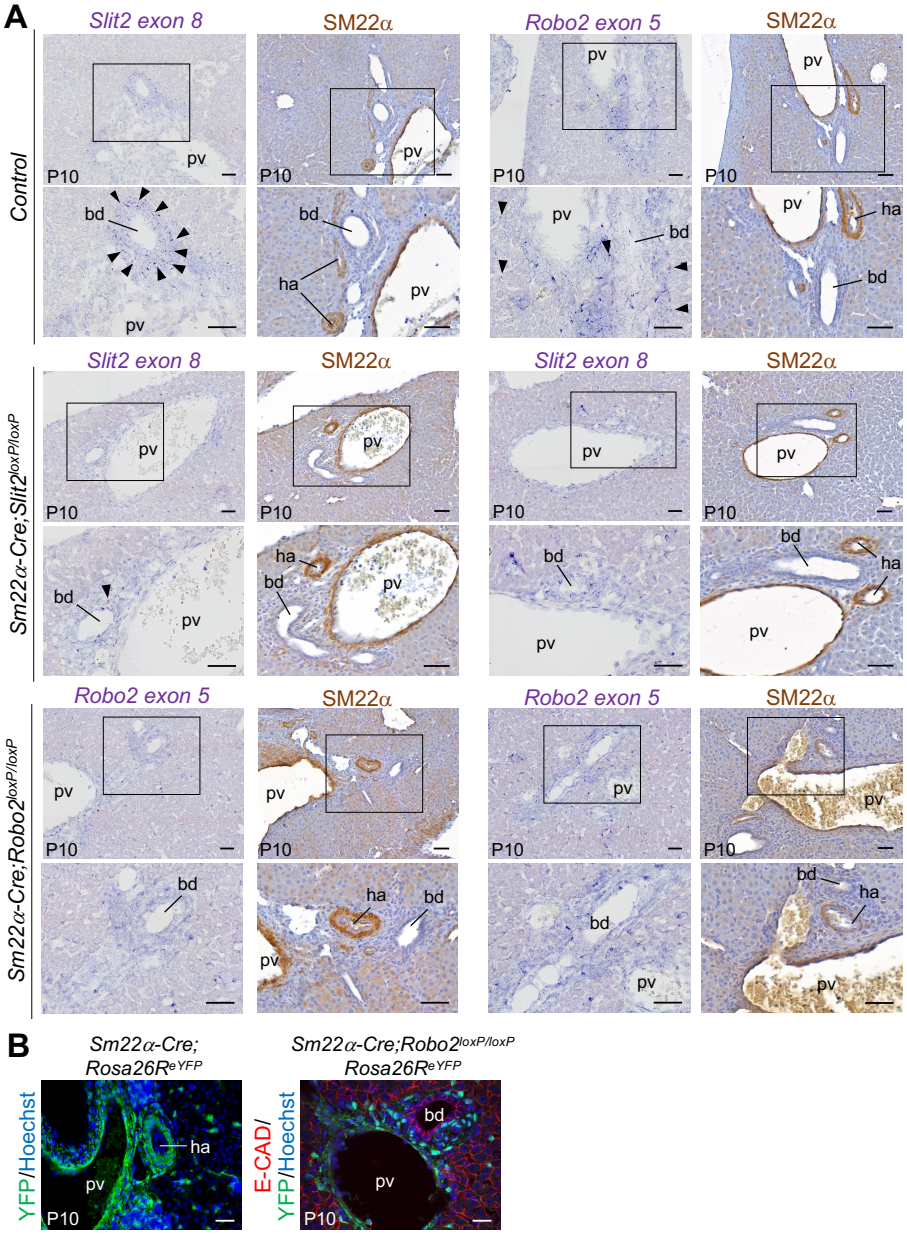


Fig. S5. Efficiency of *Sm22α-Cre* in the studied transgenic mouse models. (A) BaseScope *in situ* RNA hybridisation detecting exon 8 of *Slit2* or exon 5 of *Robo2* shows efficient inactivation of *Slit2* and *Robo2* genes in *Sm22α-Cre;Slit2*$^{loxP/loxP}$ and *Sm22α-Cre;Robo2*$^{loxP/loxP}$ mice, respectively. In parallel, staining for SM22α shows the biological heterogeneity of the arterial phenotype. The black arrowheads point to cells in which *Slit2* or *Robo2* RNA is detected. (B) Activity of *Sm22α-Cre* is confirmed by immunostaining for eYFP on *Sm22α-Cre;Robo2*$^{loxP/loxP}$*;Rosa26R*^{eYFP} livers, like in *Sm22α-Cre; Rosa26R*^{eYFP} livers. bd, bile duct; ha, hepatic artery; pv, portal vein. Scale bars: 20 µm (white) or 50 µm (black).

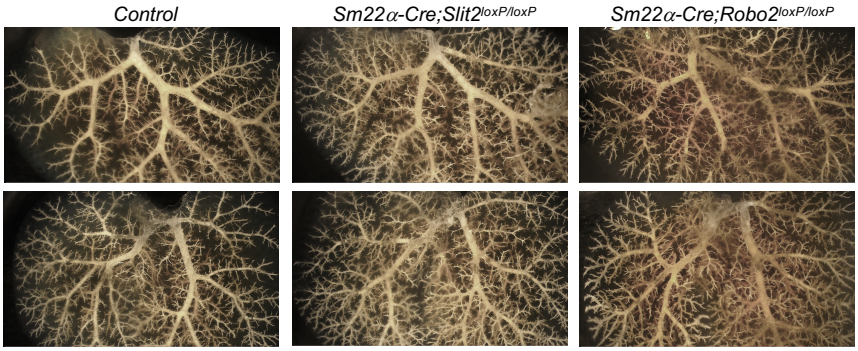


Fig. S6. Portal vein morphogenesis does not require *Slit2* or *Robo2* expression in portal mesenchymal cells. Ink injection in the portal vein followed by clearing of left lobe (upper pictures) and median lobe (bottom pictures) reveals normal portal vein branches in 2 months-old wild-type (n=3), *Sm22α-Cre;Slit2*$^{loxP/loxP}$ (n=3) and *Sm22α-Cre;Robo2*$^{loxP/loxP}$ (n=3) mice.

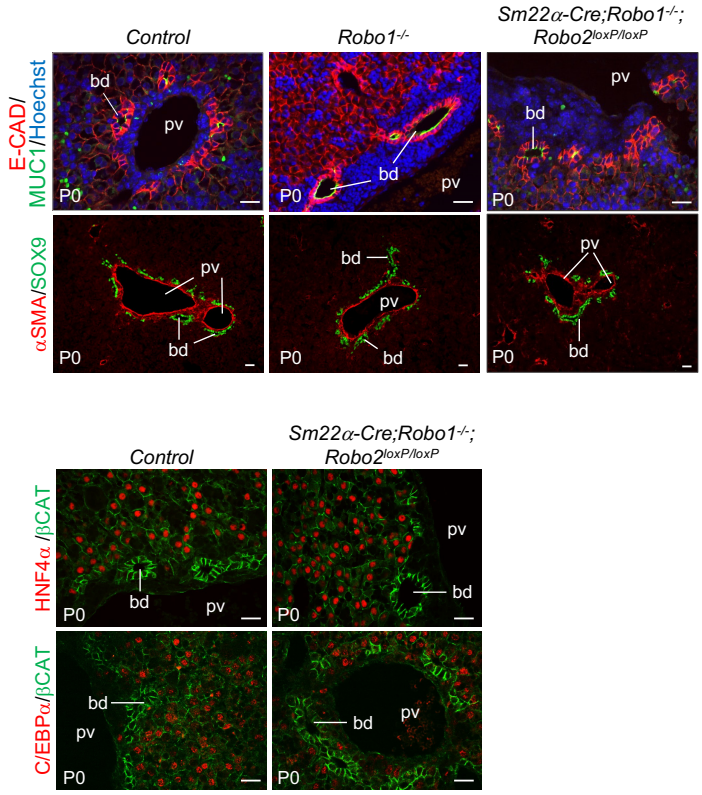


Fig. S7. *Robo1* and *Robo2* are dispensable for biliary morphogenesis. At birth, bile ducts are normal and delineated by well-differentiated and well-polarised cholangiocytes in the absence of *Robo1* and *Robo2* in *Robo1*$^{-/-}$ (n=4) and *Sm22α-Cre;Robo1*$^{-/-}$*;Robo2*$^{loxP/loxP}$ (n=6) mice. bd, bile duct; pv, portal vein. Immunostaining labels hepatocytes (HNF4α, C/EBPα, βCAT, E-CAD), cholangiocytes (SOX9, βCAT, E-CAD, MUC1), and VSMCs (αSMA). bd, bile duct; pv, portal vein. Scale bars: 20 μm.

Table S1. Number of mice and associated hepatic arteries analysed in Fig. 9B.

P10 Control (n=4)	< 2000 µm²	> 2000 µm²
#1	20	16
#2	40	15
#3	35	11
#4	15	9
P10 Sm22-Cre Slit2$^{lox/lox}$ (n=9)	**< 2000 µm²**	**> 2000 µm²**
#1	39	15
#2	23	17
#3	20	16
#4 (most severe phenotype)	16	2
#5	22	10
#6	26	18
#7	20	13
#8	16	4
#9	18	11
P10 Sm22-Cre Robo2$^{lox/lox}$ (n=7)	**< 2000 µm²**	**> 2000 µm²**
#1	22	17
#2	27	9
#3	29	14
#4	23	16
#5 (most severe phenotype)	12	3
#6	22	5
#7	15	11

Table S2 Primary antibodies

Primary antibodies	Species	Dilution	Application	Antigen retrieval	Reference
E-Cadherin	Mouse IgG2a	1/200	IF, paraffin section	MW, citrate	BD Biosciences (610181)
Sox9	Rabbit	1/1000	IF, paraffin section	MW, citrate	Homemade
Robo2	Mouse IgG1	1/200	IF, paraffin section	MW, citrate	Santa Cruz (sc-376177)
Thy-1	Rabbit	1/200	IF, paraffin section	MW, citrate	Cell Signaling (13801S)
Desmin	Mouse IgG1	1/100	IF, paraffin section	MW, citrate	Sigma-Aldrich (D1033)
Reelin	Goat	1/50	IF, paraffin or frozen section	PT-module, EDTA or water bath, citrate	R&D Systems (AF3820)
αSMA	Mouse IgG2a	1/75	IF, paraffin section	MW, citrate or EDTA	Agilent Dako (M085101-2)
GFP	Goat	1/100	IF, paraffin section	PT-module, EDTA	Abcam (#AB6673)
Sm22	Rabbit	1/100	IF, paraffin section	MW, citrate	Proteintech (10493-1-AP)
Muc-1	Armenian Hamster	1/300	IF, paraffin section	MW, citrate	Invitrogen (MA5-11202)
HNF4α	Mouse IgG2a	1/350	IF, paraffin section	MW, citrate	R&D Systems (PP-H1415-00)
β-Catenin	Mouse IgG1	1/1000	IF, paraffin section	MW, citrate	BD Biosciences (610153)
C/EBPα	Rabbit	1/300	IF, paraffin section	MW, citrate	Santa Cruz (sc-61)
TUBB3	Mouse IgG2a	1/800	IF, paraffin section	MW, citrate	Biolegend (801213)
Smoothelin	Rabbit	1/1000	IF, paraffin section	MW, EDTA	Abcam (ab219652)
Lyve1	Rabbit	1/500	IF, paraffin section	MW, citrate	Abcam (ab14917)
PECAM1 (CD31)	Rat	1/75	IF, paraffin section	MW, citrate	Dianova (DIA-310)
Vimentin	Rabbit	1/100	IF, paraffin section	MW, citrate	Cell signaling (57415)
CD45	Rat	1/50	IF, frozen or paraffin section	Water bath, citrate	BD Biosciences (550539)
Ter119	Rabbit	1/500	IF, paraffin section	MW, citrate	Biolegend (116233)
Thy1	Rat	1/100	IF, frozen section	Water bath, citrate	Abcam (ab3105)
GFP	Chicken	1/1000	IF, frozen or paraffin section	Water bath, citrate	Abcam (ab13970)
EpCAM (APC)	Rat	0.125µg/ 10^6 cells	FACS sorting	-	Invitrogen (17-5791-82)
CD45 (Brilliant Violet 421)	Rat	0.25µg/ 10^6 cells	FACS sorting	-	Biolegend (103134)
CD31 (PE/Cyanine7)	Rat	0.25µg/ 10^6 cells	FACS sorting	-	Biolegend (102418)

Table S3. Secondary antibodies

Secondary antibodies	Species	Dilution	Reference
Anti-Rabbit HRP	Goat	1/1000	Invitrogen (31460)
Anti-Rat Alexa Fluor 488	Donkey	1/1000	Invitrogen (A21208)
Anti-Rat Alexa Fluor 594	Donkey	1/1000	Invitrogen (A21209)
Anti-Mouse IgG2a Alexa Fluor 488	Goat	1/1000	Invitrogen (A21131)
Anti-Mouse IgG2a Alexa Fluor 594	Goat	1/1000	Invitrogen (A21135)
Anti-Mouse IgG2a Alexa Fluor 647	Goat	1/1000	Invitrogen (A21241)
Anti-Armenian Hamster Alexa Fluor 594	Donkey	1/500	Jackson ImmunoResearch (127-585-099)
Anti-Rabbit Alexa Fluor 594	Donkey	1/1000	Invitrogen (A21207)
Anti-Rabbit Alexa Fluor 488	Donkey	1/1000	Invitrogen (A21206)
Anti-Rabbit Alexa Fluor 647	Donkey	1/1000	Invitrogen (A31573)
Anti-Mouse IgG1 Alexa Fluor 594	Goat	1/1000	Invitrogen (A21125)
Anti-Mouse IgG1 Alexa Fluor 488	Goat	1/1000	Invitrogen (A21121)
Anti-Mouse IgG1 Alexa Fluor 647	Goat	1/1000	Invitrogen (A21240)
Anti-Goat Alexa Fluor 488	Donkey	1/1000	Invitrogen (A11055)
Anti-Goat Alexa Fluor 594	Donkey	1/1000	Invitrogen (A11058)
Anti-Chicken Alexa Fluor 488	Goat	1/1000	Invitrogen (A11039)
Anti-Mouse total Alexa fluor 594	Donkey	1/1000	Invitrogen (A21203)

Table S4. Primers designed for RT-qPCR analysis

Gene name	Forward primer sequence	Reverse primer sequence
VIM	TCCACACGCACCTACAGTCT	CCGAGGACCGGGTCACATA
COL15A1	GCCAGCGGGTTATCCTCTAC	ATCACGGGCACGGAGAAAAC
FBLN2	GCGTACAAGGAGGGTTTGTG	AATGCAGTTGGGTGGTAGCTC
DNMT1	CCTGCCAGGGCTTCAGTGGC	CAGGCAGCGCAGTGTGAGCT
ELN	TTGCTGATCCTCTTGCTCAAC	GCCCCTGGATAATAGACTCCAC
SMTN	ATGGCAGACGAGGCTTTAGC	AGTGTAGCCAGTTCTCCTTGTT
CNN1	TCTGCACATTTTAACCGAGGTC	GCCAGCTTGTTCTTTACTTCAGC

General discussion

The aim of my thesis was to improve our understanding of liver portal tract morphogenesis. The experimental work was divided into two complementary parts, namely the investigation of 3D organization of portal mesenchyme, bile ducts and hepatic artery at several developmental stages using optimized imaging technology, and the characterization of epithelial-mesenchyme interactions driving development of the liver portal tract, with focus on axon guidance molecules.

Here, I discuss the limitations of the experimental models and technologies used in this study, the role of axon guidance molecules during mouse development, the interpretation of the negative data, and the opportunities that result from our investigations opened as well as the perspectives they have raised.

I. The study of organ development in 3D

i. Imaging the liver development: the tip of the iceberg

Application of volume imaging technologies is currently at the frontline of biological studies. 3D imaging techniques, such as whole-body imaging and light-sheet microscopy, have made significant progress in recent years and have become valuable tools for studying organ development and architecture (Belle et al., 2017). Literature dealing with liver tissue optical clearing is until now limited to successful clearing of adult rodent liver with CLARITY (L. M. Molina et al., 2022), iDISCO+ (Adori et al., 2021; K. Liu et al., 2021), CUBIC (Z. Liu et al., 2022) in research studies, or seeDB as reported in methods papers (Tainaka et al., 2014; J. Xu, Ma, Yu, & Zhu, 2019).

During my work, I applied volume immunostaining and 3DISCO clearing technology combined with light-sheet fluorescence microscopy to explore the detailed 3D organization of the portal tract during mouse liver organogenesis. Anti-claudin7 antibody wholemount immunostaining of the entire liver at E18.5 revealed that cholangiocytes form a repetitive network in all liver lobes. At the lobe level, volume immunostaining with (i) anti-OPN antibody (marker of the cholangiocytes apical pole); (ii) anti-SOX9 antibody (earliest marker of cholangiocytes differentiation); (iii) anti-CK7 antibody (marker of mature cholangiocytes) and (iv) anti-SM22 antibody (mesenchymal marker), provided an in-depth description of the spatio-temporal organization of the portal tract components during late embryonic and early postnatal stages.

An unanticipated and main challenge that needed to be faced is the liver's heterogeneity. The liver is composed of several lobes, which vary in size, shape, and function. The differences between the liver lobes in mice vary depending on the stage of development. By E15.5, the liver lobes in mice are relatively well-defined and have distinct morphological features. The right lateral lobe is smaller and more rounded in shape, while the left lobe is larger and more elongated. The left and right medial lobe are intermediate in size and shape. This heterogeneity is a limitation when using 3D imaging techniques, because these techniques typically rely on the uniformity of the sample being imaged. If the different lobes of the liver are not uniformly labelled or treated, or if they have different structural characteristics, it becomes difficult to accurately visualize fine details within each lobe. To minimize this problem, I focused on individualized lobes and restricted my analysis until P6. From P13 onwards, our protocol provided results of lower quality and high variability between lobes. Beyond P13, the use of a protocol adapted to adult liver might be more suitable (Adori et al., 2021).

Newly developed protocols for optical clearing of murine adult liver tissue should be tested on embryonic samples. Two recently developed protocols bear high potential. First, a theoretically easy protocol using one simple urea-based amino sugar solution and a single incubation. This protocol efficiently clears adult liver and preserves tissue structure with excellent conservation of fluorophore emissions from endogenous proteins reporters and lipophilic tracer dyes (Hough et al., 2021). Second, liver-CUBIC improves liver transparency by introducing a lipase pretreatment. Compared to the initial CUBIC protocol it achieves good transparency of the liver within a shorter time and better fluorescence preservation. Additional advantages with the use of these two protocols are the better preservation of the tissue volume with less tissue shrinkage and the lower

toxicity of the solvents. Nevertheless, each protocol has its advantages and limitations and should be selected depending on the experimental goals. For example, in adult mouse liver, the liver-CUBIC approach was superior in the maintenance of endogenous fluorescence, whereas the 3DISCO approach achieved a better fluorescence signal with antibody labeling (Z. Liu et al., 2022).

So far, my data generated novel insight into 3D development of the liver and touched upon morphogenic description at the cellular level. The next challenge is to face the complex task of image quantification and in the future, it would be to deepen the analysis of cell-cell interactions at the molecular level. Another interesting approach to understand bile duct morphogenesis would be to study the impact of bile flow on IHBD remodeling. Similar to vascular development, the biliary plexus is created in excess and the adjustment of this network involves the regression of unnecessary ductules. Remodeling determines the formation of major large and fine channels and the establishment of a directional flow necessary for the proper functioning of the organ. Measuring the biliary flux and the associated mechanical stress could explain the intense modifications of the biliary network observed in 3D in this study.

ii. Perspectives

To study development in 3D, whole organ samples are not the only ones that would benefit from tissue-clearing. Crucial steps of morphogenesis can be modeled in organoids or in thick tissue sections (Lancaster & Knoblich, 2014), with sizes on the order of a few hundred microns. Incorporating a tissue clearing step in standard immunostaining protocols would open the door to routine high-resolution imaging a few hundred microns deep into samples with confocal microscopy. This does not

require specialized equipment and is expected to significantly impact our access to higher resolution, *i.e.* even at the subcellular level. It would be complementary to 3D imaging of large sample, as the technic still suffers from relatively low imaging resolutions.

Innovations in large-scale light-sheet microscopy is highly desirable for future work in developmental biology. For example, *de novo* lumen formation requires both subcellular resolution (imaging: cell polarization, tight junctions, basal lamina, apical polarity protein, intracellular vesicles) and visualization at the organ level. In particular, hilar-to-periphery growth of liver structures can only be fully understood using imaging of the whole liver or lobe. Such new 3D imaging data would enable to further complete computational models of lumen formation (Van Liedekerke et al., 2022), allow comparative studies of organ morphogenesis (Pierreux, 2021) and provide optimized platforms for phenotyping mutant animal models.

II. The role of axon guidance molecules during portal tract development: dream or reality?

i. Theory that holds great promise

As described in the introduction, the development of the vasculature, mesenchyme, and bile ducts in the portal area is highly interdependent (Gordillo et al., 2015; Ober & Lemaigre, 2018; Poncy et al., 2015; Tanimizu & Mitaka, 2017). With the exception of the control of cholangiocyte differentiation, which has been fairly well characterized, how this interdependence orchestrates the formation of ducts, mesenchyme, and vessels remains largely unexplored. The coexistence of these different elements in the narrow space of the portal area raises questions about potential cell-cell interactions leading to synchronized tissue morphogenesis of the portal space.

Intercellular crosstalk between epithelial and mesenchymal cells through ligands and receptors is a fundamental feature of organ biology (Xiong, Kuang, Liu, & Lin, 2020). Hepatic cells release an array of secreted factors that exert diverse biological effects and enable intercellular crosstalk necessary for tissue development and homeostasis. Several studies, including ours, have shown that many axon guidance genes are expressed by the hepatic cells and that many of these proteins are constitutively expressed in both fetal and adult liver cells (Barnault et al., 2022; Enns, Jue, & Zhang, 2021; X. Wang et al., 2020). Interestingly, axon guidance genes are now appreciated as general cell migration guidance molecules that can also pattern mesodermal and epidermal tissue morphogenesis (Hinck, 2004).These results support the hypothesis that axon guidance molecules in mesenchyme may

play a critical role in displaying guidance signals that could influence the migration and maturation of adjacent vascular and epithelial cells (H. Y. Chang et al., 2002).

Of fundamental interest, the identification of mesenchyme-epithelial interactions, occurring during liver development should also provide mechanistic information that can be implemented in the *in vitro* production of liver tissue. In addition, recent detailed mechanistic studies of mesenchymal cell biology have revealed that their functions, when defective, lead to the development of complex diseases, such as tissue fibrosis and cancer (Koliaraki, Prados, Armaka, & Kollias, 2020). This confirms our initial thoughts that it is essential to progress in the knowledge of the epithelium-mesenchyme interaction in the context of liver development with a particular focus on axon guidance genes.

ii. The study of axon guidance genes in liver development: more or no more?

Our gene profiling strategy provided high resolution and spatial expression data, which led to the selection of the NEO1-RGMA and SLIT2-ROBO2 receptor-ligand pairs as candidate for epithelial-mesenchyme interaction driving liver portal tract morphogenesis. Our choice to focus on those candidates were based on our experimental data as well as on the literature (cfr introduction chapter VI). As a quick reminder, given their many and varied roles in regulating epithelial morphogenetic events, together with their well-established roles in cell motility, netrins seemed like excellent candidates to study portal tract development (Chaturvedi & Murray, 2022; X. Lu et al., 2004; Murray, 2017; Srinivasan et al., 2003; Yebra et al., 2003). In particular, the receptor-ligand couple NEO1-RGMA was identified as a promising candidate based on previous studies highlighting its role in neuroepithelial tube formation and its ability to promote epithelial stability by

controlling junctional tension and E-cadherin dynamics (N. K. Lee et al., 2016). In parallel, we focused on the SLIT-ROBO axon guidance family, as this pathway plays essential roles in cell motility, adhesion and polarity. SLIT2-ROBO2 signaling was found to display angiogenic function and to establish islet architecture by regulation cell migration (Blockus & Chédotal, 2016; Gilbert et al., 2020).

Our phenotypic characterization of 8 knockout mouse models, unexpectedly -and disappointingly- uncovered that Slit-Robo and Neo1/Rgma signaling is not required for bile duct development, but that mesenchymal-produced SLIT2 ligand and ROBO2 receptor are needed for optimal development of the hepatic artery branches.

Why did some of our knockout mouse models generated such negative results ? Did we look for a needle in a haystack using boxing gloves or did we fail to untangle the ball of yarn? Our results raise questions on the limits of our study and selected methodology, on alternative approaches and on the positive side of negative data. These questions are discussed below.

Our contribution and its limitations

Inducible mouse models: advantages and limitations

In order to successfully isolate mesenchyme and cholangiocyte and later specifically inhibit axon guidance genes in these adjacent cell types we selected the most suitable mouse models to our knowledge. The main advantage of our two mouse models (*Sox9-Cre^{ER}* and *Sm22-Cre*) is efficient and consistent Cre recombination expression in the cell type of interest. In addition, both mouse models were previously used to successfully inhibit target genes when studying bile duct

development (Hofmann et al., 2010; Poncy et al., 2015). Even if mesenchymal cells remain a poorly described population, our current analysis extends previous data (Hofmann et al., 2010) by showing that *Sm22-Cre* is active in CD90+ and in αSMA+ periportal cells, which we consider precursors of the VSMCs. These data support that the *Sm22-Cre* line fits the goals of our study well, yet a more optimal line would drive expression of Cre^{ER} instead of Cre. This would enable time-controlled activity of Cre and allow to determine the timing at which axon guidance genes are critical for portal tract development. Another more general limitation of our Cre-line is their genetic background which potentially influenced the results of our gene inactivation strategy. Different results can be obtained when knocking genes out in different strains. Thus, we cannot rule out that the lack of phenotype in a subset of our mice results from inappropriate mouse strain selection.

Dealing with cholangiocyte and mesenchyme heterogeneity

The heterogeneity of cholangiocyte and mesenchyme was a tricky issue to address and posed several limitations and questions to our study.

First, we had to make a choice of a RNA seq technology in order to efficiently identify the gene expression profile of two small and heterogenous cell populations. As they both comprise a small percentage of the total liver, cell isolation combined with bulk RNA seq had the advantage to provide a higher sequencing depth compared to scRNAseq (Hegenbarth, Lezzoche, De Windt, & Stoll, 2022; X. Li & Wang, 2021). In addition, data processing is easier, and the technique is cost-effective. scRNA seq would have provided more data about the cellular diversity and complexity within the population. Recently it was shown that snRNA seq captures 50% more cholangiocytes and mesenchymal cells than scRNA-

seq (Paris & Henderson, 2022) and appears presently as an obvious choice for studying epithelial-mesenchymal interactions. It should allow to gain valuable biological insights into rare cellular properties and cell-to-cell variability.

Second, although selected genes were visualized *in vivo* trough immunostaining it was challenging to determine the precise subpopulation of mesenchymal cells expressing the gene of interest. High resolution spatial transcriptomics or sequential fluorescence *in situ* hybridization (Molecular Cartography™) has a designated place in this context in combination with scRNA-Seq technologies. It provides a more complete interpretation regarding the spatial organization of small cells populations and specific genes.

Third, we observed a high phenotypic heterogeneity between mutant mice with very local effects. Surprisingly, following *Sm22-Cre*-mediated inactivation of SLIT2/ROBO2 no anomaly was found in the VSMCs surrounding the branches of the portal vein. Our data indicate that when the portal mesenchyme expands during growth, the inactivation of *Slit2* or *Robo2* only impacts the artery and not the portal vein, suggesting that development of vein-associated VSMCs and artery-associated VSMCs remains independent and occurs via distinct mechanisms. These very local effects raise new question about mesenchymal niches and subpopulation specific functions.

Axon guidance pathways complexity

The lack of morphological anomalies in several of our mouse models likely indicate the high degree of similarity in the functions of axon guidance factors with functional redundancy that may occur among family members and between

families. Indeed, the complex cross talk between signaling pathways has been dramatically accelerated by the burgeoning body of structural work that sheds light on how receptor-ligand and receptor-receptor interactions control receptor activation and serve to diversify and modulate signaling outputs (Zang et al., 2021). In addition to new roles for interactions between distinct guidance pathways, significant progress has been made in understanding how proteolytic processing of axon guidance receptors can regulate receptor availability and downstream signaling. One particularly interesting emerging theme is that receptors often undergo processive proteolysis to generate intracellular domains which can signal in new ways, including by acting as direct regulators of transcription (Zang et al., 2021). Nor can we rule out that some axon guidance signaling may be supplanted by other signals at different time points as it is the case for the regulation of semaphorins on the vascular integrity. Semaphorin-Plexin signaling appears to be required during lymphatic development but is dispensable in adult tissues (Laws & Bashaw, 2022). Axon guidance receptors can be regulated at multiple level to ensure that the right complement of receptors are deployed at the right time and place (Zang et al., 2021). Thus, elucidating the roles of individual members as ligands and as receptors is hindered by the number of axon guidance members expressed and by the complexity and redundancy of their actions. It is therefore complex to search for a function, as loss of multiple cues may be required for phenotypes to be displayed (Hinck, 2004). Adding inactivation of *Ntn1* to the knockout of *Rgma* and *Neo1* seems a promising question. This could be achieved using genetic tools, but the use of NTN1 blocking antibodies should also be considered.

More or no more? More, with a different experimental approach

Guidance molecules play well-described roles in tissue patterning and morphogenesis. The four major guidance molecules are highly conserved amongst species and can either be secreted or function as cell surface-bound ligands that interact with their cognate receptors on neighboring cells (Zang et al., 2021). During the last 5 years we studied the impact of two out of four axon guidance families in the context of liver development.

As one is limited by time, budget, and available technology it made sense to start with the most reasonable candidate (aka: axon guidance family containing less members). Moreover, within those families we did our best to select our candidates based on several criteria's;

- Gene coding for secreted signaling factor and cognate signaling receptor
- Expression in cholangiocytes and portal mesenchyme, respectively, during portal tract development
- Location of expression near forming duct and arteries

Nevertheless, we still believe that additional members of these axon guidance family should be investigated. For example, since SLIT2-ROBO2 signaling was shown to impact arterial development it raises the questions about the role of ROBO4, who has been shown to stabilize blood vessel after binding with SLIT or UNC5B (Jones et al., 2009; Koch et al., 2011). ROBO4 was not considered relevant due to its very low expression in portal mesenchyme and absence in cholangiocytes. During our analysis of Wang *et al*.'s data we highlighted its expression also in endothelial cells (X. Wang et al., 2020) and found that UNC5B is highly expressed in mesenchyme. Yet our *in situ* hybridization experiments detected only rare portal endothelial cells positive for *Robo4* (L. Gannoun, *not shown*).

A candidate of the netrin family is Netrin 4. It displays anti-angiogenic properties and promotes VSMC adhesion and migration. Its overexpression increases coverage of endothelial cells tubes by VSMCs. In this context, Netrin4 is required for blood vessel integrity, through regulation of both endothelial cells and VSMCs (Lejmi et al., 2008). Netrin4 was not detected in our RNA seq data but, Wang and colleagues detected it in hepatic endothelial cells (X. Wang et al., 2020).

Moreover, the investigation of the two other axon guidance pathways deserves attention, namely Eph/Ephrin, Semaphorin/Plexin-Neuropilin, which were also identified in our gene expression profiling of embryonic cholangiocytes and mesenchymal cells. Again, scRNA sequencing by Wang et al. (X. Wang et al., 2020) confirms the expression of members of these pathways in several liver cell types, including cholangiocytes and mesenchyme (Fig. 1).

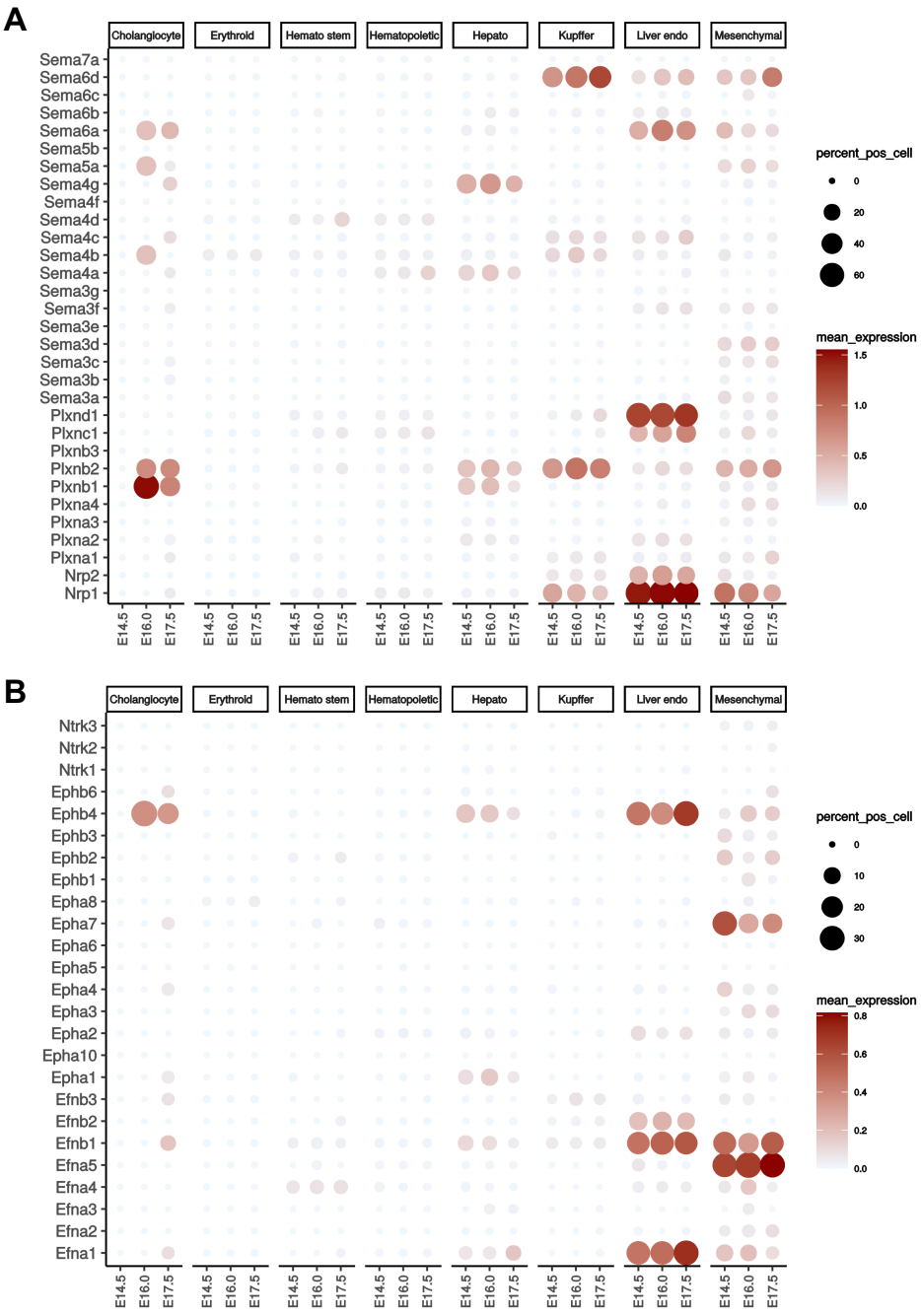


Figure 1: Expression of genes of the Semaphorin and Ephrin pathways in developing liver. Single cell RNA sequencing performed on different embryonic liver cell types (Wang et al.,

2020) shows expression of the genes belonging to the two signaling pathways in cholangiocytes and mesenchymal cells.

The role of the Ephrin and Semaphorin pathways has essentially been studied in hepatic diseases but the lack of information on these pathways during liver development would further justify research in embryonic liver. The expression pattern of these ligands and receptors during liver development as well as epithelial-mesenchyme expression of these binding pairs, suggest that Ephrin and Semaphorin axon guidance pathways could play a role in liver morphogenesis. This is also supported by previous data underlining their importance during vascular and epithelial morphogenesis (Introduction chapter VI). Closely related to our findings on hepatic arteries, mice lacking Ephrin-B2 in vascular smooth muscle develop vessel wall defects and aortic aneurysms (Lindskog et al., 2014; A. Nakayama et al., 2013)). During development Ephrin-B2 is also necessary for normal function of mural cells (Foo et al., 2006). Similar roles may exist in liver vascular development. As for the Semaphorin pathway, its involvement in VSMC development is illustrated by the observation that SEMA3A favors formation of NRP1- Plexin A1 complexes at the expense of NRP1-PDGFRβ complex, thus inhibiting phosphorylation of PDGFRβ and reducing VSMC proliferation and migration (J. H. Wu et al., 2019). SEMAs are known to interact with VEGFs on endothelial cells (Alto & Terman, 2017) and this interaction could be further investigated during hepatic artery development. Previous data already highlighted a role of VEGF signaling from the bile duct to recruit endothelial progenitors' cells and initiate arteriogenesis (Mariotti et al., 2021). Finally, Neuropilin-1 is expressed in early fetal liver hematopoietic cells and promotes blood vessel formation (Yamada et al., 2003) and we observed its prolonged expression in endothelial and mesenchymal cells (X. Wang et al., 2020).

The above data support a hitherto undescribed role of axon guidance genes in liver development. We propose to address this issue using a slightly different approach:

1. Exploit scRNA-seq and snRNA data to determine possible ligand-receptor interactions in the developing liver (Han et al., 2020; Lotto et al., 2020; Mu et al., 2020; X. Wang et al., 2020; Yang et al., 2017).

Single cell transcriptomics data provides the opportunity to computationally predict possible ligand-receptor interactions between two cell types. Existing published methods can be categorized into either (1) those that rely on known ligand-receptor pairs or (2) those that additionally rely on known downstream target genes (Armingol, Officer, Harismendy, & Lewis, 2021). While some groups have written their own code to do this analysis (Camp et al., 2017; Halpern et al., 2018), one could use computational tools such as CellPhoneDB or NicheNet (Armingol et al., 2021; Vento-Tormo et al., 2018). Interestingly, these algorithms determine possible interactions that are significantly enriched between two cell types.

2. Spatial visualization of all axon guidance members

Some of these possible interactions will not occur in developing livers, due to lack of correlation between gene and protein expression or the lack of spatial proximity between receptors and ligands. To circumvent these limitations, RNAs coding for ligand and receptors could be determined spatially using Molecular Cartography™ (Resolve BioSciences) that allows for 100-plex spatial mRNA analysis and can subsequently be visualized at low-throughput by standard immunostaining of sections

3. *In vitro* study to further select candidates

Multilineage organoid will be useful to interrogate the role of a larger numbers of ligands and receptors than would be feasible in mice (Harrison et al., 2021; Lotto et al., 2020). The goal would be to use the organoids for high throughput screening of these ligand-receptor interactions using shRNA-based knockdown of genes or small molecules to activate or inhibit the interactions or their downstream pathways. It will allow to select candidate via functional validation before using knockout mouse models. By example, available Eph receptor targeting peptides and small molecules can be found in the following reviews (Giorgio et al., 2018; Noberini, Lamberto, & Pasquale, 2012). Yet multilineage organoids do not yet recapitulate portal tract structures in the liver.

4. *In vivo* knock out mouse models

Finally, it is important to weigh the advantages of scale and tractability in organoids against the disadvantages of using an artificial system in place of the natural organ. Thus, we do believe that *in vitro* functional analysis remain complementary to *in vivo* models.

To answer the question of the title of this section: a role of axon guidance molecules during portal tract development: dream or reality? Considering the complexity of such project proposition one could think that it is more of a dream. Still, the availability of technology and opportunities for collaborative research involving experts in transcriptomics, bioinformatics, multiplex immunostaining, organoid production and transgenic mouse modeling makes it worth pursuing.

III. How far are we from applications?

Liver diseases account for approximately two million deaths worldwide yearly, or 3.5% of global mortality (Asrani, Devarbhavi, Eaton, & Kamath, 2019). A number of cases may benefit from regenerative therapy, the development of which requires substantial knowledge on liver development. The study of liver development has indeed uncovered several mechanisms of hepatic cell differentiation that were successfully transposed into protocols for programmed *in vitro* differentiation of stem cells to hepatocytes and cholangiocytes for regenerative therapy of liver disease (Asai et al., 2017; Harrison et al., 2021; Velazquez et al., 2021; F. Wu et al., 2019). However, essential knowledge is still missing to produce liver-like tissue in which hepatocyte cords, bile ducts, and vasculature are reliably connected. Key challenges also lay in the creation of a reproducible and scalable engineering process. So far cellular heterogeneity, connectivity, and complex microenvironment pose significant engineering challenges, and *in vitro* tissue engineering of the liver does so far not succeed in correctly reconstructing a functional biliary tract architecture. Such endeavor begins with a detailed understanding of the spatial and temporal biological processes that underlie hepatic morphogenesis, followed by precise implementation of these processes into a bioengineering approach (Lee & Takebe, 2022).

Our description of biliary and mesenchymal morphogenesis cannot easily be transposed into engineering protocols, neither the activation SLIT/ROBO or NEO1/RGMA signaling. Still, we hope that our contribution indicates where engineers should go for. It also underlines a hitherto unsuspected heterogeneity and complexity of developing bile ducts and VSMCs. Our identification of SLIT/ROBO as a new regulator of liver vascular development provides new markers

for benchmarking the quality of *in vitro* engineered tissue. Additional functional studies identifying soluble factors and paracrine signals that mimic secreted signals during development to generate mature, functional liver-like tissue are expected to lead to concrete applications. Our data point to mutual interactions between developing bile ducts, the adjacent portal vein mesenchyme and hepatic artery. We strongly believe that further study of the role of axon guidance genes during liver morphogenesis will uncover major cues responsible for liver organogenesis.

Finally, it is becoming increasingly apparent that the same developmental signals reappear in liver cancer and may be underappreciated oncogenic drivers. Thus, studies of liver developmental biology are paramount for improving our understanding of liver cancer biology.

Concluding remarks

At the time I started my PhD the field of developmental biology was in crisis (Wallingford, 2019; Zon, 2019). The impact factors of developmental biology journals had been declining over the years. Although impact factors are not a optimal measure of real importance, they reflect the perception of the field by other scientists and the public. With developmental biology seemingly playing second fiddle to trendier terms like stem cell biology, organoids, and high-throughput data acquisition without functional validation.

But why did the field face such drawbacks? Leading experts proposed several explanations such as a lack of inclusiveness toward these rapidly spawning news branches of the field and bad marketing (Wallingford, 2019; Zon, 2019). But could it also be due to the shift from willing to understand complex developmental processes to the need for -or public request of- more accessible and/or versatile system for applied science ? There is a risk for a growing gap between scientists aiming at solving scientific problems and public craving for short-term impact and applications. There is also a perception problem with young investigators feeling that descriptive embryonic development is already completed: this is obviously wrong since we have not more “solved” the embryo than we have “solved” cancer.

What if descriptive *in vivo* work is just as important, revealing, and fascinating as complicated molecular manipulations? As the past has already proven, developmental biology has led to tremendous impact on clinical therapies and cancer related discoveries.

What if, it is now the more exciting time for developmental biology? Technologies such as 3D imaging and single-cell sequencing are revolutionizing the way we see and understand organs.

What if, wondering about the embryos is an activity that unifies all of humanity and has done so for thousands of years? Think at all who cared about a pregnant friend or family member, and eventually contemplated the echography of the embryo. While they may not articulate it in this way, they have probably carried hopes and worries about the health of the embryo and the proper development of its organs (Wallingford, 2019).

What if, making a PhD on liver development was indeed a brilliant idea since it has nourished my scientific curiosity to the sole purpose of better understanding. Be sure that it will get me out of bed with a smile during the next years of my scientific career.

Bibliography

Adams, M. T., Gilbert, J. M., Hinojosa Paiz, J., Bowman, F. M., & Blum, B. (2018). Endocrine cell type sorting and mature architecture in the islets of Langerhans require expression of Roundabout receptors in β cells. *Sci Rep, 8*(1), 10876. doi:10.1038/s41598-018-29118-x

Adams, R. H., & Eichmann, A. (2010). Axon guidance molecules in vascular patterning. *Cold Spring Harb Perspect Biol, 2*(5), a001875. doi:10.1101/cshperspect.a001875

Adori, C., Daraio, T., Kuiper, R., Barde, S., Horvathova, L., Yoshitake, T., . . . Hökfelt, T. (2021). Disorganization and degeneration of liver sympathetic innervations in nonalcoholic fatty liver disease revealed by 3D imaging. *Sci Adv, 7*(30). doi:10.1126/sciadv.abg5733

Aida, T., Chiyo, K., Usami, T., Ishikubo, H., Imahashi, R., Wada, Y., . . . Tanaka, K. (2015). Cloning-free CRISPR/Cas system facilitates functional cassette knock-in in mice. *Genome Biol, 16*(1), 87. doi:10.1186/s13059-015-0653-x

Alagille, D., Estrada, A., Hadchouel, M., Gautier, M., Odièvre, M., & Dommergues, J. P. (1987). Syndromic paucity of interlobular bile ducts (Alagille syndrome or arteriohepatic dysplasia): review of 80 cases. *J Pediatr, 110*(2), 195-200. doi:10.1016/s0022-3476(87)80153-1

Alto, L. T., & Terman, J. R. (2017). Semaphorins and their Signaling Mechanisms. *Methods Mol Biol, 1493*, 1-25. doi:10.1007/978-1-4939-6448-2_1

Amersfoort, J., Eelen, G., & Carmeliet, P. (2022). Immunomodulation by endothelial cells — partnering up with the immune system? *Nature Reviews Immunology, 22*(9), 576-588. doi:10.1038/s41577-022-00694-4

Andersson, E. R., Chivukula, I. V., Hankeova, S., Sjöqvist, M., Tsoi, Y. L., Ramsköld, D., . . . Lendahl, U. (2018). Mouse Model of Alagille Syndrome and Mechanisms of Jagged1 Missense Mutations. *Gastroenterology, 154*(4), 1080-1095. doi:10.1053/j.gastro.2017.11.002

Andrews, T. S., Atif, J., Liu, J. C., Perciani, C. T., Ma, X. Z., Thoeni, C., . . . MacParland, S. A. (2022). Single-Cell, Single-Nucleus, and Spatial RNA Sequencing of the Human Liver Identifies Cholangiocyte and Mesenchymal Heterogeneity. *Hepatol Commun, 6*(4), 821-840. doi:10.1002/hep4.1854

Andrews, W. D., Barber, M., & Parnavelas, J. G. (2007). Slit–Robo interactions during cortical development. *Journal of Anatomy, 211*(2), 188-198. doi:https://doi.org/10.1111/j.1469-7580.2007.00750.x

Antoniou, A., Raynaud, P., Cordi, S., Zong, Y., Tronche, F., Stanger, B., . . . Lemaigre, F. P. (2009). Intrahepatic bile ducts develop according to a new mode of tubulogenesis regulated by the transcription factor SOX9. *Gastroenterology, 136*(7), 2325-2333. doi:10.1053/j.gastro.2009.02.051

Ao, J. Y., Chai, Z. T., Zhang, Y. Y., Zhu, X. D., Kong, L. Q., Zhang, N., . . . Sun, H. C. (2015). Robo1 promotes angiogenesis in hepatocellular carcinoma through the Rho family of guanosine triphosphatases' signaling pathway. *Tumour Biol, 36*(11), 8413-8424. doi:10.1007/s13277-015-3601-1

Ardito, C. M., Gruner, B. M., Takeuchi, K. K., Lubeseder-Martellato, C., Teichmann, N., Mazur, P. K., . . . Siveke, J. T. (2012). EGF receptor is required for KRAS-induced pancreatic tumorigenesis. *Cancer Cell, 22*(3), 304-317. doi:S1535-6108(12)00337-6 [pii]

10.1016/j.ccr.2012.07.024

Ariel, P. (2017). A beginner's guide to tissue clearing. *Int J Biochem Cell Biol, 84*, 35-39. doi:10.1016/j.biocel.2016.12.009

Armingol, E., Officer, A., Harismendy, O., & Lewis, N. E. (2021). Deciphering cell-cell interactions and communication from gene expression. *Nat Rev Genet, 22*(2), 71-88. doi:10.1038/s41576-020-00292-x

Asahina, K., Tsai, S. Y., Li, P., Ishii, M., Maxson, R. E., Jr., Sucov, H. M., & Tsukamoto, H. (2009). Mesenchymal origin of hepatic stellate cells, submesothelial cells, and perivascular mesenchymal cells during mouse liver development. *Hepatology, 49*(3), 998-1011. doi:10.1002/hep.22721

Asahina, K., Zhou, B., Pu, W. T., & Tsukamoto, H. (2011). Septum transversum-derived mesothelium gives rise to hepatic stellate cells and perivascular mesenchymal cells in developing mouse liver. *Hepatology, 53*(3), 983-995. doi:10.1002/hep.24119

Asai, A., Aihara, E., Watson, C., Mourya, R., Mizuochi, T., Shivakumar, P., . . . Bezerra, J. A. (2017). Paracrine signals regulate human liver organoid maturation from induced pluripotent stem cells. *Development, 144*(6), 1056-1064. doi:10.1242/dev.142794

Asrani, S. K., Devarbhavi, H., Eaton, J., & Kamath, P. S. (2019). Burden of liver diseases in the world. *J Hepatol, 70*(1), 151-171. doi:10.1016/j.jhep.2018.09.014

Avci, M. E., Konu, O., & Yagci, T. (2008). Quantification of SLIT-ROBO transcripts in hepatocellular carcinoma reveals two groups of genes with coordinate expression. *BMC Cancer, 8*, 392. doi:10.1186/1471-2407-8-392

Barnault, R., Verzeroli, C., Fournier, C., Michelet, M., Redavid, A. R., Chicherova, I., . . . Parent, R. (2022). Hepatic inflammation elicits production of proinflammatory netrin-1 through exclusive activation of translation. *Hepatology, 76*(5), 1345-1359. doi:https://doi.org/10.1002/hep.32446

Beath, S. V. (2003). Hepatic function and physiology in the newborn. *Semin Neonatol, 8*(5), 337-346. doi:10.1016/s1084-2756(03)00066-6

Belle, M., Godefroy, D., Couly, G., Malone, S. A., Collier, F., Giacobini, P., & Chédotal, A. (2017). Tridimensional Visualization and Analysis of Early Human Development. *Cell, 169*(1), 161-173.e112. doi:10.1016/j.cell.2017.03.008

Belle, M., Godefroy, D., Dominici, C., Heitz-Marchaland, C., Zelina, P., Hellal, F., . . . Chedotal, A. (2014). A simple method for 3D analysis of immunolabeled axonal tracts in a transparent nervous system. *Cell Rep, 9*(4), 1191-1201. doi:10.1016/j.celrep.2014.10.037

Benhamouche-Trouillet, S., O'Loughlin, E., Liu, C. H., Polacheck, W., Fitamant, J., McKee, M., . . . McClatchey, A. I. (2018). Proliferation-independent role of NF2 (merlin) in limiting biliary morphogenesis. *Development, 145*(9), pii: dev162123. doi:10.1242/dev.162123

Beuers, U., Hohenester, S., de Buy Wenniger, L. J., Kremer, A. E., Jansen, P. L., & Elferink, R. P. (2010). The biliary HCO(3)(-) umbrella: a unifying hypothesis on pathogenetic and therapeutic aspects of fibrosing cholangiopathies. *Hepatology, 52*(4), 1489-1496. doi:10.1002/hep.23810

Blockus, H., & Chédotal, A. (2016). Slit-Robo signaling. *Development, 143*(17), 3037-3044. doi:10.1242/dev.132829

Boyer, J. L. (2013). Bile formation and secretion. *Compr Physiol, 3*(3), 1035-1078. doi:10.1002/cphy.c120027

Brancale, J., & Vilarinho, S. (2021). A single cell gene expression atlas of 28 human livers. *J Hepatol, 75*(1), 219-220. doi:10.1016/j.jhep.2021.03.005

Brereton, M. F., Vergari, E., Zhang, Q., & Clark, A. (2015). Alpha-, Delta- and PP-cells: Are They the Architectural Cornerstones of Islet Structure and Co-ordination? *J Histochem Cytochem, 63*(8), 575-591. doi:10.1369/0022155415583535

Brevini, T., Tysoe, O. C., & Sampaziotis, F. (2020). Tissue engineering of the biliary tract and modelling of cholestatic disorders. *Journal of Hepatology, 73*(4), 918-932. doi:https://doi.org/10.1016/j.jhep.2020.05.049

Camp, J. G., Sekine, K., Gerber, T., Loeffler-Wirth, H., Binder, H., Gac, M., . . . Treutlein, B. (2017). Multilineage communication regulates human liver bud development from pluripotency. *Nature, 546*(7659), 533-538. doi:10.1038/nature22796

Campbell, S. A., Stephan, T. L., Lotto, J., Cullum, R., Drissler, S., & Hoodless, P. A. (2021). Signalling pathways and transcriptional regulators orchestrating

liver development and cancer. *Development, 148*(17). doi:10.1242/dev.199814

Cao, S., Yaqoob, U., Das, A., Shergill, U., Jagavelu, K., Huebert, R. C., . . . Shah, V. H. (2010). Neuropilin-1 promotes cirrhosis of the rodent and human liver by enhancing PDGF/TGF-beta signaling in hepatic stellate cells. *J Clin Invest, 120*(7), 2379-2394. doi:10.1172/jci41203

Carpentier, R., Suner, R. E., Van Hul, N., Kopp, J. L., Beaudry, J. B., Cordi, S., . . . Lemaigre, F. P. (2011). Embryonic ductal plate cells give rise to cholangiocytes, periportal hepatocytes, and adult liver progenitor cells. *Gastroenterology, 141*, 1432-1438. doi:S0016-5085(11)00863-8 [pii]
10.1053/j.gastro.2011.06.049

Cayuso, J., Dzementsei, A., Fischer, J. C., Karemore, G., Caviglia, S., Bartholdson, J., . . . Ober, E. A. (2016). EphrinB1/EphB3b Coordinate Bidirectional Epithelial-Mesenchymal Interactions Controlling Liver Morphogenesis and Laterality. *Dev Cell, 39*(3), 316-328. doi:10.1016/j.devcel.2016.10.009

Chakraborty, R., Chatterjee, P., Dave, J. M., Ostriker, A. C., Greif, D. M., Rzucidlo, E. M., & Martin, K. A. (2021). Targeting smooth muscle cell phenotypic switching in vascular disease. *JVS Vasc Sci, 2*, 79-94. doi:10.1016/j.jvssci.2021.04.001

Chang, H. Y., Chi, J. T., Dudoit, S., Bondre, C., van de Rijn, M., Botstein, D., & Brown, P. O. (2002). Diversity, topographic differentiation, and positional memory in human fibroblasts. *Proc Natl Acad Sci U S A, 99*(20), 12877-12882. doi:10.1073/pnas.162488599

Chang, J., Lan, T., Li, C., Ji, X., Zheng, L., Gou, H., . . . Wang, L. (2015). Activation of Slit2-Robo1 signaling promotes liver fibrosis. *J Hepatol, 63*(6), 1413-1420. doi:10.1016/j.jhep.2015.07.033

Chaturvedi, V., & Murray, M. J. (2022). Netrins: Evolutionarily Conserved Regulators of Epithelial Fusion and Closure in Development and Wound Healing. *Cells Tissues Organs, 211*(2), 193-211. doi:10.1159/000513880

Chen, Y., Bai, L., Zhou, Y., Zhang, X., Zhang, J., & Shi, Y. (2020). Fine-scale visualizing the hierarchical structure of mouse biliary tree with fluorescence microscopy method. *Biosci Rep, 40*(5). doi:10.1042/bsr20193757

Cleaver, O., & Melton, D. A. (2003). Endothelial signaling during development. *Nat Med, 9*(6), 661-668. doi:10.1038/nm0603-661

Clotman, F., Lannoy, V. J., Reber, M., Cereghini, S., Cassiman, D., Jacquemin, P., . . . Lemaigre, F. P. (2002). The onecut transcription factor HNF6 is required for normal development of the biliary tract. *Development, 129*(8), 1819-1828. Retrieved from http://www.ncbi.nlm.nih.gov/entrez/query.fcgi?cmd=Retrieve&db=PubMed&dopt=Citation&list_uids=11934848

Clotman, F., Libbrecht, L., Gresh, L., Yaniv, M., Roskams, T., Rousseau, G. G., & Lemaigre, F. P. (2003). Hepatic artery malformations associated with a primary defect in intrahepatic bile duct development. *J Hepatol, 39*(5), 686-692. doi:S0168827803004094 [pii]

Coll, M., Arino, S., Martinez-Sanchez, C., Garcia-Pras, E., Gallego, J., Moles, A., . . . Sancho-Bru, P. (2022). Ductular reaction promotes intrahepatic angiogenesis through Slit2-Roundabout 1 signaling. *Hepatology, 75*(2), 353-368. doi:10.1002/hep.32140

Collardeau-Frachon, S., & Scoazec, J. Y. (2008). Vascular development and differentiation during human liver organogenesis. *Anat Rec (Hoboken), 291*(6), 614-627. doi:10.1002/ar.20679

Cordero-Espinoza, L., Dowbaj, A. M., Kohler, T. N., Strauss, B., Sarlidou, O., Belenguer, G., . . . Huch, M. (2021). Dynamic cell contacts between periportal mesenchyme and ductal epithelium act as a rheostat for liver cell proliferation. *Cell Stem Cell, 28*(11), 1907-1921 e1908. doi:10.1016/j.stem.2021.07.002

Cordi, S., Godard, C., Saandi, T., Jacquemin, P., Monga, S. P., Colnot, S., & Lemaigre, F. P. (2016). Role of beta-catenin in development of bile ducts. *Differentiation, 91*(1-3), 42-49. doi:10.1016/j.diff.2016.02.001

Coultas, L., Chawengsaksophak, K., & Rossant, J. (2005). Endothelial cells and VEGF in vascular development. *Nature, 438*(7070), 937-945. doi:10.1038/nature04479

Cozzitorto, C., Mueller, L., Ruzittu, S., Mah, N., Willnow, D., Darrigrand, J. F., . . . Spagnoli, F. M. (2020). A Specialized Niche in the Pancreatic Microenvironment Promotes Endocrine Differentiation. *Dev Cell, 55*(2), 150-162.e156. doi:10.1016/j.devcel.2020.08.003

Crivellato, E. (2011). The role of angiogenic growth factors in organogenesis. *Int J Dev Biol, 55*(4-5), 365-375. doi:10.1387/ijdb.103214ec

De Breuck, S., Lardon, J., Rooman, I., & Bouwens, L. (2003). Netrin-1 expression in fetal and regenerating rat pancreas and its effect on the migration of human pancreatic duct and porcine islet precursor cells. *Diabetologia, 46*(7), 926-933. doi:10.1007/s00125-003-1125-5

de Jong, I. E. M., van Leeuwen, O. B., Lisman, T., Gouw, A. S. H., & Porte, R. J. (2018). Repopulating the biliary tree from the peribiliary glands. *Biochimica et Biophysica Acta (BBA) - Molecular Basis of Disease, 1864*(4, Part B), 1524-1531. doi:https://doi.org/10.1016/j.bbadis.2017.07.037

De Minicis, S., Kisseleva, T., Francis, H., Baroni, G. S., Benedetti, A., Brenner, D., . . . Marzioni, M. (2013). Liver carcinogenesis: Rodent models of hepatocarcinoma and cholangiocarcinoma. *Dig Liver Dis, 45*(6), 450-459. doi:S1590-8658(12)00406-9 [pii]

10.1016/j.dld.2012.10.008

Delgado, I., Carrasco, M., Cano, E., Carmona, R., Garcia-Carbonero, R., Marin-Gomez, L. M., . . . Rojas, A. (2014). GATA4 loss in the septum transversum mesenchyme promotes liver fibrosis in mice. *Hepatology, 59*(6), 2358-2370. doi:10.1002/hep.27005

Demarez, C., Gerard, C., Cordi, S., Poncy, A., Achouri, Y., Dauguet, N., . . . Lemaigre, F. P. (2018). MicroRNA-337-3p controls hepatobiliary gene expression and transcriptional dynamics during hepatic cell differentiation. *Hepatology, 67*(1), 313-327. doi:10.1002/hep.29475

Dent, J. A., Polson, A. G., & Klymkowsky, M. W. (1989). A whole-mount immunocytochemical analysis of the expression of the intermediate filament protein vimentin in Xenopus. *Development, 105*(1), 61-74. doi:10.1242/dev.105.1.61

DeSesso, J. M. (2017). Vascular ontogeny within selected thoracoabdominal organs and the limbs. *Reprod Toxicol, 70*, 3-20. doi:10.1016/j.reprotox.2016.10.007

Dobie, R., Wilson-Kanamori, J. R., Henderson, B. E. P., Smith, J. R., Matchett, K. P., Portman, J. R., . . . Henderson, N. C. (2019). Single-Cell Transcriptomics Uncovers Zonation of Function in the Mesenchyme during Liver Fibrosis. *Cell Rep, 29*(7), 1832-1847 e1838. doi:10.1016/j.celrep.2019.10.024

Dou, C., Wang, H., Zhou, G., Zhu, H., Wen, H., & Xu, S. (2018). Slit3 regulates migration of endothelial progenitor cells by activation of the RhoA/Rho kinase pathway. *Int J Clin Exp Pathol, 11*(7), 3398-3404.

Driskill, J. H., & Pan, D. (2021). The Hippo Pathway in Liver Homeostasis and Pathophysiology. *Annu Rev Pathol, 16*, 299-322. doi:10.1146/annurev-pathol-030420-105050

Duan, L., Woolbright, B. L., Jaeschke, H., & Ramachandran, A. (2020). Late Protective Effect of Netrin-1 in the Murine Acetaminophen Hepatotoxicity Model. *Toxicol Sci, 175*(2), 168-181. doi:10.1093/toxsci/kfaa041

Dubrac, A., Genet, G., Ola, R., Zhang, F., Pibouin-Fragner, L., Han, J., . . . Eichmann, A. (2016). Targeting NCK-Mediated Endothelial Cell Front-Rear Polarity Inhibits Neovascularization. *Circulation, 133*(4), 409-421. doi:10.1161/CIRCULATIONAHA.115.017537

Elpek, G. (2015). Neuropilins and liver. *World J Gastroenterol, 21*(23), 7065-7073. doi:10.3748/wjg.v21.i23.7065

Enns, C. A., Jue, S., & Zhang, A. S. (2021). Hepatocyte neogenin is required for hemojuvelin-mediated hepcidin expression and iron homeostasis in mice. *Blood, 138*(6), 486-499. doi:10.1182/blood.2020009485

Ertürk, A., Becker, K., Jährling, N., Mauch, C. P., Hojer, C. D., Egen, J. G., . . . Dodt, H. U. (2012). Three-dimensional imaging of solvent-cleared organs using 3DISCO. *Nat Protoc, 7*(11), 1983-1995. doi:10.1038/nprot.2012.119

Escot, S., Willnow, D., Naumann, H., Di Francescantonio, S., & Spagnoli, F. M. (2018). Robo signalling controls pancreatic progenitor identity by regulating Tead transcription factors. *Nat Commun, 9*(1), 5082. doi:10.1038/s41467-018-07474-6

Fabris, L., Cadamuro, M., Libbrecht, L., Raynaud, P., Spirli, C., Fiorotto, R., . . . Roskams, T. (2008). Epithelial expression of angiogenic growth factors modulate arterial vasculogenesis in human liver development. *Hepatology, 47*(2), 719-728. doi:10.1002/hep.22015

Feinstein, J., & Ramkhelawon, B. (2017). Netrins & Semaphorins: Novel regulators of the immune response. *Biochim Biophys Acta Mol Basis Dis, 1863*(12), 3183-3189. doi:10.1016/j.bbadis.2017.09.010

Finney, A. C., & Orr, A. W. (2018). Guidance Molecules in Vascular Smooth Muscle. *Front Physiol, 9*, 1311. doi:10.3389/fphys.2018.01311

Fiorotto, R., Raizner, A., Morell, C. M., Torsello, B., Scirpo, R., Fabris, L., . . . Strazzabosco, M. (2013). Notch signaling regulates tubular morphogenesis during repair from biliary damage in mice. *J Hepatol*. doi:S0168-8278(13)00147-5 [pii]

10.1016/j.jhep.2013.02.025

Foo, S. S., Turner, C. J., Adams, S., Compagni, A., Aubyn, D., Kogata, N., . . . Adams, R. H. (2006). Ephrin-B2 controls cell motility and adhesion during blood-vessel-wall assembly. *Cell, 124*(1), 161-173. doi:10.1016/j.cell.2005.10.034

Friedman, S. L. (2008). Mechanisms of hepatic fibrogenesis. *Gastroenterology, 134*(6), 1655-1669. doi:10.1053/j.gastro.2008.03.003

Fukushima, Y., Nishiyama, K., Kataoka, H., Fruttiger, M., Fukuhara, S., Nishida, K., . . . Uemura, A. (2020). RhoJ integrates attractive and repulsive cues in directional migration of endothelial cells. *The EMBO Journal, 39*(12), e102930. doi:https://doi.org/10.15252/embj.2019102930

Gilbert, J. M., Adams, M. T., Sharon, N., Jayaraaman, H., & Blum, B. (2020). Morphogenesis of the islets of Langerhans is guided by extra-endocrine Slit2/3 signals. *Mol Cell Biol, 41*(3). doi:10.1128/mcb.00451-20

Giorgio, C., Incerti, M., Corrado, M., Rusnati, M., Chiodelli, P., Russo, S., . . . Tognolini, M. (2018). Pharmacological evaluation of new bioavailable small molecules targeting Eph/ephrin interaction. *Biochemical Pharmacology, 147*, 21-29. doi:https://doi.org/10.1016/j.bcp.2017.11.002

Gong, J., Körner, R., Gaitanos, L., & Klein, R. (2016). Exosomes mediate cell contact-independent ephrin-Eph signaling during axon guidance. *J Cell Biol, 214*(1), 35-44. doi:10.1083/jcb.201601085

Gong, S., Zheng, C., Doughty, M. L., Losos, K., Didkovsky, N., Schambra, U. B., . . . Heintz, N. (2003). A gene expression atlas of the central nervous system based on bacterial artificial chromosomes. *Nature, 425*(6961), 917-925. doi:10.1038/nature02033

nature02033 [pii]

Gordillo, M., Evans, T., & Gouon-Evans, V. (2015). Orchestrating liver development. *Development, 142*(12), 2094-2108. doi:10.1242/dev.114215

Gouysse, G., Couvelard, A., Frachon, S., Bouvier, R., Nejjari, M., Dauge, M. C., . . . Scoazec, J. Y. (2002). Relationship between vascular development and vascular differentiation during liver organogenesis in humans. *J Hepatol, 37*(6), 730-740. doi:S0168827802002829 [pii]

Greenhalgh, S. N., Conroy, K. P., & Henderson, N. C. (2015). Cre-ativity in the liver: transgenic approaches to targeting hepatic nonparenchymal cells. *Hepatology, 61*(6), 2091-2099. doi:10.1002/hep.27606

Guilliams, M., Bonnardel, J., Haest, B., Vanderborght, B., Wagner, C., Remmerie, A., . . . Scott, C. L. (2022). Spatial proteogenomics reveals distinct and evolutionarily conserved hepatic macrophage niches. *Cell, 185*(2), 379-396.e338. doi:https://doi.org/10.1016/j.cell.2021.12.018

Halpern, K. B., Shenhav, R., Massalha, H., Toth, B., Egozi, A., Massasa, E. E., . . . Itzkovitz, S. (2018). Paired-cell sequencing enables spatial gene expression mapping of liver endothelial cells. *Nat Biotechnol, 36*(10), 962-970. doi:10.1038/nbt.4231

Hama, H., Hioki, H., Namiki, K., Hoshida, T., Kurokawa, H., Ishidate, F., . . . Miyawaki, A. (2015). ScaleS: an optical clearing palette for biological imaging. *Nature Neuroscience, 18*(10), 1518-1529. doi:10.1038/nn.4107

Han, L., Chaturvedi, P., Kishimoto, K., Koike, H., Nasr, T., Iwasawa, K., . . . Zorn, A. M. (2020). Single cell transcriptomics identifies a signaling network coordinating endoderm and mesoderm diversification during foregut organogenesis. *Nature Communications, 11*(1), 4158. doi:10.1038/s41467-020-17968-x

Hankeova, S., Salplachta, J., Zikmund, T., Kavkova, M., Van Hul, N., Brinek, A., . . . Andersson, E. R. (2021a). DUCT reveals architectural mechanisms contributing to bile duct recovery in a mouse model for Alagille syndrome. *Elife, 10*, e60916. doi:10.7554/eLife.60916

Hankeova, S., Salplachta, J., Zikmund, T., Kavkova, M., Van Hul, N., Brinek, A., . . . Andersson, E. R. (2021b). DUCT reveals architectural mechanisms contributing to bile duct recovery in a mouse model for Alagille syndrome. *Elife, 10*. doi:10.7554/eLife.60916

Harrison, S. P., Baumgarten, S. F., Verma, R., Lunov, O., Dejneka, A., & Sullivan, G. J. (2021). Liver Organoids: Recent Developments, Limitations and Potential. *Front Med (Lausanne), 8*, 574047. doi:10.3389/fmed.2021.574047

Hegenbarth, J.-C., Lezzoche, G., De Windt, L. J., & Stoll, M. (2022). Perspectives on Bulk-Tissue RNA Sequencing and Single-Cell RNA Sequencing for Cardiac Transcriptomics. *Frontiers in Molecular Medicine, 2*. doi:10.3389/fmmed.2022.839338

Henderson, N. C., Arnold, T. D., Katamura, Y., Giacomini, M. M., Rodriguez, J. D., McCarty, J. H., . . . Sheppard, D. (2013). Targeting of alphav integrin identifies a core molecular pathway that regulates fibrosis in several organs. *Nat Med, 19*(12), 1617-1624. doi:nm.3282 [pii]

10.1038/nm.3282

Herbert, S. P., Huisken, J., Kim, T. N., Feldman, M. E., Houseman, B. T., Wang, R. A., . . . Stainier, D. Y. (2009). Arterial-venous segregation by selective cell sprouting: an alternative mode of blood vessel formation. *Science, 326*(5950), 294-298. doi:10.1126/science.1178577

Hinck, L. (2004). The versatile roles of "axon guidance" cues in tissue morphogenesis. *Dev Cell, 7*(6), 783-793. doi:10.1016/j.devcel.2004.11.002

Hofmann, J. J., Zovein, A. C., Koh, H., Radtke, F., Weinmaster, G., & Iruela-Arispe, M. L. (2010). Jagged1 in the portal vein mesenchyme regulates intrahepatic bile duct development: insights into Alagille syndrome. *Development, 137*(23), 4061-4072. doi:137/23/4061 [pii]

10.1242/dev.052118

Holtwick, R., Gotthardt, M., Skryabin, B., Steinmetz, M., Potthast, R., Zetsche, B., . . . Kuhn, M. (2002). Smooth muscle-selective deletion of guanylyl cyclase-A prevents the acute but not chronic effects of ANP on blood pressure. *Proc Natl Acad Sci U S A, 99*(10), 7142-7147. doi:10.1073/pnas.102650499

Hough, M., Fenlon, M., Glazier, A., Short, C., Fernandez, G. E., Xu, J., . . . Wang, K. S. (2021). Urea-based amino sugar agent clears murine liver and preserves protein fluorescence and lipophilic dyes. *Biotechniques, 70*(2), 72-80. doi:10.2144/btn-2020-0063

Ishibashi, H., Nakamura, M., Komori, A., Migita, K., & Shimoda, S. (2009). Liver architecture, cell function, and disease. *Semin Immunopathol, 31*(3), 399-409. doi:10.1007/s00281-009-0155-6

Jhandier, M. N., Kruglov, E. A., Lavoie, E. G., Sévigny, J., & Dranoff, J. A. (2005). Portal fibroblasts regulate the proliferation of bile duct epithelia via expression of NTPDase2. *J Biol Chem, 280*(24), 22986-22992. doi:10.1074/jbc.M412371200

Jones, C. A., Nishiya, N., London, N. R., Zhu, W., Sorensen, L. K., Chan, A. C., . . . Li, D. Y. (2009). Slit2-Robo4 signalling promotes vascular stability by blocking Arf6 activity. *Nature cell biology, 11*(11), 1325-1331. doi:10.1038/ncb1976

Jongbloets, B. C., & Pasterkamp, R. J. (2014). Semaphorin signalling during development. *Development, 141*(17), 3292-3297. doi:10.1242/dev.105544

Kamimoto, K., Kaneko, K., Kok, C. Y., Okada, H., Miyajima, A., & Itoh, T. (2016). Heterogeneity and stochastic growth regulation of biliary epithelial cells dictate dynamic epithelial tissue remodeling. *Elife, 5*. doi:10.7554/eLife.15034

Kaneko, K., Kamimoto, K., Miyajima, A., & Itoh, T. (2015). Adaptive remodeling of the biliary architecture underlies liver homeostasis. *Hepatology, 61*(6), 2056-2066. doi:10.1002/hep.27685

Kania, A., & Klein, R. (2016). Mechanisms of ephrin-Eph signalling in development, physiology and disease. *Nat Rev Mol Cell Biol, 17*(4), 240-256. doi:10.1038/nrm.2015.16

Kanno, N., LeSage, G., Glaser, S., Alvaro, D., & Alpini, G. (2000). Functional heterogeneity of the intrahepatic biliary epithelium. *Hepatology, 31*(3), 555-561. doi:S0270913900409699 [pii]

10.1002/hep.510310302

Kanth, S. M., Gairhe, S., & Torabi-Parizi, P. (2021). The Role of Semaphorins and Their Receptors in Innate Immune Responses and Clinical Diseases of Acute Inflammation. *Frontiers in Immunology, 12*. doi:10.3389/fimmu.2021.672441

Kaylan, K. B., Ermilova, V., Yada, R. C., & Underhill, G. H. (2016). Combinatorial microenvironmental regulation of liver progenitor differentiation by Notch ligands, TGFbeta, and extracellular matrix. *Sci Rep, 6*, 23490. doi:10.1038/srep23490

Kellendonk, C., Opherk, C., Anlag, K., Schutz, G., & Tronche, F. (2000). Hepatocyte-specific expression of Cre recombinase. *Genesis, 26*(2), 151-153. doi:10.1002/(SICI)1526-968X(200002)26:2<151::AID-GENE17>3.0.CO;2-E [pii]

Khan, J. A., Mendelson, A., Kunisaki, Y., Birbrair, A., Kou, Y., Arnal-Estape, A., . . . Frenette, P. S. (2016). Fetal liver hematopoietic stem cell niches associate with portal vessels. *Science, 351*(6269), 176-180. doi:10.1126/science.aad0084

Kiyohashi, K., Kakinuma, S., Kamiya, A., Sakamoto, N., Nitta, S., Yamanaka, H., . . . Watanabe, M. (2013). Wnt5a signaling mediates biliary differentiation of fetal hepatic stem/progenitor cells in mice. *Hepatology, 57*(6), 2502-2513. doi:10.1002/hep.26293

Koch, A. W., Mathivet, T., Larrivée, B., Tong, R. K., Kowalski, J., Pibouin-Fragner, L., . . . Eichmann, A. (2011). Robo4 maintains vessel integrity and inhibits angiogenesis by interacting with UNC5B. *Developmental Cell, 20*(1), 33-46. doi:10.1016/j.devcel.2010.12.001

Koliaraki, V., Prados, A., Armaka, M., & Kollias, G. (2020). The mesenchymal context in inflammation, immunity and cancer. *Nature Immunology, 21*(9), 974-982. doi:10.1038/s41590-020-0741-2

Kopp, J. L., Dubois, C. L., Schaffer, A. E., Hao, E., Shih, H. P., Seymour, P. A., . . . Sander, M. (2011). Sox9+ ductal cells are multipotent progenitors throughout development but do not produce new endocrine cells in the normal or injured adult pancreas. *Development, 138*(4), 653-665. doi:138/4/653 [pii]

10.1242/dev.056499

Korzh, S., Pan, X., Garcia-Lecea, M., Winata, C. L., Pan, X., Wohland, T., . . . Gong, Z. (2008). Requirement of vasculogenesis and blood circulation in late stages of liver growth in zebrafish. *BMC Dev Biol, 8*, 84. doi:10.1186/1471-213X-8-84

Krishna, M. (2013). Microscopic anatomy of the liver. *Clin Liver Dis (Hoboken), 2*(Suppl 1), S4-S7. doi:10.1002/cld.147

Lai Wing Sun, K., Correia, J. P., & Kennedy, T. E. (2011). Netrins: versatile extracellular cues with diverse functions. *Development, 138*(11), 2153-2169. doi:10.1242/dev.044529

Lancaster, M. A., & Knoblich, J. A. (2014). Organogenesis in a dish: Modeling development and disease using organoid technologies. *Science, 345*(6194), 1247125. doi:10.1126/science.1247125

Larrivée, B., Freitas, C., Suchting, S., Brunet, I., & Eichmann, A. (2009). Guidance of vascular development: lessons from the nervous system. *Circ Res, 104*(4), 428-441. doi:10.1161/circresaha.108.188144

Larrivée, B., Freitas, C., Trombe, M., Lv, X., Delafarge, B., Yuan, L., . . . Eichmann, A. (2007). Activation of the UNC5B receptor by Netrin-1 inhibits sprouting angiogenesis. *Genes Dev, 21*(19), 2433-2447. doi:10.1101/gad.437807

Laws, K. M., & Bashaw, G. J. (2022). Diverse roles for axon guidance pathways in adult tissue architecture and function. *Natural Sciences, 2*(4), e20220021. doi:https://doi.org/10.1002/ntls.20220021

Lee, D. H., Park, J. O., Kim, T. S., Kim, S. K., Kim, T. H., Kim, M. C., . . . Lim, D. S. (2016). LATS-YAP/TAZ controls lineage specification by regulating TGFbeta signaling and Hnf4alpha expression during liver development. *Nat Commun, 7*, 11961. doi:10.1038/ncomms11961

Lee, I. S., & Takebe, T. (2022). Narrative engineering of the liver. *Current Opinion in Genetics & Development, 75*, 101925. doi:https://doi.org/10.1016/j.gde.2022.101925

Lee, N. K., Fok, K. W., White, A., Wilson, N. H., O'Leary, C. J., Cox, H. L., . . . Cooper, H. M. (2016). Neogenin recruitment of the WAVE regulatory complex maintains adherens junction stability and tension. *Nat Commun, 7*, 11082. doi:10.1038/ncomms11082

Lei, L., Bruneau, A., El Mourabit, H., Guegan, J., Folseraas, T., Lemoinne, S., . . . Housset, C. (2022a). Portal fibroblasts with mesenchymal stem cell features form a reservoir of proliferative myofibroblasts in liver fibrosis. *Hepatology*. doi:10.1002/hep.32456

Lei, L., Bruneau, A., El Mourabit, H., Guegan, J., Folseraas, T., Lemoinne, S., . . . Housset, C. (2022b). Portal fibroblasts with mesenchymal stem cell features form a reservoir of proliferative myofibroblasts in liver fibrosis. *Hepatology, 76*, 1360-1375. doi:10.1002/hep.32456

Lejmi, E., Leconte, L., Pédron-Mazoyer, S., Ropert, S., Raoul, W., Lavalette, S., . . . Plouët, J. (2008). Netrin-4 inhibits angiogenesis via binding to neogenin and recruitment of Unc5B. *Proc Natl Acad Sci U S A, 105*(34), 12491-12496. doi:10.1073/pnas.0804008105

Lemaigre, F. (2020). Development of the intrahepatic and extrahepatic biliary tract: a framework for understanding congenital diseases. *Annu Rev Pathol Mech Dis 15*(15), 1-22.

Lemoinne, S., Cadoret, A., El Mourabit, H., Thabut, D., & Housset, C. (2013). Origins and functions of liver myofibroblasts. *Biochim Biophys Acta, 1832*(7), 948-954. doi:10.1016/j.bbadis.2013.02.019

Lemoinne, S., Thabut, D., & Housset, C. (2016). Portal myofibroblasts connect angiogenesis and fibrosis in liver. *Cell Tissue Res, 365*(3), 583-589. doi:10.1007/s00441-016-2443-5

Li, C., Yang, G., Lin, L., Xuan, Y., Yan, S., Ji, X., . . . Lan, T. (2019). Slit2 signaling contributes to cholestatic fibrosis in mice by activation of hepatic stellate cells. *Experimental Cell Research, 385*(1), 111626. doi:https://doi.org/10.1016/j.yexcr.2019.111626

Li, X., & Wang, C.-Y. (2021). From bulk, single-cell to spatial RNA sequencing. *International Journal of Oral Science, 13*(1), 36. doi:10.1038/s41368-021-00146-0

Libbrecht, L., Cassiman, D., Desmet, V., & Roskams, T. (2002). The correlation between portal myofibroblasts and development of intrahepatic bile ducts and arterial branches in human liver. *Liver, 22*(3), 252-258. doi:1674 [pii]

Lindskog, H., Kim, Y. H., Jelin, E. B., Kong, Y., Guevara-Gallardo, S., Kim, T. N., & Wang, R. A. (2014). Molecular identification of venous progenitors in the

dorsal aorta reveals an aortic origin for the cardinal vein in mammals. *Development, 141*(5), 1120-1128. doi:10.1242/dev.101808

Liu, D., Hou, J., Hu, X., Wang, X., Xiao, Y., Mou, Y., & De Leon, H. (2006). Neuronal chemorepellent Slit2 inhibits vascular smooth muscle cell migration by suppressing small GTPase Rac1 activation. *Circ Res, 98*(4), 480-489. doi:10.1161/01.RES.0000205764.85931.4b

Liu, K., Yang, L., Wang, G., Liu, J., Zhao, X., Wang, Y., . . . Yang, J. (2021). Metabolic stress drives sympathetic neuropathy within the liver. *Cell Metab, 33*(3), 666-675.e664. doi:10.1016/j.cmet.2021.01.012

Liu, Z., Xu, M., Huang, S., Pan, Q., Liu, C., Zeng, F., . . . Zhang, Z. (2022). Mesoscale visualization of three-dimensional microvascular architecture and immunocyte distribution in intact mouse liver lobes. *Theranostics, 12*(12), 5418-5433. doi:10.7150/thno.71718

Long, H., Sabatier, C., Ma, L., Plump, A., Yuan, W., Ornitz, D. M., . . . Tessier-Lavigne, M. (2004). Conserved roles for Slit and Robo proteins in midline commissural axon guidance. *Neuron, 42*(2), 213-223. doi:10.1016/s0896-6273(04)00179-5

Lotto, J., Drissler, S., Cullum, R., Wei, W., Setty, M., Bell, E. M., . . . Hoodless, P. A. (2020). Single-Cell Transcriptomics Reveals Early Emergence of Liver Parenchymal and Non-parenchymal Cell Lineages. *Cell, 183*(3), 702-716 e714. doi:10.1016/j.cell.2020.09.012

Lozier, J., McCright, B., & Gridley, T. (2008). Notch signaling regulates bile duct morphogenesis in mice. *PLoS One, 3*(3), e1851. doi:10.1371/journal.pone.0001851

Lu, P., Ewald, A. J., Martin, G. R., & Werb, Z. (2008). Genetic mosaic analysis reveals FGF receptor 2 function in terminal end buds during mammary gland branching morphogenesis. *Dev Biol, 321*(1), 77-87. doi:10.1016/j.ydbio.2008.06.005

Lu, W., van Eerde, A. M., Fan, X., Quintero-Rivera, F., Kulkarni, S., Ferguson, H., . . . Maas, R. L. (2007). Disruption of ROBO2 is associated with urinary tract anomalies and confers risk of vesicoureteral reflux. *Am J Hum Genet, 80*(4), 616-632. doi:10.1086/512735

Lu, X., Le Noble, F., Yuan, L., Jiang, Q., De Lafarge, B., Sugiyama, D., . . . Eichmann, A. (2004). The netrin receptor UNC5B mediates guidance events controlling morphogenesis of the vascular system. *Nature, 432*(7014), 179-186. doi:10.1038/nature03080

Lua, I., & Asahina, K. (2016). The Role of Mesothelial Cells in Liver Development, Injury, and Regeneration. *Gut Liver, 10*(2), 166-176. doi:10.5009/gnl15226

Luo, Y., Raible, D., & Raper, J. A. (1993). Collapsin: a protein in brain that induces the collapse and paralysis of neuronal growth cones. *Cell, 75*(2), 217-227. doi:10.1016/0092-8674(93)80064-l

Macias, H., Moran, A., Samara, Y., Moreno, M., Compton, J. E., Harburg, G., . . . Hinck, L. (2011). SLIT/ROBO1 signaling suppresses mammary branching morphogenesis by limiting basal cell number. *Dev Cell, 20*(6), 827-840. doi:10.1016/j.devcel.2011.05.012

Mariotti, V., Fiorotto, R., Cadamuro, M., Fabris, L., & Strazzabosco, M. (2021). New insights on the role of vascular endothelial growth factor in biliary pathophysiology. *JHEP Reports, 3*(3), 100251. doi:https://doi.org/10.1016/j.jhepr.2021.100251

Maroni, L., Haibo, B., Ray, D., Zhou, T., Wan, Y., Meng, F., . . . Alpini, G. (2015). Functional and structural features of cholangiocytes in health and disease. *Cell Mol Gastroenterol Hepatol, 1*(4), 368-380. doi:10.1016/j.jcmgh.2015.05.005

Martens, S., Coolens, K., Van Bulck, M., Arsenijevic, T., Casamitjana, J., Fernandez Ruiz, A., . . . Rooman, I. (2021). Discovery and 3D imaging of a novel DeltaNp63-expressing basal cell type in human pancreatic ducts with implications in disease. *Gut, 71*(10), 2030-2042. doi:10.1136/gutjnl-2020-322874

Martinez Lyons, A., & Boulter, L. (2021). The developmental origins of Notch-driven intrahepatic bile duct disorders. *Dis Model Mech, 14*(9). doi:10.1242/dmm.048413

Matsuda, M., & Seki, E. (2020). The liver fibrosis niche: Novel insights into the interplay between fibrosis-composing mesenchymal cells, immune cells, endothelial cells, and extracellular matrix. *Food Chem Toxicol, 143*, 111556. doi:10.1016/j.fct.2020.111556

Mederacke, I., Hsu, C. C., Troeger, J. S., Huebener, P., Mu, X., Dapito, D. H., . . . Schwabe, R. F. (2013). Fate tracing reveals hepatic stellate cells as dominant contributors to liver fibrosis independent of its aetiology. *Nat Commun, 4*, 2823. doi:ncomms3823 [pii]

10.1038/ncomms3823

Mehta, V., Pang, K. L., Rozbesky, D., Nather, K., Keen, A., Lachowski, D., . . . Tzima, E. (2020). The guidance receptor plexin D1 is a mechanosensor in endothelial cells. *Nature, 578*(7794), 290-295. doi:10.1038/s41586-020-1979-4

Meijers, R., Smock, R. G., Zhang, Y., & Wang, J. H. (2020). Netrin Synergizes Signaling and Adhesion through DCC. *Trends Biochem Sci, 45*(1), 6-12. doi:10.1016/j.tibs.2019.10.005

Mescher, A. (2010). *Junqueira's Basic Histology: Text & Atlas (12th ed.), by Anthony L. Mescher*.

Mimche, P. N., Lee, C. M., Mimche, S. M., Thapa, M., Grakoui, A., Henkemeyer, M., & Lamb, T. J. (2018). EphB2 receptor tyrosine kinase promotes hepatic fibrogenesis in mice via activation of hepatic stellate cells. *Sci Rep, 8*(1), 2532. doi:10.1038/s41598-018-20926-9

Miyajima, A., Tanaka, M., & Itoh, T. (2014). Stem/progenitor cells in liver development, homeostasis, regeneration, and reprogramming. *Cell Stem Cell, 14*(5), 561-574. doi:S1934-5909(14)00147-7 [pii]

10.1016/j.stem.2014.04.010

Molbay, M., Kolabas, Z. I., Todorov, M. I., Ohn, T. L., & Ertürk, A. (2021). A guidebook for DISCO tissue clearing. *Mol Syst Biol, 17*(3), e9807. doi:10.15252/msb.20209807

Molina, L., Nejak-Bowen, K., & Monga, S. P. (2022). Role of YAP1 Signaling in Biliary Development, Repair, and Disease. *Semin Liver Dis, 42*(1), 17-33. doi:10.1055/s-0041-1742277

Molina, L. M., Krutsenko, Y., Jenkins, N. E. C., Smith, M. C., Tao, J., Wheeler, T. B., . . . Monga, S. P. (2022). LiverClear: A versatile protocol for mouse liver tissue clearing. *STAR Protoc, 3*(1), 101178. doi:10.1016/j.xpro.2022.101178

Morini, S., Carpino, G., Carotti, S., & Gaudio, E. (2020). Anatomy and Embryology of the Liver. In (pp. 3-16).

Mu, T., Xu, L., Zhong, Y., Liu, X., Zhao, Z., Huang, C., . . . Hou, Y. (2020). Embryonic liver developmental trajectory revealed by single-cell RNA sequencing in the Foxa2eGFP mouse. *Communications Biology, 3*(1), 642. doi:10.1038/s42003-020-01364-8

Murray, M. J. (2017). The Role of Netrins and Their Receptors in Epithelial Mesenchymal Plasticity during Development. *Cells Tissues Organs, 203*(2), 71-81. doi:10.1159/000447424

Naito, Y., Hino, K., Bono, H., & Ui-Tei, K. (2015). CRISPRdirect: software for designing CRISPR/Cas guide RNA with reduced off-target sites. *Bioinformatics, 31*(7), 1120-1123. doi:10.1093/bioinformatics/btu743

Nakayama, A., Nakayama, M., Turner, C. J., Höing, S., Lepore, J. J., & Adams, R. H. (2013). Ephrin-B2 controls PDGFRβ internalization and signaling. *Genes Dev, 27*(23), 2576-2589. doi:10.1101/gad.224089.113

Nakayama, H., Kusumoto, C., Nakahara, M., Fujiwara, A., & Higashiyama, S. (2018). Semaphorin 3F and Netrin-1: The Novel Function as a Regulator of Tumor Microenvironment. *Frontiers in Physiology, 9*. doi:10.3389/fphys.2018.01662

Negulescu, A.-M., & Mehlen, P. (2018). Dependence receptors – the dark side awakens. *The FEBS Journal, 285*(21), 3909-3924. doi:https://doi.org/10.1111/febs.14507

Neufeld, G., Mumblat, Y., Smolkin, T., Toledano, S., Nir-Zvi, I., Ziv, K., & Kessler, O. (2016). The semaphorins and their receptors as modulators of tumor progression. *Drug Resist Updat, 29*, 1-12. doi:10.1016/j.drup.2016.08.001

Ng, L., Chow, A. K. M., Man, J. H. W., Yau, T. C. C., Wan, T. M. H., Iyer, D. N., . . . Law, W. L. (2018). Suppression of Slit3 induces tumor proliferation and chemoresistance in hepatocellular carcinoma through activation of GSK3β/β-catenin pathway. *BMC Cancer, 18*(1), 621. doi:10.1186/s12885-018-4326-5

Noberini, R., Lamberto, I., & Pasquale, E. B. (2012). Targeting Eph receptors with peptides and small molecules: progress and challenges. *Semin Cell Dev Biol, 23*(1), 51-57. doi:10.1016/j.semcdb.2011.10.023

Ober, E. A., & Lemaigre, F. P. (2018). Development of the liver: Insights into organ and tissue morphogenesis. *J Hepatol, 68*, 1049-1062. doi:10.1016/j.jhep.2018.01.005

Ochoa-Espinosa, A., & Affolter, M. (2012). Branching morphogenesis: from cells to organs and back. *Cold Spring Harb Perspect Biol, 4*(10). doi:10.1101/cshperspect.a008243

Ohtani, O., & Ohtani, Y. (2008). Lymph Circulation in the Liver. *The Anatomical Record, 291*(6), 643-652. doi:https://doi.org/10.1002/ar.20681

Owens, G. K., Kumar, M. S., & Wamhoff, B. R. (2004). Molecular regulation of vascular smooth muscle cell differentiation in development and disease. *Physiol Rev, 84*(3), 767-801. doi:10.1152/physrev.00041.2003

Pan, F. C., & Wright, C. (2011). Pancreas organogenesis: from bud to plexus to gland. *Dev Dyn, 240*(3), 530-565. doi:10.1002/dvdy.22584

Paris, J., & Henderson, N. C. (2022). Liver zonation, revisited. *Hepatology, 76*(4), 1219-1230. doi:https://doi.org/10.1002/hep.32408

Park, K. W., Crouse, D., Lee, M., Karnik, S. K., Sorensen, L. K., Murphy, K. J., . . . Li, D. Y. (2004). The axonal attractant Netrin-1 is an angiogenic factor. *Proc Natl Acad Sci U S A, 101*(46), 16210-16215. doi:10.1073/pnas.0405984101

Pauerstein, P. T., Tellez, K., Willmarth, K. B., Park, K. M., Hsueh, B., Efsun Arda, H., . . . Kim, S. K. (2017). A radial axis defined by semaphorin-to-neuropilin signaling controls pancreatic islet morphogenesis. *Development, 144*(20), 3744-3754. doi:10.1242/dev.148684

Paysan, J. (2021). *The Art of Tissue Clearing*.

Pepe-Mooney, B. J., Dill, M. T., Alemany, A., Ordovas-Montanes, J., Matsushita, Y., Rao, A., . . . Camargo, F. D. (2019). Single-Cell Analysis of the Liver Epithelium Reveals Dynamic Heterogeneity and an Essential Role for YAP in

Homeostasis and Regeneration. *Cell Stem Cell, 25*(1), 23-38 e28. doi:10.1016/j.stem.2019.04.004

Pi, L., Sun, C., Jn-Simon, N., Basha, S., Thomas, H., Figueroa, V., . . . Petersen, B. (2022). CCN2/CTGF promotes liver fibrosis through crosstalk with the Slit2/Robo signaling. *J Cell Commun Signal*. doi:10.1007/s12079-022-00713-y

Pierreux, C. E. (2021). Shaping the thyroid: From peninsula to de novo lumen formation. *Mol Cell Endocrinol, 531*, 111313. doi:10.1016/j.mce.2021.111313

Poncy, A., Antoniou, A., Cordi, S., Pierreux, C. E., Jacquemin, P., & Lemaigre, F. P. (2015). Transcription factors SOX4 and SOX9 cooperatively control development of bile ducts. *Dev Biol, 402*(2), 136-148. doi:10.1016/j.ydbio.2015.05.012

Popescu, D.-M., Botting, R. A., Stephenson, E., Green, K., Webb, S., Jardine, L., . . . Haniffa, M. (2019). Decoding human fetal liver haematopoiesis. *Nature, 574*(7778), 365-371. doi:10.1038/s41586-019-1652-y

Rama, N., Dubrac, A., Mathivet, T., Ni Charthaigh, R. A., Genet, G., Cristofaro, B., . . . Chedotal, A. (2015). Slit2 signaling through Robo1 and Robo2 is required for retinal neovascularization. *Nat Med, 21*(5), 483-491. doi:10.1038/nm.3849

Ramachandran, P., Matchett, K. P., Dobie, R., Wilson-Kanamori, J. R., & Henderson, N. C. (2020). Single-cell technologies in hepatology: new insights into liver biology and disease pathogenesis. *Nature Reviews Gastroenterology & Hepatology, 17*(8), 457-472. doi:10.1038/s41575-020-0304-x

Ramadori, G., Saile, B., Ramadori, G., & Saile, B. (2002). Mesenchymal cells in the liver – one cell type or two? *Liver, 22*(4), 283-294. doi:https://doi.org/10.1034/j.1600-0676.2002.01726.x

Raudvere, U., Kolberg, L., Kuzmin, I., Arak, T., Adler, P., Peterson, H., & Vilo, J. (2019). g:Profiler: a web server for functional enrichment analysis and conversions of gene lists (2019 update). *Nucleic Acids Res, 47*(W1), W191-W198. doi:10.1093/nar/gkz369

Renier, N., Wu, Z., Simon, D. J., Yang, J., Ariel, P., & Tessier-Lavigne, M. (2014). iDISCO: a simple, rapid method to immunolabel large tissue samples for volume imaging. *Cell, 159*(4), 896-910. doi:10.1016/j.cell.2014.10.010

Ribatti, D. (2006). Genetic and epigenetic mechanisms in the early development of the vascular system. *J Anat, 208*(2), 139-152. doi:10.1111/j.1469-7580.2006.00522.x

Richardson, D. S., Guan, W., Matsumoto, K., Pan, C., Chung, K., Ertürk, A., . . . Lichtman, J. W. (2021). TISSUE CLEARING. *Nat Rev Methods Primers, 1*(1). doi:10.1038/s43586-021-00080-9

Richardson, D. S., & Lichtman, J. W. (2015). Clarifying Tissue Clearing. *Cell, 162*(2), 246-257. doi:10.1016/j.cell.2015.06.067

Robinson, R. A., Griffiths, S. C., van de Haar, L. L., Malinauskas, T., van Battum, E. Y., Zelina, P., . . . Siebold, C. (2021). Simultaneous binding of Guidance Cues NET1 and RGM blocks extracellular NEO1 signaling. *Cell, 184*(8), 2103-2120.e2131. doi:10.1016/j.cell.2021.02.045

Rogers, A. B., & Dintzis, R. Z. (2018). 13 - Hepatobiliary System. In P. M. Treuting, S. M. Dintzis, & K. S. Montine (Eds.), *Comparative Anatomy and Histology (Second Edition)* (pp. 229-239). San Diego: Academic Press.

Rosenthal, S. B., Liu, X., Ganguly, S., Dhar, D., Pasillas, M. P., Ricciardelli, E., . . . Brenner, D. A. (2021). Heterogeneity of HSCs in a Mouse Model of NASH. *Hepatology, 74*(2), 667-685. doi:10.1002/hep.31743

Sampaziotis, F., Cardoso de Brito, M., Madrigal, P., Bertero, A., Saeb-Parsy, K., Soares, F. A., . . . Vallier, L. (2015). Cholangiocytes derived from human induced pluripotent stem cells for disease modeling and drug validation. *Nat Biotechnol, 33*(8), 845-852. doi:10.1038/nbt.3275

Schlegel, M., Köhler, D., Körner, A., Granja, T., Straub, A., Giera, M., & Mirakaj, V. (2016). The neuroimmune guidance cue netrin-1 controls resolution programs and promotes liver regeneration. *Hepatology, 63*(5), 1689-1705. doi:10.1002/hep.28347

Serini, G., Valdembri, D., Zanivan, S., Morterra, G., Burkhardt, C., Caccavari, F., . . . Bussolino, F. (2003). Class 3 semaphorins control vascular morphogenesis by inhibiting integrin function. *Nature, 424*(6947), 391-397. doi:10.1038/nature01784

Sheu, A. Y., Zhang, Z., Omary, R. A., & Larson, A. C. (2013). Invasive catheterization of the hepatic artery for preclinical investigation of liver-directed therapies in rodent models of liver cancer. *Am J Transl Res, 5*(3), 269-278. Retrieved from https://www.ncbi.nlm.nih.gov/pubmed/23634238

Shi, N., & Chen, S.-Y. (2016). Smooth Muscle Cell Differentiation: Model Systems, Regulatory Mechanisms, and Vascular Diseases. *Journal of Cellular Physiology, 231*(4), 777-787. doi:https://doi.org/10.1002/jcp.25208

Shinozaki, K., Ebert, O., Kournioti, C., Tai, Y. S., & Woo, S. L. (2004). Oncolysis of multifocal hepatocellular carcinoma in the rat liver by hepatic artery infusion of vesicular stomatitis virus. *Mol Ther, 9*(3), 368-376. doi:10.1016/j.ymthe.2003.12.004

Si-Tayeb, K., Lemaigre, F. P., & Duncan, S. A. (2010). Organogenesis and development of the liver. *Dev Cell, 18*(2), 175-189. doi:S1534-5807(10)00055-9 [pii]

10.1016/j.devcel.2010.01.011

Silberstein, G. B. (2001). Postnatal mammary gland morphogenesis. *Microscopy Research and Technique, 52*(2), 155-162. doi:https://doi.org/10.1002/1097-0029(20010115)52:2<155::AID-JEMT1001>3.0.CO;2-P

Soares-da-Silva, F., Peixoto, M., Cumano, A., & Pinto-do-Ó, P. (2020). Crosstalk Between the Hepatic and Hematopoietic Systems During Embryonic Development. *Frontiers in Cell and Developmental Biology, 8*. doi:10.3389/fcell.2020.00612

Sosa-Pineda, B., Wigle, J. T., & Oliver, G. (2000). Hepatocyte migration during liver development requires Prox1. *Nat Genet, 25*(3), 254-255. doi:10.1038/76996

Srinivas, S., Watanabe, T., Lin, C. S., William, C. M., Tanabe, Y., Jessell, T. M., & Costantini, F. (2001). Cre reporter strains produced by targeted insertion of EYFP and ECFP into the ROSA26 locus. *BMC Dev Biol, 1*, 4. Retrieved from http://www.ncbi.nlm.nih.gov/entrez/query.fcgi?cmd=Retrieve&db=PubMed&dopt=Citation&list_uids=11299042

Srinivasan, K., Strickland, P., Valdes, A., Shin, G. C., & Hinck, L. (2003). Netrin-1/neogenin interaction stabilizes multipotent progenitor cap cells during mammary gland morphogenesis. *Dev Cell, 4*(3), 371-382. doi:10.1016/s1534-5807(03)00054-6

Stoeckli, E. T. (2018). Understanding axon guidance: are we nearly there yet? *Development, 145*(10). doi:10.1242/dev.151415

Strazzabosco, M., & Fabris, L. (2008). Functional anatomy of normal bile ducts. *Anat Rec (Hoboken), 291*(6), 653-660. doi:10.1002/ar.20664

Strickland, P., Shin, G. C., Plump, A., Tessier-Lavigne, M., & Hinck, L. (2006). Slit2 and netrin 1 act synergistically as adhesive cues to generate tubular bi-layers during ductal morphogenesis. *Development, 133*(5), 823-832. doi:10.1242/dev.02261

Sugiyama, Y., Takabe, Y., Nakakura, T., Tanaka, S., Koike, T., & Shiojiri, N. (2010). Sinusoid development and morphogenesis may be stimulated by VEGF-Flk-1 signaling during fetal mouse liver development. *Dev Dyn, 239*(2), 386-397. doi:10.1002/dvdy.22162

Susaki, Etsuo A., & Ueda, Hiroki R. (2016). Whole-body and Whole-Organ Clearing and Imaging Techniques with Single-Cell Resolution: Toward Organism-Level Systems Biology in Mammals. *Cell Chemical Biology, 23*(1), 137-157. doi:https://doi.org/10.1016/j.chembiol.2015.11.009

Swartley, O. M., Foley, J. F., Livingston, D. P., Cullen, J. M., & Elmore, S. A. (2016). Histology Atlas of the Developing Mouse Hepatobiliary Hemolymphatic Vascular System with Emphasis on Embryonic Days 11.5–18.5 and Early

Postnatal Development. *Toxicologic Pathology, 44*(5), 705-725. doi:10.1177/0192623316630836

Tada, M., Hatano, E., Taura, K., Nitta, T., Koizumi, N., Ikai, I., & Shimahara, Y. (2006). High volume hydrodynamic injection of plasmid DNA via the hepatic artery results in a high level of gene expression in rat hepatocellular carcinoma induced by diethylnitrosamine. *J Gene Med, 8*(8), 1018-1026. doi:10.1002/jgm.930

Tainaka, K., Kubota, S. I., Suyama, T. Q., Susaki, E. A., Perrin, D., Ukai-Tadenuma, M., . . . Ueda, H. R. (2014). Whole-body imaging with single-cell resolution by tissue decolorization. *Cell, 159*(4), 911-924. doi:10.1016/j.cell.2014.10.034

Tainaka, K., Kuno, A., Kubota, S. I., Murakami, T., & Ueda, H. R. (2016). Chemical Principles in Tissue Clearing and Staining Protocols for Whole-Body Cell Profiling. *Annu Rev Cell Dev Biol, 32*, 713-741. doi:10.1146/annurev-cellbio-111315-125001

Takashima, Y., Terada, M., Kawabata, M., & Suzuki, A. (2015). Dynamic three-dimensional morphogenesis of intrahepatic bile ducts in mouse liver development. *Hepatology, 61*(3), 1003-1011. doi:10.1002/hep.27436

Takebe, T., Sekine, K., Enomura, M., Koike, H., Kimura, M., Ogaeri, T., . . . Taniguchi, H. (2013). Vascularized and functional human liver from an iPSC-derived organ bud transplant. *Nature, 499*(7459), 481-484. doi:10.1038/nature12271

Tanaka, M., & Iwakiri, Y. (2016). The Hepatic Lymphatic Vascular System: Structure, Function, Markers, and Lymphangiogenesis. *Cell Mol Gastroenterol Hepatol, 2*(6), 733-749. doi:10.1016/j.jcmgh.2016.09.002

Tanimizu, N. (2022). The neonatal liver: Normal development and response to injury and disease. *Semin Fetal Neonatal Med, 27*(1), 101229. doi:10.1016/j.siny.2021.101229

Tanimizu, N., Ichinohe, N., & Mitaka, T. (2018). Intrahepatic bile ducts guide establishment of the intrahepatic nerve network in developing and regenerating mouse liver. *Development, 145*(9), pii: dev159095. doi:10.1242/dev.159095

Tanimizu, N., Kaneko, K., Itoh, T., Ichinohe, N., Ishii, M., Mizuguchi, T., . . . Mitaka, T. (2016). Intrahepatic bile ducts are developed through formation of homogeneous continuous luminal network and its dynamic rearrangement in mice. *Hepatology, 64*(1), 175-188. doi:10.1002/hep.28521

Tanimizu, N., Kikkawa, Y., Mitaka, T., & Miyajima, A. (2012). alpha1- and alpha5-containing laminins regulate the development of bile ducts via beta1 integrin signals. *J Biol Chem, 287*(34), 28586-28597. doi:10.1074/jbc.M112.350488

Tanimizu, N., & Mitaka, T. (2017). Epithelial Morphogenesis during Liver Development. *Cold Spring Harb Perspect Biol, 9*(8). doi:10.1101/cshperspect.a027862

Tanimizu, N., Miyajima, A., & Mostov, K. E. (2007). Liver progenitor cells develop cholangiocyte-type epithelial polarity in three-dimensional culture. *Mol Biol Cell, 18*(4), 1472-1479. doi:E06-09-0848 [pii]

10.1091/mbc.E06-09-0848

Taylor, H., Campbell, J., & Nobes, C. D. (2017). Ephs and ephrins. *Curr Biol, 27*(3), R90-r95. doi:10.1016/j.cub.2017.01.003

Terada, T., & Nakanuma, Y. (1993). Development of human peribiliary capillary plexus: a lectin-histochemical and immunohistochemical study. *Hepatology, 18*(3), 529-536. doi:S0270913993002113 [pii]

Teulière, J., Faraldo, M. M., Deugnier, M. A., Shtutman, M., Ben-Ze'ev, A., Thiery, J. P., & Glukhova, M. A. (2005). Targeted activation of beta-catenin signaling in basal mammary epithelial cells affects mammary development and leads to hyperplasia. *Development, 132*(2), 267-277. doi:10.1242/dev.01583

Trávníčková, M., Filová, E., Matějka, R., Stepanovska, J., Musílková, J., Zarubova, J., & Molitor, M. (2018). The Role of Vascular Smooth Muscle Cells in the Physiology and Pathophysiology of Blood Vessels. In.

Trefts, E., Gannon, M., & Wasserman, D. H. (2017). The liver. *Curr Biol, 27*(21), R1147-r1151. doi:10.1016/j.cub.2017.09.019

Troeger, J. S., Mederacke, I., Gwak, G. Y., Dapito, D. H., Mu, X., Hsu, C. C., . . . Schwabe, R. F. (2012). Deactivation of hepatic stellate cells during liver fibrosis resolution in mice. *Gastroenterology, 143*(4), 1073-1083 e1022. doi:10.1053/j.gastro.2012.06.036

Tuchin, V. V. (1997). Light scattering study of tissues. *Physics-Uspekhi, 40*, 495 - 515.

Van Liedekerke, P., Gannoun, L., Loriot, A., Johann, T., Lemaigre, F. P., & Drasdo, D. (2022). Quantitative modeling identifies critical cell mechanics driving bile duct lumen formation. *PLoS Comput Biol, 18*(2), e1009653. doi:10.1371/journal.pcbi.1009653

Vartak, N., Drasdo, D., Geisler, F., Itoh, T., P.J.Oude Elferink, R., van de Graaf, S. F. J., . . . Hengstler, J. G. (2021). On the Mechanisms of Biliary Flux. *Hepatology, 74*(6), 3497-3512. doi:https://doi.org/10.1002/hep.32027

Vaught, D., Chen, J., & Brantley-Sieders, D. M. (2009). Regulation of mammary gland branching morphogenesis by EphA2 receptor tyrosine kinase. *Mol Biol Cell, 20*(10), 2572-2581. doi:10.1091/mbc.e08-04-0378

Velazquez, J. J., LeGraw, R., Moghadam, F., Tan, Y., Kilbourne, J., Maggiore, J. C., . . . Ebrahimkhani, M. R. (2021). Gene Regulatory Network Analysis and Engineering Directs Development and Vascularization of Multilineage

Human Liver Organoids. *Cell Syst, 12*(1), 41-55.e11. doi:10.1016/j.cels.2020.11.002

Vento-Tormo, R., Efremova, M., Botting, R. A., Turco, M. Y., Vento-Tormo, M., Meyer, K. B., . . . Teichmann, S. A. (2018). Single-cell reconstruction of the early maternal-fetal interface in humans. *Nature, 563*(7731), 347-353. doi:10.1038/s41586-018-0698-6

Vestentoft, P. S., Jelnes, P., Hopkinson, B. M., Vainer, B., Mollgard, K., Quistorff, B., & Bisgaard, H. C. (2011). Three-dimensional reconstructions of intrahepatic bile duct tubulogenesis in human liver. *BMC Dev Biol, 11*, 56. doi:10.1186/1471-213X-11-56

Vieites-Prado, A., & Renier, N. (2021). Tissue clearing and 3D imaging in developmental biology. *Development, 148*(18). doi:10.1242/dev.199369

Villeneuve, J., Pelluard-Nehme, F., Combe, C., Carles, D., Chaponnier, C., Ripoche, J., . . . Lepreux, S. (2009). Immunohistochemical study of the phenotypic change of the mesenchymal cells during portal tract maturation in normal and fibrous (ductal plate malformation) fetal liver. *Comp Hepatol, 8*, 5. doi:1476-5926-8-5 [pii]

10.1186/1476-5926-8-5

Wallingford, J. B. (2019). We Are All Developmental Biologists. *Developmental Cell, 50*(2), 132-137. doi:https://doi.org/10.1016/j.devcel.2019.07.006

Walter, T. J., Vanderpool, C., Cast, A. E., & Huppert, S. S. (2014). Intrahepatic bile duct regeneration in mice does not require Hnf6 or Notch signaling through Rbpj. *Am J Pathol, 184*(5), 1479-1488. doi:10.1016/j.ajpath.2014.01.030

Wang, H. U., Chen, Z. F., & Anderson, D. J. (1998). Molecular distinction and angiogenic interaction between embryonic arteries and veins revealed by ephrin-B2 and its receptor Eph-B4. *Cell, 93*(5), 741-753. doi:10.1016/s0092-8674(00)81436-1

Wang, X., Yang, L., Wang, Y. C., Xu, Z. R., Feng, Y., Zhang, J., . . . Xu, C. R. (2020). Comparative analysis of cell lineage differentiation during hepatogenesis in humans and mice at the single-cell transcriptome level. *Cell Res, 30*(12), 1109-1126. doi:10.1038/s41422-020-0378-6

Wang, Y., Wang, E., Zhang, Y., Madamsetty, V. S., Ji, B., Radisky, D. C., . . . Mukhopadhyay, D. (2019). Neuropilin-1 maintains dimethylarginine dimethylaminohydrolase 1 expression in endothelial cells, and contributes to protection from angiotensin II-induced hypertension. *Faseb j, 33*(1), 494-500. doi:10.1096/fj.201800499R

Waters, B. J., & Blum, B. (2022). Axon Guidance Molecules in the Islets of Langerhans. *Front Endocrinol (Lausanne), 13*, 869780. doi:10.3389/fendo.2022.869780

Weiler, S., Rohrbach, V., Pulvirenti, T., Adams, R., Ziemiecki, A., & Andres, A. C. (2009). Mammary epithelial-specific knockout of the ephrin-B2 gene leads to precocious epithelial cell death at lactation. *Dev Growth Differ, 51*(9), 809-819. doi:10.1111/j.1440-169X.2009.01140.x

Weiss, K. R., Voigt, F. F., Shepherd, D. P., & Huisken, J. (2021). Tutorial: practical considerations for tissue clearing and imaging. *Nature Protocols, 16*(6), 2732-2748. doi:10.1038/s41596-021-00502-8

Wells, R. G. (2014). The portal fibroblast: not just a poor man's stellate cell. *Gastroenterology, 147*(1), 41-47. doi:10.1053/j.gastro.2014.05.001

Wilkinson, D. G. (2014). Regulation of cell differentiation by Eph receptor and ephrin signaling. *Cell Adh Migr, 8*(4), 339-348. doi:10.4161/19336918.2014.970007

Williams, J. M., & Daniel, C. W. (1983). Mammary ductal elongation: differentiation of myoepithelium and basal lamina during branching morphogenesis. *Dev Biol, 97*(2), 274-290. doi:10.1016/0012-1606(83)90086-6

Wilson, B. D., Ii, M., Park, K. W., Suli, A., Sorensen, L. K., Larrieu-Lahargue, F., . . . Li, D. Y. (2006). Netrins promote developmental and therapeutic angiogenesis. *Science (New York, N.Y.), 313*(5787), 640-644. doi:10.1126/science.1124704

Wilson, N. H., & Key, B. (2006). Neogenin interacts with RGMa and netrin-1 to guide axons within the embryonic vertebrate forebrain. *Dev Biol, 296*(2), 485-498. doi:10.1016/j.ydbio.2006.06.018

Wu, F., Wu, D., Ren, Y., Huang, Y., Feng, B., Zhao, N., . . . Xu, A. (2019). Generation of hepatobiliary organoids from human induced pluripotent stem cells. *J Hepatol, 70*(6), 1145-1158. doi:10.1016/j.jhep.2018.12.028

Wu, J. H., Zhou, Y. F., Hong, C. D., Chen, A. Q., Luo, Y., Mao, L., . . . Hu, B. (2019). Semaphorin-3A protects against neointimal hyperplasia after vascular injury. *EBioMedicine, 39*, 95-108. doi:10.1016/j.ebiom.2018.12.023

Wu, M. F., Liao, C. Y., Wang, L. Y., & Chang, J. T. (2017). The role of Slit-Robo signaling in the regulation of tissue barriers. *Tissue Barriers, 5*(2), e1331155. doi:10.1080/21688370.2017.1331155

Xiong, X., Kuang, H., Liu, T., & Lin, J. D. (2020). A Single-Cell Perspective of the Mammalian Liver in Health and Disease. *Hepatology, 71*(4), 1467-1473. doi:10.1002/hep.31149

Xu, J., Ma, Y., Yu, T., & Zhu, D. (2019). Quantitative assessment of optical clearing methods in various intact mouse organs. *J Biophotonics, 12*(2), e201800134. doi:10.1002/jbio.201800134

Xu, K., Wu, Z., Renier, N., Antipenko, A., Tzvetkova-Robev, D., Xu, Y., . . . Nikolov, D. B. (2014). Neural migration. Structures of netrin-1 bound to two receptors

provide insight into its axon guidance mechanism. *Science, 344*(6189), 1275-1279. doi:10.1126/science.1255149

Yagai, T., Miyajima, A., & Tanaka, M. (2014). Semaphorin 3E secreted by damaged hepatocytes regulates the sinusoidal regeneration and liver fibrosis during liver regeneration. *Am J Pathol, 184*(8), 2250-2259. doi:10.1016/j.ajpath.2014.04.018

Yamada, Y., Oike, Y., Ogawa, H., Ito, Y., Fujisawa, H., Suda, T., & Takakura, N. (2003). Neuropilin-1 on hematopoietic cells as a source of vascular development. *Blood, 101*(5), 1801-1809. doi:10.1182/blood-2002-01-0119

Yan, W., Han, P., Zhou, Z., Tu, W., Liao, J., Li, P., . . . Fu, Y. (2014). Netrin-1 induces epithelial-mesenchymal transition and promotes hepatocellular carcinoma invasiveness. *Dig Dis Sci, 59*(6), 1213-1221. doi:10.1007/s10620-013-3016-z

Yang, L., Wang, W. H., Qiu, W. L., Guo, Z., Bi, E., & Xu, C. R. (2017). A single-cell transcriptomic analysis reveals precise pathways and regulatory mechanisms underlying hepatoblast differentiation. *Hepatology, 66*(5), 1387-1401. doi:10.1002/hep.29353

Yebra, M., Diaferia, G. R., Montgomery, A. M., Kaido, T., Brunken, W. J., Koch, M., . . . Cirulli, V. (2011). Endothelium-derived Netrin-4 supports pancreatic epithelial cell adhesion and differentiation through integrins α2β1 and α3β1. *PLoS One, 6*(7), e22750. doi:10.1371/journal.pone.0022750

Yebra, M., Montgomery, A. M., Diaferia, G. R., Kaido, T., Silletti, S., Perez, B., . . . Cirulli, V. (2003). Recognition of the neural chemoattractant Netrin-1 by integrins alpha6beta4 and alpha3beta1 regulates epithelial cell adhesion and migration. *Dev Cell, 5*(5), 695-707. doi:10.1016/s1534-5807(03)00330-7

Yin, C., Evason, K. J., Asahina, K., & Stainier, D. Y. (2013). Hepatic stellate cells in liver development, regeneration, and cancer. *J Clin Invest, 123*(5), 1902-1910. doi:10.1172/jci66369

Yuan, M., Guo, H., Li, J., Sui, C., Qin, Y., Wang, J., . . . Ye, J. (2016). Slit2 and Robo1 induce opposing effects on metastasis of hepatocellular carcinoma Sk-hep-1 cells. *Int J Oncol, 49*(1), 305-315. doi:10.3892/ijo.2016.3506

Yuasa-Kawada, J., Kinoshita-Kawada, M., Tsuboi, Y., & Wu, J. Y. (2022). Neuronal guidance genes in health and diseases. *Protein & Cell*, pwac030. doi:10.1093/procel/pwac030

Zang, Y., Chaudhari, K., & Bashaw, G. J. (2021). New insights into the molecular mechanisms of axon guidance receptor regulation and signaling. *Curr Top Dev Biol, 142*, 147-196. doi:10.1016/bs.ctdb.2020.11.008

Zaret, K. S. (2016). From Endoderm to Liver Bud: Paradigms of Cell Type Specification and Tissue Morphogenesis. *Curr Top Dev Biol, 117*, 647-669. doi:10.1016/bs.ctdb.2015.12.015

Zeng, Z., Wu, Y., Cao, Y., Yuan, Z., Zhang, Y., Zhang, D. Y., . . . Guo, J. (2018). Slit2-Robo2 signaling modulates the fibrogenic activity and migration of hepatic stellate cells. *Life Sci, 203*, 39-47. doi:10.1016/j.lfs.2018.04.017

Zhang, B., Dietrich, U. M., Geng, J. G., Bicknell, R., Esko, J. D., & Wang, L. (2009). Repulsive axon guidance molecule Slit3 is a novel angiogenic factor. *Blood, 114*(19), 4300-4309. doi:10.1182/blood-2008-12-193326

Zhang, H., Pu, W., Tian, X., Huang, X., He, L., Liu, Q., . . . Zhou, B. (2016). Genetic lineage tracing identifies endocardial origin of liver vasculature. *Nat Genet, 48*(5), 537-543. doi:10.1038/ng.3536

Zhang, J., Zhong, W., Cui, T., Yang, M., Hu, X., Xu, K., . . . Chen, Y. E. (2006). Generation of an adult smooth muscle cell-targeted Cre recombinase mouse model. *Arterioscler Thromb Vasc Biol, 26*(3), e23-24. doi:10.1161/01.ATV.0000202661.61837.93

Zhang, N., Bai, H., David, K. K., Dong, J., Zheng, Y., Cai, J., . . . Pan, D. (2010). The Merlin/NF2 tumor suppressor functions through the YAP oncoprotein to regulate tissue homeostasis in mammals. *Dev Cell, 19*(1), 27-38. doi:S1534-5807(10)00305-9 [pii]
10.1016/j.devcel.2010.06.015

Zon, L. (2019). Improving the visibility of developmental biology: time for induction and specification. *Development, 146*(2). doi:10.1242/dev.174631

Zong, Y., Panikkar, A., Xu, J., Antoniou, A., Raynaud, P., Lemaigre, F., & Stanger, B. Z. (2009). Notch signaling controls liver development by regulating biliary differentiation. *Development, 136*(10), 1727-1739. doi:dev.029140 [pii]
10.1242/dev.029140

Zong, Y., & Stanger, B. Z. (2012). Molecular mechanisms of liver and bile duct development. *Wiley Interdiscip Rev Dev Biol, 1*(5), 643-655. doi:10.1002/wdev.47

Zorn, A. M., & Wells, J. M. (2007). Molecular basis of vertebrate endoderm development. *Int Rev Cytol, 259*, 49-111. doi:10.1016/S0074-7696(06)59002-3